SOCIETÀ GEOLOGICA ITALIANA
FONDATA NEL 1881 - ENTE MORALE R. D. 17 OTTOBRE 1885

Geological Field Trips and Maps

2023
Vol. 15 (1.2)

ISPRA
Istituto Superiore per la Protezione e la Ricerca Ambientale
Sistema Nazionale per la Protezione dell'Ambiente

INDEXED IN EMERGING SOURCES CITATION INDEX THOMSON REUTERS

ISSN: 2038-4947

Fossil rifted margins in the Alps

https://doi.org/10.3301/GFT.2023.02

GFT&M - *Geological Field Trips and Maps*

Periodico semestrale del Servizio Geologico d'Italia - ISPRA e della Società Geologica Italiana
Geol. F. Trips Maps, Vol.**15** No.1.2 (2023), 207 pp., 122 figs. (https://doi.org/10.3301/GFT.2023.02)

Fossil rifted margins in the Alps

Gianreto Manatschal[1] & Pauline Chenin[1]

[1] Université de Strasbourg - CNRS UMR7063 ITES, 5 rue Descartes, 67084 Strasbourg, France.

* Corresponding author e-mail: manat@unistra.fr

with contributions from

PhD students:
Laurent Desmurs, Andreas Hölker, Anna Engström, Geoffroy Mohn, Emmanuel Masini, Victor Hugo Pinto, Isabelle Haupert, Benoît Petri, Marie-Eva Epin, Nicolò Incerpi, Méderic Amann, Rémi Coltat, Flora Hochscheid, Nicolas Dall'Asta

Post-doctoral researchers:
Marco Beltrando, Suzanne Picazo, Alessandro Decarlis, Charlotte Ribes

Senior researchers:
Daniel Bernoulli, Nikolaus Froitzheim, Peter Nievergelt, Othmar Müntener, Jean-François Ghienne, Anne-Marie Karpoff, Marc Ulrich, Philippe Boulvais

Special thanks to:
Nick Kusznir (MM consortia), Patrick Unternehr (Total), Garry Karner (ExxonMobil), Adriano Viana (Petrobras)

Cover page Figure: Outcrop of the former Err detachment system, expressed as a sub-horizontal planar contact, in the neighbourhood of Piz Laviner. View toward the east taken from 46°32'48.8" N – 9°43'30.8" E.

ISSN: 2038-4947 [online]

http://gftm.socgeol.it/

https://doi.org/10.3301/GFT.2023.02

INDEX

INFORMATION

EXCURSION NOTES

ITINERARY

https://doi.org/10.3301/GFT.2023.02

https://doi.org/10.3301/GFT.2023.02

https://doi.org/10.3301/GFT.2023.02

ABSTRACT

The significant progress achieved over the last fifty years in understanding continental rifting and oceanization processes demonstrates the benefit of an iterative workflow between onshore field studies and offshore geophysical studies. On the one hand, geophysical studies can image intact present-day rifted margins in their entirety. However, the resolution of refraction and reflection seismic sections is relatively low, and most parts of the margin remain largely inaccessible, even to deep-sea drilling. On the other hand, field studies of rifted margin remnants exposed in orogens offer easy-to-access, high-resolution outcrops. Yet, they provide only local, discontinuous, and often overprinted insights into the former margins and their evolution.

With more than one century of published research into the geology of the European Alps, the present-day Alpine orogen and former Alpine Tethys rift system are among the best-described tectonic systems in the world. In the present document, we provide a guide for recognizing key remnants of the former Alpine Tethys rift system (Fig. I.0) and discuss how the derived observations can be integrated into the study of present-day rifted margins. This document is structured around three parts:

- **Excursion notes: we first provide an overview of the state of the art on rifted margins and its historical evolution. Second, we outline the paleogeographic framework of the Alpine rift system and discuss its uncertainties. Third, we describe the structural and stratigraphic relationships of well-preserved remnants of the Alpine Tethys rift system and propose a crustal-scale reconstruction for one transect across the former Alpine Tethys rift system. Finally, we provide insights into the spatio-temporal evolution of the Alpine Tethys rift system.**
- **Excursions: through a series of excursions at illustrative remnants of the Alpine Tethys rift system, we propose a journey across the proximal part, the distal part, and the so-called ocean-continent transition (OCT) of the former North-Adriatic margin. In particular, we display the scale of the considered geological objects, report the nature of the crust, mantle, and sediments, and highlight the structural and stratigraphic relationships between the different domains.**
- **Thematic sheets: we provide a series of short syntheses on different geological themes and illustrate them with examples from the Alps. Themes include the petrology of the Alpine Tethys lithosphere, the tectono-stratigraphic record and fluid signature during the Alpine Tethys rifting, the tectono-structural characteristics of the Alpine Tethys rift system and Alpine orogen, the impact of inheritance vs rift-induced and orogenic processes, and the isostatic evolution of future distal margins during rifting, with special focus on the Briançonnais domain in the Alps.**

Keywords: Alpine Tethys rift system, Alpine Orogen, Tectonics, Stratigraphy.

PROGRAM SUMMARY

The present field trip describes a journey across the Adriatic margin and an ocean-continent transition of the former Alpine Tethys. It focuses on the major rift-related structures, their field evidence and the tracking of timelines (isochrons) from one domain to the other based on stratigraphic markers.

The first excursion takes place near Il Motto (IM in Fig. I.1), an Early Jurassic half-graben depocenter that was inverted during the Late Cretaceous. This excursion provides an overview of the pre-rift paleogeographic and stratigraphic setting in which the Alpine Tethys rifting took place. It focuses on the style of both rift-related and Alpine deformation style in the (former) proximal domain of the fossil Adriatic margin.

The second excursion takes place near Diavolezza (D in Fig. I.1), where the Piz Alv mountain represents a former extensional allochthon. This

https://doi.org/10.3301/GFT.2023.02

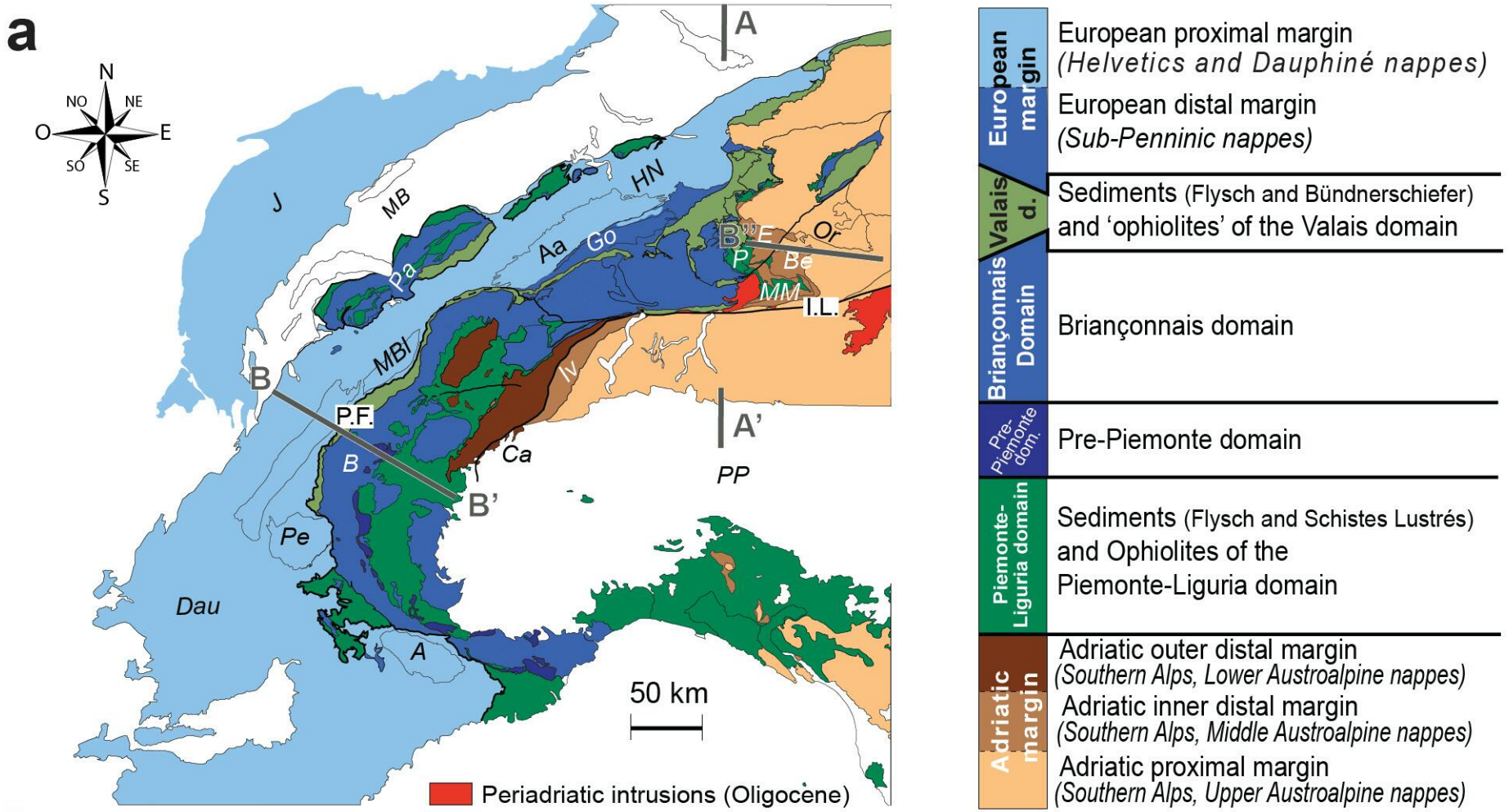

Fig. I.0 - a) A: Argentera massif, Aa: Aar massif, B: Briançonnais nappes, Be: Bernina Ca: Cannavese nappes, Dau: Dauphiné nappes, E: Errnappe, Go: Gothard massif, HN: Helvetic nappes, I.L.: Insubric Line; Iv: Ivrea, J: Jura, MB: Molasse basin, MBl: Mont Blanc massif, MM: Malenco-Margna nappes, Or: Ortler nappe, P: Platta nappe, Pa: Prealps, Pe: Pelvoux massif, P.F.: Penninic Front; PP: Po Plain. Simplified tectonic map of the Alpine orogen straddling France, Switzerland, and Italy (modified from Schmid et al., 2004)

excursion displays evidence for extensional detachment faults in the necking/inner part of the hyperextended domain of the former Adriatic margin and discusses their role in the significant crustal thinning achieved during the necking phase of rifting. It also highlights that such first-order structural features largely seeded Alpine deformation, and hence that much of the apparent Alpine structural complexity can be linked to the architecture of the margins involved in the collision.

https://doi.org/10.3301/GFT.2023.02

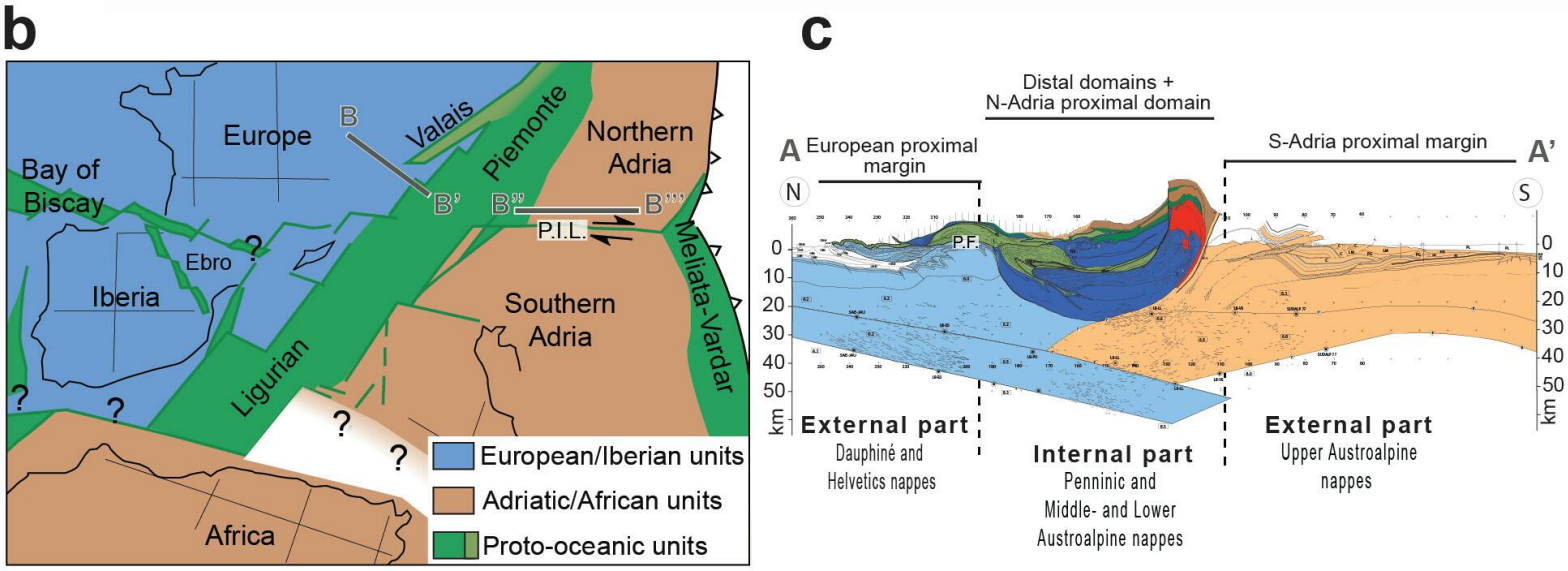

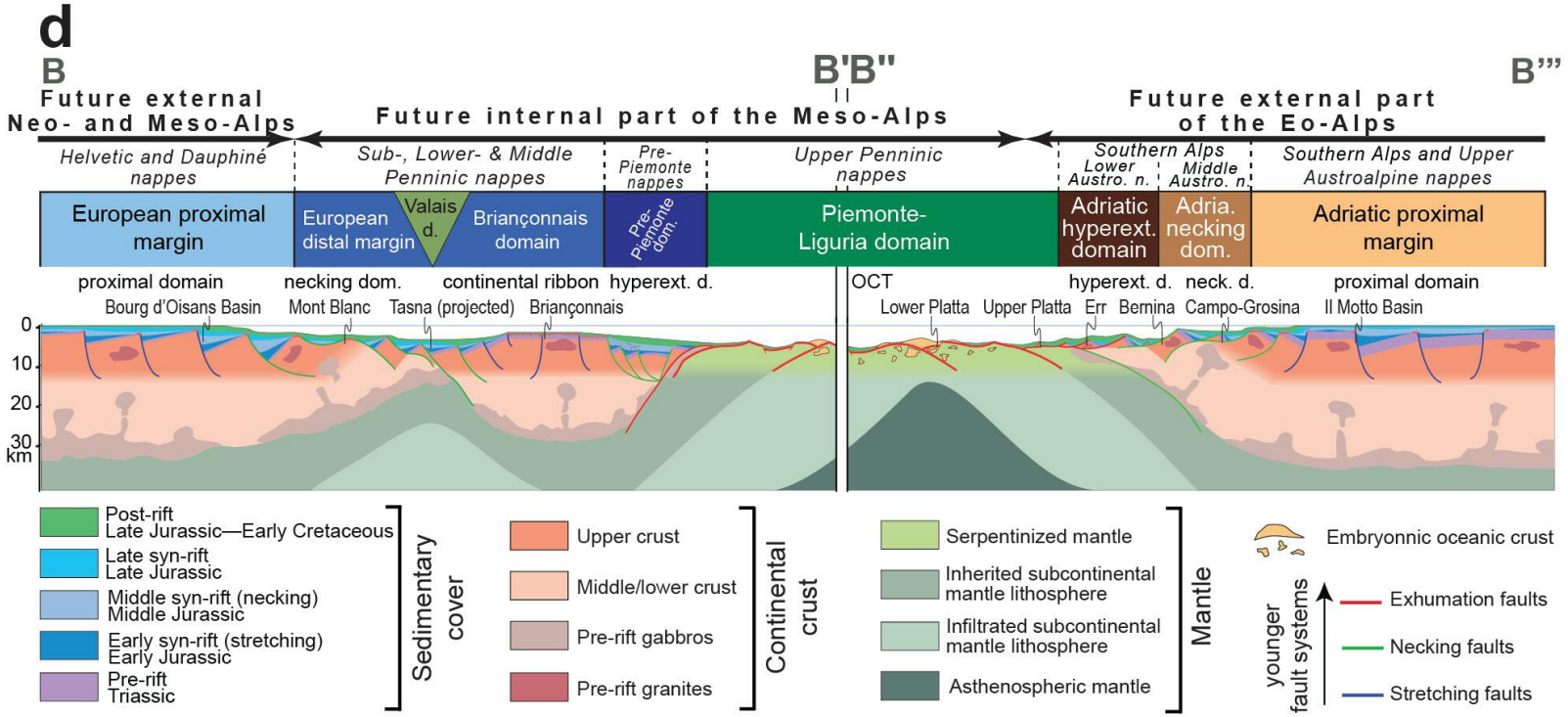

Fig. I.0 - b) schematic paleogeographic map of the Alpine Tethys region during the Early Cretaceous (modified from Manatschal and Müntener, 2009; see Appendix 1 for a geological time scale); Abbreviation: P.I.L.: Paleo-Insubric Line; c) interpretation of the NFP 20 seismic profile across the Central Alps in terms of paleogeographic domains (from Schmid et al., 1996). From a large-scale perspective, collisional orogens can be regarded as comprised of two buttresses (the "external domains") formed by the former proximal margins on either side of an "internal domain" comprised of the former distal margins and its sedimentary cover that was scraped off during the closure of the "ocean"/ hyperextended rift system (see the *Tectono-Structural thematic sheet*); d) reconstruction of a synthetic section across the former Alpine Tethys rift system during the Late Jurassic (from Manatschal et al., 2022). See panels a and b for location and note that section B-B' across the European margin is offset from section B''-B''' across the northern Adriatic margin. Note also that pre, syn- and post-rift are relative to the Alpine Tethys rifting. Abbreviations: d./dom.: domain; hyperext.: hyperextended; Austro. n.: Austroalpine nappes; neck.: necking; OCT: Ocean–Continent Transition.

https://doi.org/10.3301/GFT.2023.02

The third excursion takes place in the region of Piz Laviner, Piz Bardella and Piz Nair (PL, PB and PN in Fig. I.1), which display the spectacularly well-preserved and exposed Err extensional detachment system. This excursion provides a three-dimensional overview of the hyperextended domain of the former Adriatic margin with a special focus on the associated stratigraphic record. It also highlights the importance of rheological interfaces/decoupling levels in controlling the style of alpine reactivation.
The fourth excursion takes place in the region of Falotta and the Marmorera Lake (Fa and ML in Fig. I.1), which preserves remnants of the inner part of the Adriatic margin exhumed mantle domain. This excursion provides an overview of the three-dimensional architecture of a proto-oceanic core complex, the nature and location of related magmatic additions and sedimentary systems, as well as the fluid-rock-sediment interactions during mantle exhumation. It also highlights the importance of rift-related topography in controlling the style of alpine reactivation.
The fifth and last excursion takes place in the region of Tasna (Ta in Fig. I.1), which spectacularly preserves the ocean-continent transition between the Briançonnais continental ribbon and the Valais Basin. This excursion displays the structures that accommodated crustal thinning and mantle exhumation and describes the nature of the crust and mantle rocks involved. It also describes the nature of the sediments present in the ocean-continent transition and the insights they provide into the regional paleogeographic setting.

SAFETY

All attendees participate to the excursions at their own risk. Your attendance to an excursion constitutes your acceptance not to hold the field leader or their institutions responsible or liable for any mishap while on the excursion.
All field trips are accessible to any healthy person. The excursions involve walking in strenuous but not dangerous terrains at high altitudes (up to 3000 m above sea level). Adequate mountain gear is necessary (appropriate hiking shoes, warm clothes, and rainwear).

HOSPITALS

Excursion A: International Medical Center; Via Canton, 474, 23041 Livigno SO, Italy; +39 0342 978112; Italian Alpine rescue system (emergency number 112)

Excursions B, C, and D: Hospital Oberengadin, Via Nouva 3, 7503 Samedan, Switzerland; +41 81 851 81 11; Swiss Alpine rescue system (emergency number 1414)

Excursion E: Hospital Lower Engadine, Via da l'Ospidal 280, 7550 Scuol, Switzerland; +41 81 861 10 00; Swiss Alpine rescue system (emergency number 1414)

https://doi.org/10.3301/GFT.2023.02

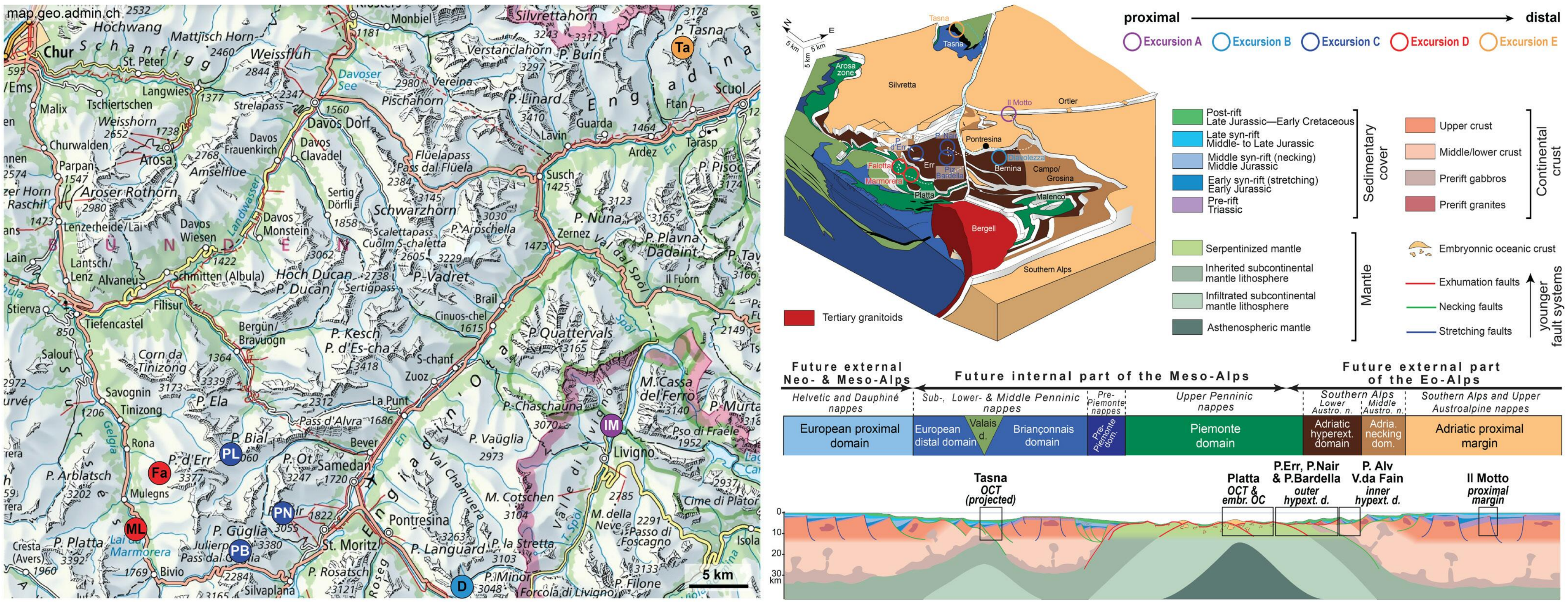

Fig. I.1 - Location of the excursion sites on: (a) a regional map; (b) a schematic diagram block of SE Grisons region and adjacent Italy (modified from Froitzheim et al., 1994); (c) a synthetic cross section through the former Alpine Tethys rift system (see location of transect B–B' in Fig. I.0a, I.0b and I.12); Abbreviations: Austro. n.: Austroalpine nappes; d./dom.: domain; embr. OC: embryonic oceanic crust; hypext./hypertext.: hyperextended; OCT: Ocean–Continent Transition.

ACCOMMODATIONS

Tourist offices:

- Pontresina tourist office : Via Maistra 133, 7504 Pontresina; tel.: +41 81 838 83 00 ; email: pontresina@engadin.ch; website: https://www.engadin.ch/pontresina
- St. Moritz Tourist Information Village: Via Maistra 12, 7500 St. Moritz; tel.: +41 81 837 33 33; email: info@stmoritz.ch; website: https://www.stmoritz.com

Hotels:

- Sporthotel Pontresina: Via Maistra 145, 7504 Pontresina; tel.: +41818389400; https://www.sporthotel.ch/
- Hotel Station: Cuntschett 2, 7504 Pontresina; tel.: +41818388000; https://www.station-pontresina.ch/en/
- Hotel Baer & Post, Curtins 108, 7530 Zernez; tel.: +41818515500; http://www.baer-post.ch/
- Hotel Solaria, Vea Valetta 113, 7457 Bivio; tel.: +41816591991; http://www.hotelsolariabivio.ch/

B&B:

- B&B Chesa Albris: 7500 Saint-Moritz, Suisse; tel.: +41818335465 ; https://www.engadin.ch/de/privatzimmer/chesa-albris/

Youth Hotel:

- Jugendherberge Pontresina; Via Da la Staziun 46, 7504 Pontresina, Suisse; tel.: +41818427223; http://www.youthhostel.ch/pontresina

Camping sites:

- Camping Morteratsch: Plauns 13, 7504 Pontresina; tel.: +41818426285; http://www.camping-morteratsch.ch/
- Camping St. Moritz: Via San Gian 55, 7500 St. Moritz; tel.: +41818334090; http://camping-stmoritz.ch/

https://doi.org/10.3301/GFT.2023.02

PROGRESS IN UNDERSTANDING RIFTED MARGINS AND RIFTING PROCESSES: A HISTORICAL OVERVIEW

From naturalist observations to plate tectonics

As early as the 1700s, naturalists, and geologists started to report lithological and structural observations from the European Alps (e.g., de Saussure 1779). The Alps became rapidly a popular natural laboratory to study the functioning of the Earth. During the next century, the Alps both inspired and benefited from scientific advances in geology (Şengör 1990).

The Austrian palaeontologist Eduard Suess (Fig. I.2a) was presumably the most influent player in the change of paradigm from fixism to mobilism. He was one of the first to support the existence of horizontal displacements at the scale of the Earth and suggested that "folded orogens" resulted from the compression of basins filled with pelagic sediments between two continental blocks (Suess, 1875). He recognized the former existence of such a basin in the Alps, which he named Tethys (Suess, 1875).

Suess's hypothesis laid the ground for the nappe concept introduced by Marcel Bertrand (1884) (Fig.I.2b). Subsequently, Hans Schardt (1898), Maurice Lugeon (1902), and Pierre Termier (1904) established that the Alpine orogen was primarily constructed by the stacking of nappes, settling the nappe theory. At the same time, Gustav Steinmann (1905) (Fig. I.2c) suggested that the association of (serpentinized) peridotite, "diabase" and radiolarite, which can be mapped throughout the Alps, was characteristic of a deep ocean floor. These studies inspired the first-ever paleogeographic and tectonic reconstructions of the Alps by Emile Argand (1911, 1916, 1924a,b) (Fig. I.2d).

Contemporaneously, Alfred Wegener (Fig. I.2e) published his theory of Continental Drift (Wegener, 1915), which however met a cold reception from the scientific community because the author was unable to resolve what was driving the movements of the tectonic plates. Arthur Holmes (Fig. I.2f) envisioned the mechanism of mantle convection only fifteen years later (Holmes, 1931), and it took a few more decades for the concept of seafloor spreading to emerge with Otto Ampferer (1941) and Harry Hess (1962) (Fig. I.2g). Frederick Vine and Drummond Matthews (Fig. I.2h) confirmed this hypothesis when they evidenced parallel and symmetrical magnetic stripes on either side of so-called mid-oceanic ridges worldwide (Vine et al., 1963). Shortly after, the Deep-Sea Drilling Program (DSDP, 1968) revealed the positive correlation between the age of the sediments directly overlying the ocean floor and their distance to the mid-oceanic ridge, establishing the reality of seafloor spreading, and hence plate tectonics.

Characterization of rifted margins, ocean floors, and ocean-continent transitions

In the 1950s, the first refraction seismic exploration of oceans revealed significant differences between the basement flooring continental platforms and slopes and that flooring abyssal plains (e.g., Officer and Ewing, 1954; see Green, 1974 for a review): on the one hand, the basement of continental platforms is thick (30±5 km), the basement of continental slopes wedges oceanward from ca. 30 km to 0 km, and both are seismically complex and heterogeneous. On the other hand, the basement of the abyssal plains is thin (ca. 7 km) and characterized by a uniform seismic signature.

https://doi.org/10.3301/GFT.2023.02

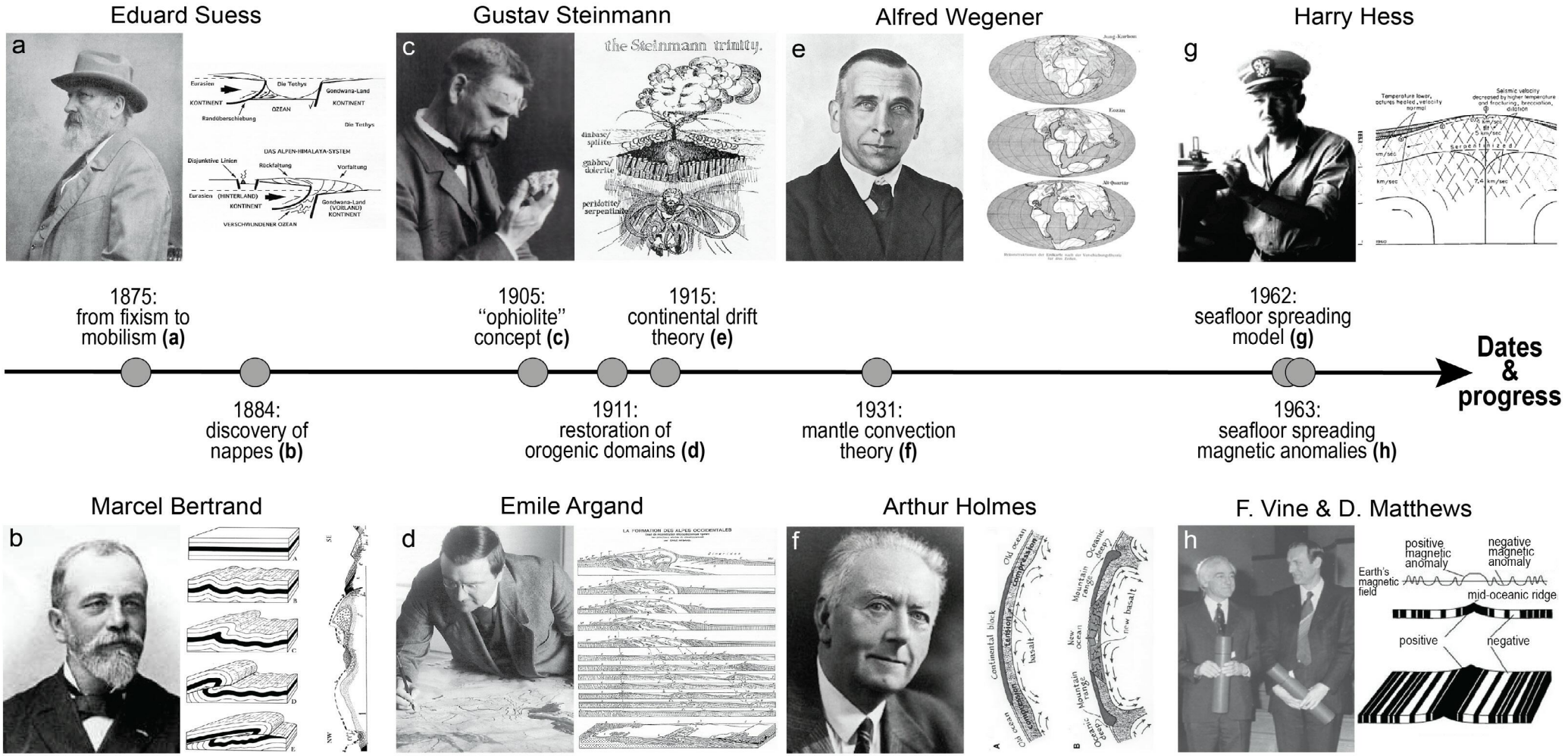

Fig. I.2 - Major players of the Plate Tectonics revolution: a) Eduard Suess and his first model of a Tethyan basin whose closure was at the origin of the Alpine orogeny (Suess, 1875); b) Marcel Bertrand suggested that the architecture of the Alpine orogen was controlled by the stacking of nappes; c) Gustav Steinmann related the association of serpentinized peridotite, "diabase" and radiolarite (later named "Steinmann's Trinity") observed in the Alps to a deep ocean floor (Steinmann, 1905; picture from Coleman, 1977); d) Emile Argand is the author of the first detailed paleogeographic and tectonic restoration of the Alps (Argand, 1916); e) Alfred Wegener is the author of the Theory of Continental drift (Wegener, 1915), a premise of the Plate Tectonic theory; f) Arthur Holmes envisioned mantle convection as a potential driver for plate tectonics as early as 1931 (Holmes, 1931); g) Harry Hess was one of the discoverers of seafloor spreading (Hess, 1962); h) Frederic Vine and Drummond Matthews established that seafloor spreading was achieved via magmatic accretion when they evidenced parallel and symmetrical magnetic stripes on either side of mid-oceanic ridges worldwide.

https://doi.org/10.3301/GFT.2023.02

Until the latest 1960s drilling and dredging of continental margins were essentially limited to their proximal parts. As a result, rifted margins were envisioned as continental rifts, namely comprised of quartz-feldspathic crust (Fig. A2a in Appendix 2) essentially structured by oceanward-dipping normal faults (Figs. I.3c and 3d). These faults were separating a series of tilted blocks whose size decreased oceanward (Fig. I.3a).

Spurred by the Plate Tectonic revolution, the basement flooring abyssal plains was consensually interpreted as a mafic oceanic crust formed by steady-state seafloor spreading at a mid-oceanic ridge (Penrose conference of 1972; Anonymous, 1972). At that time, the thinned continental crust was thought to be structured by tilted blocks and to terminate abruptly against the above-mentioned Penrose-type oceanic crust (Fig. I.3a). This sharp contact was supposed to mark an "instantaneous" onset of seafloor spreading.

Advances in reflection seismic techniques enabled to image of ever-deeper parts of rifted margins with ever-higher resolutions. However, as seismic interpretation is generally biased by the conceptual model the interpreter has in mind, the next steps in the understanding of rifted margins arose essentially from field studies at "fossil" rifted margins exposed on land.

Alpine geologists highlighted that the basement underlying the continental platform was essentially affected by high-angle normal faults (blue faults on Fig. I.0d; Bernoulli, 1964), while more distal parts of the margins were affected by both high-angle normal faults and low-angle extensional detachment faults (green and red faults on Fig. I.0d; Froitzheim and Eberli, 1990; Manatschal and Nievergelt, 1997; Mohn et al., 2012). Extensional detachment faults initiate preferentially in weak materials, as evidenced by the mylonitic front associated with these structures (Lister et al., 1986; Wernicke, 1985). Detachment faults are much more efficient thinning structures than high-angle normal faults: they may exhume relatively deep material (e.g., mid- to lower crustal levels or upper mantle rocks) to the seafloor, favouring an efficient cooling of the lithosphere (e.g., mylonitic structures evolving into cataclastic breccias as the detachment approaches the seafloor). Recently, Epin and Manatschal (2018) highlighted the oceanward in-sequence migration of the successive extensional detachment faults (each one cross-cutting the previous one) in the most distal part of the fossil Adriatic margin (Err and Platta nappes; cf. Excursions C and D).

Since their discovery in the Alpine orogen, extensional detachment structures have been increasingly recognized at present-day rifted margins, from ultra-distal (e.g., Reston et al., 1995) to less distal environments (i.e., necking domain; Osmundsen and Péron-Pinvidic, 2018). Growing evidence confirms that the proximal domain of rifted margins is generally comprised of little thinned (30±5 km) continental crust essentially affected by high-angle normal faults, while the significantly thinned (25-0 km) continental crust of the distal domain is affected by both high-angle normal faults and low-angle detachment faults (Fig. I.3b).

The dredging (Boillot et al., 1980) and drilling (Boillot et al., 1987) of serpentinized peridotites directly overlain by post-rift sediments offshore the Iberian margin laid the ground for a change of paradigm in the interpretation of the OCT. In the Alps, mantle rock exposures that had been described as early as 1905 (e.g., Steinmann, 1905) and interpreted as exhumed along extensional detachment faults by Decandia and Elter (1969, 1972) received renewed interest after having been discarded, disregarded, or misinterpreted following the emergence of the Plate Tectonics theory. For instance, Trommsdorff et al. (1993) and Hermann and Müntener (1996) interpreted

https://doi.org/10.3301/GFT.2023.02

geological field trips and maps 2023 - 15(1.2)
15
excursion notes

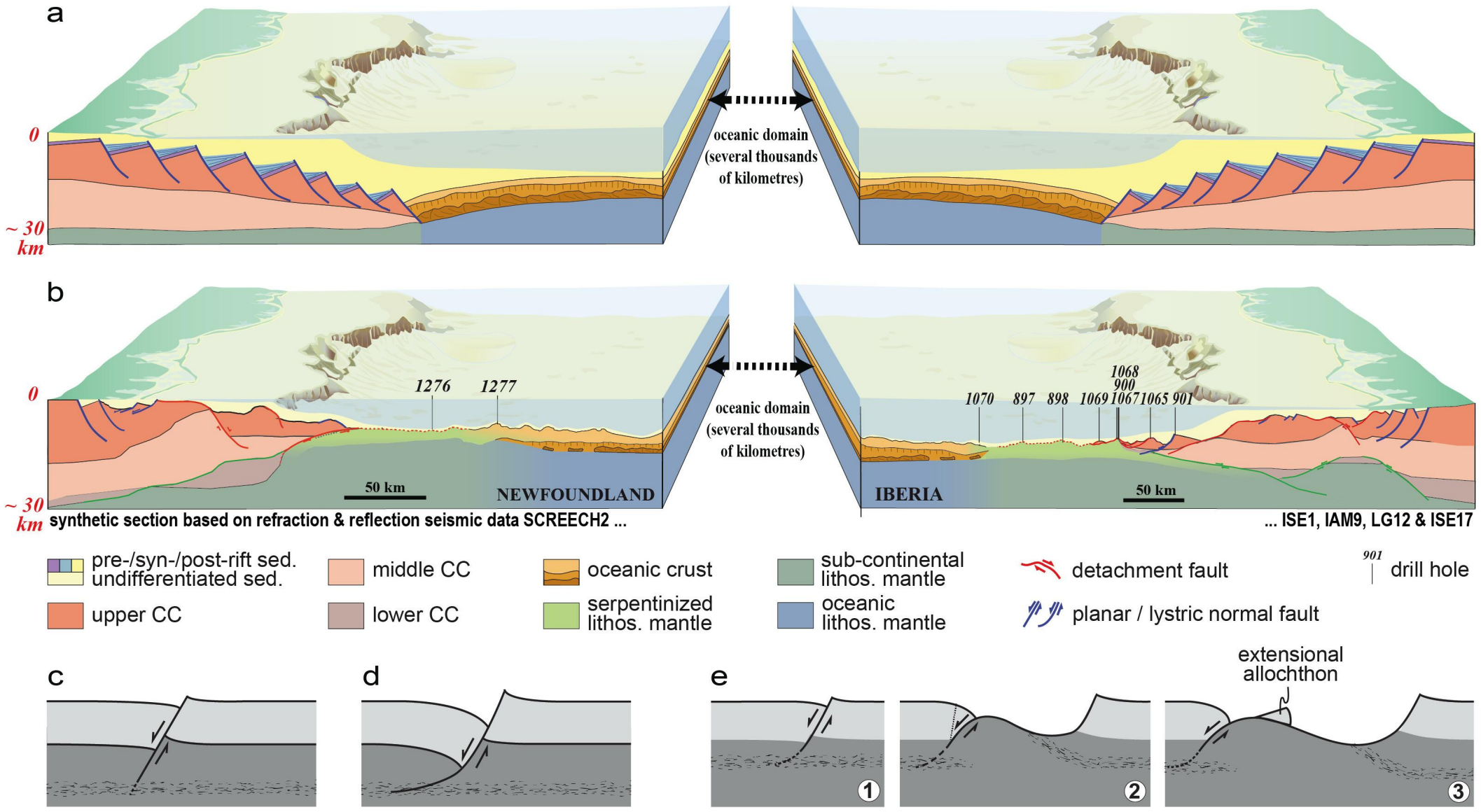

Fig. I.3 – a) Generic conceptual model for rifted margins and associated sedimentary fill as envisioned during the 1970-1980s; b) one of the most recent models proposed for the Iberian-Newfoundland conjugate rifted margins (modified from Péron-Pinvidic and Manatschal, 2009); c) planar and (d) listric normal faults dip typically at a relatively high angle of ca. 60°; e) extensional detachment faults initiate with a comparable dip as high-angle normal faults (ca. 60° - see panel 1) but exhume material at low angle (<15° - see panel 2). The activity of a detachment fault may form extensional allochthons and can explain the exhumation of deep-seated rocks to the seafloor (see panel 3). Abbreviations: CC: continental crust; lithos.: lithospheric; sed.: sediments.

https://doi.org/10.3301/GFT.2023.02

the Malenco serpentinites as syn-rift exhumed subcontinental mantle. And Florineth and Froitzheim (1994), Froitzheim and Manatschal (1996), and Whitmarsh et al. (2001) suggested that the play of extensional detachment faults could explain, on the one hand, the presence of subcontinental mantle at the seafloor offshore Iberia, and on the other hand the existence of allochthonous blocks of continental crust over exhumed mantle both in the former distal Adriatic margin of the Alpine Tethys and offshore Iberia (Fig.I.3e).
Later, Reston and McDermott (2011), Sauter et al. (2013) and Gillard et al. (2016a) advocated for the activity of successive in-sequence, out-of-sequence and/or flip-flop extensional detachment faults in the process of subcontinental mantle exhumation and highlighted the variability in morphology of detachment systems.

Unravelling rifting evolution: from a monophase to polyphase extension

Improvements in understanding rifting have been intimately tied to stratigraphic studies on rifted margins. Indeed, when the sedimentation rate is sufficiently high with respect to the rate of accommodation space creation, sediments (and magma) efficiently record the tectonic evolution.
The stratigraphic record of a margin can be split up into three sedimentary megasequences, namely a pre-, a syn- and a post-rift megasequence, deposited respectively prior to the onset of rifting, during rifting and after the termination of rifting (Hubbard, 1988). In the absence of pre-rift tectonic events, pre-rift deposits are essentially comprised of parallel strata (i.e., without growth structures; violet sediments in Figs. I.3a and I.4). Post-rift deposits are made of un-extended sedimentary packages that drape or onlap against pre-existing topography and offlap oceanward (green sediments in Fig. I.4g). The architecture of syn-rift deposits is more complex and has been the matter of much research and many debates (compare blue sediments in Figs. I.3a and I.4g).
Until the late 1980s, the “rigid domino fault block” model prevailed for interpreting rifted margins (Fig. I.3a). This conceptual model assumes that upper crustal blocks rotate rigidly with a diffuse accommodation zone at their base (Hardy, 1993). All faults and intervening tilted blocks are required to move and stop moving simultaneously, and thus, according to this model, the syn-rift megasequence must be synchronous across the entire margin. When the sedimentation rate is high enough, syn-rift deposits must all display a wedge-shape architecture that thickens toward the adjacent normal fault (blue sediments in Fig. I.3a). In this model, both the base and top of the syn-rift megasequence are ideally marked by an isochronous change in the strata dip across the entire margin, either between parallel pre-rift deposits and wedge-shape syn-rift deposits in the former case, or between wedge-shape syn-rift deposits and parallel post-rift deposits in the latter (Fig. I.3a).
From the 1990s to the early 2000s stratigraphic studies from both the Alps (Froitzheim et al., 1990) and the Iberia-Newfoundland margins (Murillas et al., 1990; Wilson et al., 2001) highlighted that the Alpine Tethys and southern North-Atlantic rifting were achieved via two main, distinct, and successive extensional phases. During the first, so-called low-β phase (where β corresponds to the ratio length prior to extension/length at the end of extension; McKenzie, 1978), numerous and broadly distributed half-graben basins bounded by high-angle normal faults formed over a wide region (Fig. I.4b), resulting in only minor crustal and lithospheric thinning ($1/\beta<1.5$). During the second, so-called

https://doi.org/10.3301/GFT.2023.02

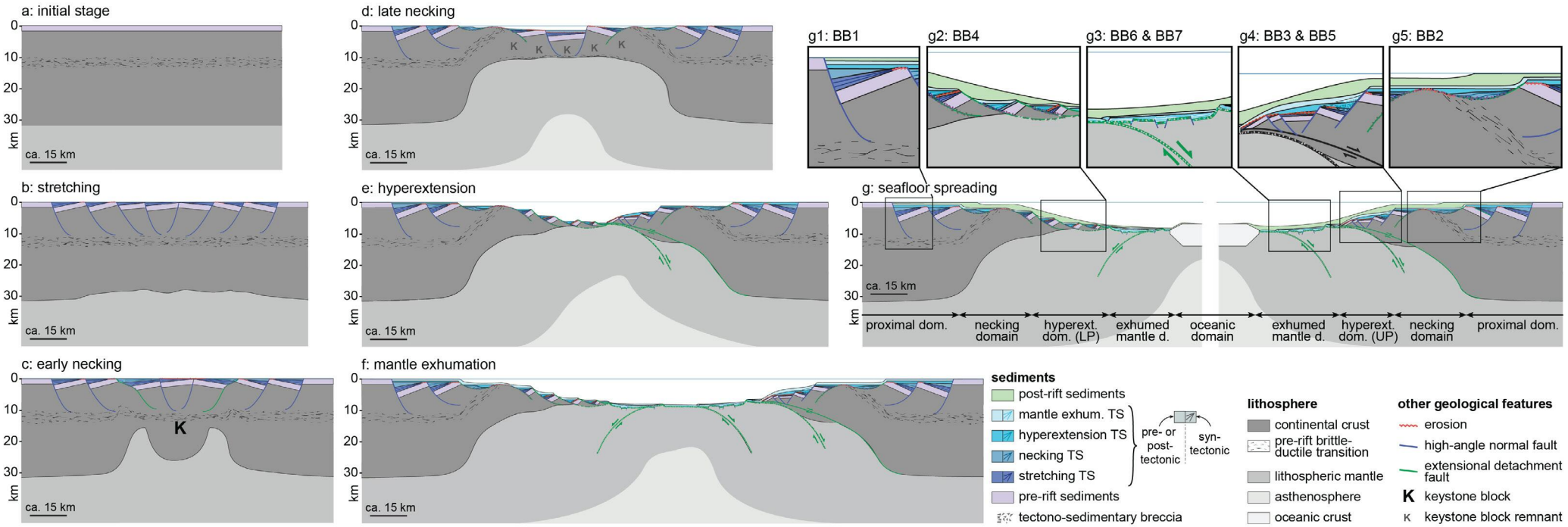

Fig. I.4 - Illustration of the polyphase rift model where the area of continental crust (dark grey) and the length of pre-rift sediments (violet) are preserved (modified from Chenin et al., 2022). a) Pre-rift stage; b) stretching phase (low-β phase): broadly distributed high-angle normal faulting rooting in the brittle-ductile transition; c) early necking phase (onset of the high-β phase): individualization of the keystone block; d) late necking phase: basement exhumation via extensional detachment faults and onset of keystone thinning/disintegration; e) hyperextension phase: onset of asymmetric deformation with the individualization of an upper-plate- (right-hand side) and a lower-plate (left-hand side) margin; f) mantle exhumation phase achieved via flip-flop extensional detachment faulting; g) onset of seafloor spreading; g1-g5: close-up on the stratigraphic architecture in the different rift domains of the passive margins. Abbreviations: d. and dom.: domain; LP: Lower Plate; TS: Tectonic Sequence; UP: Upper Plate. BB1–BB7 refer to the margin Building Blocks defined in section 4.

high-β phase, tectonic activity was localized in the future distal margins only (Figs. I.4b-I.4f) and significant crustal thinning (1/β>1.5) was achieved via both normal and detachment faulting, and via the attenuation of ductile middle- and/or lower crustal layers (Manatschal et al., 2001).

In the mid-2000s, Lavier and Manatschal (2006) suggested that rifting was achieved via successive and distinct deformation modes. In their numerical models, deformation evolves from initially distributed extension with limited crustal and lithospheric thinning (the so-called stretching phase; Fig. I.4b) to increasingly localized deformation with significant crustal and lithospheric thinning (the so-called thinning phase; Figs.I.4c-I.4e) and (mantle) exhumation phases (Fig. I.4f). A few years later, the thinning phase was subdivided into a necking phase (Chenin et al., 2018a; Ribes et al., 2020; Figs. I.4c and I.4d) and a hyperextension phase (Epin and Manatschal, 2018; Nirrengarten

https://doi.org/10.3301/GFT.2023.02

et al., 2016; Fig. I.4e). Here we name polyphase rifting the succession of the stretching, necking, hyperextension, and mantle exhumation deformation modes that is thought to consistently rule magma-poor rifting (Chenin et al., 2022).
Recent field observations from the Alps (Ribes et al., 2019a), seismic interpretation at the South China Sea (Chao et al., 2021; Luo et al., 2021), and numerical models (Pérez-Gussinyé et al., 2020) suggest that the different deformation modes play sequentially (one after the other) and affect successively ever narrower regions. This implies that at the shift between two deformation modes, extension stops (and thus passive infill sedimentation starts) in some regions, while rifting continues in others (cf. sections 2.2.1, 5.2, and 5.3).

https://doi.org/10.3301/GFT.2023.02

STATE OF THE ART ON MAGMA-POOR RIFTED MARGINS AND RIFTING PROCESSES

Margin architecture: rift domains and related deformation modes

Definition of rift domains

Based on the dip angle of the top basement and Moho, which are usually the two most consensual interfaces recognized on seismic sections (red lines in Fig. I.5a), Sutra et al. (2013) identified four systematic rift domains. From the continent toward the ocean, these domains are:

- the proximal domain where the top basement and Moho are sub-horizontal and parallel and where the crust is only a little thinned (30±5 km);
- the necking domain where the crust is thinned from 30±5 km to ca. 10 km;
- the hyperextended domain where the crust is thinned from ca. 10 km to 0 km. Compared with the necking domain, the angle of the aperture between the top basement and Moho is lower and more consistent in the hyperextended domain (Sutra and Manatschal, 2012; Nirrengarten et al., 2016; Fig. I.5a);
- the exhumed mantle domain where the subcontinental lithospheric mantle is exhumed to the seafloor.

Based on a worldwide compilation of seismic sections, Chenin et al. (2017) proposed that each domain displays a typical range of width, namely: necking domains range between ca. 10 and 100 km with an average of 55 km; hyperextended domains between ca. 20 and 70 km with an average of 50 km; and exhumed mantle domains between 20 and 110 km with an average of 60 km (Fig. I.5b). They also highlighted the lack of correlation between the width of the different domains for a given margin (Fig. I.5c).

Linking rift domains to lithologies, rheologies, and deformation processes

The variability in the angle of the aperture between the top basement and Moho among the different domains of rifted margins (red lines in Fig. I.5a) is interpreted to reflect changes in the rheology and/or in the composition of the continental crust and underlying mantle (Sutra and Manatschal, 2012; Nirrengarten et al., 2016; Chenin et al., 2017; Figs. I.5d and I.5e). Recently, Chenin et al. (2022) proposed that each domain is linked to a specific deformation mode at play during rifting (Fig. I.5f).

In the proximal domain, crustal thinning is minor and broadly distributed. It is accommodated by the formation of numerous and broadly distributed half-graben basins in the brittle upper crust and by ductile deformation within the middle- to lower crust (i.e., decoupled deformation). The proximal domain is associated with the stretching phase of Lavier and Manatschal (2006). Its tectono-thermal evolution is essentially ruled by the pure-shear/depth-uniform thinning model of McKenzie (1978). In the proximal domain, neither the composition of

https://doi.org/10.3301/GFT.2023.02

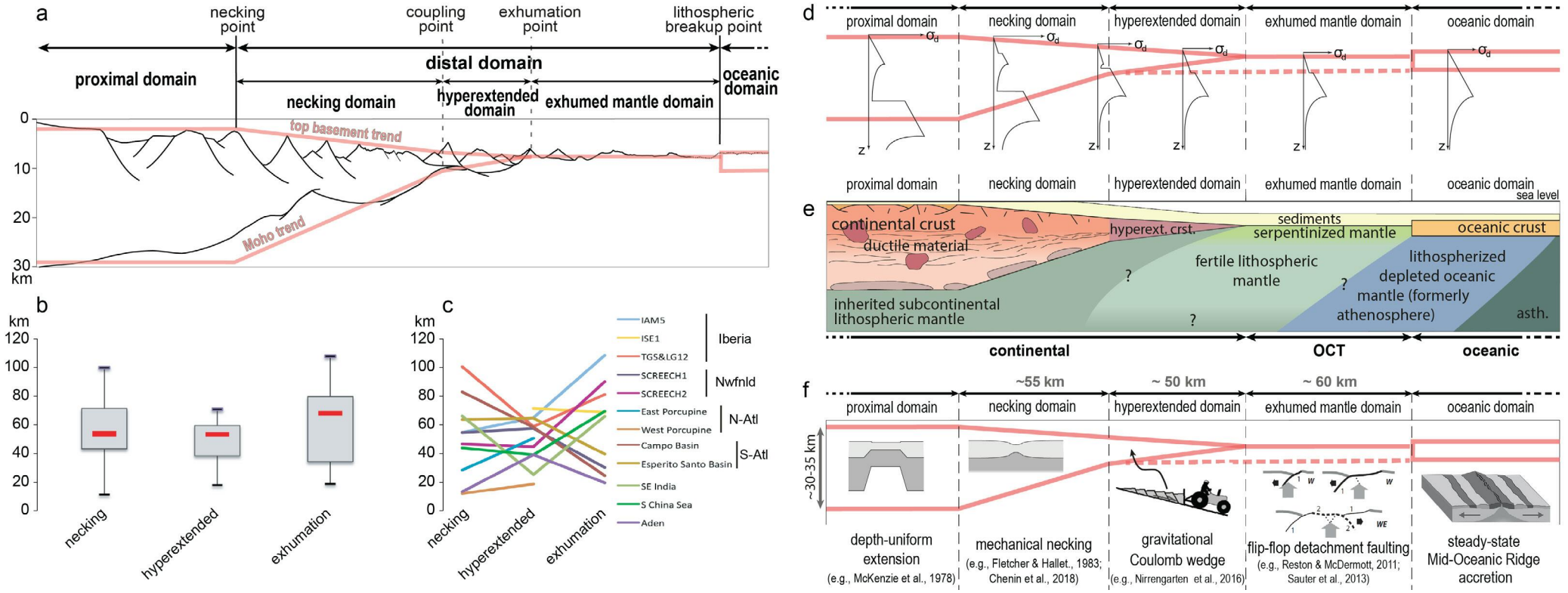

Fig. I.5 – a) Schematic cross-section highlighting the primary morphology of a "magma-poor" rifted margin and its relationship with the different rift domains (from Chenin et al., 2017); b) width of the different distal domains (necking, hyperextended and exhumation (from Chenin et al., 2017); c) width relationships among the different distal domains (from Chenin et al., 2017); d) schematic cross-section displaying the first-order rheological profile associated with each rift domain; e) schematic cross-section showing the first-order lithological architecture of a rifted margin (modified from Chenin et al., 2017); f) schematic cross-section displaying the dominant deformation mechanism associated with each domain (Chenin et al., 2022). Abbreviations: Atl: Atlantic; asth.: asthenosphere; hyperext. crst.: hyperextended crust; Nwfnld: Newfoundland.

the crust, nor that of the mantle is significantly modified, and thus their lithology is comparable to that of the pre-rift (or adjacent non-rifted) lithosphere (Chenin et al., 2017; Fig. I.5e).

In the necking domain, the convergence between the top basement and Moho is interpreted to reflect the progressive removal of ductile layers (Pérez-Gussinyé et al., 2003; Sutra et al., 2013). Significant crustal thinning is achieved via detachment faulting (Mohn et al., 2012; Osmundsen et al., 2018; Ribes et al., 2020), which is interpreted to result from viscoplastic necking of the lithosphere (Chenin et al., 2018a). Compared with the early stretching phase, the necking phase is characterized by a focalization of the deformation into a narrower region (ca. 20-100 km) according to the analytical study by Fletcher and Hallet (1983), the seismic observations by Chenin et al. (2017), and the numerical models by Chenin et al. (2018a). In the necking domain, neither the composition of the crust, nor that of the mantle is significantly

https://doi.org/10.3301/GFT.2023.02

modified, and thus their lithology can also be approximated by that of the pre-rift (or adjacent non-rifted) lithosphere (Chenin et al., 2017; Fig. I.5e).

In the hyperextended domain, there are no decoupling ductile layers left in the crust, and thus faults cut through it and propagate down into the upper mantle (i.e., coupled deformation). The relatively uniform dip angle between the top basement and Moho among margins is interpreted to express the frictional thinning of a fully brittle continental crust over a weak serpentinized mantle, which was recognized to follow the extensional Coulomb's Wedge Theory (Nirrengarten et al., 2016). Field observations show that crustal thinning is achieved via in-sequence detachment faulting that progresses oceanward (Epin et al., 2018). In the hyperextended domain, the continental crust is highly fractured, and efficient fluid circulation occurs along faults, forming convection cells (e.g., Manatschal, 1999; Pinto et al., 2015; Incerpi et al., 2018; see also the Fluids thematic sheet). At the same time, the asthenosphere rise generated by lithosphere thinning results in its partial melting. The produced melts migrate upwards and (re)fertilize the inherited subcontinental lithospheric mantle (i.e., Mantle type 2 in Picazo et al., 2016; Fig. I.5e; see also the Petrology thematic sheet).

The exhumed mantle domain corresponds to the domain where the subcontinental lithospheric mantle is exhumed to the seafloor (top basement = Moho; Fig. I.5a). The mantle exhumation phase is controlled by the play of successive, either in- or out-of-sequence detachment faults (e.g., Reston and McDermott, 2011; Sauter et al., 2013; Gillard et al., 2016a; Fig. I.5f). On seismic sections in depth, the exhumed mantle domain is characterized by a relatively corrugated top basement, which results from extensive normal faulting of the detachment surface (e.g., Gillard et al., 2016b). The top 6 km of the basement is comprised of a decreasingly serpentinized mantle (Gillard et al., 2019). The underlying mantle is infiltrated/(re)fertilized (i.e., Mantle type 2 in Picazo et al., 2016; Fig. I.5e) and displays an increasing number of intrusive magmatic bodies oceanward (Gillard et al., 2019). The oceanic domain is characterized by homogeneous, 5-7 km-thick Penrose-type oceanic crust underlain by depleted oceanic mantle, or by asthenospheric mantle at the mid-oceanic ridge (Fig. I.5e). On seismic sections, the top basement and Moho are largely flat and parallel (Fig. I.5a). At present, no evidence for such a mature oceanic domain could be found in the former Alpine Tethys rift system (Picazo et al., 2016).

The stratigraphic record of rifting

Definition of Tectonic Sequences and notions of pre-, syn- and post-tectonic

Considering that each rift domain (proximal, necking, hyperextended, and exhumed mantle domain) is dominantly controlled by one specific deformation mode (pure shear, viscoplastic necking, frictional thinning, and flip-flop detachment faulting, respectively), and assuming that these deformation modes are active during distinct periods of time (see previous section), Ribes et al. (2019a) defined four system tracts, namely the stretching, necking, hyperextension, and mantle exhumation system tract. Here we follow Chenin et al. (2022) in referring to these as Tectonic Sequences.

https://doi.org/10.3301/GFT.2023.02

A Tectonic Sequence (TS) encompasses all the sediments deposited during the period of activity of the corresponding deformation mode (see the Tectono-stratigraphy thematic sheet).

The recognition of passive infill deposits emplaced during rifting in the proximal domain of the Alpine Tethys margins led Masini et al. (2013) to redefine the term syn-rift. They suggested restricting the use of syn-rift to its temporal dimension with respect to the overall rifting event and using the terms pre-, syn- and post-tectonic to characterize the architecture of sedimentary deposits with respect to the local tectonic activity (Figs. I.6a-I.6d). In this perspective, pre-rift sediments are necessarily pre-tectonic and post-rift sediments are necessarily post-tectonic. However, syn-rift sediments may be either pre-, syn- or post-tectonic (Fig. I.6e).

In the absence of pre-rift tectonic events and inherited topography, pre-tectonic sediments display horizontal and parallel strata of a constant thickness (Fig. I.6a). Syn-tectonic sediments are usually wedge-shaped, but their architecture varies depending on the type of fault they are associated with. We name them half-graben wedge-shaped when associated with the play of a high-angle normal fault (Fig. I.6b) and supra-detachment wedge-shaped when related to an extensional detachment fault (Fig. I.6c). Note that supra-detachment wedge-shaped sediments may be hard to distinguish from pre- and post-tectonic deposits because the wedge morphology may be little expressed, especially when sedimentation rate is low compared to the extension rate along the fault (Fig. I.6f). However, extensional detachment faults are generally associated with cataclastic breccias and black gouges (Chester et al., 1986; Manatschal et al., 2000) and the surface of an exhumed

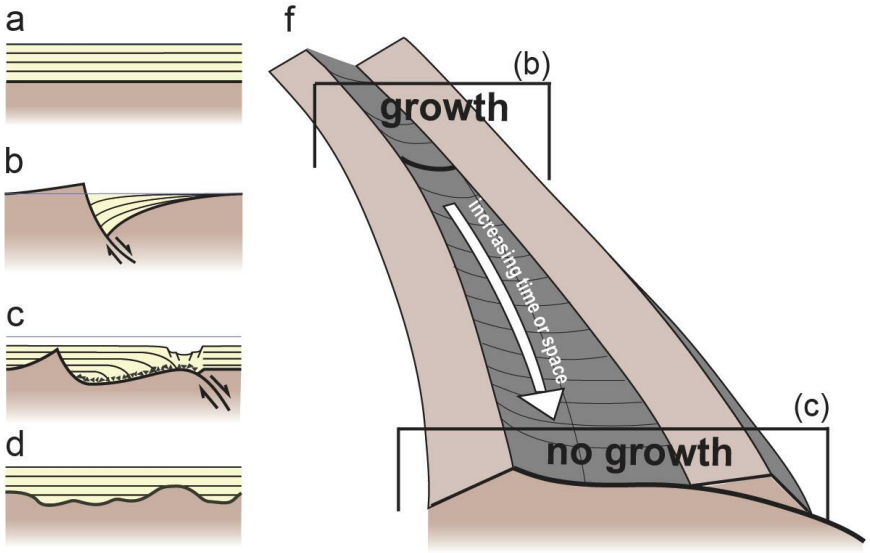

e

sediment architecture	timing with respect to rifting: pre-rift	syn-rift	post-rift
pre-tectonic	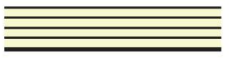	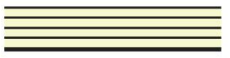	
syn-tectonic		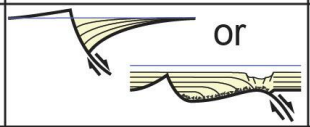	
post-tectonic			

Fig. I.6 (modified from Chenin et al. 2022) – a-d) Stratigraphic architecture of sedimentary deposits (a) pre-tectonic; (b) syn-tectonic normal fault-related; (c) syn-tectonic detachment fault-related; and (d) post-tectonic; e) table synthetizing the time-sediment architecture relationships during the different rift megasequences; f) cartoon displaying the evolution from a high-angle normal fault into a long-offset detachment fault when the amount of exhumed basement increases.

https://doi.org/10.3301/GFT.2023.02

detachment is typically overlain with tectono-sedimentary breccias (Collettini, 2011; Masini et al., 2011; Fig. I.6c). Post-tectonic deposits are either made of horizontal strata onlapping against/draping residual rift-related topography, or of strata offlapping/downlapping onto exhumed basement or oceanic crust (Fig. I.6d). In the absence of rift-related topography or syn-tectonic deposits between them, pre- and post-tectonic deposits are practically indistinguishable.

The Wheeler diagram of an ideal magma-poor rifting event

The Wheeler diagram is a powerful graphic representation of the tectono-stratigraphic evolution of a geological system through both space and time. Fig. I.7 synthesizes into Wheeler diagrams the major paradigm shifts achieved between the tectono-stratigraphic model of the 20th century ("tilted block rift model"; Fig. I.7a) and the "polyphase rift model" currently admitted/in progress (Fig. I.7b; for details see the Tectono-Stratigraphy thematic sheet).

The most important changes in the polyphase tectono-stratigraphic model compared to the tilted block model arises from (1) the consideration of new real estate creation owing to basement exhumation via extensional detachment faults, and (2) the recognition that rifting is a localizing extensional process during which the size and/or location of the actively deforming region varies with time. This model will be illustrated with the example of the Alpine Tethys rifting in section 5.2.

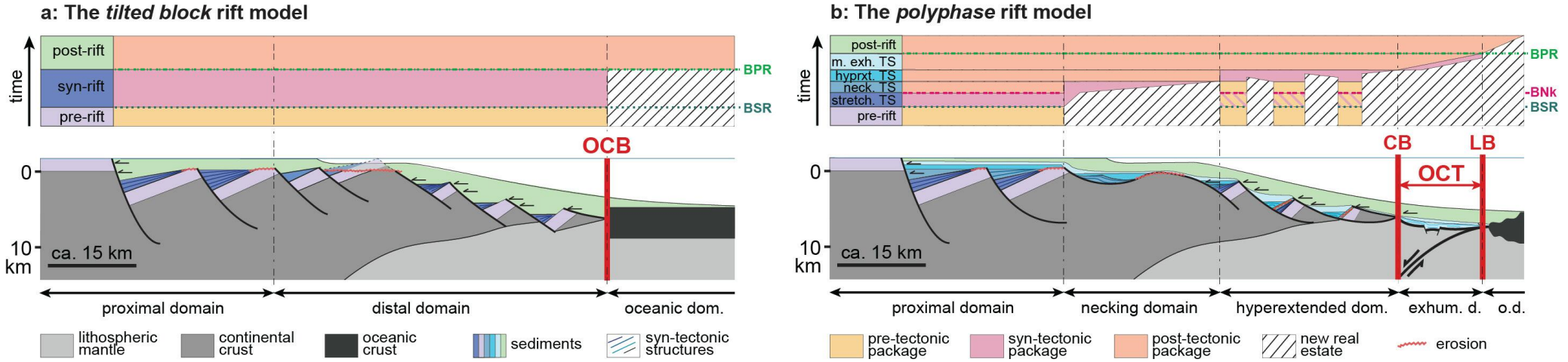

Fig. I.7 (modified from Chenin et al., 2022) - Schematic view of a rifted margin and corresponding Wheeler diagram according to (a) a "tilted block" tectono-stratigraphic model; (b) a "polyphase" tectono-stratigraphic model. Abbreviations: BPR: Base of the Post-Rift megasequence; BNk: Base of the Necking Tectonic Sequence; BSR: Base of the Syn-Rift megasequence; CB: Continental Breakup; dom.: domain; exhum. d.: exhumed mantle domain; hyprxt. TS: hyperextension Tectonic Sequence; LB: Lithospheric Breakup; m. exh. TS: mantle exhumation Tectonic Sequence; neck. TS: necking Tectonic Sequence; o.d.: oceanic domain; OCB: Ocean-Continent Boundary; OCT: Ocean-Continent Transition; stretch. TS: stretching Tectonic Sequence; TS: Tectonic Sequence.

https://doi.org/10.3301/GFT.2023.02

PALEOGEOGRAPHIC FRAMEWORK AND TECTONIC EVOLUTION OF THE ALPINE TETHYS REALM

The Alpine Tethys realm: a large-scale perspective

The late Palaeozoic paleogeographic evolution was dominated by the agglomeration of the Pangea supercontinent (Fig. I.8a), which was manifested in Western Europe by the Variscan orogeny (Fig. I.8b). Rifting of the Alpine Tethys took place in the framework of the subsequent world-wide rifting event that led to the fragmentation of Pangea from latest Triassic onward (e.g., Müller et al., 2016).
In the future North Atlantic and western Mediterranean regions, the latest Triassic to Early Cretaceous rifting seeded largely around the core of the Variscan orogen (Chenin et al., 2015; Chenin et al., 2019a). During the Late Jurassic, the resulting oceanic basins were part of an equatorial spreading system that extended from the Caribbean to the western Mediterranean region via the Central Atlantic Ocean, continued eastward between the Iberian and African plates into the Alpine Tethys rift system and beyond into the Paleo- and/or Neo-Tethys Ocean(s) (Fig. I.8c).
The tectonic evolution of the Alpine Tethys rift system was controlled by the movements of three major tectonic plates (the North American, African, and Eurasian plates), and two smaller plates (the Iberian and Adriatic plates, e.g., Hosseinpour et al., 2016). While the movements of the major plates are reasonably well constrained, that of the smaller plates is still a matter of debate (Frasca et al., 2021; Le Breton et al., 2017; Schmid et al., 2017). Basically, the opening of the Alpine Tethys in the Early Jurassic separated the Eurasian/Iberian plates from the Adriatic/African plates.

Paleogeographic evolution of the Alpine Tethys realm

Three main successive rifting phases can be distinguished in the Alpine Tethys region:

- the first episode of rifting took place during the Middle- to Late Triassic and led to seafloor spreading in the Meliata-Vardar domain, east of the Adriatic plate. This rifting event is documented and dated by magmatic intrusions and sedimentary deposits (e.g., Anders et al., 2007). It was contemporaneous with rifting of the future Central Atlantic Ocean. The relationships between the Meliata-Vardar domain and the Paleo- and/or Neo-Tethys Ocean(s) to the east remain, however, poorly constrained.
- Subsequently, rifting of the Alpine Tethys started west of the future Adriatic plate with the opening of the Liguria, Piemonte, and Valais branches during the Early Jurassic (ca. 185 Ma; Galster et al., 2012; Manatschal et al., 2006). The age of this second rifting event is documented, among others, by cooling ages of middle- to lower crustal rocks (e.g., Mohn et al., 2012) and by sedimentary deposits (e.g., Masson et al., 2008; Ribes et al., 2019a). No evidence of a steady-state seafloor spreading is recorded in the ophiolites of any branch of the Alpine rift system (Picazo et al., 2016).

https://doi.org/10.3301/GFT.2023.02

- The third rifting event recorded in the peri-Tethyan region corresponds to the opening of the future North Atlantic Ocean and Bay of Biscay during the Late Jurassic to Early Cretaceous (Nirrengarten et al., 2018). Seafloor spreading initiated during the late Early Cretaceous in the North Atlantic segment (late Aptian-early Albian; Tucholke et al., 2007) and in the Bay of Biscay (earliest Albian; Montadert et al., 1979; Thinon et al., 2003).

The details of the Alpine Tethys region paleogeography remain a matter of much controversy and debate. The main problems arise from (1) the lack of magnetic anomalies from the former Alpine Tethys "Ocean"; (2) the identification and restoration of hyperextended domains; and (3) the recognition of strike-slip and intracontinental movements.

Today's challenges in the paleogeographic reconstruction of the Alpine Tethys include, among others: (1) determining the oceanic

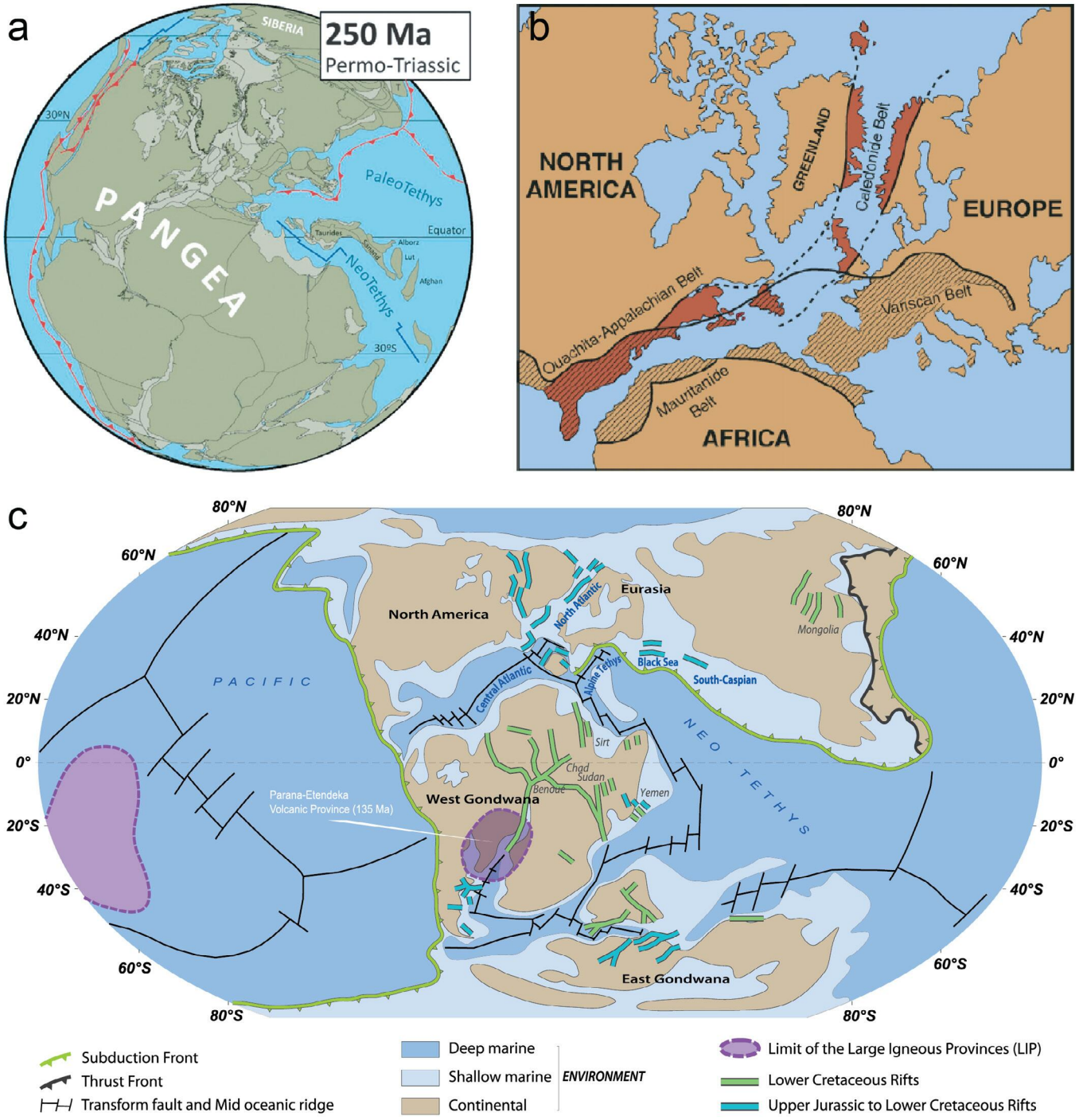

Fig. I.8 – a) Worldwide paleogeographic reconstruction at ca. 250 Ma (Permo-Triassic) by Torsvik et al. (2012); b) Palaeozoic orogenic belts in Europe, North America and Africa in latest Palaeozoic (modified from Nance et al., 2010); c) worldwide paleogeographic reconstruction at ca. 120 Ma by Frizon de Lamotte et al. (2015).

https://doi.org/10.3301/GFT.2023.02

versus non-oceanic nature of the rift basins; (2) assessing the movements of the Iberian and Eurasian plates; (3) recognizing the former conjugate margins and determining the importance of rift-related segmentation in the Alpine Tethys rift system; and (4) integrating realistic margin architectures in (deformable) plate reconstructions.

Alpine tectonic evolution

By and large, the Alps are the product of the convergence between the Eurasian and African plates and their interference with the smaller Iberia and Adriatic plates. The Alpine orogen was essentially constructed through three successive, but not coaxial, phases of convergence, namely the Eoalpine, Mesoalpine, and Neoalpine orogenic phases (Fig. I.9; Hunziker et al., 1992; see also the Tectono-Structural thematic sheet).

i) The Eoalpine orogenic phase (Figs.I.9a and I.9d). From the Late Jurassic to the Late Cretaceous, NNE-directed closure of the Meliata-Vardar domain led to the construction of a strike-slip dominated thrust wedge that propagated from the north-eastern margin of Adria towards the WNW (Kley et al., 2008). During this event, the proximal margin, distal margin, and OCT of north-western Adria (i.e., the Adriatic margin that faced the Piemonte branch of the Alpine Tethys) were telescoped into a number of thrust sheets, so-called Eoalpine Austroalpine and Upper Penninic thrust complexes, which are today exposed in the Eastern and Central Alps (Froitzheim et al., 1994, 1996; Schmid et al., 2004). The geological record of this orogenic event is essentially limited to the former northern Adriatic margin.

ii) The Mesoalpine orogenic phase (Figs. I.9b and I.9d). At ca. 84 Ma (Late Cretaceous), the NNE-directed movement of the African plate relative to Europe rotated counterclockwise to an NNW-directed contraction (Kley et al., 2008), which led to the subduction of parts of the Alpine Tethys beneath the Adriatic plate. This event resulted in the telescoping of the European passive margin, and eventually in the emplacement of the Eoalpine Austroalpine and Penninic thrust complexes as an orogenic lid over the European shelf (Helvetic units; e.g., Pfiffner et al., 2002; Schmid et al., 1996).

Eocene subduction-related metamorphism affected parts of the Piemonte-Liguria and Valais basins, and later the most distal parts of the European margin. In contrast, shallow crustal levels of the European margin were scraped off and accumulated in crystalline basement units and sedimentary décollement nappes (Pfiffner et al., 1997). Thrust sheets derived from the Adriatic margin and OCT were always in the hanging wall of the subducting European plate during the Mesoalpine phase, therefore they escaped subduction, and hence high-pressure metamorphism.

In the Grisons region, the Cenozoic continental collision between the Adriatic margin and the Briançonnais unit-European margin affected only the northern parts of the former distal Adriatic margin and OCT. In contrast, the rear of the margin was only weakly reactivated. The Late Cretaceous nappe stack was thrust more or less “en bloc” to the north, over the Briançonnais and Valais units (i.e., the Middle- and North Penninic units, respectively). In the South Alpine domain, a southward propagating thrust wedge affected the southern Adriatic domain, whose southwestern part had escaped the previous Eoalpine orogeny (Doglioni et al., 1987; Schumacher et al., 1997; Zanchetta et al., 2015).

https://doi.org/10.3301/GFT.2023.02

iii) The Neoalpine orogenic phase (Fig. I.9c). From late Eocene onward (ca. 35 Ma), a substantial shift from essentially N-directed to WNW-directed shortening occurred at the scale of the entire Alpine orogen (Handy et al., 2010). This shift was linked to the anticlockwise rotation of the Adriatic indenter following the kinematic reorganization of the Alpine orogenic system (transition from the collision in the Mesoalpine system to subduction in the Eastern Mediterranean). This final phase is largely responsible for the arcuate shape of the Alpine orogen. It also formed most of the relief of the Western Alps along the Franco-Italian boundary. The kinematic reorganization was accompanied by substantial magmatic activity (e.g., Periadriatic plutons emplacement between 33 and 31 Ma), a drastic increase in the sedimentary budget (e.g., overfill of the eastern and western foreland basins) and the onset of dextral strike-slip movements in the Periadriatic system. These events are usually regarded as linked to the onset of slab breakoff beneath the Central Alps (von Blanckenburg and Davies, 1995; see also Ji et al., 2019, for an alternative interpretation).

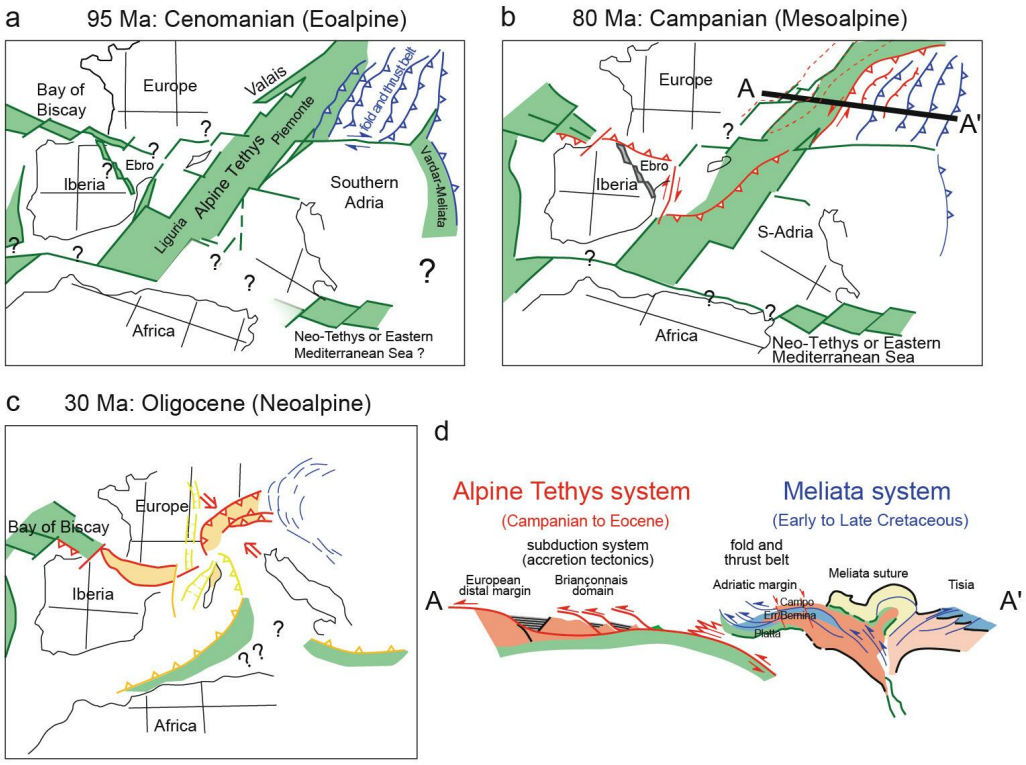

Fig. I.9 (modified from Mohn et al., 2011) - Paleogeographic evolution in the Alpine Tethys region during (a) the Early- to Late Cretaceous closure of the Meliata-Vardar domain; (b) the Late Cretaceous-late Eocene closure of the Alpine Tethys rift system; (c) the Oligocene-Miocene subduction in the Eastern Mediterranean; d) schematic cross-section through North-Adria and the east European margin (see panel b for location) showing the first-order nappe stack during the Campanian (Mesoalpine orogeny).

https://doi.org/10.3301/GFT.2023.02

RECONSTRUCTING THE FORMER ALPINE TETHYS RIFTED MARGINS

The Alpine Tethys margins have been partly accreted and subducted during the Cretaceous and Cenozoic Alpine compressional events (see previous section). Thus, only remnants of the former margins are now embedded in the Alpine nappe stack. The restoration of the Alpine Tethys margins relies on our capacity to (1) identify such remnants, and (2) put them back into a pre-Alpine rift system template.
Until the late 2010s, the restoration of the Alpine Tethys margin was based on the identification of Alpine paleogeographic domains and geological units, which relied on: (i) their tectonic position within the orogenic nappe stack; (ii) the facies and stratigraphic successions observed in their pre-, syn- and post-rift sedimentary cover; and to a lesser degree (iii) the nature of their basement (i.e., pre-rift upper-, middle- or lower continental crust, exhumed mantle or oceanic crust). Recently, Manatschal et al. (2022) proposed an approach relying on the identification of Building Blocks (BBs) characteristic of specific rift domains and their restoration into a generic magma-poor rifted margin template.
In the following, we first briefly introduce the main Alpine paleogeographic domains and relate them to the former Alpine Tethys rift system. Second, we summarize the characteristics of the seven different types of BBs identified in the Alps. Third, we describe how transects across the former Alpine Tethys were reconstructed and paleogeographic maps were drawn.

Main Alpine paleogeographic domains

The Alps can be subdivided into three main paleogeographic domains, namely the Helvetic/Dauphiné, Penninic, and Austroalpine/South Alpine units. These correspond respectively to the proximal European margin, the distal European margin and OCT(s)/proto-oceanic domain(s), and the Adriatic margin. Each of these domains is comprised of several nappes and units (Figs. I.0c and I.0d).

The Helvetic/Dauphiné domain - The proximal European margin

The Helvetic/Dauphiné domain corresponds to the light-blue domain in Figs. I.0a, I.0c, and I.0d. It represents the proximal part of the European margin. The Dauphiné domain in the Western Alps is the equivalent of the Helvetic domain in the Swiss Alps.
The basement of the Helvetic/Dauphiné domain is made of polymetamorphic Variscan rocks and in some places Permian sedimentary basins that formed during the post-orogenic collapse of the Variscan range. These are overlain with pre-rift Permo-Triassic sub-aerial and shallow-marine sedimentary rocks (essentially sandstones, dolostones, and evaporites; 1 in Fig. I.10a). The Variscan basement crops out at the so-called External Massifs (i.e., the Argentera, Pelvoux, Belledonne, Mont Blanc, Aiguilles Rouges, Aar, and Gotthard massifs; Fig. I.0a).
The limit between the northern external part of the Alpine orogen (i.e., the Helvetic/Dauphiné domain) and the internal part (i.e., the Penninic domain - see next paragraph) is a major thrust fault named the Penninic Front (P.F. in Figs. I.0a and I.0c).

https://doi.org/10.3301/GFT.2023.02

The Penninic domain - The distal European margin and Alpine Tethys proto-oceanic domains

The Penninic domain comprises ophiolitic and continental remnants derived from the distal European margin (dark-blue domain in Figs. I.0a, I.0c, and I.0d) and proto-oceanic parts of the Alpine Tethys, namely the Valais domain (olive-green domain) and the Ligurian and Piemonte domains (dark-green domain).
Remnants from the distal European margin are comprised of polymetamorphic Variscan basement rocks intruded and/or underplated by magmatic bodies (Fig. I.10b). Some of the Penninic nappes locally carry relics of Permo-Triassic sediments.
Remnants from the Valais Basin comprise serpentinized subcontinental mantle, metabasalts, and metagabbros, as well as calcschists that represent their former sedimentary cover (Fig. I.10a).
Remnants from the Liguria-Piemonte domain display relics of serpentinized subcontinental mantle covered with deep-water sediments (Fig. I.10a5) but no evidence for a depleted oceanic mantle indicative of a mature oceanic spreading system (Picazo et al., 2016; Petrology thematic sheet).
In the Western Alps, nappes comprised of shallow-water pre- and syn-rift sediments and pelagic deep-water post-rift sediments can be found in-between the nappes sampling the former Valais and Liguria-Piemonte domains. These relationships suggest the existence of a ribbon of continental crust between the Valais and Liguria-Piemonte basins (Figs. I.0b and I.0d). This ribbon of unknown thickness and lateral extent is referred to as the Briançonnais domain.

The Austroalpine/South Alpine domain - The Adriatic margin

The Austroalpine/South Alpine domain comprises remnants from the former Adriatic margin. At present, the Austroalpine unit is separated from the South Alpine unit by the Insubric Line (Schmid et al., 1987), which represents both a major orogenic structure and a former transfer zone between the former Northern- and Southern Adria (Fig. I.0b). Although Northern- and Southern Adria were never separated by an ocean, these two domains display different tectonic histories. In contrast to the Austroalpine domain (N-Adria) where nappe stacking occurred during the Late Cretaceous in the framework of the NNW-SSE Eoalpine contractional event, the South Alpine domain (S-Adria) recorded essentially N-S convergence (i.e., perpendicular to the margin dip) during the Cenozoic Meso- and Neoalpine events. In this field guide, we only discuss the Austroalpine domain.
The Austroalpine domain can be subdivided into a Lower- Middle- and Upper Austroalpine nappe system (Figs. I.0a, I.0c, and I.0d; Mohn et al., 2011):

- the Lower Austroalpine Nappe (dark-brown domain in Figs. I.0a, I.0c, and I.0d) sample the hyperextended domain of the former north-western Adriatic margin. Remnants of the hyperextended domain include essentially fragments of upper continental crust capped by low-angle extensional detachment fault systems (Manatschal and Nievergelt, 1997; Epin and Manatschal, 2018). Extensional detachment faults are overlain with allochthons of the upper crust and/or pre-rift sediments, as well as with deep-water syn- to post-tectonic sedimentary deposits (Fig. I.10a).

https://doi.org/10.3301/GFT.2023.02

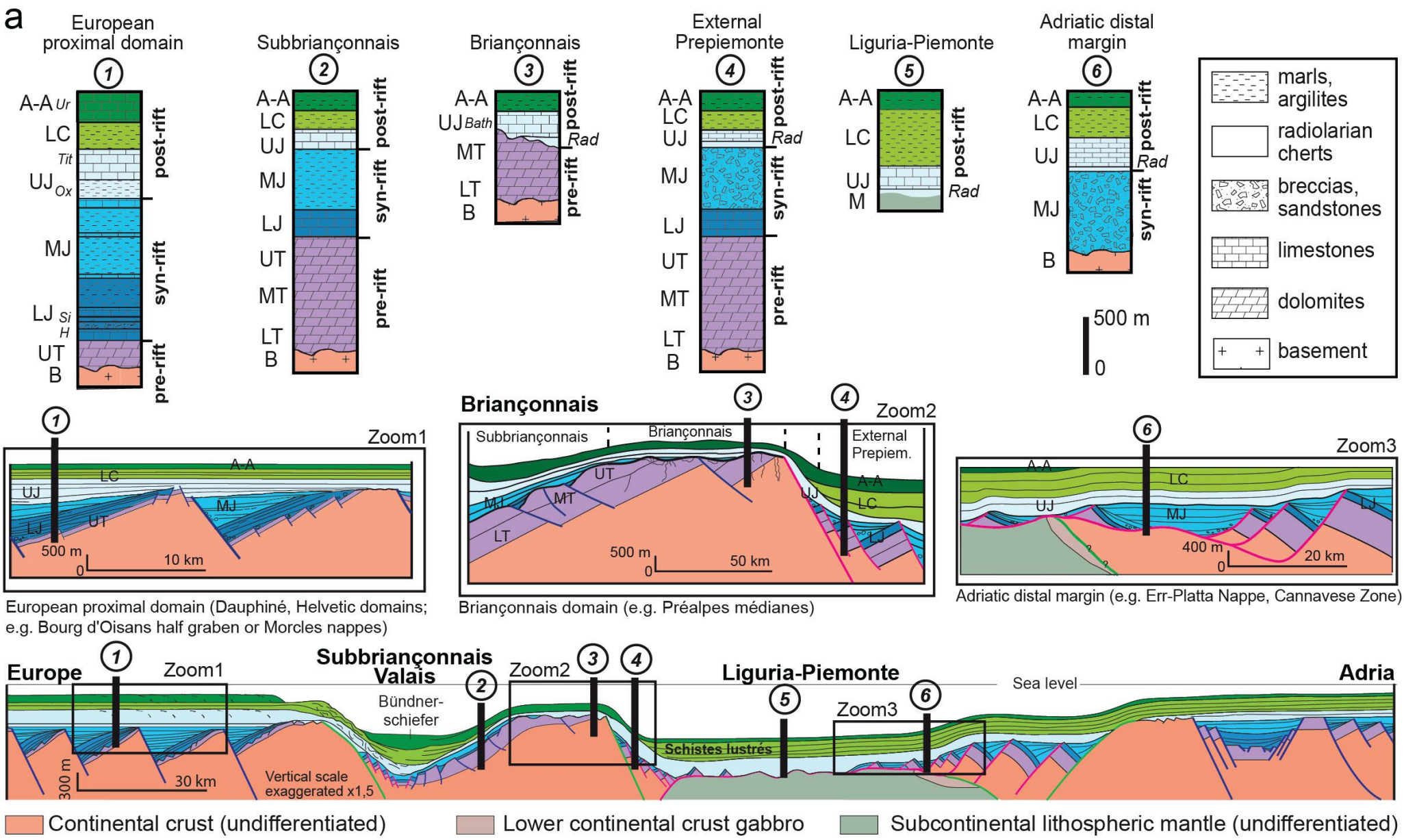

Fig. I.10 - a) Stratigraphic log of the different Alpine units and reconstruction of a synthetic cross-section through the former Alpine Tethys rift system. A-A: Aptian-Albian; LC: Lower Cretaceous; UJ: Upper Jurassic; MJ: Middle Jurassic; LJ: Lower Jurassic; UT: Upper Triassic; MT: Middle Triassic; LT: Lower Triassic; B: basement; M: mantle; Ur: Urgonian; Tit: Tithonian; Ox: Oxfordian; Bath: Bathonian ; Si: Sinemurian; H: Hettangian; Rad: radiolarian cherts (modified from Mohn et al., 2010).

https://doi.org/10.3301/GFT.2023.02

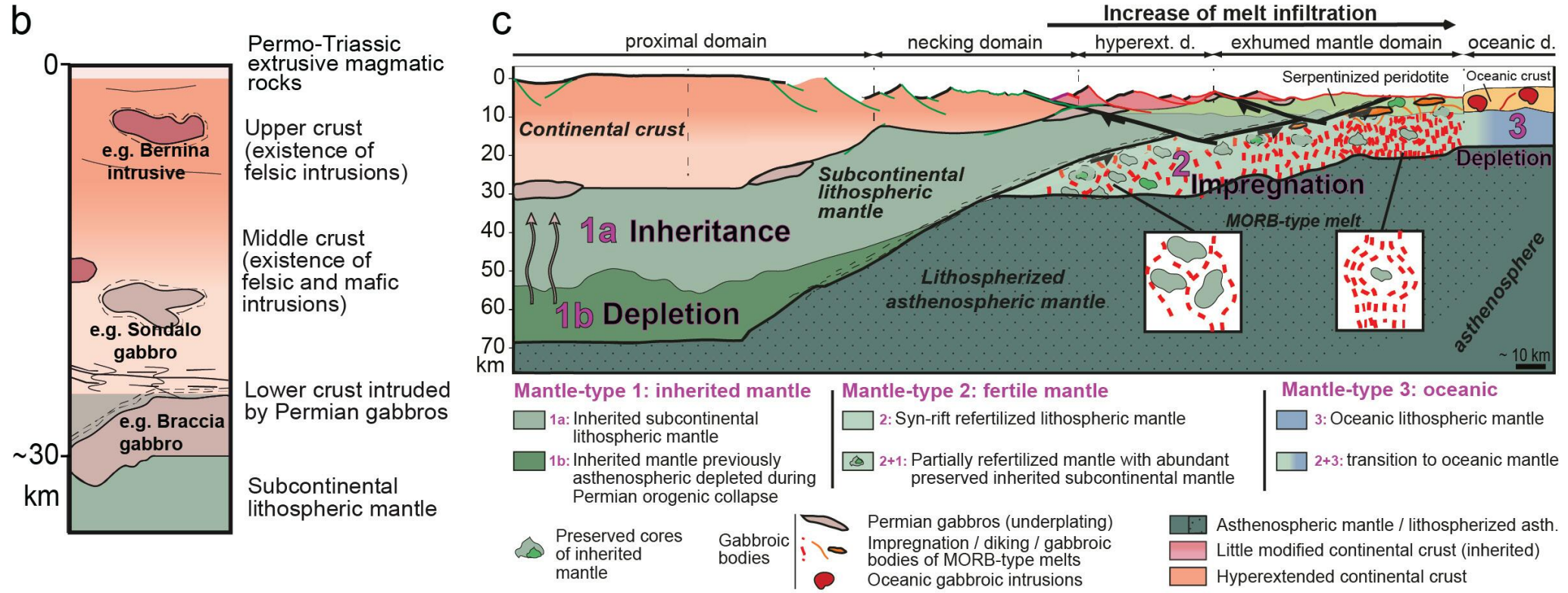

Fig. I.10 - b) Permian basement composition (modified from Mohn et al., 2011); c) Synthetic cross section showing the mantle composition along a rifted margin (modified from Picazo et al., 2016). Abbreviations: hyperext.: hyperextended; d.: domain.

- The Middle Austroalpine Nappe (light-brown domain in Figs. I.0a, I.0c, and I.0d) sample the necking domain of the former Adriatic margin. Remnants of the necking domain display mid-crustal levels that were exhumed to the seafloor via intra-crustal shear zones and a crustal-scale extensional detachment system (Mohn et al., 2012). This detachment system allowed for the exhumation of mid-crustal rocks, including Permian magmatic intrusions (e.g., the Sondalo gabbro; Petri et al., 2019; Fig. I.10b). No syn-rift sedimentary deposits are preserved over this detachment system.
- The Upper Austroalpine Nappe (sand-colour domain in Figs. I.0a, I.0c, and I.0d) correspond to the proximal domain of the Adriatic margin. Like in the Helvetic/Dauphiné unit, the continental basement is polymetamorphic, sometimes underplated and/or intruded by mafic to acidic magmatic rocks and includes locally Permian basins filled with volcano-sedimentary deposits (Fig. I.10b). This domain is characterized by thick shallow- to deep-water Triassic carbonates filling and sealing half-grabens bounded by high-angle normal faults.

https://doi.org/10.3301/GFT.2023.02

Building Blocks (BBs) of the Alpine Tethys rift system

BBs are ideally kilometre-scale outcrops, where primary rift relationships between basement rocks, fault structures, and syn-rift stratigraphic levels are preserved. BBs provide therefore information about (1) the nature of the basement (continental crust, exhumed mantle, or magmatic crust); (2) depositional environments and stratigraphic thickness, and hence indications on accommodation space. The latter can be used as a proxy for first-order crustal thickness by applying isostatic principles (e.g., Tugend et al., 2014); and (3) the geometry and age of rift structures. In the Alps, seven types of BBs can be described (Manatschal et al., 2022). In the following, we refer to them as BB1, BB2, … BB7, and exemplify each one with one or several type-localities.

BB1 (Fig. I.11) displays classical tilted blocks bounded by high-angle normal faults. The normal faults affect a 30±5 km thick crust, including possible pre-rift sedimentary layers. The syn-tectonic deposits thicken towards the bounding faults. Basins can reach several tens of kilometres in width and several kilometres in depth. The crustal extension is typically low (ß<1.5), and the total accommodation space is minor, in line with a syn- and post-rift bathymetry remaining shallow to moderately deep (<500 m). The type locality of BB1 is the Il Motto block in the Upper Austroalpine unit exposed near Livigno in northern Italy (Eberli, 1988; Figs. I.12.d and I.12.e; see also Excursion A). Other examples are the Generoso Basin in the Southern Alps (Bernoulli, 1964) and the Bourg d'Oisans Basin in the Western Alps (Lemoine et al., 1986).

BB2 (Fig. I.11) shows crustal-scale shear zones responsible for major crustal thinning/necking. They typically juxtapose upper- and middle-crustal levels via the attenuation of ductile crustal layers. The total accommodation space and sediments related to BB2 are yet little investigated but were recently discussed by Chenin et al. (2022). An example of BB2 is the Eita shear zone and Grosina extensional detachment fault exposed in the Middle Austroalpine Grosina/Campo nappe at the Swiss-Italian border (Mohn et al., 2012, 2014; Figs. I.12.d and I.12.e). However, the link between basement structures and the stratigraphic record is not well preserved in this area. More recent studies in the Mont Blanc area (Western Alps; Ribes et al., 2020) and in the Cusio-Biellese zone (Southern Alps; Beltrando et al., 2015; Decarlis et al., 2017a), both interpreted as remnants of BB2 (Figs. I.12.d and I.12.e), show a complex isostatic evolution consisting in uplift and sometimes erosion, followed by fast subsidence and aggradation.

BB3 (Fig. I.11) displays a major stratigraphic gap, also referred to as "the Briançonnais unconformity". This prominent unconformity separates tilted and eroded Triassic and Lower Jurassic platform carbonates from late Middle- to Upper Jurassic pelagic carbonates. It is recognized throughout the Western and Central Alps in the so-called Briançonnais nappes (e.g., Lory, 1860; Lemoine, 1961) and is characteristic of the former distal European margin. BB3 is best exposed in the Briançonnais nappes near the city of Briançon (south-eastern France; Claudel and Dumont, 1999; Figs. I.12.d and I.12.e).

BB4 (Fig. I.11) shows an exhumation system comprised of successive in-sequence extensional detachment faults. These detachment faults exhume mainly upper crustal levels to the seafloor and can accommodate large offsets (>10 km; Epin and Manatschal, 2018). The exhumed basement is locally overlain with allochthonous fragments of the upper crust, pre-rift, and early syn-rift sediments. These structures are covered by syn-tectonic deposits and sealed by post-tectonic deep-water sediments. The type-locality of BB4 is the Err detachment system

https://doi.org/10.3301/GFT.2023.02

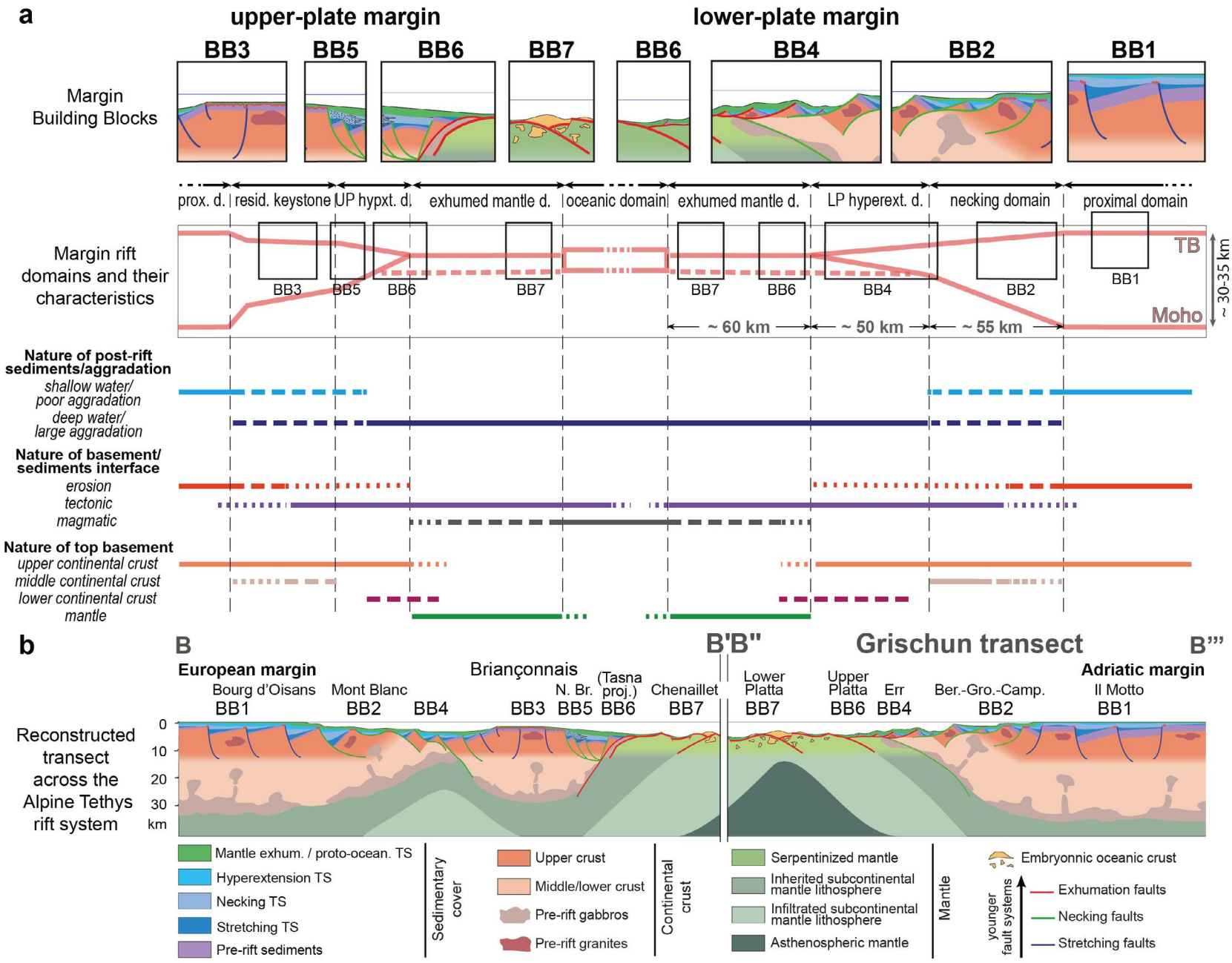

Fig. I.11 - The Building Block (BB) concept applied to the Alpine Tethys margins (modified from Manatschal et al., 2022 and Tugend et al., 2014). a) Idealized section across conjugate magma-poor rifted margins and location of the building blocks (BB) defined in the text. The nature of top basement, post-rift sediments, and of their interface vary across the margin and are diagnostic to specific rift domains; b) synthetic reconstruction of a composite transect across the Alpine Tethys rift system (see Figures I.0a and I.0b for location of B-B' and B''-B''' transects) with location of BBs and projected position of type localities. Abbreviations: Ber.-Gro.-Camp.: Bernina-Grosina-Campo; d.: domain; hypxt./ hyperext.: hyperextended; LP: Lower Plate; UP: Upper Plate; prox.: proximal; resid.: residual; TS: Tectonic Sequence; TB: Top Basement.

https://doi.org/10.3301/GFT.2023.02

exposed in the Lower Austroalpine Err nappe north of the Julier Pass (e.g., Masini et al., 2012; Epin and Manatschal, 2018; Figs. I.12.d and I.12.e; see also Excursion C). Another nearby example is the Bernina extensional detachment system (Mohn et al., 2012).

BB5 (Fig. I.11) is the least known block and, in contrast to the others, it is not preserved in one single outcrop. It corresponds to major breccia bodies of Jurassic and/or Late Cretaceous age that occur preferentially along the boundary between the Briançonnais and the Piemonte units or are linked to the Valais Basin. These breccias were first interpreted as related to one or several submarine slopes owing to either large faults or flexure (Haug, 1909; Lemoine, 1961, 1967). Ribes et al. (2019b) linked these breccias to submarine mega-fault scarps that are more favourably formed in the distal part of upper-plate margins (Haupert et al., 2016). Type localities of BB5 are (Figs. I.12.d and I.12.e) the Breccia Nappe in the Préalpes (e.g., Chessex, 1958; Steffen et al., 1993) and the Falknis breccia (Ribes et al, 2019b).

BB6 (Fig. I.11) displays a tectonically exhumed serpentinized mantle capped by extensional detachment faults and ophicalcites. These are typically overlain by silica-rich deep-water sediments (radiolarian cherts). The nature of the exhumed mantle is subcontinental (Mantle type 1 of Picazo et al., 2016). Type-localities of BB6 are (Figs. I.12.d and I.12.e) the Tasna Ocean-Continent Transition (OCT) exposed north of Scuol in the Lower Engadin valley (Florineth and Froitzheim, 1994; Manatschal et al., 2006; Ribes et al., 2019c; see Excursion E) and the Upper Platta Nappe (Epin and Manatschal, 2018; see Excursion D).

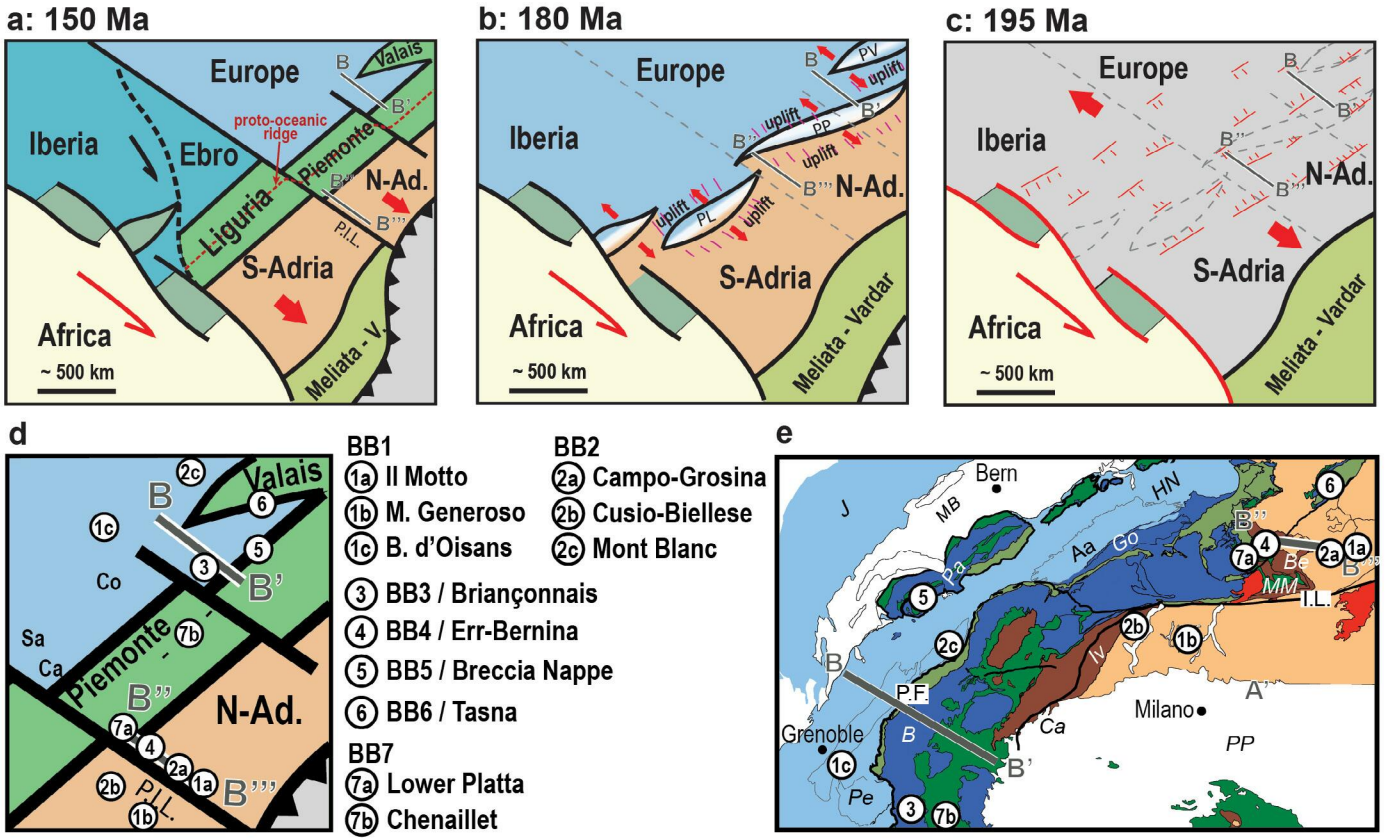

Fig. I.12 (modified from Manatschal et al. 2022) - a-c) Schematic maps showing the paleogeographic evolution of the Alpine Tethys during the: (a) Late Jurassic (150 Ma; assumed end of rifting/spreading in the Alpine Tethys); (b) late Pliensbachian (180 Ma; end of necking phase); (c) Early Jurassic (195 Ma; stretching phase). Interpretation based on Decarlis et al. (2017a); d) zoom on (a) showing the locations of the BBs described in this study at Late Jurassic time; e) location of the BBs on the present-day structural map shown in Figure I.0.a. See also Figures I.0a and I.0b for position of transects B-B' and B''-B'''. Abbreviations: B. d'Oisans: Bourg d'Oisans Basin; M. Generoso: Monte Generoso Basin; N-Ad.: northern Adria; P.I.L.: Paleo Insubric Line; PL: Proto-Liguria basin; PP: Proto-Piemonte basin; PV: Proto-Valais basin; see caption of Fig. I.0 for the abbreviations used in panel (e).

https://doi.org/10.3301/GFT.2023.02

BB7 (Fig. I.11) shows syn-tectonic magmatic additions related to mantle exhumation, as well as high- and low-angle faults affecting the infiltrated subcontinental mantle (Mantle type 2 of Picazo et al., 2016). Extrusive magmatic products include OCT basalts related to incipient magma production (Amann et al., 2020). Type-localities are (Figs. I.12.d and I.12.e) the Lower Platta Nappe exposed in the Surses valley in the Grischun region of SE Switzerland (Desmurs et al., 2001; see Excursion D) and the Chenaillet Ophiolite (Manatschal et al., 2011).
All observations derived from field studies in the Alps are not considered in terms of BBs, and yet they are important for the restoration of the former Alpine Tethys rifted margins. Such observations include the discovery of a fossil Moho in the Malenco Nappe (Hermann et al., 1997), as well as the identification of lower crustal granulites linked to the intrusion of Permian gabbros in the Ivrea zone (Quick et al., 1992; Barboza et al., 1999) and in the Sondalo region (Petri et al., 2016). These outcrops enabled us to understand the pre-rift crustal structure and to reckon the pre-rift lithospheric conditions, determine the exhumation history, and assess the Pressure-Temperature-time (PTt) evolution of the basement rocks during rifting (cf. Petrology thematic sheet). Studies on fluid inclusions and neo-formed minerals provide insights into the hydrothermal processes at play during rifting (cf. Fluids thematic sheet).

Reconstructing the Alpine Tethys rift system

Reconstructing the transect across the Alpine Tethys shown in Fig. I.0d required replacing the BBs along a generic magma-poor and sediment-starved rifted margin such as the one described in Fig. I.5. Overall, it took more than 50 years to find and define all BBs and determine the characteristics common to magma-poor rifted margins (Fig. I.11; Manatschal et al., 2022).
BB1 (tilted blocks) have been imaged since the 1970ties in the proximal margin (Montadert et al., 1979). Until the late 1980ties, the entire margin was assumed to be formed by such structures only. BB4 (in-sequence, oceanward dipping extensional detachment faults) was the next BB to be identified when Froitzheim and Eberli (1990) demonstrated that the proximal and distal margins of the Alpine Tethys were controlled by different fault systems. They recognized pre-Sinemurian high-angle faults (BB1) in the proximal margin and post-Sinemurian extensional detachment faults in the distal margin (BB4). The recognition of BB6 (exhumed mantle) and BB7 (proto-oceanic crust) arose from both the discovery of exhumed mantle along the Iberian margin (Boillot et al., 1987) and field evidence for extensional detachment faults related to mantle exhumation in the Alpine Tasna and Platta nappes (Decandia and Elter, 1969; Florineth and Froitzheim, 1994; Manatschal and Nievergelt, 1997). BB2 (necking detachment systems) was identified only in the early 2010s by Mohn et al. (2012) as they studied how and when the crust underwent major crustal thinning. The recognition of BB5 required a detailed tectono-stratigraphic investigation of the distal European margin, which enabled Ribes et al. (2019b) to link massive breccia bodies with rift models.
To reconstruct the three-dimensional architecture of the Alpine Tethys rift system, the lateral continuity of the margins needs to be integrated. This requires first determining the extent of the different rift domains along the dip (proximal, necking, hyperextended, and exhumed mantle/proto-oceanic domains), which can be approximated assuming that the width/scales of the Alpine margins are comparable to those of present-day rifted margin domains (section 2.1.1.). Second, it requires correlating rift domains along strike. To do that, it is essential to determine

https://doi.org/10.3301/GFT.2023.02

whether the rift system was segmented and if so to locate the position of the main transfer zones. BB3 and BB5, which are characteristic of upper-plate margins (e.g., Haupert et al., 2016), are missing in the Grischun transect of Northern Adria. This, together with the polarity of exhumation faults at BB4 (i.e., location of fault breakaways and transport direction) leaves little doubt about the Grischun transect being a lower plate margin (Epin et al., 2018). Based on the distribution of the BBs described above, Decarlis et al. (2017b) proposed a change in the polarity from an upper- to a lower-plate margin across a transfer fault that corresponds to the present-day Insubric Line (Figs. I.0a and I.12). Its counterpart on the European margin has not been located yet, which makes the paleogeographic restoration of the Alpine Tethys non-unique for the time being.

Our preferred view, which needs however to be confirmed by future studies, is that this conjugate pinpoint lies at the southern limit of Sardinia and corresponds to the paleo-Iberia-Europe plate boundary (Fig. I.12a). In this view, the conjugate of the Grischun lower plate transect (B''-B''') would correspond to the Sardinia-Calabria section, that would consequently be an upper-plate margin. The Southern Alps and Apennine would correspond to an upper-plate margin and its conjugate Ebro/Balearian would be a lower-plate margin.

https://doi.org/10.3301/GFT.2023.02

THE SPATIO-TEMPORAL EVOLUTION OF THE ALPINE TETHYS RIFT SYSTEM

Unravelling the spatio-temporal evolution of a rift system requires the dating of specific rift events. Dating can be relative to other events; or dating can be absolute when an age can be assigned (e.g., dating with radiogenic isotopes or stratigraphic ages).

Identification of the pre-, syn- and post-rift intervals

In the Alpine Tethys rift system, the onset of rifting is manifested by the first syn-tectonic deposits, the latest Triassic-earliest Jurassic in age (ca. 201 Ma), best preserved in the proximal domain (e.g., Eberli, 1988; Ribes et al., 2019a). The end of rifting is more difficult to identify due to the lack of evidence for a steady-state seafloor spreading system in the Alpine Tethys. Scattered basalts indicate only an embryonic spreading system (Picazo et al., 2016; Amann et al., 2020). The end of rifting is often assumed to coincide with the deposition of the Callovian-Bathonian radiolarian cherts (Bill et al., 2001), which are the first sediments overlying these basalts. However, in the absence of a mature spreading system, this assumption can be questioned (Ribes et al., 2019a).

Definition and recognition of timelines

To establish absolute timelines that can be recognized across the entire margin, Ribes et al. (2019a) relied on the characteristic deposits of three global events (Fig. I.13): (i) the Toarcian Oceanic Anoxic Event (T-OAE; ca. 183 Ma); (ii) the Bajocian-Bathonian Bio-Siliceous Event (BB-SiE; ca. 170 Ma); and (iii) the Tithonian Carbonate Event (T-CaE; ca. 152 Ma):

i) the T-OAE has been interpreted as a global anoxic event that induced a large enhancement of organic carbon deposition during the early Toarcian (ca. 183 Ma). It translates to the worldwide deposition of black shales, a large drop in $\delta^{13}C$ values framed by two positive excursions, a faunal turnover including the collapse of calcareous nannofossils, and a major transgression (Jenkyns, 1988; Bailey et al., 2003; McArthur et al., 2008; Jenkyns, 2010; Huang and Hesselbo, 2014; Ullmann et al., 2014).
ii) The BB-SiE is marked by the onset of bio-siliceous sedimentation in the Alpine Tethys realm, following a drop in the biodiversity of the calcareous organisms (Bartolini et al., 1996; Chiari et al., 2008). In the distal domain of the Alpine Tethys, it translates to a shift from siliceous pelagic limestones to lime-free radiolarites during the Bajocian (ca. 170 Ma; Bill et al., 2001; Baumgartner et al., 2013).
iii) The T-CaE is marked by a shift from bio-siliceous sedimentation to carbonate sedimentation in most of the Tethyan basins (Baumgartner et al., 2013). This change was interpreted as the result of a rapid decrease in nutrients availability during the late Oxfordian-early Tithonian, which lessened radiolarian productivity. As a result, Tithonian nannofossils developed and formed the first planktonic-derived pelagic limestone across the Alpine Tethys (Bornemann et al., 2003; Cecca et al., 2005).

https://doi.org/10.3301/GFT.2023.02

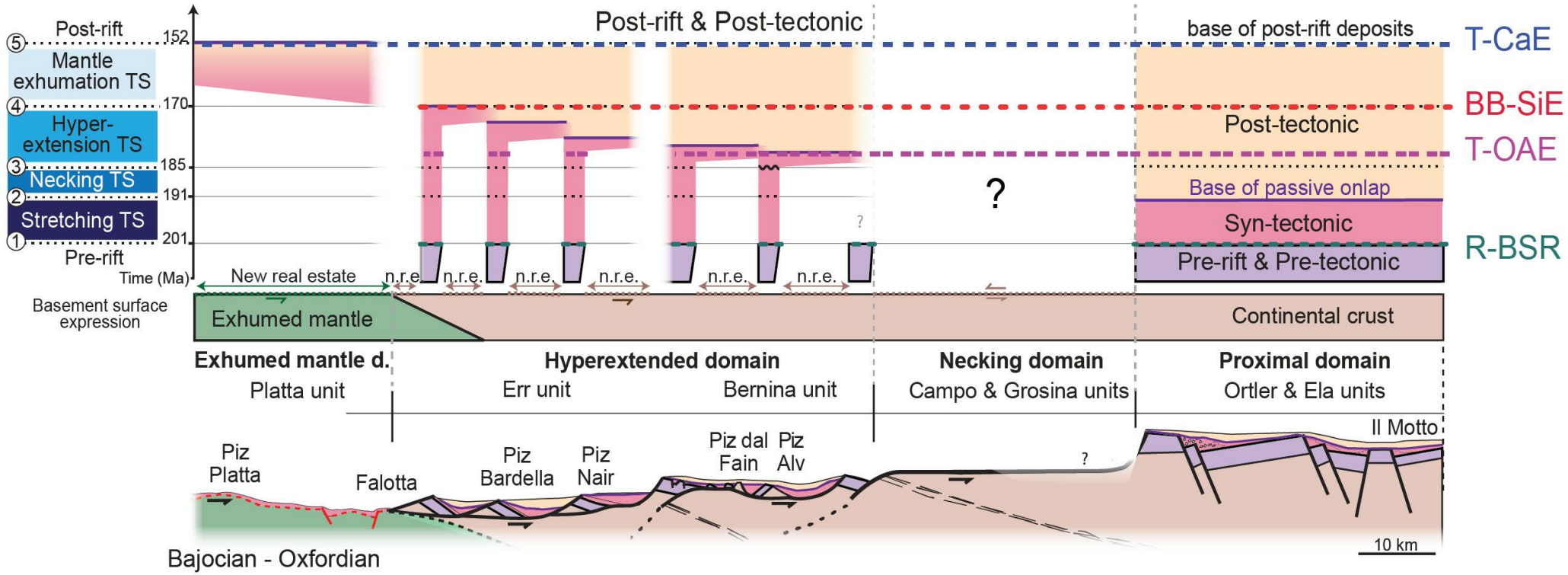

Fig. I.13 (modified from Ribes et al., 2019a) - Primary stratigraphic evolution along the north-western Adriatic margin of the Alpine Tethys schematically represented in the form of a Wheeler Diagram. Abbreviations: d.: domain; n.r.e.: new real estate; R-BSR: Rhaetian Base of the Syn-rift megasequence; T-OAE: Toarcian Oceanic Anoxic Event; BB-SiE: Bajocian–Bathonian bio-Siliceous Event; T-CaE Tithonian Carbonate Event.

Here we add the Rhaetian Base of the Syn-Rift interval (R-BSR), a timeline that corresponds to the Trias-Jurassic transition. In the proximal domain, the R-BSR corresponds to the onset of Alpine Tethys rift-related deformation.
Ribes et al. (2019a) emphasized that, although the T-OAE, BB-SiE, and T-CaE belong to the syn-rift time interval, the pre-, syn- or post-tectonic nature of associated deposits varies across the Adriatic margin:

- in the proximal domain (Ortler and Ela nappes), the T-OAE, BB-SiE, and T-CaE timelines lie in post-tectonic deposits, and hence related deposits are largely continuous through space (Fig. I.13);
- in the necking domain (Campo-Grosina nappes), no syn-rift sediments are preserved therefore no assumption can be made on the stratigraphic position of the T-OAE, BB-SiE, and T-CaE timelines (Fig. I.13);

https://doi.org/10.3301/GFT.2023.02

- in the inner part of the hyperextended domain (Bernina Nappe) the T-OAE timeline lies at the top of the syn-tectonic deposits, while in the outer part of the hyperextended domain (Err Nappe), it lies at the base of the syn-tectonic deposits. In both places, T-OAE deposits are largely discontinuous. In contrast, the BB-SiE and T-CaE timelines lie within post-tectonic deposits and related deposits are largely continuous throughout the hyperextended domain (Fig. I.13);
- in the exhumed mantle domain, the T-OAE timeline does not exist since mantle exhumation occurred later than the anoxic event. The BB-SiE timeline lies within syn-tectonic deposits and the T-CaE timeline lies within the first post-tectonic sediments, onto the rare basalts present in the exhumed mantle domain (Fig. I.13).

Synthesis of the Alpine Tethys rifting

The transition of the T-OAE and BB-SiE timelines from post-tectonic settings in the proximal domain to syn-tectonic settings in more distal parts of the Adriatic margin demonstrates that the rifting of the Alpine Tethys was a localizing deformation process, as expected for a polyphase rifting event. Its evolution is interpreted as follows.

Rifting began in the latest Triassic-earliest Jurassic (at ca. 201 Ma) with differential tectonic subsidence throughout the future Alpine Tethys realm via the formation of numerous, both east- and west-oriented, half-grabens (Fig. I.14b). These depocenters were bounded by listric high-angle normal faults that sold out in the brittle-ductile transition at 10-12 km depth (see Excursion A). This period of widely distributed extension is referred to as the stretching phase (Lavier and Manatschal, 2006).

During the Sinemurian-Pliensbachian (at ca. 191 Ma), deformation ceased abruptly in the future proximal domains of the rift system while it started focusing on the future distal domain (e.g., Eberli, 1988; Ribes et al., 2019a). The switch from distributed to focused extension is defined as the onset of the necking phase. It is indicated by: (i) the start of post-tectonic deposits sealing most of the half-graben depocenters in the proximal domain (the so-called necking unconformity of Chenin et al., 2015); and (ii) the play of crustal-scale extensional detachment faults exhuming mid-crustal levels to the seafloor (e.g., the Grosina detachment of Mohn et al., 2012; Fig. I.14c). Contemporaneously, the future Briançonnais domain became transitorily emerged and eroded, and a thermal pulse was recorded at the base of the crust in the future distal domain of the Alpine Tethys rift system (Chenin et al., 2019b, cum ref.). These events are interpreted to reflect the early mechanical necking of the upper mantle beneath a yet little-thinned keystone of continental crust framed by two major fault zones (Manatschal, et al., 2019; Schmalholz, et al., 2018).

Right after the Pliensbachian (at ca. 185 Ma), the first occurrence of Ni, Cr, and V in syn-tectonic minerals in extensional detachment faults of the distal Adriatic margin evidenced the onset of crust and mantle mechanical coupling (Pinto et al., 2015; see the Fluids thematic sheet), in other words, the onset of the hyperextension phase. This event was largely contemporaneous with the T-OAE (ca. 183 Ma), which is observed in the syn-tectonic deposits overlying the detachment fault systems of the Adriatic hyperextended domain (Ribes et al., 2019a). The play of successive in-sequence extensional detachment faults (Fig. I.14d) was associated with the formation of cataclasites, gouges,

https://doi.org/10.3301/GFT.2023.02

geological field trips and maps 2023 - 15(1.2)

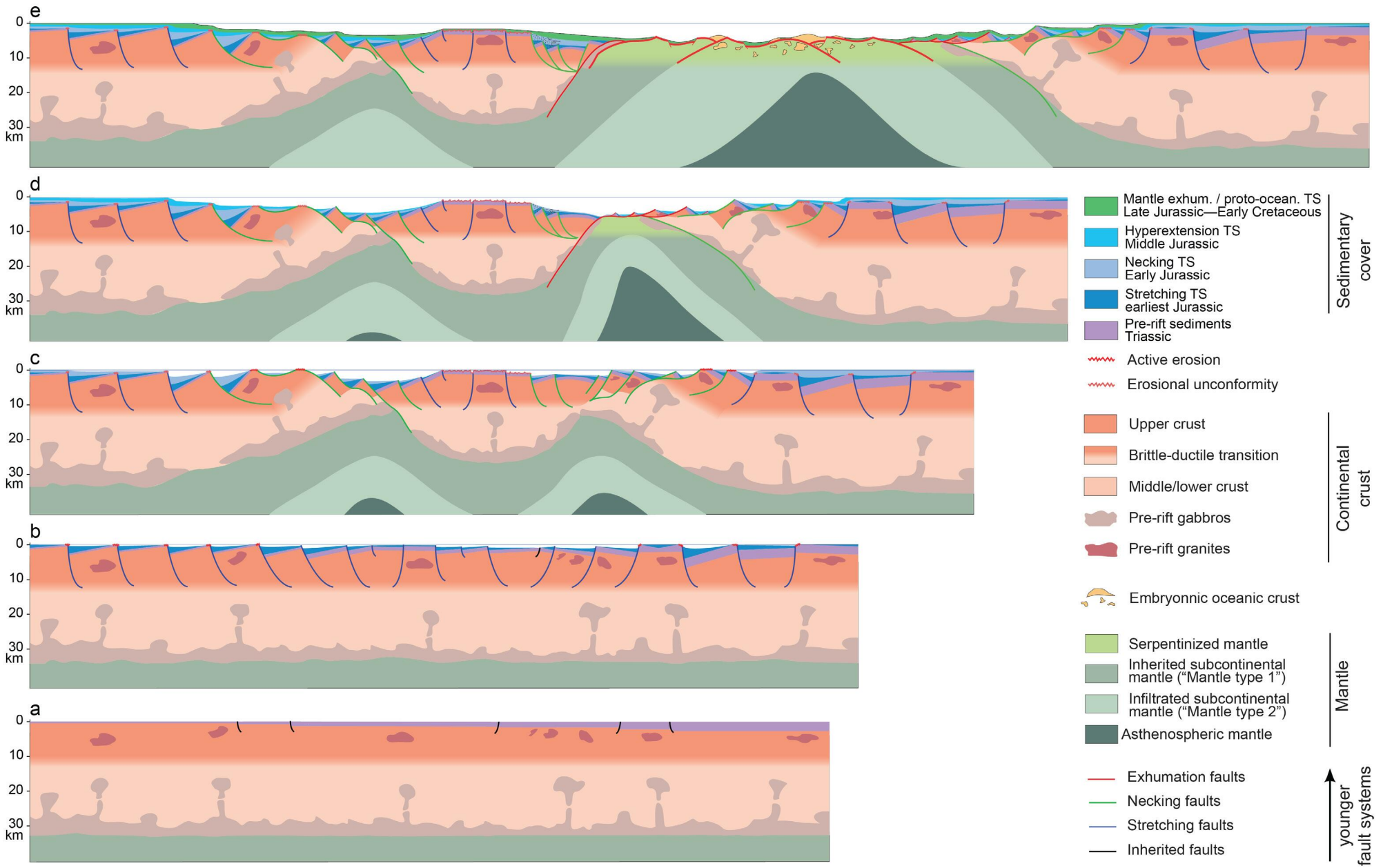

Fig. I.14 - Schematic evolution of the Alpine Tethys rifting (modified from Manatschal et al., 2022). a) Late Triassic pre-rift setting; b) latest Triassic to Early Jurassic stretching phase; c) Early Jurassic (Sinemurian–Pliensbachian) necking phase; d) late Early Jurassic (Pliensbachian–Toarcian) hyperextension phase; e) Middle Jurassic mantle exhumation phase. Abbreviation: TS: Tectonic Sequence.

https://doi.org/10.3301/GFT.2023.02

and syn-tectonic phyllosilicates in their footwall, and tectono-sedimentary breccias in their hanging wall (Epin et al., 2017, 2018). At the same time, hydrothermal fluid circulations caused the breakdown of feldspar into phyllosilicates within the continental crust and the onset of subcontinental mantle serpentinization (Manatschal, 1999; Pinto et al., 2015; see also Appendix A3).

During the Bajocian-Bathonian (ca. 170 Ma), the subcontinental lithospheric mantle started to be exhumed to the seafloor via long-offset extensional detachment faults (mantle exhumation phase; Fig. I.14e; Epin et al., 2019; Ribes et al., 2019a). The time interval of active mantle exhumation is characterized by a strong enrichment in Ni, Cr, V, Fe, and Mn in the fault rocks of the detachment faults (gouges and cataclasites), and in the syn-tectonic sediments deposited contemporaneously in adjacent basins (e.g., the Saluver C Formation; Pinto et al., 2015). This enrichment resulted from the intense serpentinization of the uppermost mantle caused by efficient hydrothermal fluid circulation along active detachment- and normal faults (Pinto et al., 2015; Incerpi et al., 2020a). Mantle was exhumed via both in- and out-of-sequence detachment faults that played dominantly in the brittle regime (cataclasites and gouges imply temperature < 350°C; e.g., Picazo et al., 2013; Epin et al., 2019). Mantle exhumation was also associated with nascent magmatic activity, as evidenced by deformed gabbros at depth and deformed basalts at the paleo seafloor (Epin et al., 2019). Mantle exhumation formed dome-shaped topographies extending over ca. 15 x 20 km, similar to those observed at present-day oceanic core complexes (Epin et al., 2019; see Excursion D). Evidence for such relief includes a local accumulation of (tectono-)sedimentary breccias and volcanic additions around the edges of the proto-oceanic core complex (Picazo et al., 2013; Epin et al., 2019). Local ophicalcites found at the top of exhumed serpentinized mantle indicate either post-tectonic carbonation at the seafloor at temperatures less than 150-100 °C (Picazo et al., 2013), or carbonatation at ca. 100 °C linked to the emplacement of basalts (Coltat et al., 2019a).

The mantle exhumation stage is assumed to cease when the first MORB-type basalts and overlying radiolarian cherts are emplaced, that is during the Callovian-Bathonian (ca. 165 Ma; Bill et al., 2001). Yet, since a mature seafloor spreading system is lacking, this age may be questioned (Ribes et al., 2019a).

https://doi.org/10.3301/GFT.2023.02

EXCURSIONS

In the following, we propose five excursions to visit the north-western Adriatic margin, the Piemonte OCT/proto-oceanic domain, and the distal European margin (Fig. II.1).

Excursion A: The proximal domain of the Adriatic margin: Il Motto in the Ortler Nappe (p. 43-55)

Excursion B: The inner part of the hyperextended domain of the Adriatic margin: Piz Alv-Diavolezza in the Bernina Nappe (p. 56-69)

Excursion C: The outer part of the hyperextended domain of the Adriatic margin: Bardella-Piz Nair in the Err Nappe (p. 70-89)

Excursion D: The exhumed mantle/proto-oceanic domain of the Ligurian-Piemonte Basin adjacent to the Adriatic margin: Val Julier-Falotta in the Platta Nappe (p. 90-106)

Excursion E: The transition between the Briançonnais domain (distal European margin) and the Valais exhumed mantle domain: Motta-Naluns in the Tasna Nappe (p. 107-131)

https://doi.org/10.3301/GFT.2023.02

EXCURSION A
The proximal domain of the Adriatic margin: Il Motto (Ortler Nappe, northern Italy)

ABSTRACT

Il Motto is a 2716 m high mountain close to the village of Livigno in northern Italy. It belongs to the Upper Austroalpine Ortler Nappe, which samples the proximal domain of the former northern Adriatic margin. Il Motto preserves structural and stratigraphic relationships between a high-angle master fault bounding an extensional basin and its pre-, syn- and post-tectonic sedimentary infill. It is a representative example of the numerous extensional basins that formed all over the proximal domain of both the European and Adriatic margins of the Alpine Tethys.

This excursion aims to highlight (1) the structural and stratigraphic architecture of the former rift basin exposed at Il Motto; (2) the pre-rift geological setting in the Alpine Tethys realm; and (3) the inversion of the Il Motto basin and reactivation of rift-related structures during Alpine convergence.

MAIN TAKE-AWAY OF THE EXCURSION

- **Age of rift-related deformation:** Lower Jurassic (Hettangian to Sinemurian, ca. 200 to 190 Ma), before the Toarcian oceanic anoxic event.
- **Deformation style:** distributed deformation (so-called “stretching”). The continental crust remained thick, as indicated by the moderate creation of accommodation.
- **Paleogeographic framework at the onset of rifting:** the Alpine Tethys system overprinted an older rift system (Meliata-Vardar) that used to be east of the Adria microcontinent (i.e., Alpine Tethys rifting was part of a so-called multistage rifting).
- **Onset of Alpine reactivation:** Late Cretaceous (Santonian/Campanian).
- **Reactivation style:** thin-skinned tectonics controlled by rift-inherited structures (decoupling salt layers).
- **Main remaining questions:** what is the nature of the contact between the Ortler and Campo nappes (i.e., Zebru thrust): why young on old? Is it a rift-inherited structure? why is there no sediment on the Campo Nappe?

INTRODUCTION

The Ortler Nappe exposed in south-eastern Switzerland and northern Italy belongs to the Upper Austroalpine Nappe complex (Fig. I.0). It preserves remnants of the proximal domain of the former Adriatic margin. As it was only weakly deformed during Alpine convergence, the Ortler Nappe provides good insights into the architecture and stratigraphy of the former Adriatic proximal margin. It also enlightens us on the paleo-environmental settings at the onset of the Alpine Tethys rifting.

https://doi.org/10.3301/GFT.2023.02

ITINERARY

The field trip takes place in northern Italy, close to the Passo d'Eira, above the village of Livigno. From Livigno, drive on road SS301 towards Bormio and leave the car in the parking of the Passo d'Eira (P on Fig. II.A.1; GPS: 46°32'19.1"N 10°09'54.3"E, i.e., 46.538643, 10.165090).

Stop 1: Il Motto (Viewpoint 1 in Fig. II.A.1; GPS: 46°32'31.0"N 10°09'49.7"E, i.e., 46.541939, 10.163795). From the northern end of the parking, take the hiking trail heading north-northeast and walk-up ca. 300 m; look into the northwest toward Il Motto.
Stop 2: Monte Crapene (Viewpoint 2 in Fig. II.A.1; GPS 46°32'49.6"N 10°10'09.7"E, i.e., 46.547113, 10.169358). From Stop 1, keep walking up ca. 500 m to the summit (Monte Crapene). From there, you have a panoramic view on the Livigno region. Look into the north toward the Punt dal Gall dam.
Stop 3: Cima di Pozzin (Viewpoint 3 in Fig. II.A.1; GPS: 46°32'19.0"N 10°10'03.9"E, i.e., 46.538616, 10.167745). Back to the parking, walk ca. 100 m heading east to bypass the houses; look into the east toward Cima di Pozzin.

Stop 1: Il Motto (46°32'31.0"N - 10°09'49.7"E)

l Motto displays a stratigraphic contact between the pre-rift Triassic Hauptdolomit formation (Fm) and the syn-rift Early Jurassic Allgäu Fm (Figs. II.A.2 and II.A.3). This contact was interpreted as the expression of a high-angle normal fault that separates basement and overlying pre-rift sediments from the syn-rift sedimentary infill of the resulting half-graben depocenter (Eberli, 1985; Furrer, 1985). Within the former Il Motto Basin, the Allgäu Fm is comprised of marls and limestones originating from background sedimentation, interbedded with redeposited carbonates such as breccias, conglomerate, and calciturbidites (Eberli, 1988). Redeposited carbonates are sourced from the pre-rift cover of adjacent footwall highs and related fault scarps, which became emerged and eroded due to flexural footwall uplift (e.g., Kusznir et al., 1991). Ammonite stratigraphy allowed to date the Allgäu formation early Hettangian to late Sinemurian (e.g., Eberli, 1985; Furrer, 1985; Dommergues and Meister, 1991).

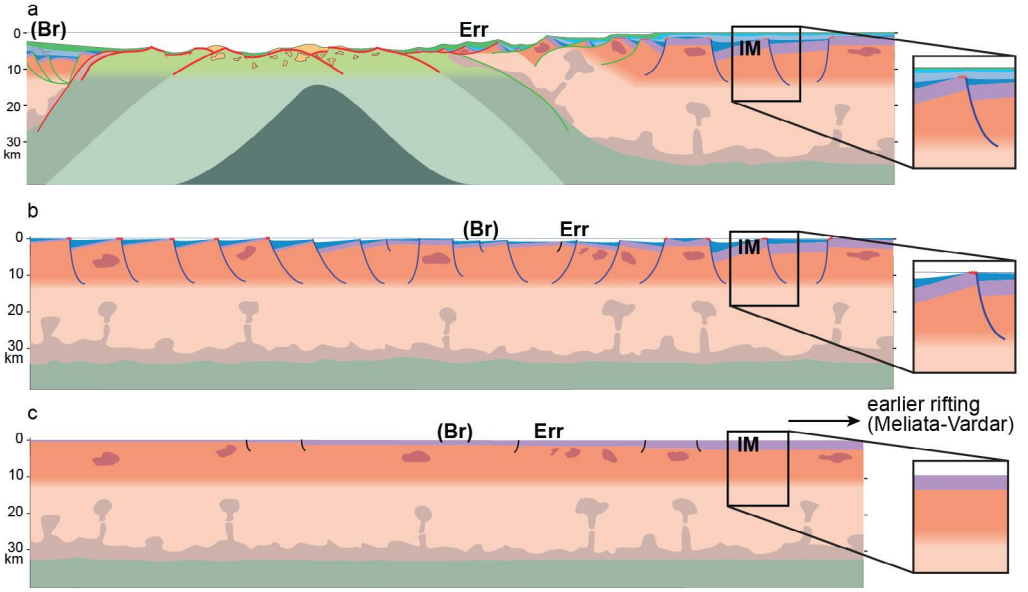

Fig. II.A.0 - Schematic section across the Alpine Tethys rift system showing the position of the Briançonnais (Br), Err and Il Motto (IM) domains during the (a) Middle Jurassic mantle exhumation phase; (b)latest Triassic to Early Jurassic stretching phase; and (c) Late Triassic pre-rift setting (modified from Manatschal et al., 2022).

https://doi.org/10.3301/GFT.2023.02

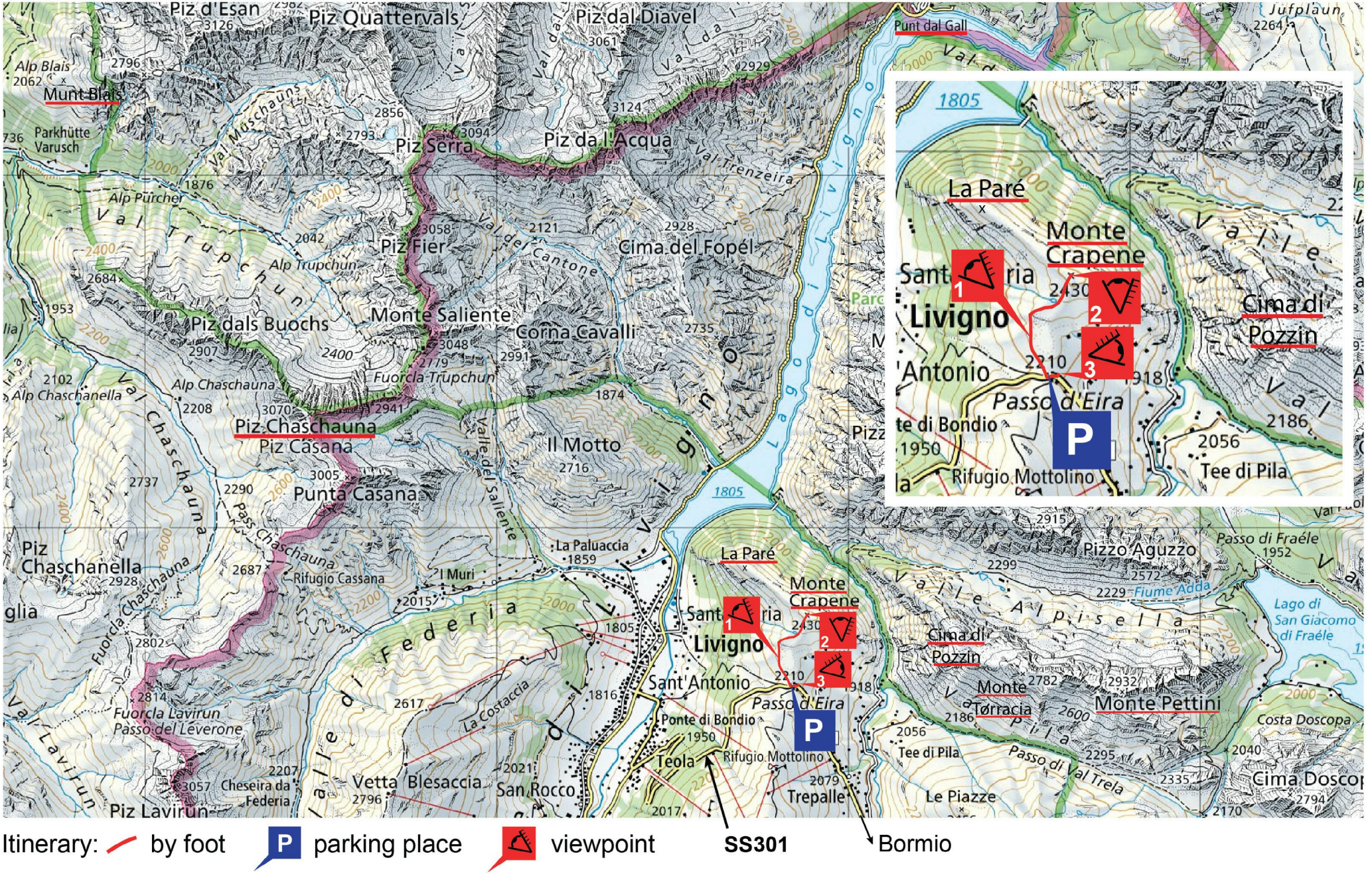

Fig. II.A.1 - Map of the Il Motto/Livigno area and route to the viewpoints (background map from https://map.geo.admin.ch/).

https://doi.org/10.3301/GFT.2023.02

Stop 2: Monte Crapene (46°32'49.6"N - 10°10'09.7"E)

The pre-rift paleogeography of the future Alpine Tethys realm can be deduced from the pre-rift stratigraphic record, which is excellently preserved and well described across most of the Alpine realm (e.g., Fig. II.A.4). Apart from local exceptions, the pre-rift Triassic stratigraphy of the Alpine Tethys realm shows a general evolution from continental siliciclastics in the northwest, to sabkha- and shallow-marine carbonate-dominated depositional systems toward the southeast (Bosellini, 1973; see Fig. III.B.2 of the Stratigraphy thematic sheet).
The Triassic sedimentary sequence is thicker in the east and southeast (1 to 5 km in the Upper Austroalpine and Southern Alps), thins towards the west and northwest, and is only a few tens of meter-thick in the future proximal European margin (bottom panel of the take-away Fig. II.A.0). In the future distal margin, Triassic pre-rift sediments are only present as extensional allochthons (e.g., Err in the top panel of the take-away Fig.; see also Fig. I.1 and Excursions B and C).

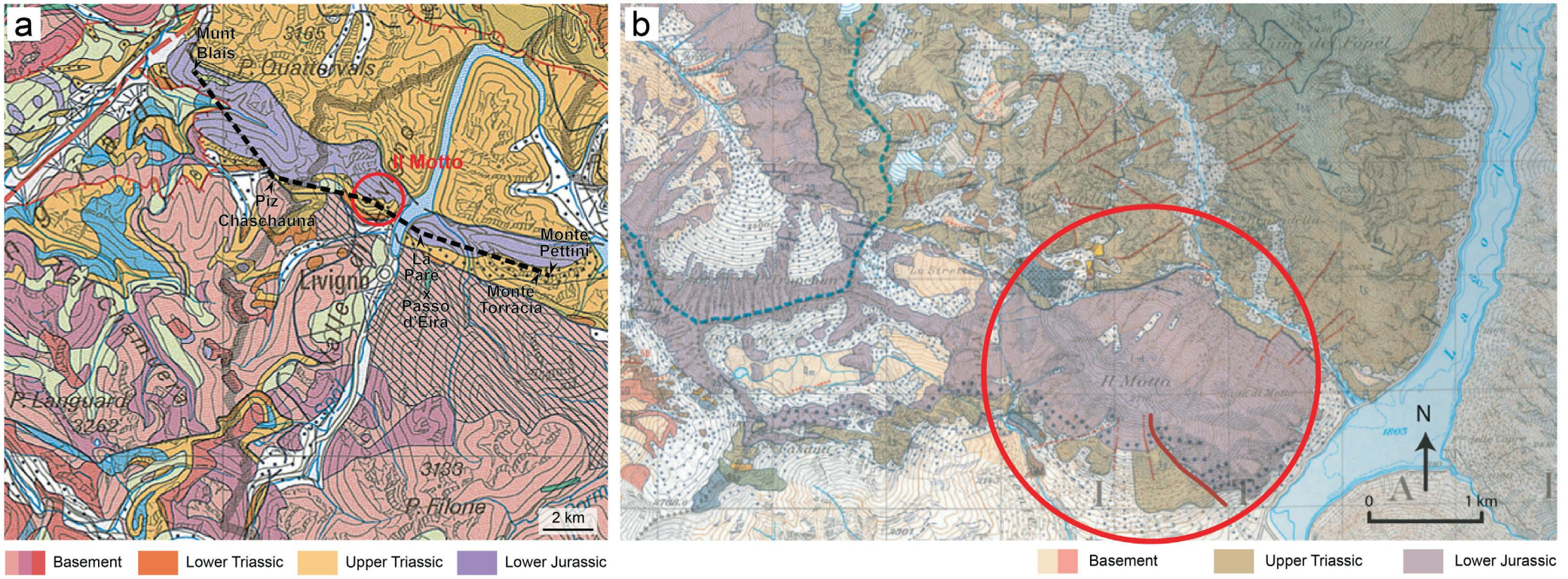

Fig. II.A.2 - Geological maps of the Livigno-Il Motto region. a) excerpt from the Swiss geological map 1:500.000. The black dashed line in the upper panel represents the trace of the profile shown in Fig. II.A.6; b) excerpt from the geological map of the Swiss National Park 1:50.000 (Trümpy et al., 1997).

https://doi.org/10.3301/GFT.2023.02

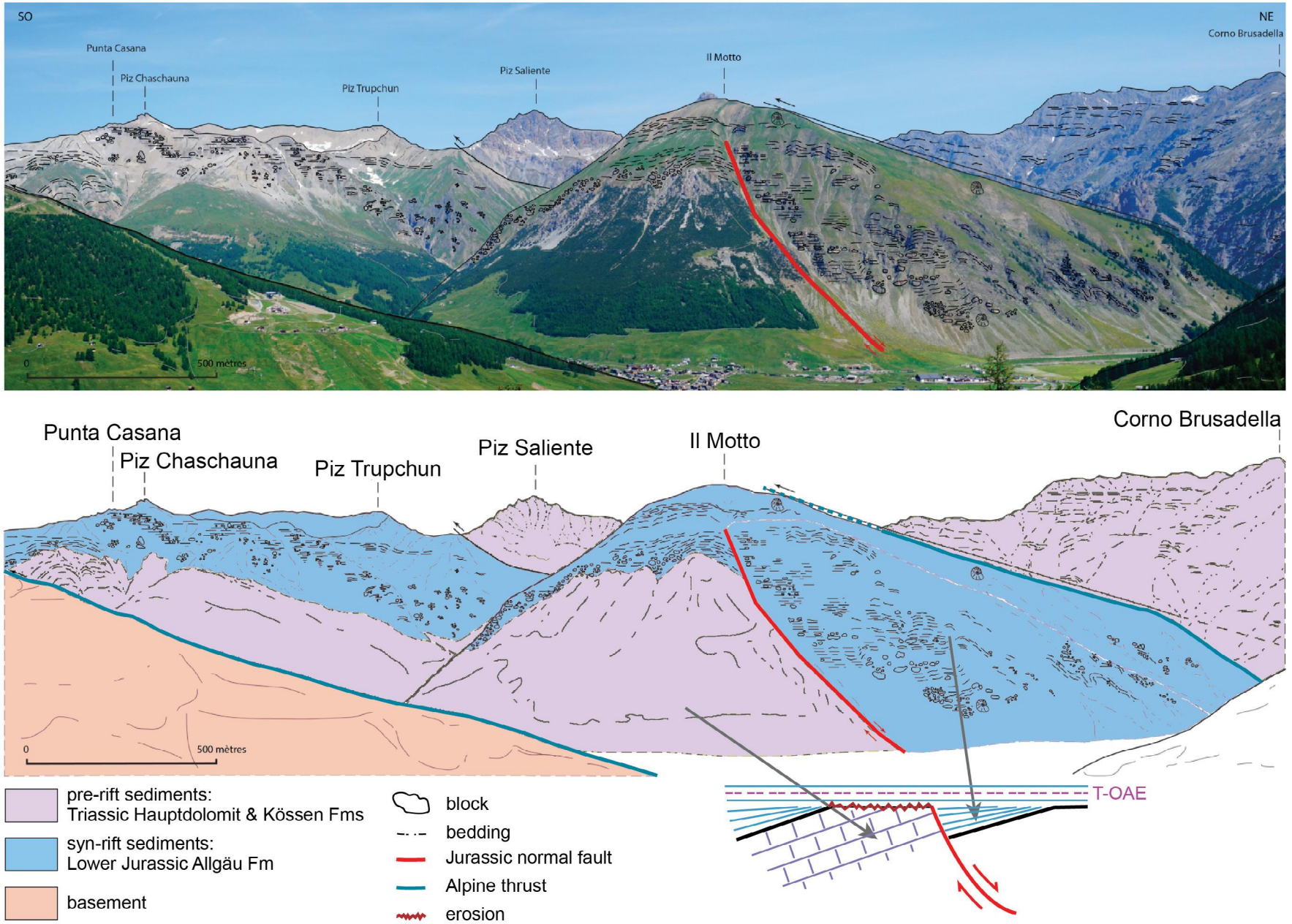

Fig. II.A.3 - Panorama of the Il Motto area taken from the Monte Sponda chairlift station (GPS: 46°31'48.6"N 10°09'04.1"E; 46.530170, 10.151136) and its geological interpretation. Abbreviation: T-OAE: Toarcian Oceanic Anoxic Event.

https://doi.org/10.3301/GFT.2023.02

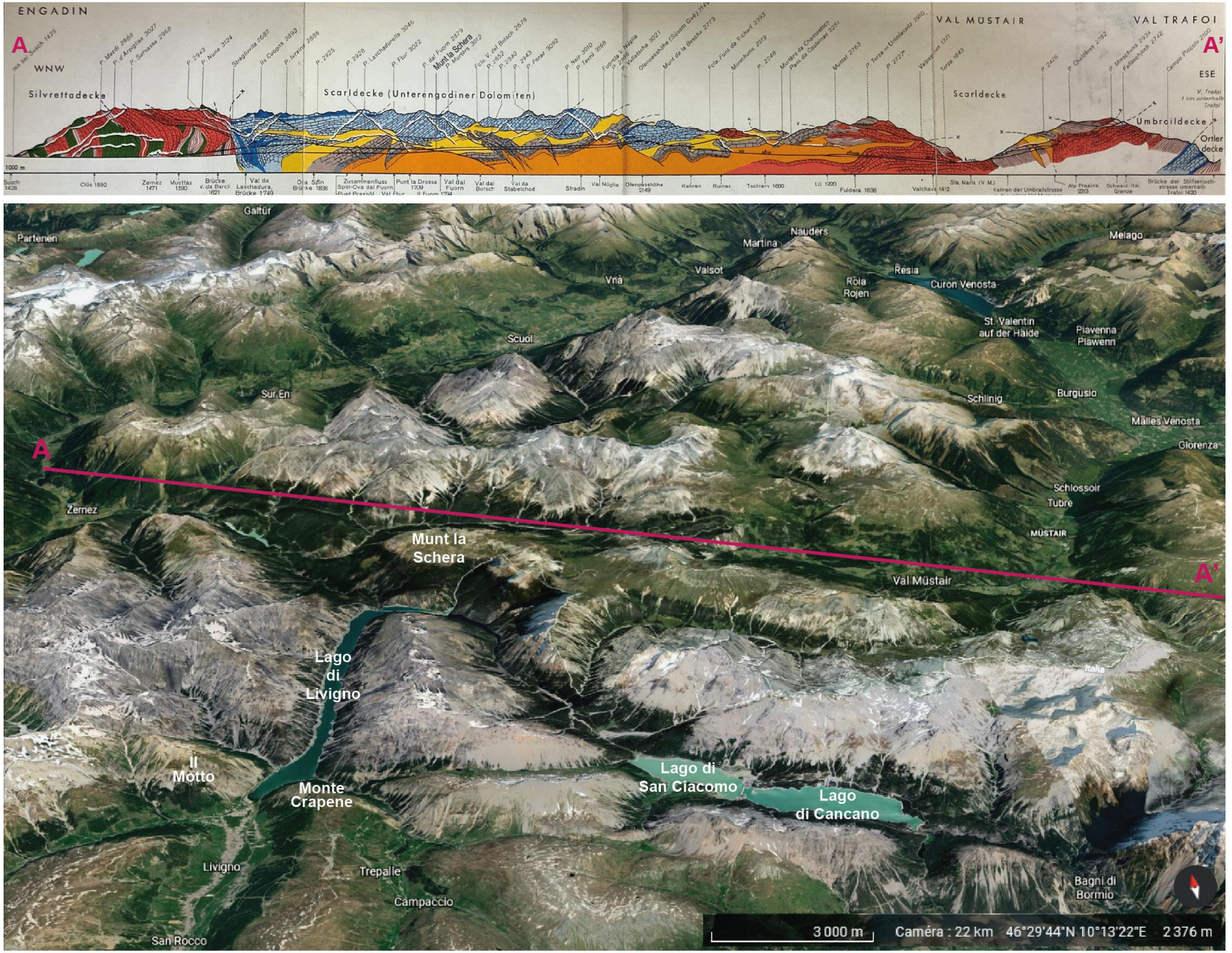

Fig. II.A.4 - Panoramic view of the Ortler region toward the north-northeast showing the Triassic stratigraphy (background picture from Google Earth) and geological section across the Engadine Dolomites (see panorama for location; Switzerland Generaldirektion der Post-, Telegraphen- und Telephonverwaltung, 1955).

https://doi.org/10.3301/GFT.2023.02

Triassic deposits overlay Carboniferous to Permian clastic sediments and volcano-sedimentary sequences, which form the base of the sedimentary succession. These Permo-Carboniferous volcano-sedimentary rocks and clastic sedimentary sequences were presumably deposited in fault-bounded basins during the post-orogenic extensional collapse of the Variscan orogen (Handy and Zingg, 1991; Handy et al., 1999; Froitzheim et al., 2008).

Stop 3: Cima di Pozzin (46°32'19.0"N - 10°10'03.9"E)

At Cima di Pozzin, large-scale sheath folds are spectacularly exposed (Fig. II.A.5a). These folds display a north-dipping axial plan, sub-parallel to the overlying Quattervals Thurst and the underlying Zebru Thrust (Fig. II.A.5b).
The Cima di Pozzin folds represent D1 sheath folds that were in turn folded by a later, long-wavelength D3 event. The folded marker bed is the Culment limestone that represents the limit between the Triassic Kössen Fm and the base of the Lower Jurassic Allgäu Fm (Figs. II.A.5b-II.A.5d). These fold structures result from the inversion of a rift basin located further east, as discussed below.

DISCUSSION

From field observations to a tectono-stratigraphic interpretation

Structural and stratigraphic architecture of the former rift basin exposed at Il Motto

In the Livigno region, the Allgäu Fm displays a large-scale wedge-shaped architecture thickening towards the master fault identified at Il Motto (Figs. II.A.6 and II.A.7). Deposits show a general fining and thinning upward megacycle. Basal deposits close to the fault scarp are largely comprised of megabreccias, which evolve into finer breccias and calciturbidites both upwards and away from the master fault (Eberli, 1985). Ribes et al. (2019a) noticed that, within the entire proximal domain of the Adriatic margin, all the T-OAE, BB-SiE, and T-CaE timelines (cf. section 5.2. of the excursion notes) belong to the post-tectonic sequence (Fig. II.A.6). This means that extension ceased in the future Adriatic proximal domain before the T-OAE, and consequently before the BB-SiE, which is considered to coincide with the end of the Alpine Tethys rifting/mantle exhumation.
The proximal domain of both the Adriatic and European margins used to comprise several similar graben and half-graben basins bounded by east- and/or west-facing high-angle normal faults (Eberli, 1987; Froitzheim, 1988). Il Motto is a representative example of these basins, like the Generoso Basin on the former southern Adriatic margin (Bernoulli, 1964; Bertotti, 1991) and the Bourg d'Oisans Basin on the former European margin (Chevalier et al., 2003; for a general discussion see Manatschal et al., 2022). The dip angle of the Jurassic normal faults in the Ortler Nappe is typically 60°±10° and their vertical offset ranges from 100 m to more than 1000 m (Froitzheim, 1988), and even several thousand meters in the case of the Generoso Basin (e.g., Bernoulli, 1964). Based on geological mapping, Bertotti (1991) concluded that

https://doi.org/10.3301/GFT.2023.02

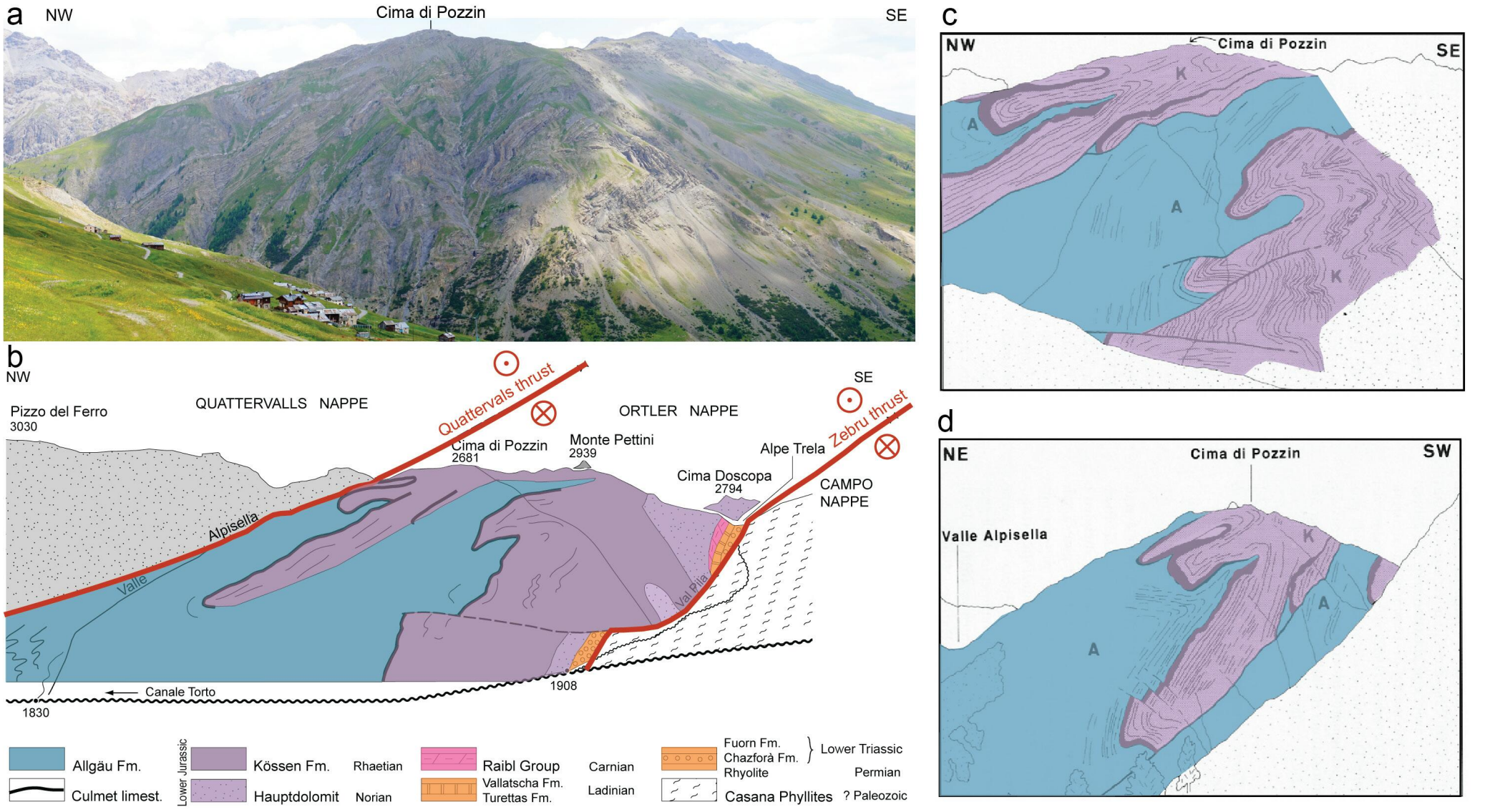

Fig. II.A.5 - Cima di Pozzin: Alpine structures resulting from the reactivation of a rift basin. a) SW face of Cima di Pozzin (photograph taken from Passo d'Eira) and (b) its geological interpretation from Furrer (1995); c-d) fold geometry in the SW face of Cima di Pozzin from Conti (1997). Abbreviations: A: Allgäu Fm; K:Kössen Fm.

https://doi.org/10.3301/GFT.2023.02

these faults had a listric geometry characterized by high-angle localized brittle faulting in the pre-rift and uppermost basement layers, and soling out into a ductile mylonitic shear zone at greenschist facies conditions, that is at 300 to 350 °C. Assuming a normal temperature gradient of 30 °C/km, the depth of this brittle-ductile transition is expected to occur at 10 to 12 km depth.

Triassic to Early Jurassic paleogeography and "pre-rift" evolution

The thick Triassic sequences in the eastern and south-eastern parts of the Alpine realm can be partly explained by its proximity to the Triassic Meliata margin, which underwent post-rift thermal subsidence (Gawlick et al., 2015). Further west, over the European domain, the shallow marine pre-rift deposits, and the lack of subsidence during the Late Triassic suggest that the continental crust was in isostatic equilibrium and was ca. 30±5 km thick prior to the onset of rifting. The distribution and thickness of Triassic vs. Lower Jurassic depocenters suggest that the locus of rifting jumped from the east/southeast of Adria to the west/northwest of Adria. Rifting in the Alpine Tethys realm was thus a multistage process involving several extension phases that were spatially and temporally offset (see the Stratigraphy thematic sheet).

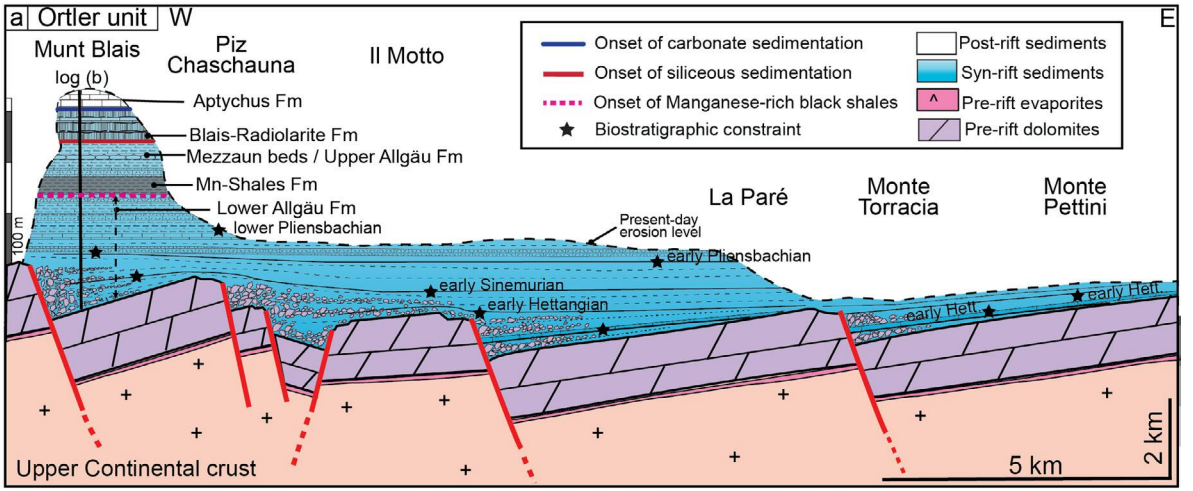

b **Representative sedimentary succession of Val Trupchun (Munt Blais & Piz Chaschauna) - Ortler Nappe**

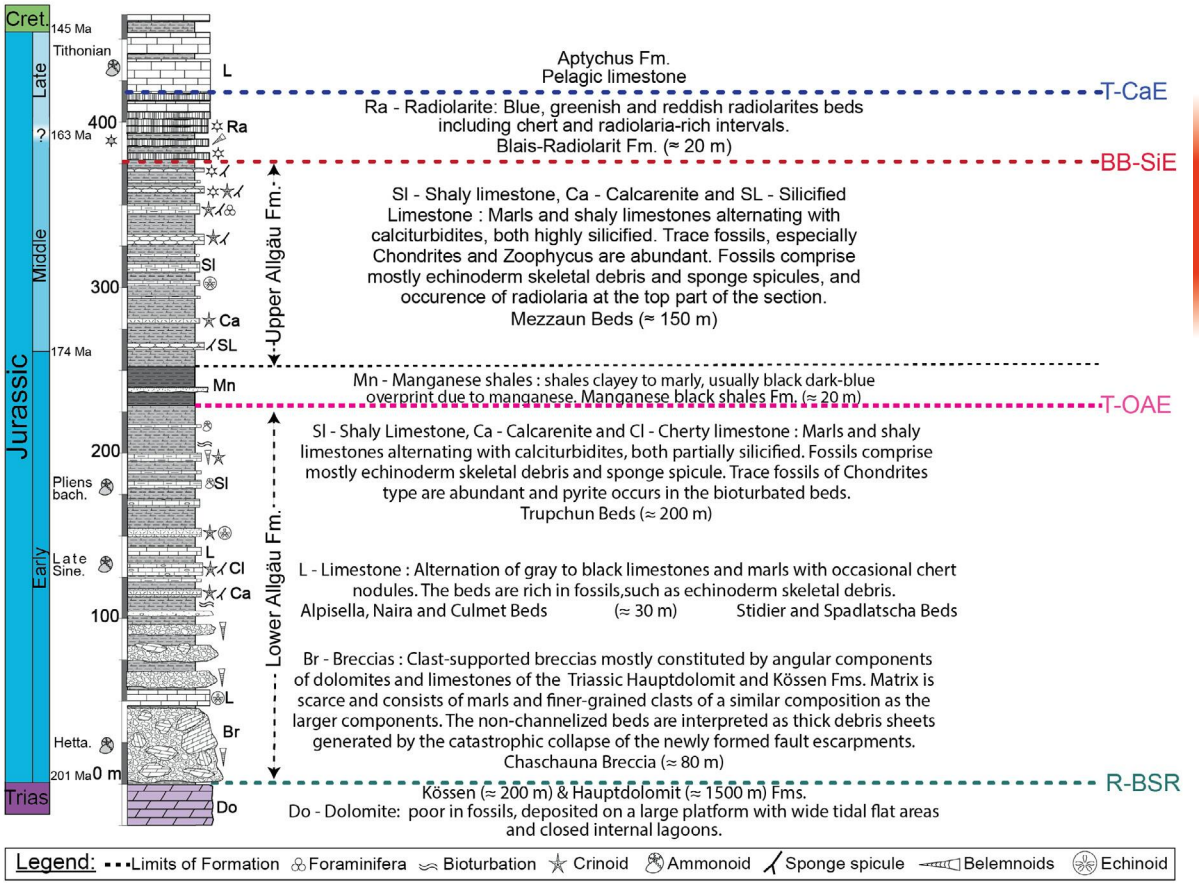

Fig. II.A.6 – a) Palinspastic reconstruction across the Ortler Nappe by Ribes et al. (2019a); see the black dotted line in panel a of Fig. II.A.2 for location. Note that the scale for syn-rift sediments is different from that for pre-rift sediments and basement; b) representative sedimentary successions of the Ortler Nappe by Ribes et al. (2019a). Abbreviation: R-BSR: Rhaetian Base of the Syn-Rift; T-OAE: Toarcian Oceanic Anoxic Event; BB-SiE Bajocian–Bathonian bio-Siliceous Event; T-CaE: Tithonian Carbonate Event (see section 5.2. of the excursion notes).

https://doi.org/10.3301/GFT.2023.02

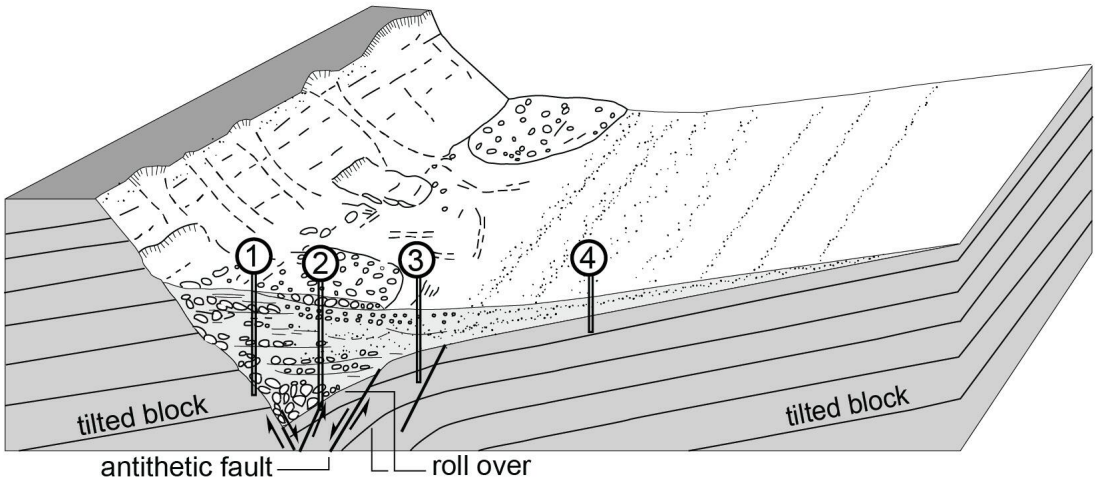

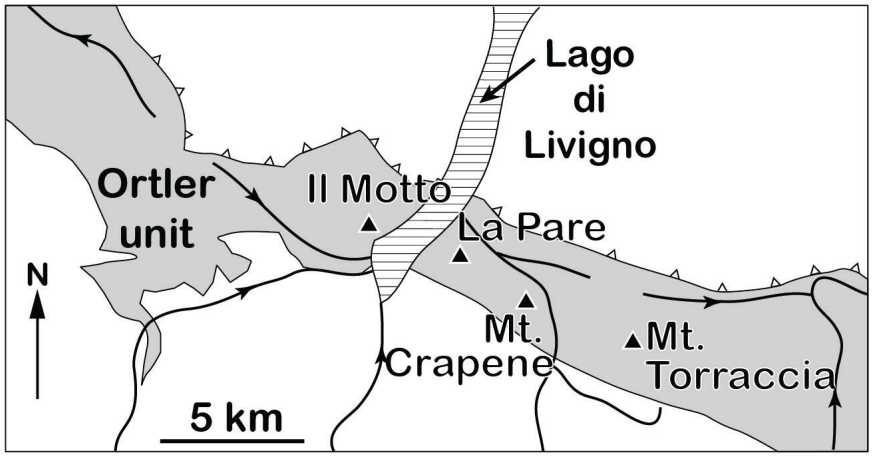

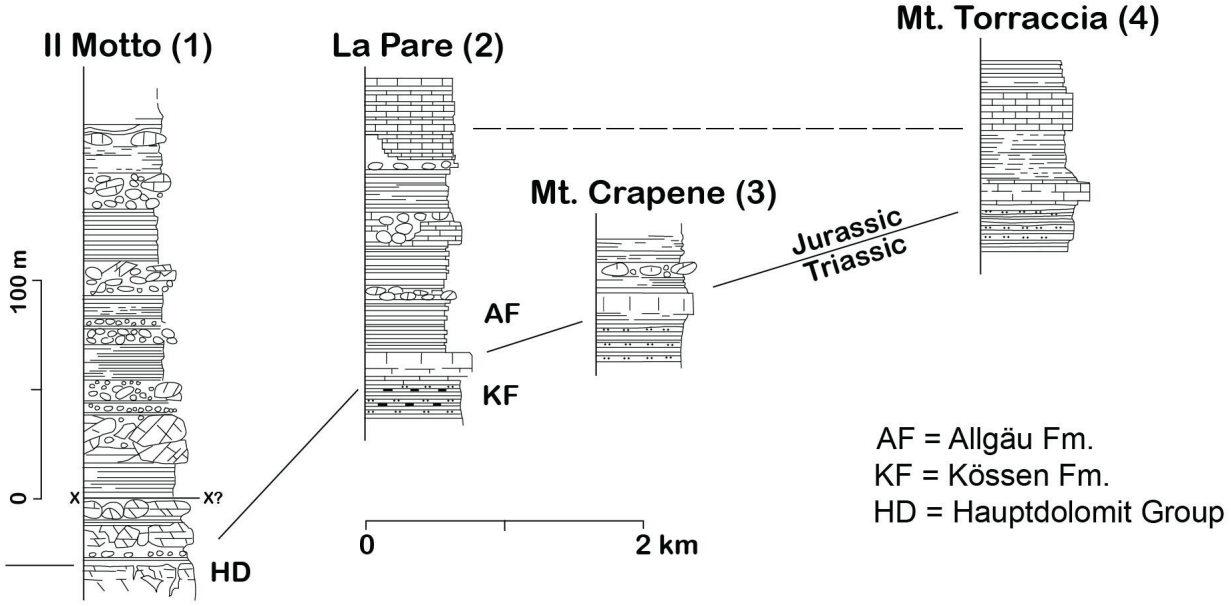

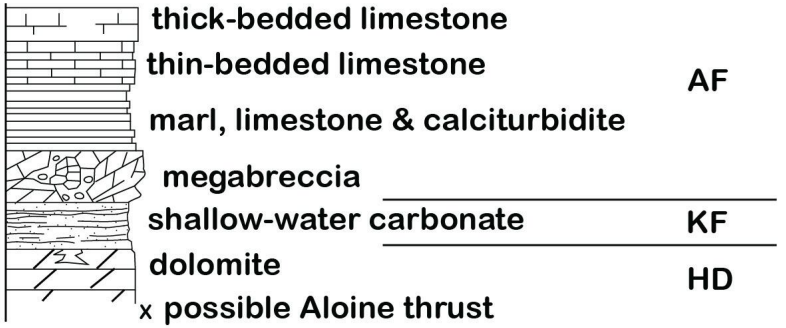

Fig. II.A.7 - Sedimentological model for the deposition of syn-tectonic sediments based on the vertical and lateral distribution of the Allgäu Fm in the Il Motto basin (from Eberli 1987).

https://doi.org/10.3301/GFT.2023.02

Alpine convergence and associated rift basin reactivation

Primary architecture of the Alpine nappe stack in the Ortler-Campo region

The Ortler Nappe and overlying Quattervals Nappe belong to the Upper Austroalpine nappe system (Fig. I.0). The underlying Campo-Grosina-Languard Nappe (including the Filladi di Bormio) belongs to the Middle Austroalpine nappe system (Mohn et al., 2011). It is separated from the Ortler Nappe by the Albula-Zebru Movement Zone (Fig. II.A.8a; Mohn et al., 2011).
The Campo-Grosina-Languard Nappe is essentially comprised of upper- and middle-crustal rocks and lacks largely pre- and syn-rift sediments (Fig. II.A.8). The Ortler and Quattervals nappes are décollement sedimentary nappes that sample essentially the pre- and/or syn-rift sedimentary cover, although some slivers of crystalline basement overlain by Permo-Triassic pre-rift sequences can be locally observed (Fig. II.A.8).
The Zebru Thrust between the Campo-Grosina-Languard and Ortler nappes is part of the Albula-Zebru Movement Zone. The latter is a complex tectonic contact that corresponds largely (but not only) to the boundary between the Variscan basement and its sedimentary cover (Fig. II.A.8). It may be rooted in a pre-existing (inherited) structure; however, this assumption remains to be confirmed.
In contrast, the Quattervals Thrust between the Quattervals and Ortler nappes followed an evaporite layer that was deposited during the Meliata rifting (Carnian). This salt layer acted as a décollement level during Alpine convergence.

Reactivation during Alpine convergence

The Alpine orogeny included three main deformation phases, namely the Eoalpine, Mesoalpine and Neoalpine orogenic phases (see section 3.3. of the excursion notes). In the Ortler Nappe, the Eoalpine orogenic phase is equivalent to the local D1 deformation phase. The Mesoalpine orogenic phase is expressed by the D2 and D3 deformation phases. The Neoalpine phase is only recorded by minor deformation structures in the Ortler Nappe. In the Il Motto area, the D1 and D3 deformation phases are clearly identified, while the D2 phase is less well expressed.

- D1 phase (i.e., Trupchun phase of Froitzheim et al., 1994). During the D1 deformation phase, the Quattervals Nappe was thrust over the Ortler Nappe along the Quattervals Thrust, and the Ortler Nappe was thrust over the Campo-Grosina-Languard Nappe along the Zebrù Thrust (Fig. II.A.4c). Both thrusts are top the west-northwest and the age of thrusting is Late Cretaceous (post-Cenomanian, for details see Mohn et al., 2011).

  The Allgäu Fm was strongly folded during the D1 deformation phase (e.g., sheath folds in Fig. II.A.8). Folds are increasingly tight when approaching the Quattervals Thrust plane, and a gradual transition into calcite mylonites is observed. Close to the thrust plane, fold axial plans become parallel with the mylonite foliation, which implies that the Quattervals Nappe thrusting (i.e., basin inversion) was contemporaneous with both folding and mylonitization (Conti, 1997).
- Orientation of the D1 sheath fold axes varies largely in the Il Motto area. Yet, as their axial planes are consistently northward plunging, this non-cylindrical folding cannot result from a subsequent folding event (Conti et al., 1994). Escher and Watterson (1974) and Cobbold

https://doi.org/10.3301/GFT.2023.02

and Quinquis (1980) suggested that a possible mechanism to form such a non-cylindrical folding could be a reorientation of the early-formed folds parallel to the transport direction during progressive simple-shear deformation.

- D2 phase (Ela-Duncan phase of Froitzheim et al., 1994). The D2 deformation phase is poorly recorded in the Il Motto area, despite it is well documented in the Austroalpine nappes north of the Engadine Line. There, it corresponds to an extensional event that is Late Cretaceous to Palaeocene (see also Mohn et al., 2011).

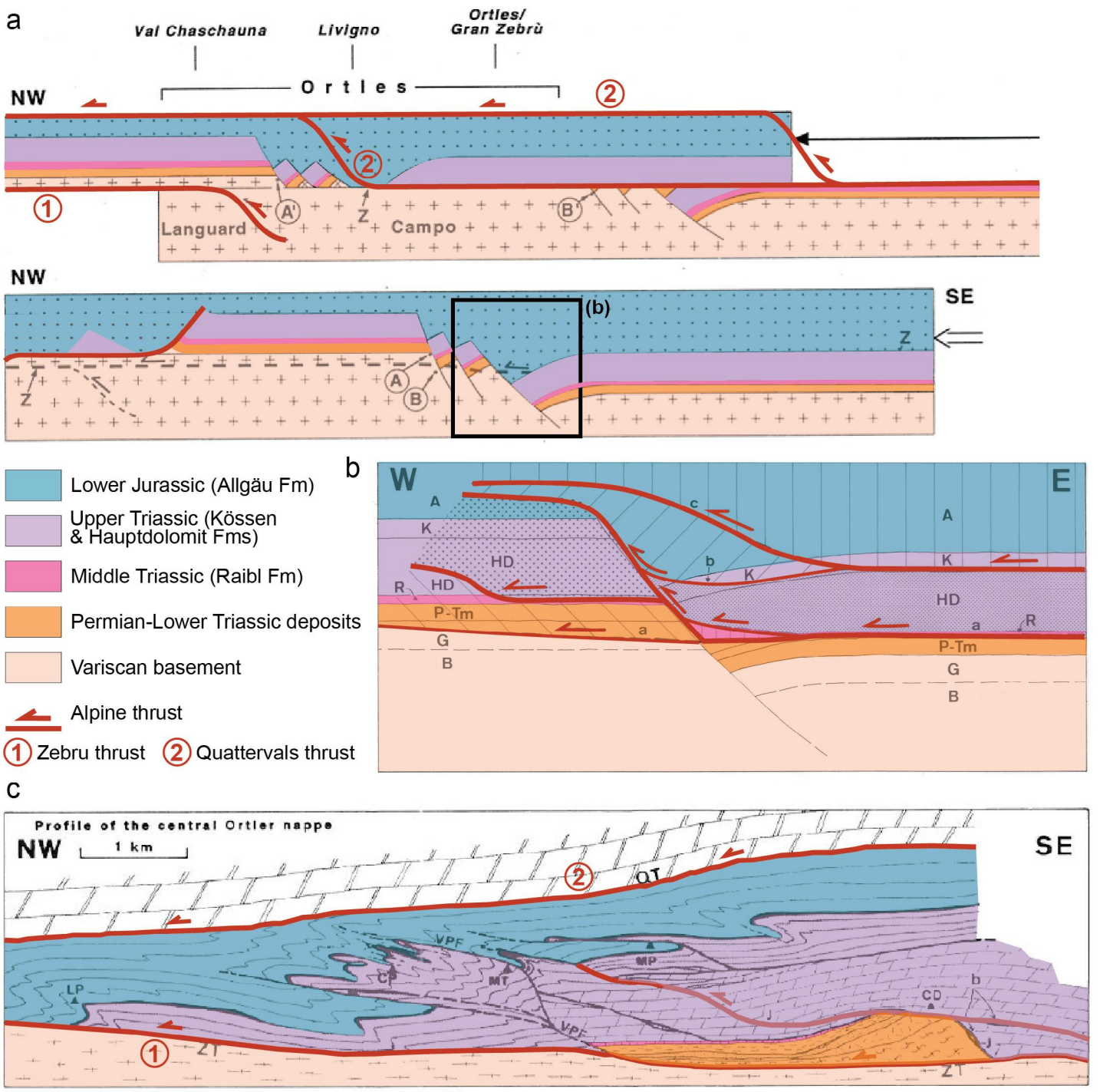

Fig. II.A.8 - Restoration of a transect through the Quattervals, Ortler and Campo–Grosina–Languard nappes from Conti et al. (1994). a) Reconstruction at the end of the Jurassic; dashed lines highlight future D1 thrust planes. b) Reconstruction after W-thrusting along the Zebru thrust and before reactivation of the Monte Torraccia fault; c) Reconstructed present-day profile across the central part of the Ortler Nappe. Note that scale in (a) is different scale from that in (b) and (c). Abbreviation: A: Allgäu Fm; B: basement; C: Campo Nappe; CD: Cima Doscopa; CP: Cima di Pozzin; HD: Hauptdolomit Fm; K: Kössen Fm; LP: La Paré; MT: Monte Torraccia; MP: Monte Pettini; P-Tm: Permian–Middle Triassic sediments; QT: Quattervals Thrust; VPF: Val Pila Fault; ZT: Zebru Thrust.

https://doi.org/10.3301/GFT.2023.02

- D3 phase (Blaisun phase of Froitzheim et al., 1994). In the Il Motto area, the D3 phase resulted in large-scale buckling and formation of east-west trending, km-scale upright folds (Fig. II.A.5; see also Mohn et al., 2011). These structures are of the same age as the north-directed thrusts in the proto-wedge in the north, and south-vergent folds in the retro-wedge in the south. In the Passo d'Eira area, the northern limb of a D3 anticline can be observed. Consequently, the whole D1 nappe pile was tilted to the north in an N-S section (Fig. II.A.5). Details of this reactivation can be mapped along the Monte Pettini southern slope (see map in Fig. II.A.1).

The overall evolution of the Ortler domain exposed at Il Moto - Passo d'Eira can be summarized as follows: globally east-dipping normal faults were created during the early rifting stages of the Alpine Tethys. These faults were properly oriented to be reactivated during the west(-northwest)-directed Eoalpine phase of convergence (D1 deformation phase). During rift basin inversion, the deep parts of normal faults were reactivated while their upper part was often preserved due to shortcuts of the Alpine D1 thrusts. In other proximal basins, normal faults were sometimes reactivated as ramps while major interfaces (e.g., the base of the Hauptdolomit Fm) were reactivated as décollement/flats.

FURTHER READING

For an overview of the Alpine Tectonic evolution of the Austroalpine units see Froitzheim et al. (1994) and Trümpy et al. (1997).
For more detailed studies of the Il Motto region, see Eberli (1988), Froitzheim (1988), and Conti et al. (1994).

https://doi.org/10.3301/GFT.2023.02

EXCURSION B
The inner part of the Adriatic hyperextended domain: Diavolezza-Piz Alv and Val da Fain (Bernina Nappe, southeast Switzerland)

ABSTRACT

Diavolezza, Piz Alv and Val da Fain lie in the Bernina region, south of the village of Pontresina. They belong to the Bernina Nappe, which samples the inner part of the former Adriatic hyperextended domain. The stratigraphic and structural relationships between basement rocks and pre- to syn-rift sediments preserved at Piz Alv and Val da Fain indicate the existence of an extensional allochthonous block made of pre-rift sediments, and of early syn-rift sediments that directly overlie exhumed basement and are sealed by post-tectonic sediments. The occurrence of cataclasites and gouges along a low-angle interface separating the tectonized exhumed basement from either the extensional allochthon or late Lower Jurassic sediments, suggests that this contact is a former rift-related detachment fault.
This excursion aims to: (1) describe the structural and stratigraphic architecture; (2) discuss the type of sediments and basement and structures observed in the inner part of the Adriatic hyperextended domain; and (3) highlight how the former necking zone controlled the style and location of subsequent Alpine deformation.

MAIN TAKE-AWAY OF THE EXCURSION

- **Age of rift-related deformation:** the Bernina detachment fault is younger than the Toarcian Oceanic Anoxic Event (T-OAE; ca. 185 Ma), and older than the Bathonian-Bajocian Bio-siliceous Event (BB-SiE Radiolarian cherts; ca.170 Ma).
- **Deformation style:** essentially controlled by brittle extensional detachment faults.
- **Paleogeographic framework:** extension occurred after the necking phase, at the onset of crust-mantle mechanical coupling. At that time, the proximal margin was tectonically inactive, conversely to the future distal margin.
- **Onset of Alpine reactivation:** Late Cretaceous (Santonian/Campanian).
- **Reactivation style:** essentially thick-skinned tectonics. Involved basement and reactivated pre-existing faults, also thin-skinned tectonics. Reactivation of decoupling levels (e.g., Triassic salt layers).
- **Main remaining question:** what are the age and importance of the Val da Fain normal fault and of its reactivation?

https://doi.org/10.3301/GFT.2023.02

INTRODUCTION

The Lower Austroalpine Bernina Nappe in SE-Switzerland samples the inner part of the Adriatic hyperextended domain. Despite numerous studies, the structure and architecture of this region have long remained unclear and controversial. Main problems arose from apparently conflicting observations, for instance: (1) the sedimentary sequences show both tectonic and primary contacts with the underlying basement; and (2) in some places, syn-rift Jurassic sediments overly directly basement rocks with primary contacts, questioning how and when the thick pre-rift Triassic sequence was removed (by erosion or tectonics? Before or during the Jurassic?).

Based on new mapping and structural, petrological, and thermochronological studies, Mohn et al. (2011) proposed that the present-day observed tectonic complexity is largely inherited from the Jurassic rifting. They suggested that the basement was juxtaposed against the pre- and early syn-rift Mesozoic cover via one extensional detachment fault during the Jurassic rifting. This detachment fault, referred to as the Bernina detachment fault, displays similarities with those previously described in the Err nappe (see Manatschal, 2004 and Excursion C). Observations from the Bernina Nappe reveal a strong control of rift-related structures at all scales during the Alpine reactivation of the distal margin.

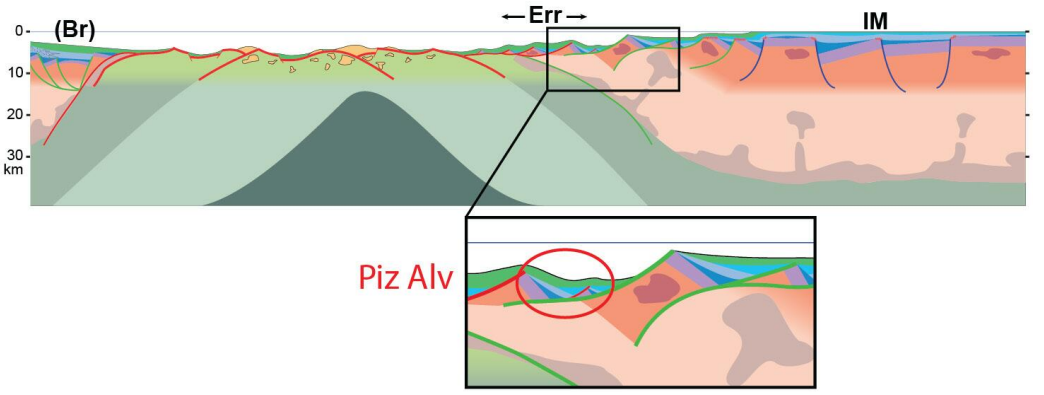

Fig. II.B.0 - Schematic section across the Alpine Tethys rift system showing the position of the Briançonnais (Br), Err and Il Motto (IM) and Piz Alv domains during the Middle Jurassic (modified from Manatschal et al., 2022).

ITINERARY

This excursion takes place in the Diavolezza-Piz Alv-Val da Fain area in south-eastern Switzerland, on road 29 between the town of Pontresina and the Bernina Pass.

Stop 1: Park the car on the Bernina Lagalb parking (P1 on Fig. II.B.1; GPS: 46°26'13.2"N 9°59'37.1"E, i.e., 46.437002, 9.993632). Walk ca. 300 m toward the northwest and look at the rocks (Outcrop 1 on Fig. II.B.1).

Stop 2: Park the car on the Bernina Diavolezza parking (P2 on Fig. II.B.1; GPS: 46°26'31.3"N 9°58'57.7"E, i.e., 46.442040, 9.982703).

Stop 2a: From P2, take the cable car to Diavolezza. Look into the north-northeast toward Piz Alv and Val da Fain (Viewpoint 2a on Fig. II.B.1; GPS: 46°24'44.2"N 9°57'56.2"E, i.e., 46.412274, 9.965613).

Stop 2b: From P2, walk along road 29 toward the west ca. 550 m and take the path on your right-hand side. After 1.8 km, turn left and walk ca. 2.5 km up to the outcrop (total ascending elevation ca. 680 m; Outcrop 2b on Fig. II.B.1; GPS: 46°27'43.6"N 9°58'46.5"E, i.e., 46.462120, 9.979569).

https://doi.org/10.3301/GFT.2023.02

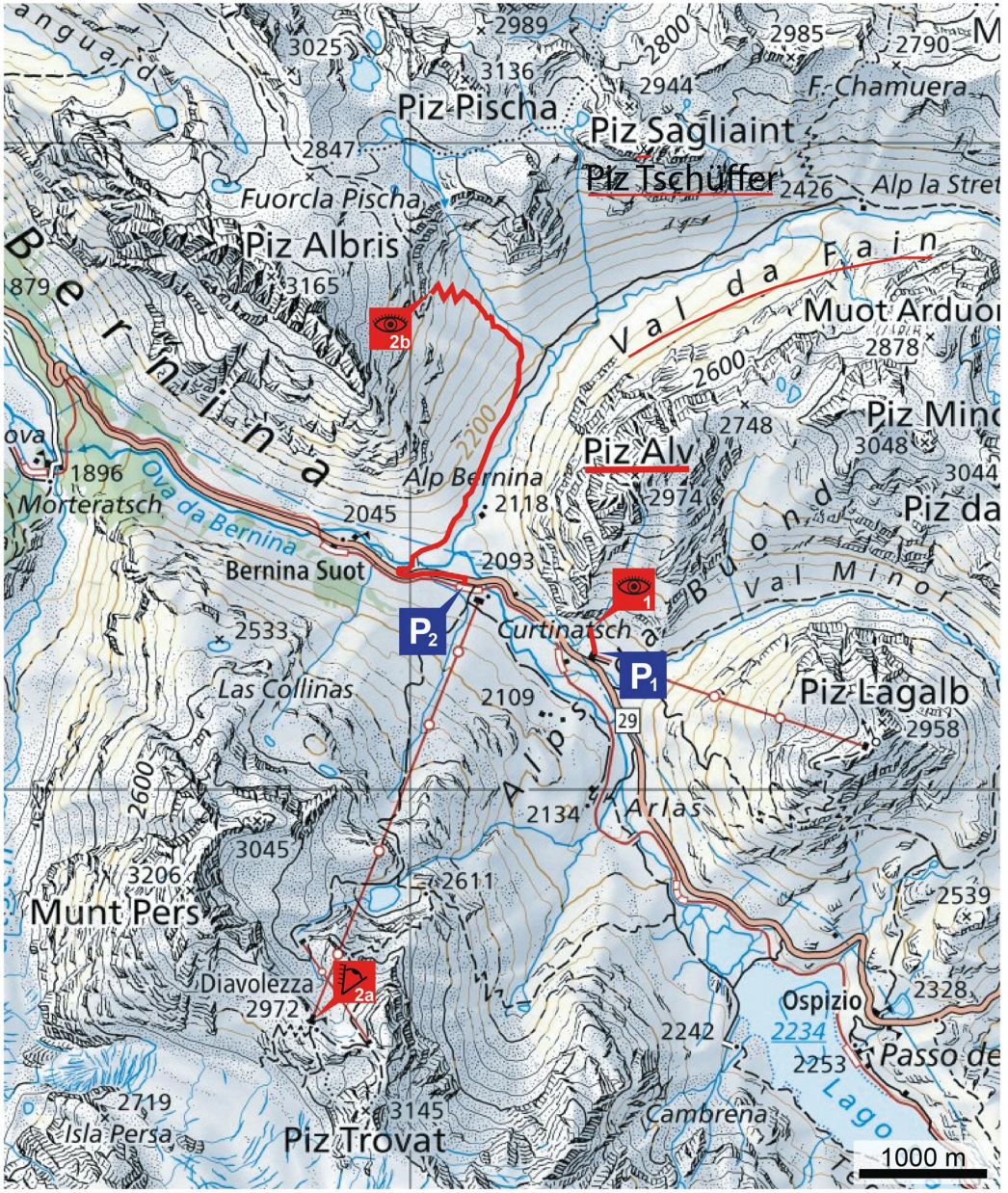

Fig. II.B.1 - Map of the Diavolezza-Piz Alv-Val da Fain area and route to the outcrops and viewpoints (background map from map.geo.admin.ch).

Stop 1: Alv Breccias (46°26'19.0" N - 9°59'33.8" E)

The Alv Fm, also called Alv Breccias, is best exposed near P1 at the Lagalb cable car station (Figs. II.B.1 and II.B.2). There it corresponds to a 200-300 m-thick succession comprised of coarse breccias and megabreccias (Decarlis et al., 2015; Ribes et al., 2019a; Incerpi et al., 2020a). It is constituted of a few millimetres- to tens of meters-scale angular clasts derived from the Triassic Kössen and Hauptdolomit Fms, embedded into a reddish to a yellowish matrix (Fig. II.B.3e). The same reddish-yellowish sediments also occur as clasts and as neptunian sills and dykes infill within the breccias (Decarlis et al., 2015; Incerpi et al., 2020a; Fig. II.B.3). Significant facies variations occur over short distances within the Alv Fm, hindering regional stratigraphic correlations.

Fig. II.B.3 displays some of the key observations concerning sedimentary facies and diagenetic products. For details, see Incerpi et al. (2020a).

Stop 2a (46°24'44.2" N - 9°57'56.2" E) and 2b (46°27'43.6" N 9°58'46.5" E): Panoramic view and view of the contact, respectively

Field observations

Piz Alv and Val da Fain display a Variscan polymetamorphic basement topped by a flat surface (Fig. II.B.4), which is locally overlain by blackish fault rocks and cataclasites (Figs. II.B.5b and II.B.5c; Manatschal, 1999). The flat surface is overlain by an Upper Triassic to Middle Jurassic(? - age based on lithostratigraphic correlations) sedimentary succession (Fig. II.B.4), which includes, from the bottom up (Fig. II.B.6; Decarlis et al., 2015; Ribes et al, 2019a): (1) a ca. 10 m-thick Triassic evaporite layer; (2) a ca. 350

https://doi.org/10.3301/GFT.2023.02

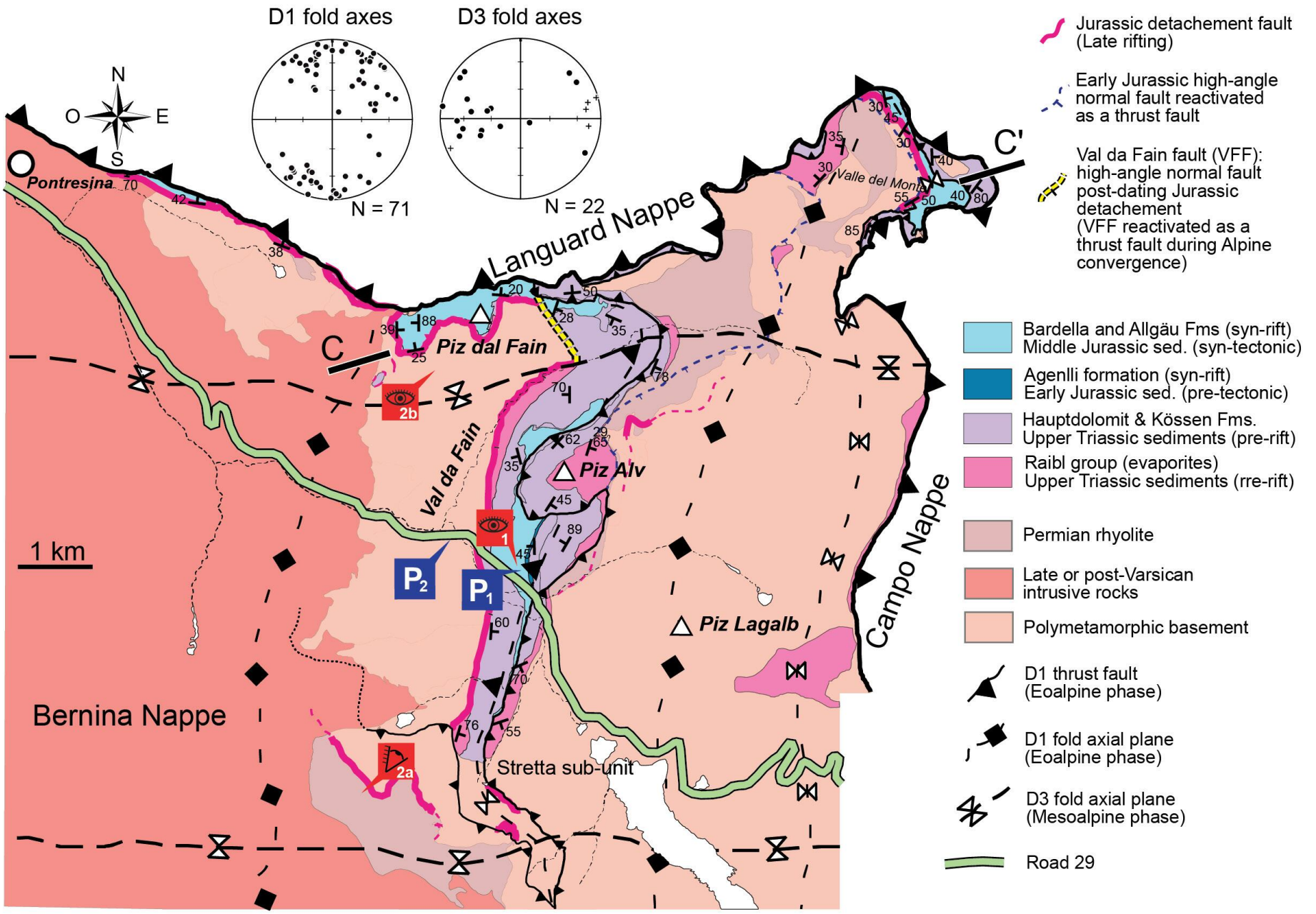

Fig. II.B.2 - Geological map of the Diavolezza-Piz Alv-Val da Fain area (modified from Mohn et al., 2011). The geological cross-section (C-C') is showed in Fig. II.B.6a.

https://doi.org/10.3301/GFT.2023.02

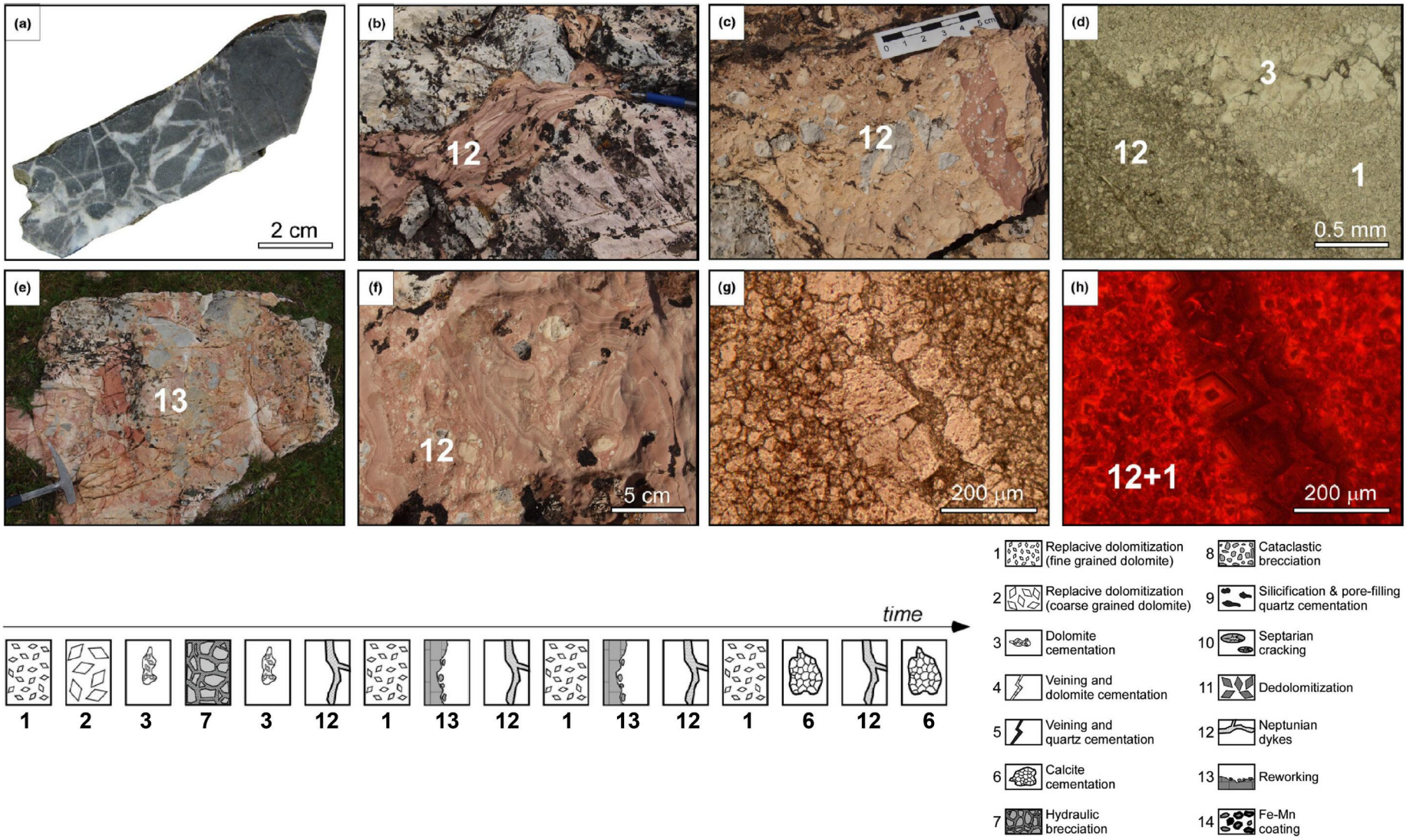

Fig. II.B.3 (from Incerpi et al., 2020b) - a) Polished slab of mosaic breccia affecting the Hauptdolomit Fm. The centimetre-large angular clasts are cemented by dolomite; b) Neptunian dyke within the breccia of Alv Fm made up of reddish laminated and dolomitized micritic sediment; c) detail of a neptunian dyke filling. It is made up of centimetre-large clasts of grey dolostones as well as reddish clasts composed of older neptunian dyke filling. It points to a polyphase opening and filling of fractures; d) TL photomicrograph showing a clast of dolostone, belonging to the Hauptdolomite Fm, cut by a dolomite-filled vein confined within the clast edges. Both are then cut by a neptunian dyke whose filling is dolomitized; e) typical aspect of the Alv Breccia made up of grey Triassic dolostone clasts as well as reddish to yellowish clasts consisting of dyke-filling sediments; f) the largest fissure infills often show convoluted laminae; g) photomicrograph and CL image (h) of a dolomitized dyke filling, which is cut by a dolomite vein. Both the replacement dolomite and the cement are characterized by bright orange to brown concentric CL zoning. The synthetic diagenetic log on the left side represents on a timescale the succession of the main diagenetic processes recorded at Piz Alv. For details, see Incerpi et al. (2020b).

https://doi.org/10.3301/GFT.2023.02

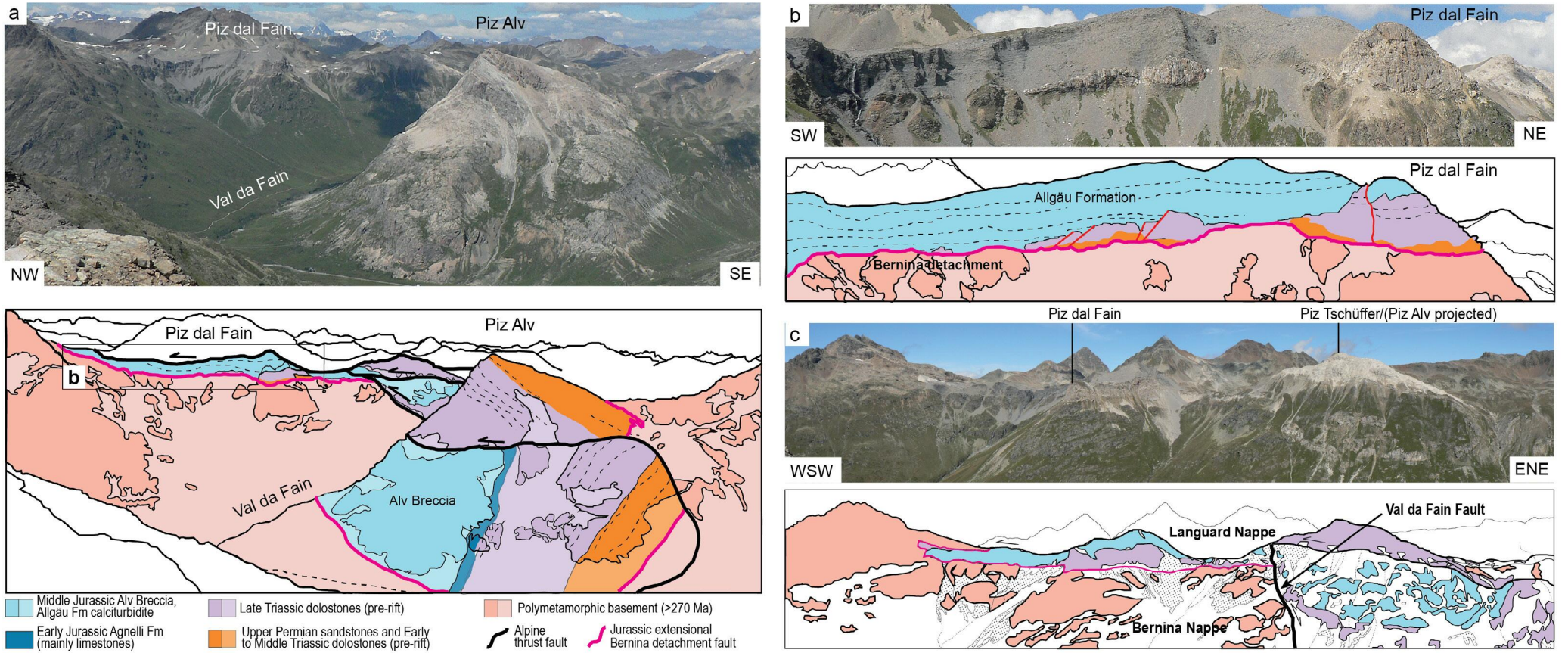

Fig. II.B.4 - Panorama of the Piz Alv and Val da Fain areas and their geological interpretation (modified from Mohn et al., 2011).

m-thick Triassic dolostone succession (Hauptdolomit and locally Kössen Fms); (3) a ca. 10 m-thick Early Jurassic limestone layer (Agnelli Fm); (4) a 100-300 m-thick succession of Early Jurassic breccias and mega-breccias (Alv Fm); (5) a ca. 10 m-thick manganese-rich layer, known as the Black Shale Fm, that is presumably of Toarcian age (Ribes et al., 2019a; T-OAE in Fig. II.B3b); and (6) a succession of calciturbidites (ca. 100 m-thick preserved) of Middle Jurassic age, which was correlated to the Upper Allgäu Fm (cf. Excursion A).

Basement nature and exhumation timing

The basement of the Bernina Nappe is made of Carboniferous to early Permian calc-alkaline and alkaline igneous rocks (333-295 Ma; Spillmann and Büchi, 1993; Von Quadt et al., 1994) intrusive into polymetamorphic Variscan basement. The occurrence of Permian rhyolitic

https://doi.org/10.3301/GFT.2023.02

bodies that formed near or at the surface indicates that the Bernina basement was in an upper crustal position already during the Permian (i.e., prior to the onset of rifting).

Stratigraphic indicators

The Triassic pre-rift succession observed at Piz Alv and Val da Fain is comparable to that of the proximal domain (cf. Excursion A). At Piz Alv, the pre-rift deposits are conformably overlain by the syn-rift (but pre-tectonic) Agnelli Fm, which is interpreted as a former starved carbonate platform. It was dated from late Sinemurian to Pliensbachian with ammonites (Finger 1978; Manatschal and Nievergelt 1997). The next deposits are the syn-tectonic Alv Breccias. The Agnelli and Alv Fms were deposited contemporaneously to the Lower Allgäu Fm in the proximal domain (cf. Excursion A). This tectono-sedimentary succession indicates that rift-related deformation started later in the future distal domain (Bernina Nappe) compared to the proximal domain (Ortler Nappe).
The Alv Breccias are sealed by a manganese-rich layer, which can be correlated to that separating the Lower- from the Upper Allgäu Fm in the proximal domain (T-OAE time marker; cf. Excursion A). In contrast to the Ortler Nappe where the T-OAE clearly belongs to the post-tectonic sequence, the T-OAE lies within the uppermost part of the syn-tectonic in the Bernina Nappe (Ribes et al., 2019a).
To the northwest, at Piz dal Fain, the syn-rift Allgäu formation overlies directly fragments of pre-rift sediments (Fig. II.B.5a). Deformed basement beneath the contact and deformation structures in the overlying sediments suggest that this contact represents a former extensional detachment fault.

DISCUSSION

From field observations to a tectono-stratigraphic interpretation

The Alv Fm corresponds to the first syn-tectonic sequence recorded in the inner part of the Adriatic hyperextended domain, now exposed in the Lower Austroalpine Bernina Nappe (Schüpbach, 1974; Finger, 1978). The Alv Fm generally overlies the Agnelli Fm, which is dated Sinemurian-Pliensbachian.
Where the Alv Fm overlies the Agnelli Fm, the contact between the two formations is an erosional unconformity (Incerpi et al., 2020a). Locally, however, Alv Breccias are interfingered with Agnelli-type sediments, suggesting that both formations were deposited contemporaneously (Incerpi et al., 2020a). The Alv Fm is overlain by the Black Shale Fm, which is interpreted to reflect the Toarcian Oceanic Anoxic Event (T-OAE; Ribes et al., 2019a; cf. section 5.2. of the excursion notes).
Schüpbach (1974), Furrer (1985), and Froitzheim (1988) suggested that Alv breccias formed in situ in response to the activity of nearby high-angle normal faults. More recently, Ribes et al. (2019a) highlighted that the Alv Fm was extended subsequently to its deposition and prior to

https://doi.org/10.3301/GFT.2023.02

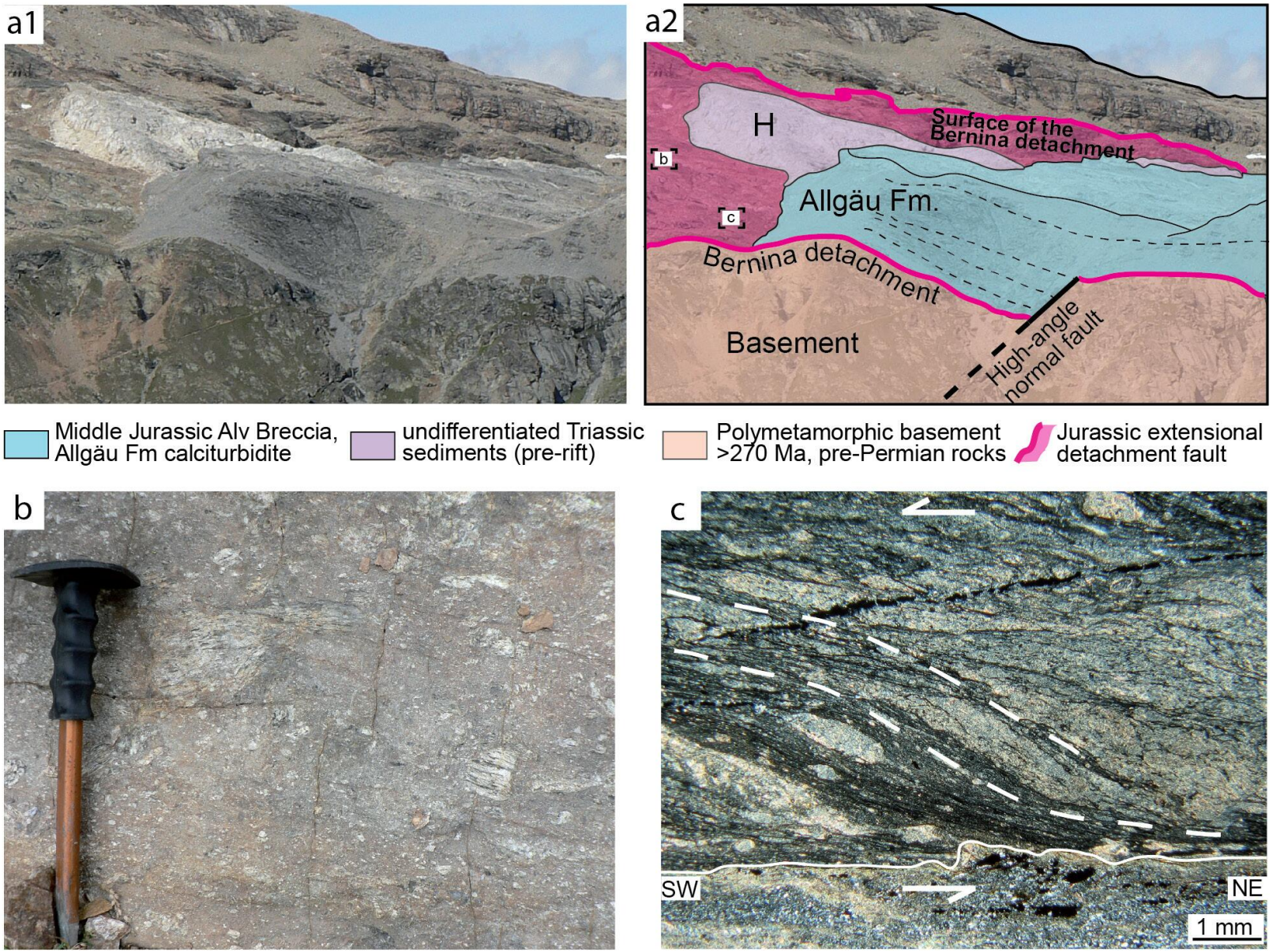

Fig. II.B.5 - Outcrop observations from Mohn et al. (2012). a1) Photograph and line drawing (a2) of the Bernina detachment (Bernina Nappe; view from the south). A high-angle normal faults crosscutting the Bernina detachment can be observed. The syn-rift Allgäu Fm thickens into this fault, indicating that these sediments were deposited during the fault activity; b–c) view of the fault rocks related to the Bernina detachment. (b) Cataclastic Palaeozoic basement of the Bernina Nappe, and (c) photomicrograph of a fault rock (crossed polarizers) showing rotation s-c fabric indicating a top to the SW sense of shear.

https://doi.org/10.3301/GFT.2023.02

Alpine convergence (cf. neptunian dykes and sills affecting the Alv Fm). They interpreted this deformation to have resulted from the activity of the detachment fault underlying the Alv allochthon (Fig. II.B.6a).

During the late Pliensbachian time, deformation started to focus on the future distal margin. Localization of the deformation is indicated by (1) the sealing of extensional basins in the proximal margin with post-tectonic deposits; and (2) the deposition of thick syn-rift sediments in the distal margin, including the up to 200-300 m-thick Alv Breccias (Schüpbach 1974).

Alv breccias were deposited contemporaneously with the Lower Allgäu Fm and after the Agnelli Fm. Alv Breccias were interpreted to have initially formed in a high-angle fault basin environment comparable to that of Il Motto (cf. Excursion A) and to have been subsequently deformed due to continuing activity of the normal fault as it evolved into a long-offset detachment fault (Ribes et al. 2019a).

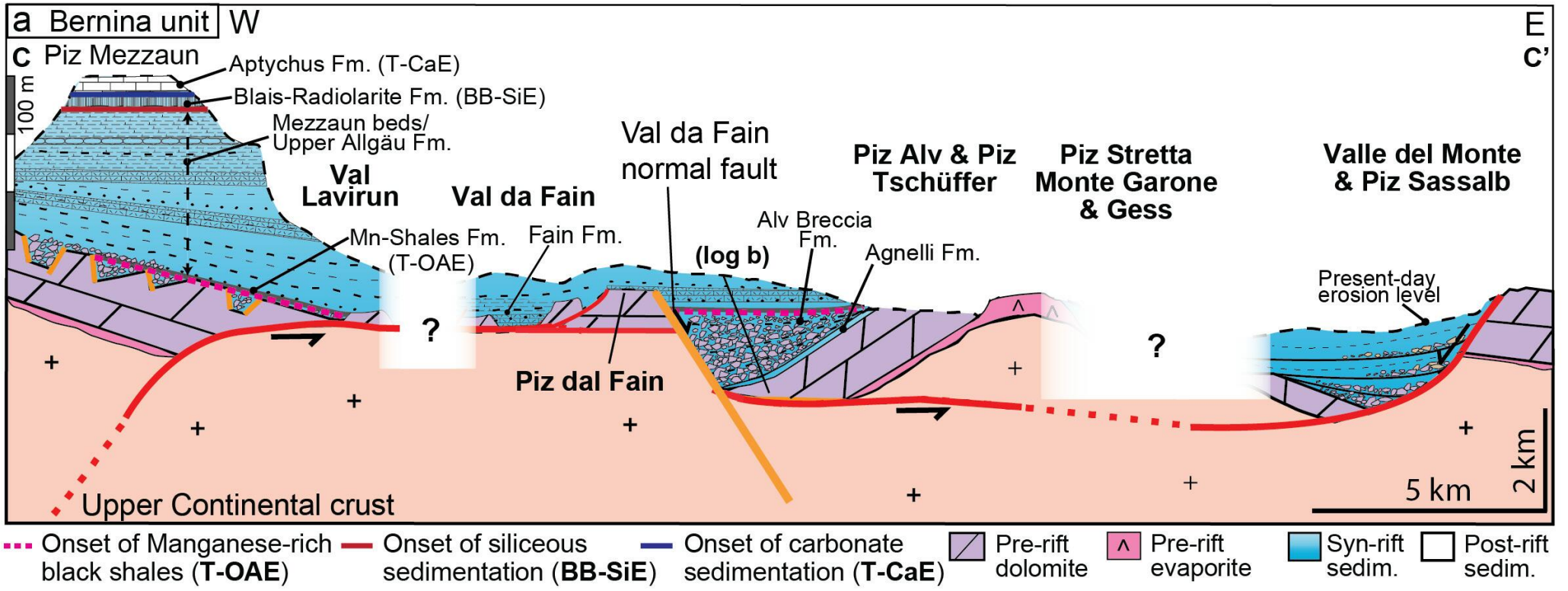

Fig. II.B.6 - a) Palinspastic reconstruction of the Bernina Nappe by Ribes et al. (2019a, modified). Note that the scale for the syn-rift sediments is different from that for the pre-rift sediments and basement; see location of transect C–C' in Fig. II.B.2).

https://doi.org/10.3301/GFT.2023.02

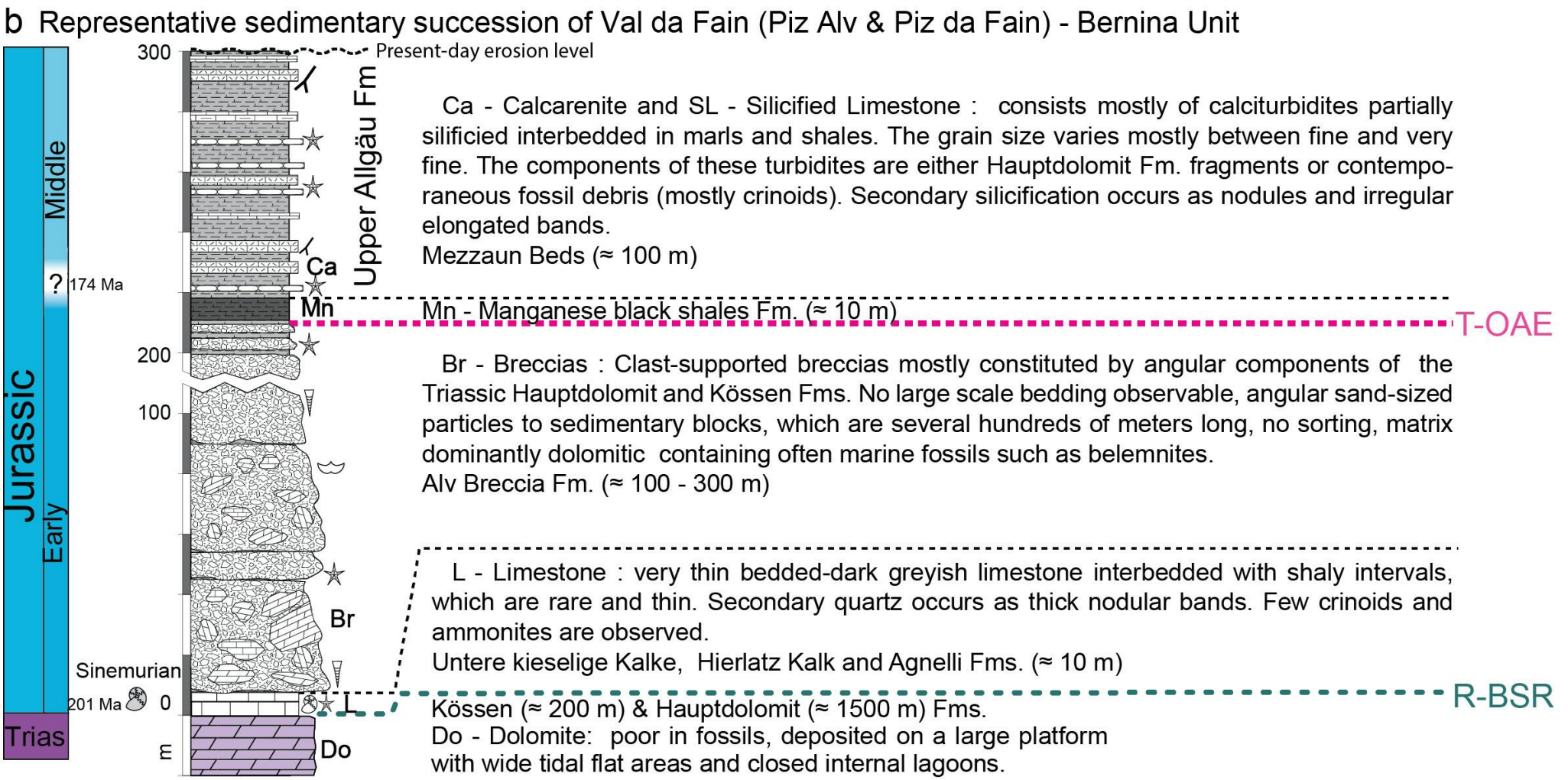

Fig. II.B.6 - b) representative sedimentary successions of Piz Alv and Val da Fain by Ribes et al. (2019a). Abbreviation: R-BSR: Rhaetian Base of the Syn-Rift; T-OAE: Toarcian Oceanic Anoxic Event; BB-SiE: Bajocian-Bathonian bio-Siliceous Event; T-CaE: Tithonian Carbonate Event (see section 5.2 of the excursion notes).

Detachment systems in the necking zone and inner hyperextended margin

Remnants of the necking zone and inner hyperextended domain are exposed in the Campo-Grosina and Bernina nappes (Fig. II.B.7). These domains contain extensional detachment faults that can be mapped in the field (e.g., Fig. II.B.7). Two extensional detachment faults can be distinguished, namely the Grosina and the Bernina detachments. The relationships between these two detachment faults are shown in

https://doi.org/10.3301/GFT.2023.02

Fig. II.B.7c and sections across these domains are shown in Figs. II.B.8a and II.B.8b. In the sections of Fig. II.B.8, the relative and absolute ages of the detachment systems and related fault rocks are provided, which allow us to reckon the timing of necking to be 185±5 Ma (Sinemurian to Pliensbachian).

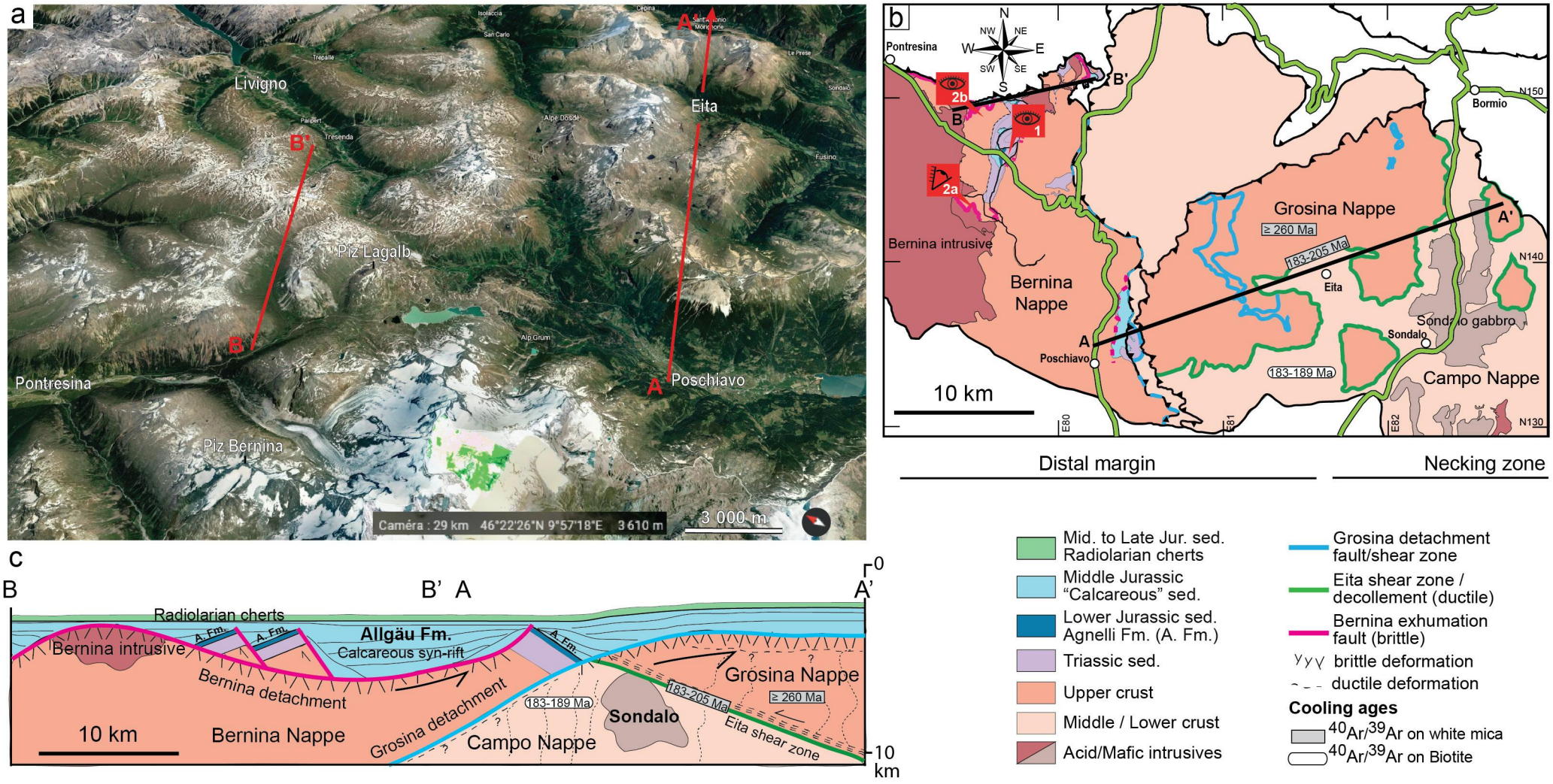

Fig. II.B.7 - View of the fossil Adriatic necking zone and location of detachments faults. a) Panorama of the Bernina region (background picture from Google Earth); b) present-day geological map and (c) restored cross-section of the Adriatic necking zone across the Bernina–Campo–Grosina nappes. The cross section summarizes the sediment architecture, fault geometry, $^{40}Ar/^{39}Ar$ data and strain distribution observed in these nappes (from Mohn et al., 2012). Abbreviation: A. Fm: Agnelli Formation; Jur.: Jurassic; Mid.: Middle; sed.: sediments.

https://doi.org/10.3301/GFT.2023.02

Alpine reactivation

The overall Alpine structure in the Piz Alv-Val da Fain region is quite clear when looking into a WSW-ENE-striking section, i.e., parallel to the main Alpine transport direction (Fig. II.B.8b). Piz Alv, like Piz Tschüffer, form a W-facing recumbent fold truncated by a west-vergent, second-order, late Cretaceous thrust fault (Fig. II.B.8b). This thrust juxtaposes an inverted limb in the hanging wall against a sub-vertical hinge in the footwall. At a larger scale, it can be observed that Alpine deformation reactivated and overprinted rift-related decoupling levels so that the necking zone and overriding nappes display an antiformal shape (Fig. II.B.9).

FURTHER READING

Mohn et al. (2011, 2012); Epin et al. (2017); Ribes et al. (2019a).
Ph.D. thesis: Mohn (2010).

https://doi.org/10.3301/GFT.2023.02

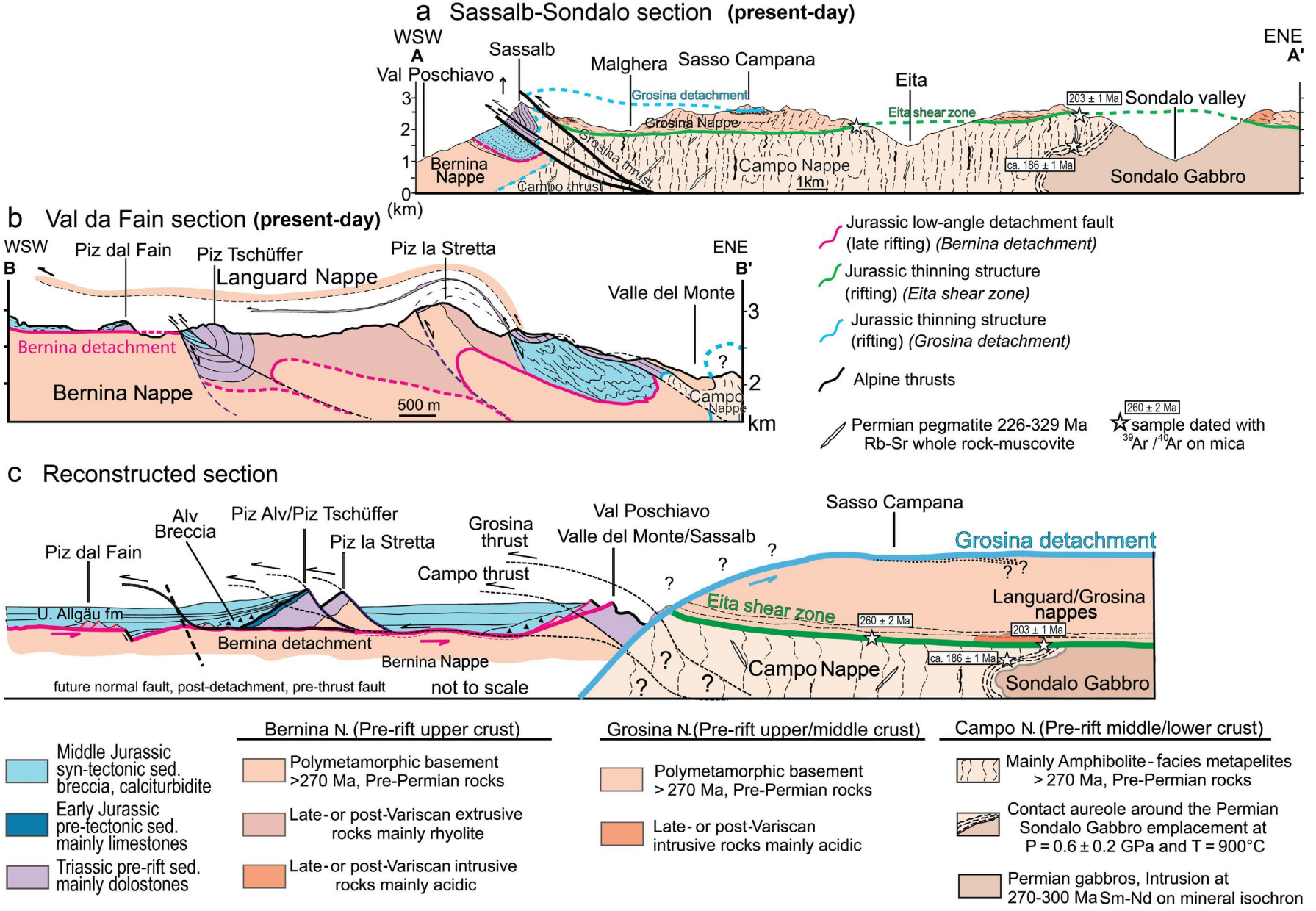

Fig. II.B.8 (modified from Mohn et al., 2012) - Geological sections across (a) Sassalb–Sondalo, and (b) parallel to the Alpine shortening direction across the Piz dal Fain–Piz la Stretta area (see Figure II.B.7 for location); c) restoration of the two sections above showing the pre-Alpine structures and their relation to the sediments and basement rocks in the Bernina, Campo-Grosina nappes. Abbreviation:; N.: Nappe; sed.: sediments.

https://doi.org/10.3301/GFT.2023.02

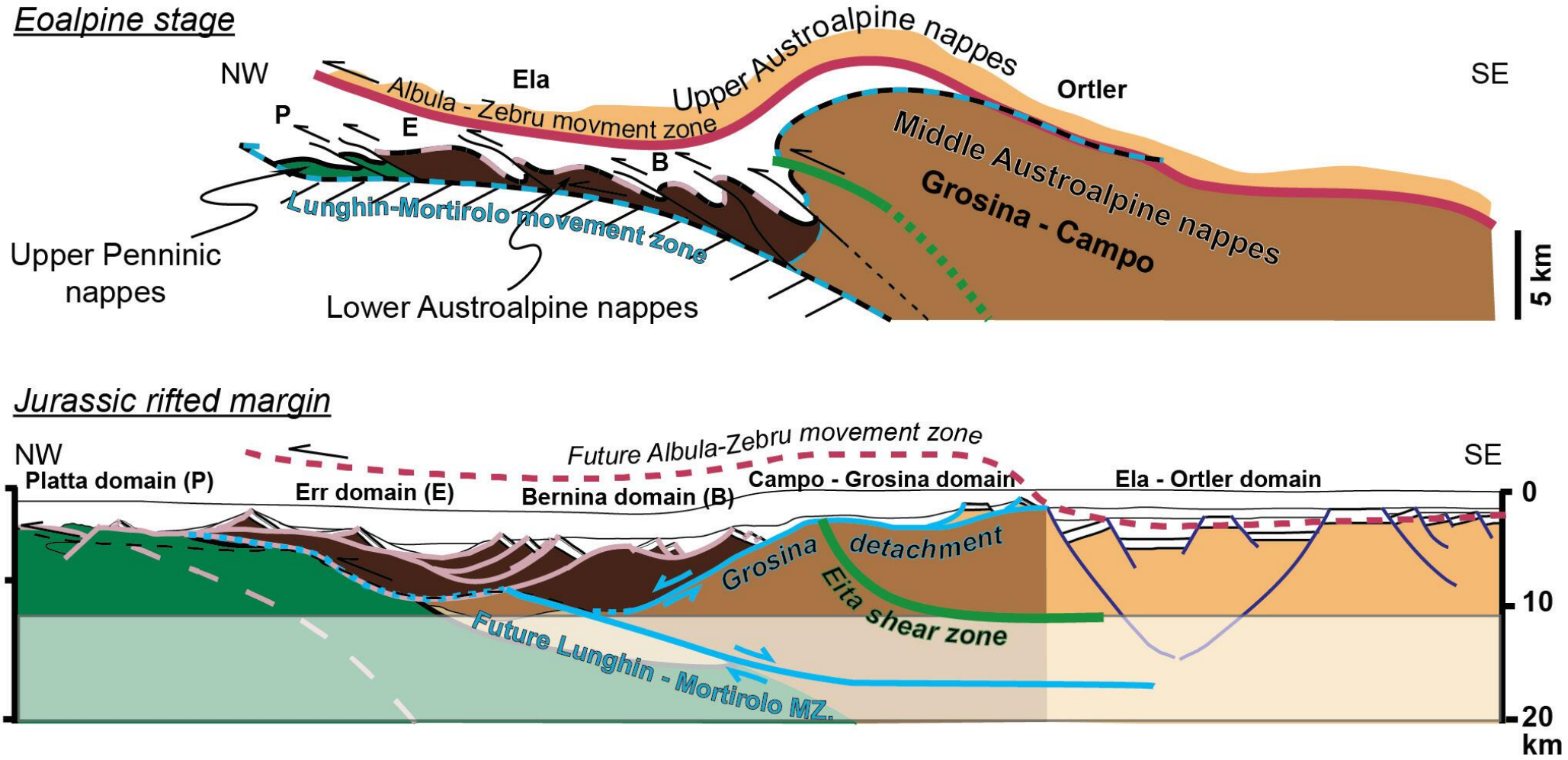

Fig. II.B.9 (modified from Mohn et al., 2011) - Large-scale tectonic restoration of the Austroalpine and Upper Penninic nappes in SE-Switzerland and N-Italy. Top panel: reactivation of the former rift structure during the Eoalpine phase: the Upper Austroalpine, Ela and Ortler nappes are thrust over Middle and Lower Austroalpine nappes. Note the importance of the Albula-Zebru and Lunghin-Mortirolo movement zones in accommodating most of the Alpine deformation, so that the Upper Penninic and Lower and Middle Austroalpine nappes in-between the two movement zones are only moderately overprinted by Alpine deformation. Lower Panel: architecture of the former Adriatic margin.

https://doi.org/10.3301/GFT.2023.02

EXCURSION C
The outer part of the Adriatic hyperextended domain: The Err detachment system at Piz Lavinier, Piz Bardella and Piz Nair (Err Nappe, southeast Switzerland)

ABSTRACT

The Err detachment system belongs to the Err Nappe, which samples the outer part of the Adriatic hyperextended domain. The Err detachment system is comprised of at least three in-sequence long-offset detachment faults, namely, in order of activity, the Err, Jenatsch and Agnel extensional detachment faults. The length of detachment faults and the size of associated breakaway blocks decrease oceanward. The three-dimensional architecture of the Err detachment system was largely controlled by inherited structures and compositional heterogeneities within the basement and pre-rift sediments.

This excursion aims to display: (1) the three-dimensional architecture of the Err detachment system; (2) the sedimentary facies and stratigraphic architecture of supra-detachment basins; (3) the characteristics of fluid flow linked to detachment systems; (4) the importance of inheritance in controlling the architecture of the Err detachment system; and (5) the importance of rift-related structures in controlling Alpine reactivation.

MAIN TAKE-AWAY OF THE EXCURSION

- **Age of rift-related deformation:** the Err detachment system is younger than the Agnelli formation, which is dated Sinemurian (196.5-189.6 Ma), and older than the Radiolarian Cherts (ca. 165 Ma).
- **Deformation style:** essentially controlled by long-offset detachment faults (so-called “hyperextension”). The continental crust was thinned from ca. 10 km to 0 km over a distance of ca. 30 km while significant accommodation space was created.
- **Paleogeographic framework:** extension occurred after the necking phase when the crust was mechanically coupled to the upper mantle; syn-tectonic minerals and pre- to syn-rift sediments show evidence for mantle-reacted fluid contamination.

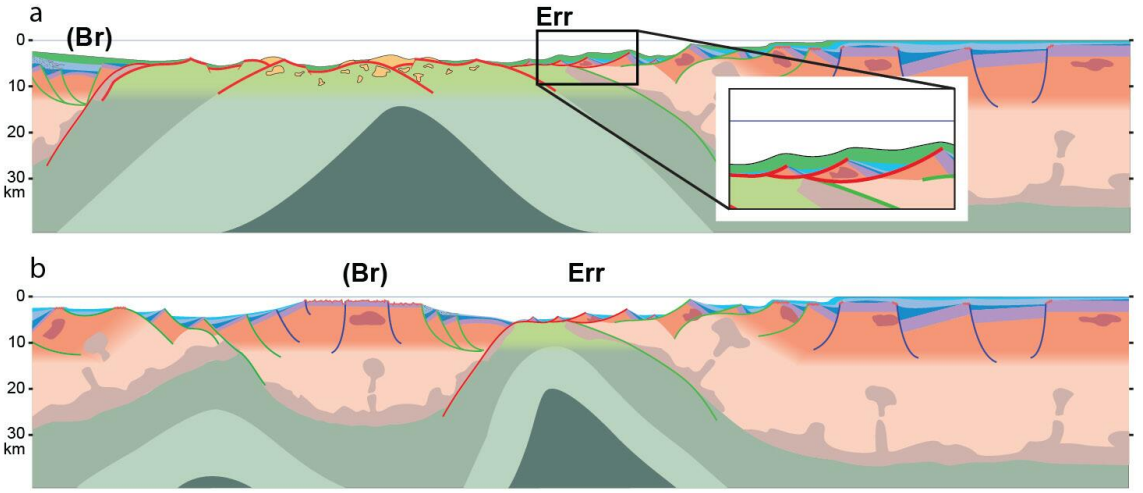

Fig. II.C.0 - Schematic section across the Alpine Tethys rift system showing the position of the Briançonnais (Br) and Err domains during the (a) Middle Jurassic mantle exhumation phase, and (b) late Early Jurassic (Pliensbachian–Toarcian) hyperextension phase (modified from Manatschal et al., 2022).

https://doi.org/10.3301/GFT.2023.02

- **Onset of Alpine reactivation:** Late Cretaceous (Santonian/Campanian).
- **Reactivation style:** essentially thick-skinned tectonics; involves basement and sometimes reactivation of pre-existing faults; also thin-skinned: reactivation of decoupling layers (e.g., Triassic salt).
- **Main remaining questions:** where and how do the detachment faults root at depth?

INTRODUCTION

The Lower Austroalpine Err Nappe samples the outer part of the former Adriatic hyperextended domain. Already in the early 1990s, Froitzheim and Eberli (1990) pointed out the existence of low-angle faults in the Err Nappe, which contrast with the high-angle faults observed in the proximal domain. Mapping of the Err Nappe by Manatschal and Nievergelt (1997), Masini et al. (2011), and Epin and Manatschal (2018) confirmed that the Err detachment system likely formed via a rolling hinge model succession (e.g., Buck and Poliakov, 1998; Wernicke and Axen, 1988). Epin and Manatschal (2018) also highlighted that the Err detachment system is comprised of three successive detachment faults. These faults formed in-sequence with an oceanward progression. They were linked with fluid flow and deposition of syn-tectonic sequences (Manatschal, 1999; Pinto et al., 2015).

ITINERARY

This excursion takes place in the Julier Pass - Piz Neir region (Fig. II.C.1).

Stop 1 (virtual): Piz Lavinier.
Stop 2: Piz Nair. In San Murezzan, park the car in the Sarletta parkaus (P2 on Fig. II.C.1; GPS: 46°29'47.7"N 9°50'33.5"E, i.e., 46.496594, 9.842637). Take the escalators and walk to the funicular station (St Moritz SMBB; GPS: 46°29'55.6"N 9°50'15.2"E, i.e., 46.498779, 9.827546). Take the funicular to the Corviglia station, and from Corviglia take the cable car to Piz Nair. Walk up ca. 50 m to the antenna (GPS: 46°30'23.1"N 9°47'14.6"E, i.e., 46.506403, 9.787398). Enjoy the panoramic view on the Err Nappe. Walk down the path through the sedimentary section back to Corviglia station.
Stop 3: Bardella allochthon; From San Murezzan, take route 27 toward the southeast and then head towards Julier Pass on route 3. Drive over the Julier Pass and park the car on the first parking to the right (P1 on Fig. II.C.1; GPS: 46°28'12.5"N 9°43'03.8"E, i.e., 46.470141, 9.717715). From the parking, cross the road and walk 250 m toward the southwest to the top of the hill. Look west toward Piz Bardella (Viewpoint 1 on Fig. II.C.1; GPS: 46°28'07.2"N 9°42'58.8"E, i.e., 46.468672, 9.716343).
Alternative stop 3: walk up to Fuorcla Cotschna (GPS: 46°38'31.5"N 9°01'26.1"E, i.e., 46.642095, 9.023911; see Fig. II.C.1) where the detachment is exposed and syn-rift sediments onlap directly onto the detachment surface (Fig. II.C.3).

https://doi.org/10.3301/GFT.2023.02

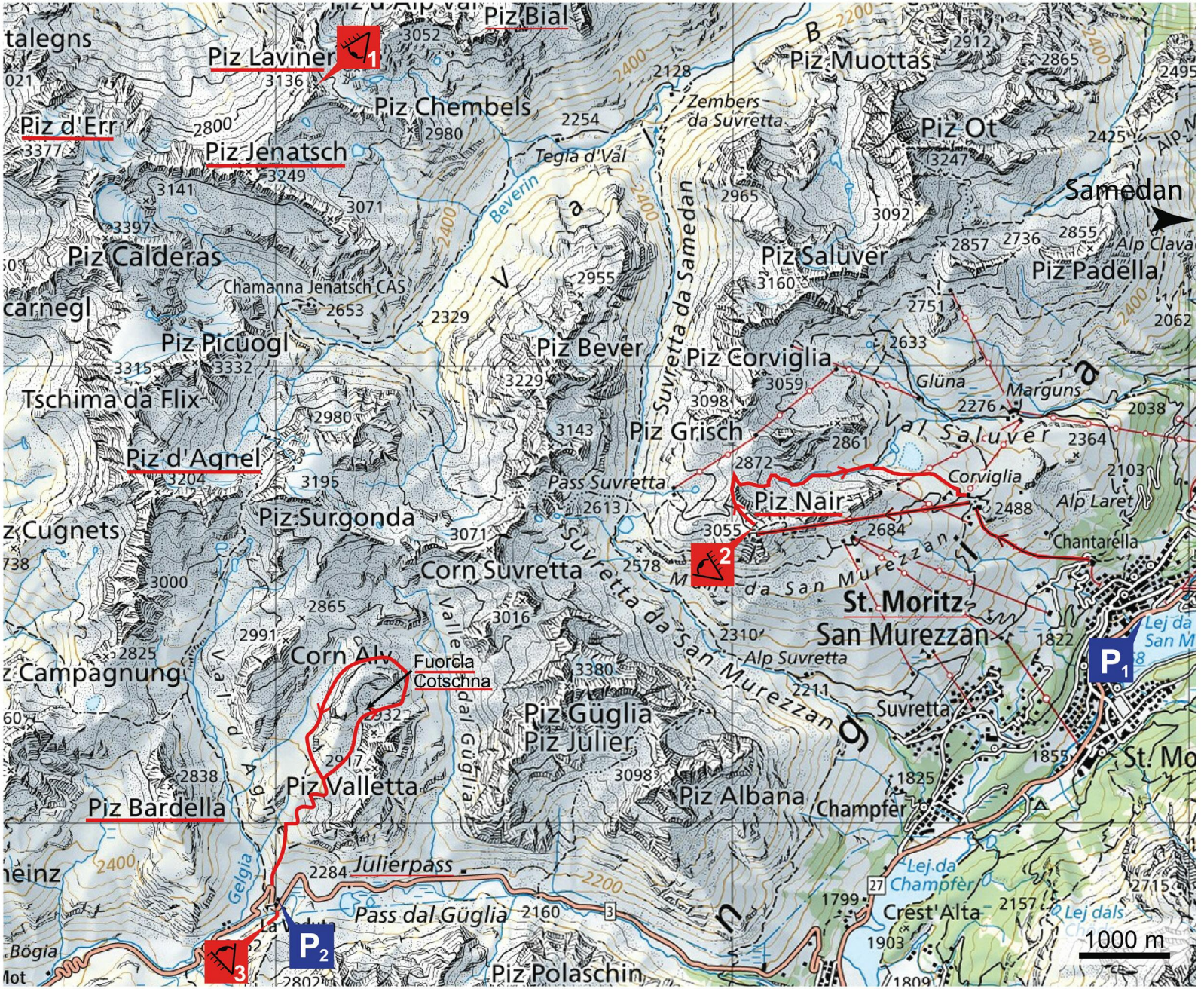

Fig. II.C.1 - Map of the Err detachment system area and route to the viewpoints (background map from https://map.geo.admin.ch/).

https://doi.org/10.3301/GFT.2023.02

Stop 1: Piz Lavinier (virtual: https://sketchfab.com/3d-models/3a19ff2890394f2ba81283c89e1b9d4b; Betlem et al., 2023)

The Err detachment system is exposed over ca. 6 km in the region of Piz d'Err-Piz Bial and, except from a few gaps due to later erosion, it can be traced over more than 200 km^2 (Figs. II.C.2 and II.C.3; Epin and Manatschal, 2018).

Characteristics of the fault zone of the Err detachment system

Sections across the footwall of the Err detachment system exhibit an evolution from an undeformed granitic basement to a damage zone formed of green cemented cataclasites (log in Fig. II.C.4). These cataclasites display angular clasts of variable size cemented by a matrix comprised of quartz, albite, illite, and chlorite (Epin and Manatschal, 2018). Manatschal (1999) and Pinto et al. (2017) showed that albite, illite, and chlorite formed during rifting as a result of an intense fluid-assisted breakdown of feldspars. The lack of quartz mylonite suggests that deformation occurred in the brittle regime, at relatively low temperatures (<300 °C). The main slip surface of the extensional detachment faults, which corresponds to the core zone of the damaged zone, is made of a few cm- to meters-thick layer of indurated black gouges that shows sharp limits to the cataclastic zone (Fig. II.C.4d; Froitzheim and Eberli, 1990; Manatschal and Bernoulli, 1999; Manatschal et al., 2000; Epin and Manatschal, 2018). These black gouges define the upper limit of the footwall.

Where a hanging wall is preserved in the Err detachment system, it is made of continental basement and/or pre-rift sediments that form extensional allochthons. They can be either tilted toward the east (continentward) or the west (oceanward) (Fig. II.C.4a). These fault blocks are typically a few hundred meters to several km across.

Where a hanging wall is missing, syn-rift sediments overly directly the detachment surface (e.g., Fuorcla Cotschna). In that case, black gouges are usually reworked within the tectono-sedimentary breccias that form the base of the overlying syn-tectonic sequence. Manatschal (1999) showed that the black gouges along the Err detachment system display relatively high concentrations in Ni, Cr, and V. These elements of mantle chemical affinity were released during mantle serpentinization (c.f. the Fluids thematic sheet; Appendix A3; Pinto et al. 2015).

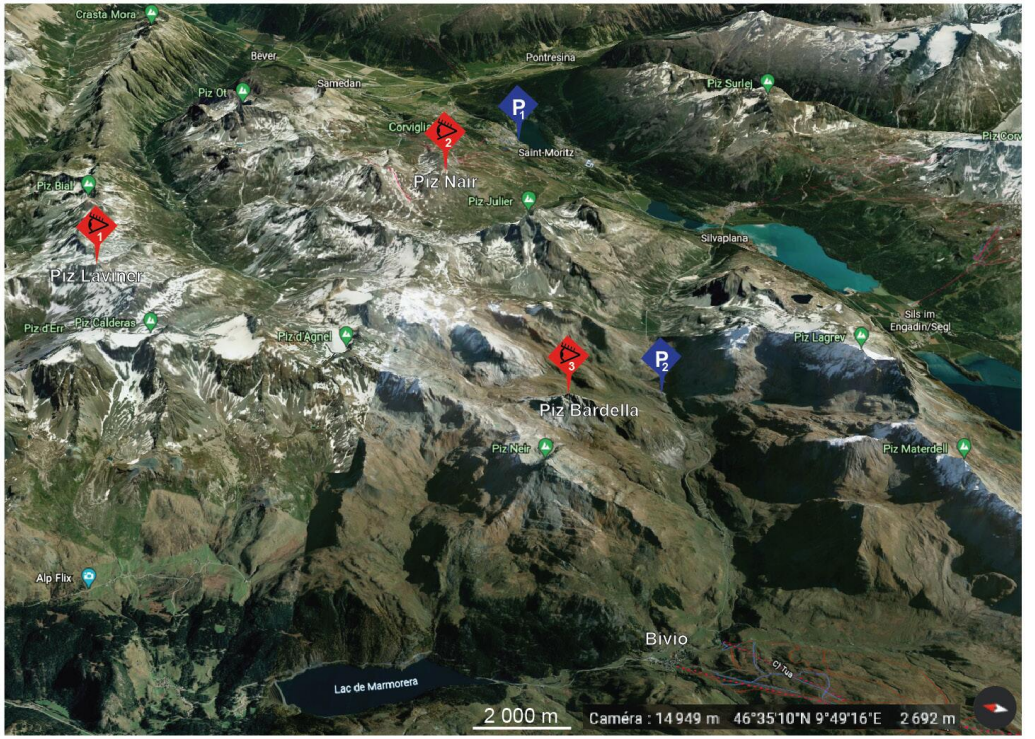

Fig. II.C.2 - View of the Err detachment system area looking eastward (background picture from Google Earth).

https://doi.org/10.3301/GFT.2023.02

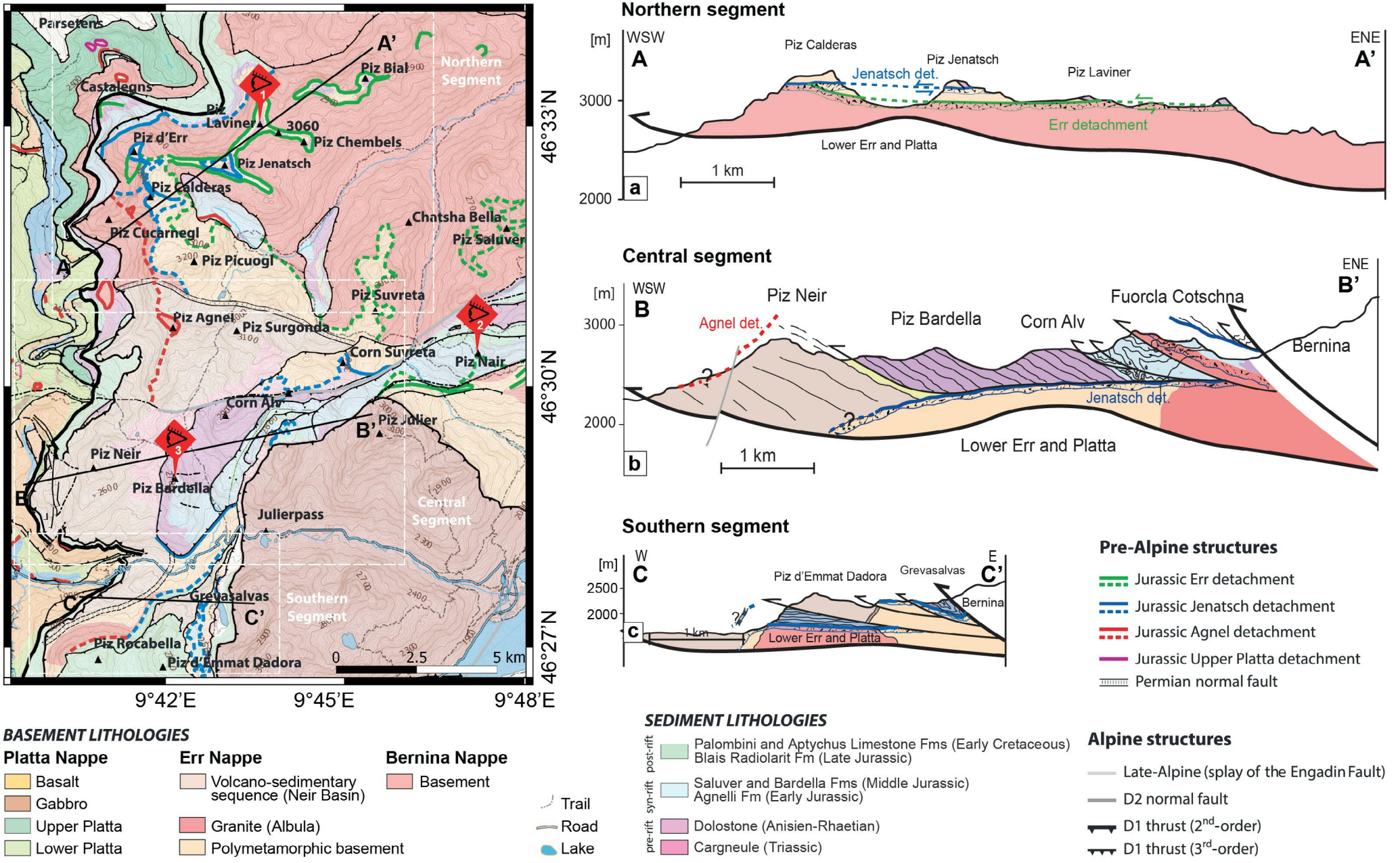

Pre-Alpine structures

- Jurassic Err detachment
- Jurassic Jenatsch detachment
- Jurassic Agnel detachment
- Jurassic Upper Platta detachment
- Permian normal fault

BASEMENT LITHOLOGIES

Platta Nappe
- Basalt
- Gabbro
- Upper Platta
- Lower Platta

Err Nappe
- Volcano-sedimentary sequence (Neir Basin)
- Granite (Albula)
- Polymetamorphic basement

Bernina Nappe
- Basement

- Trail
- Road
- Lake

SEDIMENT LITHOLOGIES

post-rift
- Palombini and Aptychus Limestone Fms (Early Cretaceous) Blais Radiolarit Fm (Late Jurassic)

syn-rift
- Saluver and Bardella Fms (Middle Jurassic) Agnelli Fm (Early Jurassic)

pre-rift
- Dolostone (Anisien-Rhaetian)
- Cargneule (Triassic)

Alpine structures

- Late-Alpine (splay of the Engadin Fault)
- D2 normal fault
- D1 thrust (2nd-order)
- D1 thrust (3rd-order)

Fig. II.C.3 (modified from Epin and Manatschal, 2018) - Geological map of the Err detachment system area and sections through the northern (a), central (b) and southern (c) part. Abbreviation: det.: detachment.

https://doi.org/10.3301/GFT.2023.02

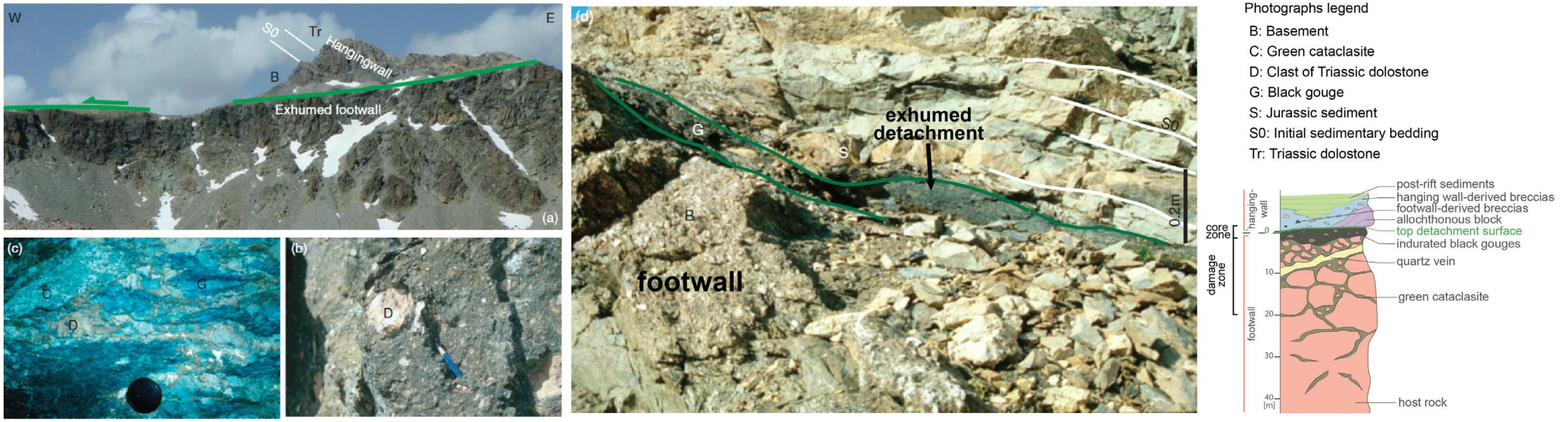

Fig. II.C.4 - Fault rocks and relation to footwall and hanging wall observed along the Err detachment system (modified from Masini et al., 2011; Log modified from Epin et al., 2017). a) View of the Err detachment fault in the Piz Lavinier area. The hanging wall is made of an extensional allochthon, which is comprised of polymetamorphic basement and Triassic dolostones that are tilted to the east (i.e., continentward). The underlying Err detachment (green line) shows a top-to-the-west transport direction; b) clasts of black gouge, green cataclasite and Triassic dolostone reworked into Jurassic sediments (Saluver Fm); c) clast of Triassic dolostone in black gouges; d) Fuorcla Cotschna outcrop. The Err detachment fault is sealed by Jurassic sediments. Green lines highlight the black fault gouges (G) that are onlapped by syn-rift sediments of the Saluver Fm (S). The Saluver Fm was deposited after the Sinemurian Agnelli limestones (ca. 190 Ma) and before the Bathonian radiolarian cherts (ca. 165 Ma).

Stop 2: Piz Nair (46°30'23.1" N - 9°47'14.6" E)

The sedimentary record of hyperextension

Piz Nair lies approximately in the centre of the Samedan Basin, which is floored by the Err detachment system (Fig. II.C.3). At Piz Nair, the basement is topped by cataclasites and locally also gouges, which are directly overlain by Jurassic syn-tectonic sediments (Saluver Fm). The reworking of the gouges and cataclasites within syn-tectonic sediments suggests that an extensional detachment fault was exhumed to the seafloor. From base to top, the Saluver Fm consists in (Fig. II.C.5): massive breccias (Member A of the Saluver Fm); turbiditic sandstones (Member B of the Saluver Fm); and shale-dominated hemipelagic sediments (Member C of the Saluver Fm). The progressive finning upward of the sedimentary deposits in the Saluver Fm indicates a progressive deepening of the basin. Members B and C of the Saluver Fm were essentially deposited during axial basin sedimentation, conversely to Member A.

The Saluver Fm was deposited at least partially at the same time as the Bardella Fm, as indicated by the local interfingering of the two formations. However, in contrast to the Bardella Fm that is exclusively comprised of hanging wall-derived carbonate rocks, the Saluver

https://doi.org/10.3301/GFT.2023.02

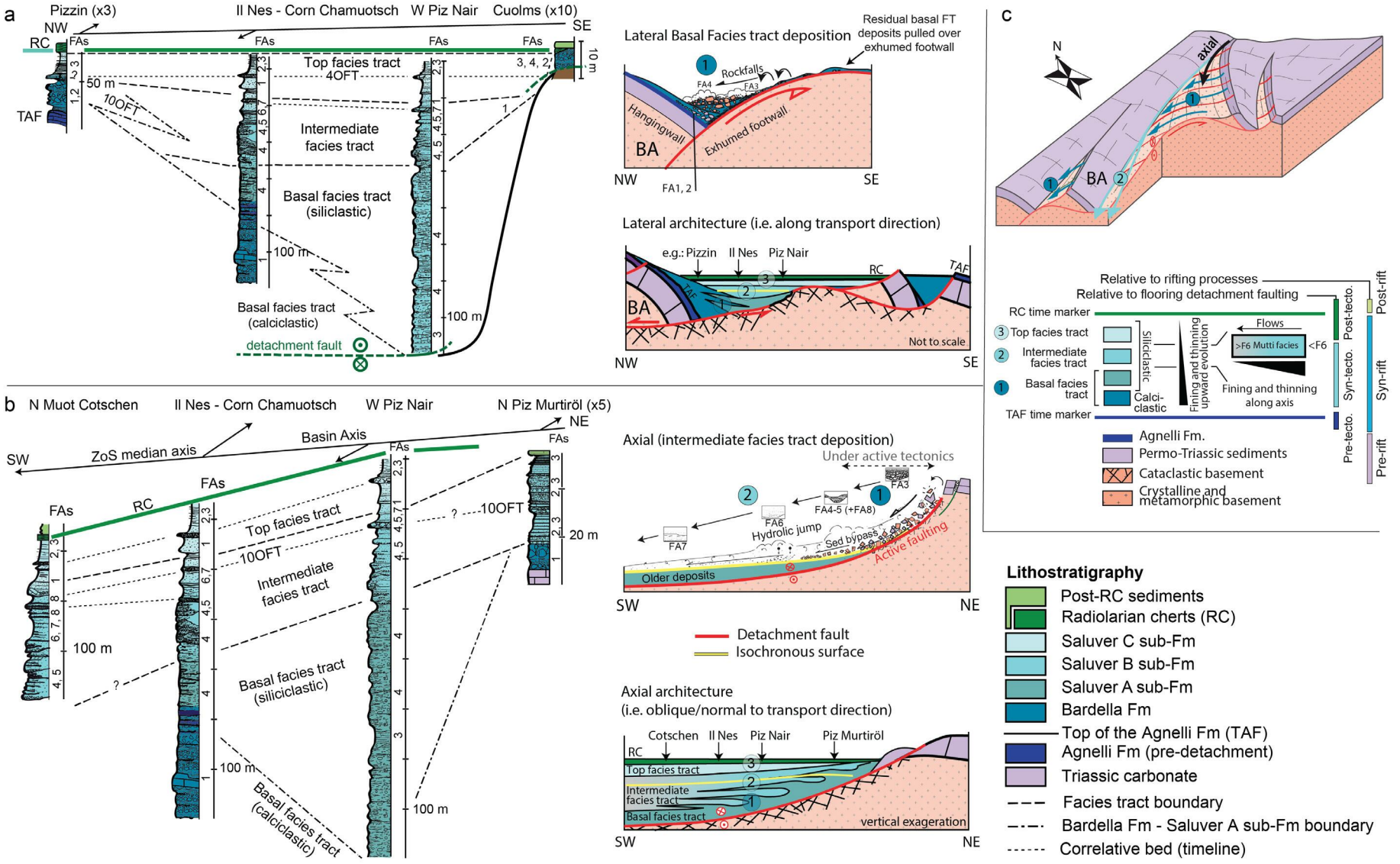

Fig. II.C.5 (modified from Masini et al. 2011) – a) Lithostratigraphic log and schematic sections along a NW–SE transect across the Samedan Basin showing correlations perpendicular to the main axis of the basin (i.e., in transport direction of the detachment fault). Note that the intermediate- and top facies tracts onlap the Bardella allochthon to the NW and the exhumed basement to the SE; b) lithostratigraphic log and schematic sections along a NE–SW transect across the Samedan Basin showing correlations along the basin depot-axis (i.e., in the sediment transport direction); c) 3-dimensional model of the Samedan Basin morphology during its opening (intermediate facies tract deposition); arrows indicate the paleoenvironment directions of basal (1) and intermediate (2) facies tract deposits. Abbreviations: BA, Bardella allochthon block; FAs: Facies Associations, i.e., beds or group of beds with consistent texture, composition and sedimentary structures; FT: Facies tract; OFT: Out of facies tract; TAF: Top of the Agnelli Fm; RC: Radiolarian cherts; tecto.: tectonique; ZoS: Zone of Samedan.

https://doi.org/10.3301/GFT.2023.02

Fm is essentially made of siliciclastic, basement-derived material. Masini et al. (2011) interpreted the different compositions of the Bardella and Saluver Fms to reflect a change from hanging wall-derived to footwall-derived breccias due to increasing extension along the detachment fault underlying the basin (Figs. II.C.5 and II.C.6). The Saluver Fm is overlain by post-rift radiolarian cherts, which are interpreted to represent the Bathonian-Bajocian Bio-Siliceous Event (BB-SiE; Ribes et al., 2019a; cf. section 5.2 of the excursion notes). The last sedimentary sequence corresponds to the Aptychus Limestone Fm, which is interpreted to mark the Tithonian Carbonate Event (Ti-CaE; Ribes et al., 2019a).

Mantle-derived fluids linked to hyperextension

Crustal thinning and mantle exhumation during hyperextension were achieved via a series of extensional detachment faults (Epin and Manatschal, 2018). These processes are intimately linked with fluid migration, which leads to changes in the mineralogy and chemistry of the related mantle, crustal, and sedimentary rocks. Using field observations and analytical methods, Manatschal et al. (2000) and Pinto et al. (2015) showed that Cr, Ni, V, and Mn, together with some major elements (Si, Fe, and Mg), were transported by fluids that were channelized along the extensional detachment faults. These fluids first reacted with the encompassing fault rocks (crust and/or mantle), before they reached the seafloor, where they reacted with surrounding syn-tectonic sediments (see Fig. II.C.6a).

In the early stages of hyperextension, mantle-reacted fluids released their element surplus directly within the syn-tectonic sediments they percolated through (e.g., Member A of the Saluver Fm). In the later stages of hyperextension, over-saturated fluids reached the seafloor, and their transported elements surplus were released within seawater. As a consequence, these elements were absorbed by post-tectonic sediments (e.g., Member C of the Saluver Fm).

The significant enrichment of syn-rift sediments in mantle-derived elements suggests that a significant amount of serpentinization occurred beneath the hyperextended continental crust and that mantle-reacted fluids modified the chemical composition of the local sediments and seawater (Fig. II.C.6b). It also shows that mantle serpentinization initiated before the mantle was exhumed to the seafloor (Fig. II.C.6a; Pinto et al., 2015).

Stop 3: The Bardella Allochthon (46°28'07.2" N - 9°42'58.8" E)

Compared to the Piz Nair, the Bardella site displays an extensional allochthon made of (from the bottom up): a few hundred meters of pre-rift Triassic carbonates (Hauptdolomit and Kössen Fms); and ca. 40 m of Lower Jurassic Agnelli Fm (Fig. II.C.7). Despite the Agnelli Fm is syn-rift in age, it lies in a pre-tectonic position in the Err Nappe.

The Agnelli Fm is capped by a ferromanganese crust, which is interpreted to represent the Toarcian Oceanic Anoxic Event (T-OAE; Ribes et al., 2019a). Thus, in the Err Nappe, the T-OAE marker lies at the top of the pre-tectonic sequence, while it lied at the top of the syn-tectonic

https://doi.org/10.3301/GFT.2023.02

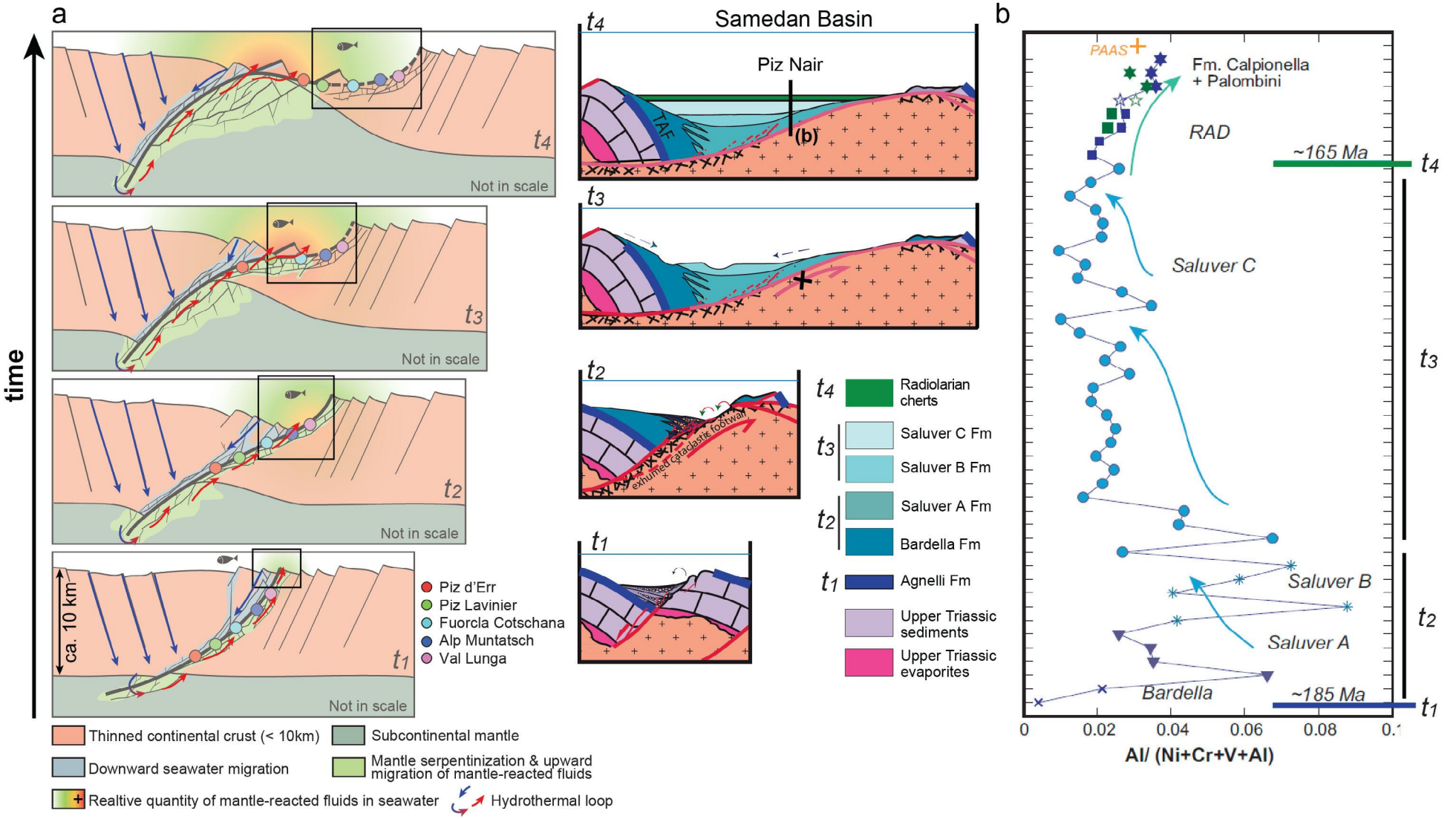

Fig. II.C.6 (modified from Masini et al. 2011 and Pinto et al. 2015) – a) Progressive gain of Ni-Cr-V along the Err detachment fault (left hand-side panel) with a close up showing the tectono-sedimentary evolution of the Samedan Basin (right hand-side panel). The panels to the left show the concept of the progressive increase of serpentinized area and degree of serpentinization that are linked to the detachment fault evolution. This increase is registered along the Err Detachment (coloured dots). The light blue zone is the downward migration of the seawater along normal faults in the hanging-wall. Seawater reaches the mantle, triggering its serpentinization, which produces the mantle-reacted fluids that migrate upward (light green zone). In t1 stage, deformation is distributed along a high-angle normal fault and a set of fractures. From t2 to t4, deformation is localized along the detachment fault.; b) Ni-Cr-V trends from the sedimentary rocks (from Pinto et al., 2015). Samples are from Piz Nair and Murtiröl in the Err nappe (blue symbols). Samples from the Platta Nappe (dark green symbols) are from Bracciali et al. (2014) and the reference value of PAAS (orange cross) are from Condie (1993). Abbreviations: PAAS: Post-Archean Australian Shale standard; RAD: Radiolarian cherts; t: time; TAF: Top of the Agnelli Fm.

https://doi.org/10.3301/GFT.2023.02

sequence in the Bernina Nappe and belonged to the post-tectonic sequence in the Ortler Nappe (cf. Excursions B and A, respectively; see also the Stratigraphy thematic sheet).

The Bardella allochthon overlies exhumed basement. The local presence of evaporitic remnants (cargneules) between the basement and overlying pre-rift sediments indicates that this contact was a décollement level (Figs. II.C.7 and II.C.8). Where evaporitic remnants are lacking, the contact between the basement and overlying pre- to syn-rift sediments is characterized by cataclasites and black gouges, which are typical fingerprints of Jurassic detachment faults (see Fuorcla Cotschna outcrop, Fig. II.C.4d).

The Bardella allochthon is overlain by syn-tectonic Jurassic sediments of the Bardella Fm (Figs. II.C.7 and II.C.8). The Bardella Fm is essentially comprised of stacking of 1-5 m-thick beds of clast-supported, unsorted breccias. These breccias are exclusively comprised of Triassic dolostones, and, in rare cases, of Agnelli limestones. The Bardella Fm is interpreted to result from debris flow processes. A finning-up trend of the sedimentary deposit is locally observable (breccias calcarenite calcilutites). Up-section, Masini et al. (2011) recognized a 90° counterclockwise rotation of the paleocurrent. This observation may be explained by a change from gravitational sediment transport along slopes (debris-flows) to axial turbiditic currents (Figs. II.C.5 and II.C.6).

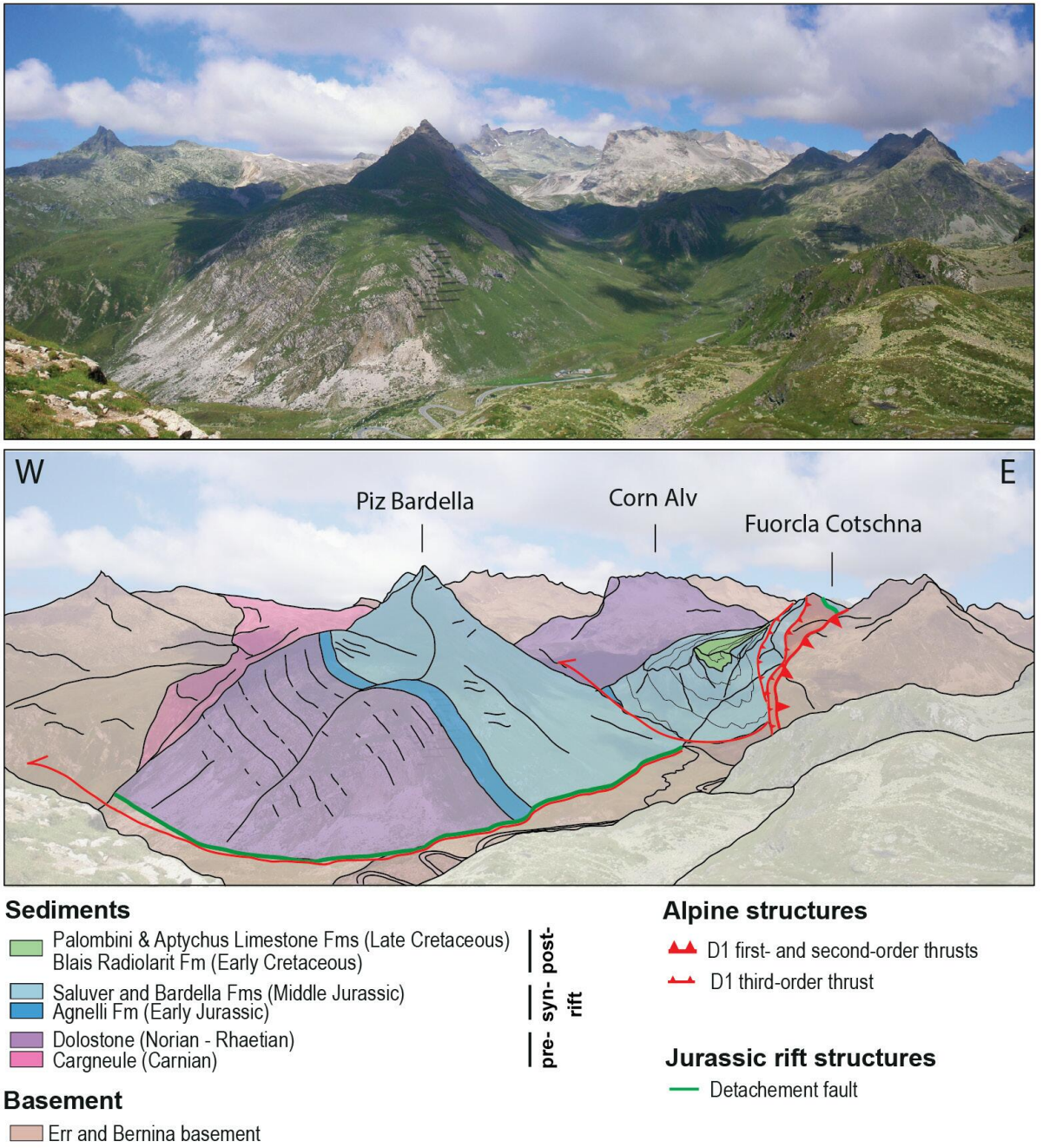

Fig. II.C.7 - Panorama of the Piz Bardella–Fuorcla Cotschna region (from Epin et al., 2017).

https://doi.org/10.3301/GFT.2023.02

DISCUSSION

From outcrop observations to a tectono-stratigraphic interpretation

The challenge to upscale outcrop observations to a tectono-stratigraphic interpretation is a long-standing problem and has been tackled by numerous studies, including litho-stratigraphic and sequence-stratigraphic approaches. At modern rifted margins, because of the lack of direct observations and the scarcity of drill hole data in distal domains, syn-tectonic sediments were often assumed to be of the same age along the dip of the entire margin (i.e., it was assumed that syn-rift equals syn-tectonic; see section 2.2 of the excursion notes for more details and Chenin et al., 2022 for a more comprehensive review). The Piz Bardella outcrop played a major role in the change of paradigm toward the modern view of a localizing rifting process. By dating the top of the Agnelli Fm with ammonites and correlation of this time horizon, which coincides with the T-AOE (Fig. II.C.8a), along the dip of the fossil Adriatic margin, Ribes et al. (2019a) demonstrated that the syn-tectonic sequence becomes younger in increasingly distal settings. Indeed, while the syn-tectonic sequence is older than the T-AOE in the proximal domain (e.g., Il Motto; see Fig. II.A.6a in excursion A), it post-dates the T-OAE at Piz Bardella (Fig. II.C.8a). A more comprehensive description of the margin-scale tectono-stratigraphic evolution is provided in the Tectono-stratigraphy thematic sheet and more extensively reviewed in Ribes et al. (2019a) and Manatschal et al. (2022).

Three-dimensional architecture of the Err detachment system

Mapping of the Err detachment system allowed defining three successive detachment faults that formed in-sequence with an oceanward younging and sense of shear. The footwall of the Err detachment system is mainly formed by the Albula granite, a late Variscan granite that was emplaced at upper crustal levels into polymetamorphic Palaeozoic gneisses and schists. In contrast, the rocks of the hanging wall are more heterogeneous (Fig. II.C.4e): in the northern and southern parts of the Err region the hanging wall is made of the polymetamorphic basement; in contrast, the central part of the hanging wall consists dominantly of volcano-sedimentary sequences that belong to a former Permian basin (Fig. II.C.10d). This variable lithology has important implications in the localization and evolution of the detachment system (Fig. II.C.9a). For instance, the Jenatsch detachment seeded at the base of the Permian basin so that the footwall of the Jenatsch detachment is made of the Palaeozoic basement and its hanging wall of a Permian volcano-sedimentary sequence (Fig. II.C.10d-h). Upper Triassic evaporitic sequences within the pre-rift succession also controlled the style of Jurassic extension as they acted as decollement layers (Fig. II.C.9e).
In the north of the Err region (Fig. II.C.9c), three in-sequence extensional detachment faults can be identified: the Err, Jenatsch, and Agnel detachments. Each of these detachments is crosscut by the next one with an angle of 20-30° (i.e., the footwall of a given detachment corresponds to the hanging wall of the next detachment). Both the size of the breakaway blocks and the length of the detachment faults decrease oceanward (Figs. II.C.10a and II.C.10b).

https://doi.org/10.3301/GFT.2023.02

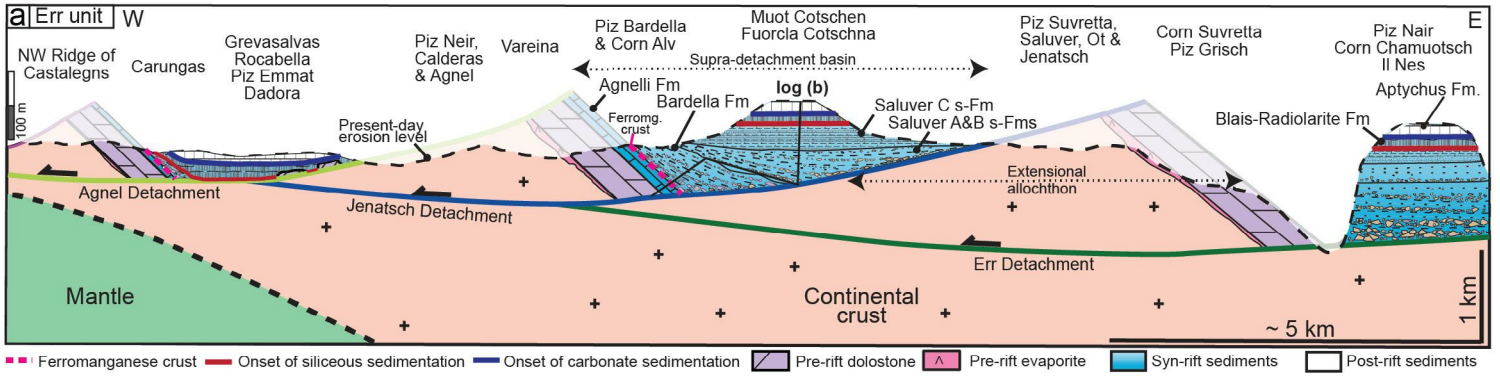

b Representative sedimentary succession of Fuorcla Alva (Piz Bardella & Fuorcla Cotschna) - Err unit

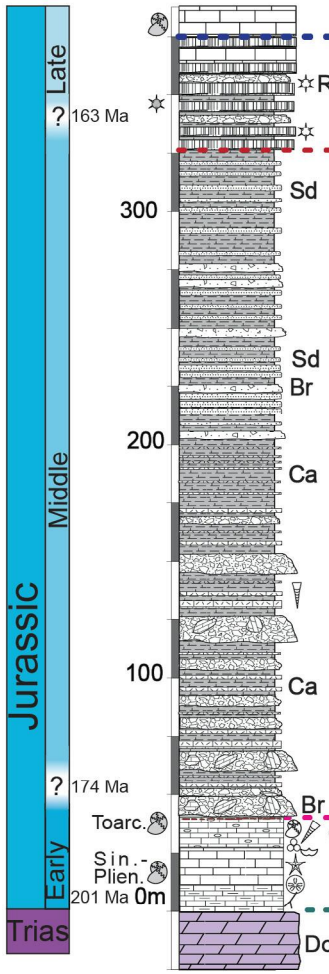

Aptychus Limestone Fm

T-CaE

Ra - Radiolarite: Blue, greenish and reddish radiolarite beds including chert and radiolaria-rich intervals.
Blais Radiolarit Fm (≈ 20 m)

BB-SiE

Sd - Sandstone: interleaved black, red, green and brown shales and thin distal turbidite beds with subordinate conglomerates and mature arkosic beds.
Member C of the Saluver Fm (≈ 40 m)

Br - Breccias and Sd - Sandstone: Matrix-supported breccias and reddish fine-grained sandstone consisting of the resedimented Triassic strata and the reworked basement with an important contribution of the Permo-Triassic Chazfora source. The size of clasts decreases upsection. Matrix of breccias consists of red arkoses.
Member B of the Saluver Fm (≈ 100 m)

Br - Breccias and Ca - Calcarenites: Clast-supported breccias constituted by angular components of the Triassic Hauptdolomit and Kössen Fms, the Jurassic Agnelli Fm and crystalline components. Breccias are interbedded with gray to brown marl/shales and calcarenites.
Bardella Fm and Member A of the Saluver Fm (≈ 100 - 300 m)

T-OAE

L - Limestone and Ca - Calcarenites: At the base dark thin-bedded spiculitic limestones, then 20 m of gray massive limestone capped by a 10 m thick body of calcarenite. Beds generally contain siliceous spiculae, echinoderms and crinoids debris. The upper limit is capped by a belemnite-rich horizon that predates the deposition of a ferromanganese hardground which contains a rich encrusted ammonite fauna.
Agnelli Fm (≈ 40 m)

R-BSR

Kössen (≈ 200 m) & Hauptdolomit (≈ 1500 m) Fms
Do - Dolostone: poor in fossils, deposited on a large platform with wide tidal flat areas and closed internal lagoons.

Fig. II.C.8 – a) Palinspastic reconstruction across the Err Nappe from Ribes et al. (2019a). Note that the scale for syn-rift deposits is not the same as that for basement and pre-rift deposits; b) representative sedimentary succession of the distal hyperextended domain from Ribes et al. (2019a). Abbreviations: R-BSR: Rhaetian Base of the Syn-Rift; T-OAE: Toarcian Oceanic Anoxic Event; BB-SiE Bajocian–Bathonian bio-Siliceous Event; T-CaE: Tithonian Carbonate Event (see section 5.2 of the excursion notes). Plien.: Pliensbachian; Sin.: Sinemurian; Toarc.: Toarcian.

https://doi.org/10.3301/GFT.2023.02

In the central part (Fig. II.C.9d), only two in-sequence detachments can be identified: the Jenatsch and Agnel detachments.
In the south (Fig. II.C.9e) a single detachment surface covered by post-rift sediments can be identified. This detachment surface has been interpreted to correspond to the merging of the Jenatsch and Agnel detachments (Epin and Manatschal, 2018).

Anatomy of a supra-detachment basin: the example of the Samedan Basin

The Samedan Basin formed as a result of the Err detachment activity. Remnants of the Samedan Basin extend from Piz Bardella to the town of Samedan and further east to Murtiröl (Figs. II.C.1 and II.C.11; Masini et al., 2011, 2012).
Based on structural and stratigraphic relationships and on the restoration of Alpine sections (Fig. II.C.11), Masini et al (2011) reconstructed the tectono-stratigraphic architecture and history of the Samedan Basin (Fig. II.C.12).

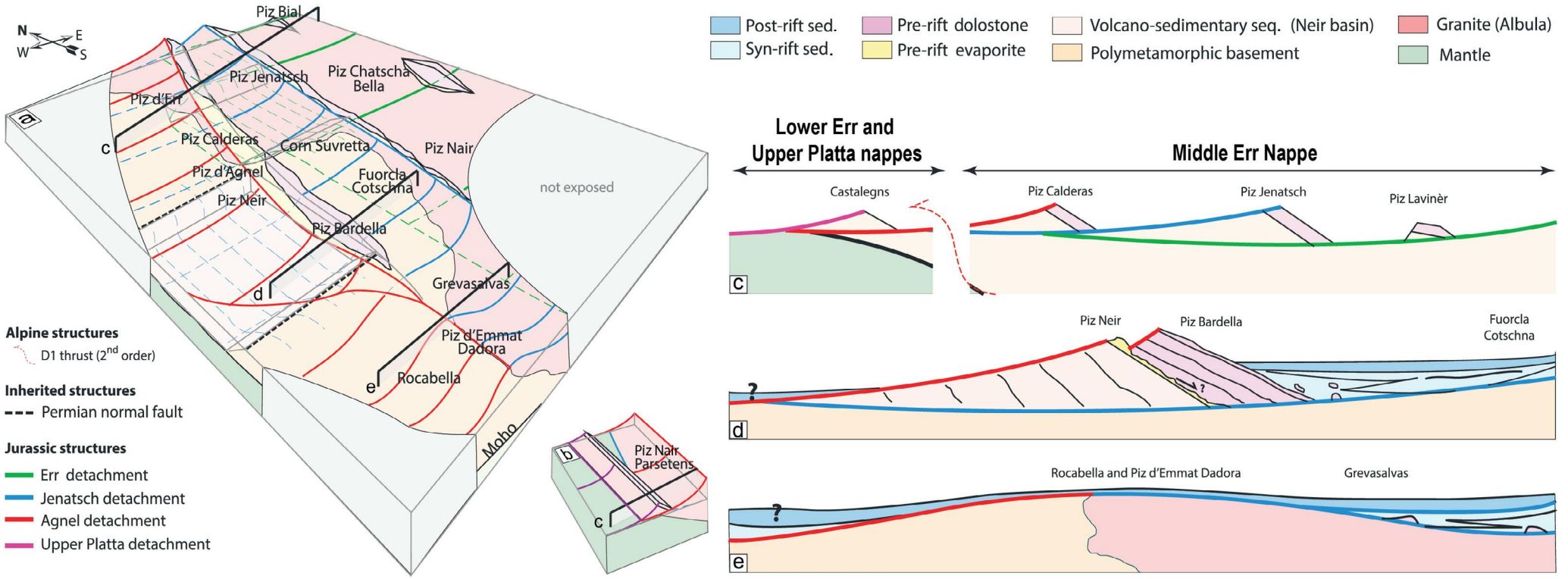

Fig. II.C.9 (modified from Epin and Manatschal (2018) – a) Restored block of the Err Nappe showing the location of the different detachment faults; b) restored block of the Lower Err and Upper Platta nappes showing the transition between the hyperextended and exhumed mantle domains. c-d) and (e) simplified restored sections through the Err Nappe (see panels a and b for location). Abbreviations: sed.: sediments; seq.: sequence.

https://doi.org/10.3301/GFT.2023.02

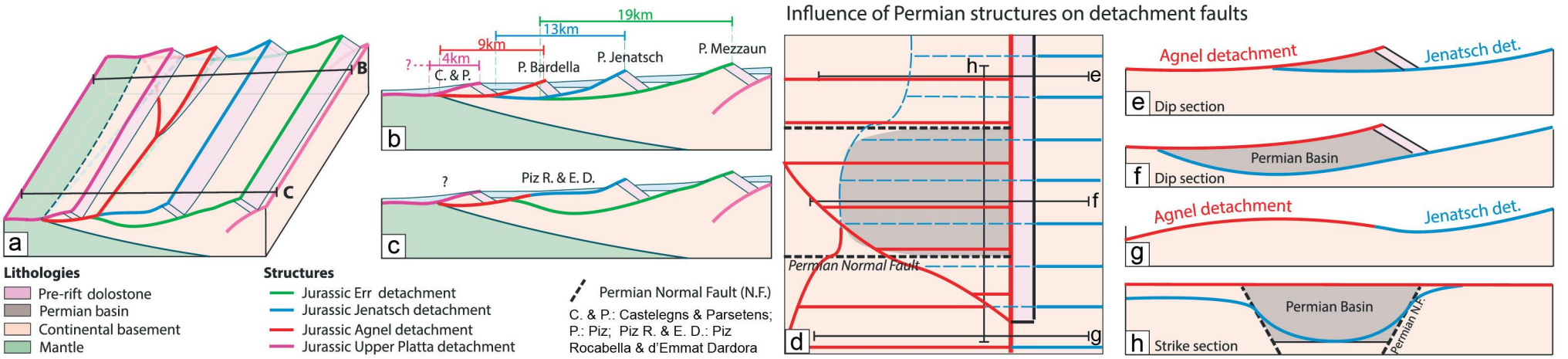

Fig. II.C.10 (modified from Epin and Manatschal, 2018) - a) Schematic block representing the lateral extent of allochthonous blocks related to the Err, Jenatsch and Agnel detachments of the Err detachment system; note: the pink detachment to the left corresponds to the Upper Platta detachment, which is responsible for mantle exhumation to the seafloor. It does not belong to the Err Nappe but to the more distal Platta domain; b-c) sections through the schematic block showing the lateral variability of allochthonous blocks; d) schematic map of the Jenatsch and Agnel detachment faults and their relation to the Permian basin (see sections e, f, g and h).

The Samedan Basin initiated as a classical high-angle fault-bounded basin (Figs. II.C.12b and II.C.12c). Continued extension on the high-angle fault led to the flattening of its inactive portion as it moved away (roll-over), and to the exhumation of relatively deep basement levels at a low angle to the seafloor. At this stage, the initial high-angle fault had become a long-offset extensional detachment fault where syn-tectonic sediments were deposited directly onto exhumed basement (Fig. II.C.12d).

Alpine reactivation

The Err Nappe underwent little metamorphic imprint during the Eo-Alpine orogeny (late Cretaceous closure of the northern Meliata-Vardar domain; cf. section 3.3. of the excursion notes). It was also little reactivated during the Eocene-Oligocene N-S shortening because it was in the neutral zone located above the singular point that separates the pro-wedge from the retro-wedge.
At present, the Err Nappe is sandwiched between the Bernina Nappe (above) and the Platta Nappe (below) along second-order D1 Alpine thrusts (Epin et al., 2017). The Err Nappe itself is essentially affected by third-order D1 Alpine thrusts (Fig. II.C.13). Most of these thrusts seed at lithological contacts between basement and sediments or between the basement and serpentinized mantle, suggesting that most of the Alpine orogen complexity is inherited from the architecture of the former Alpine Tethys margins (Fig. II.C.13; Epin et al. 2017).

https://doi.org/10.3301/GFT.2023.02

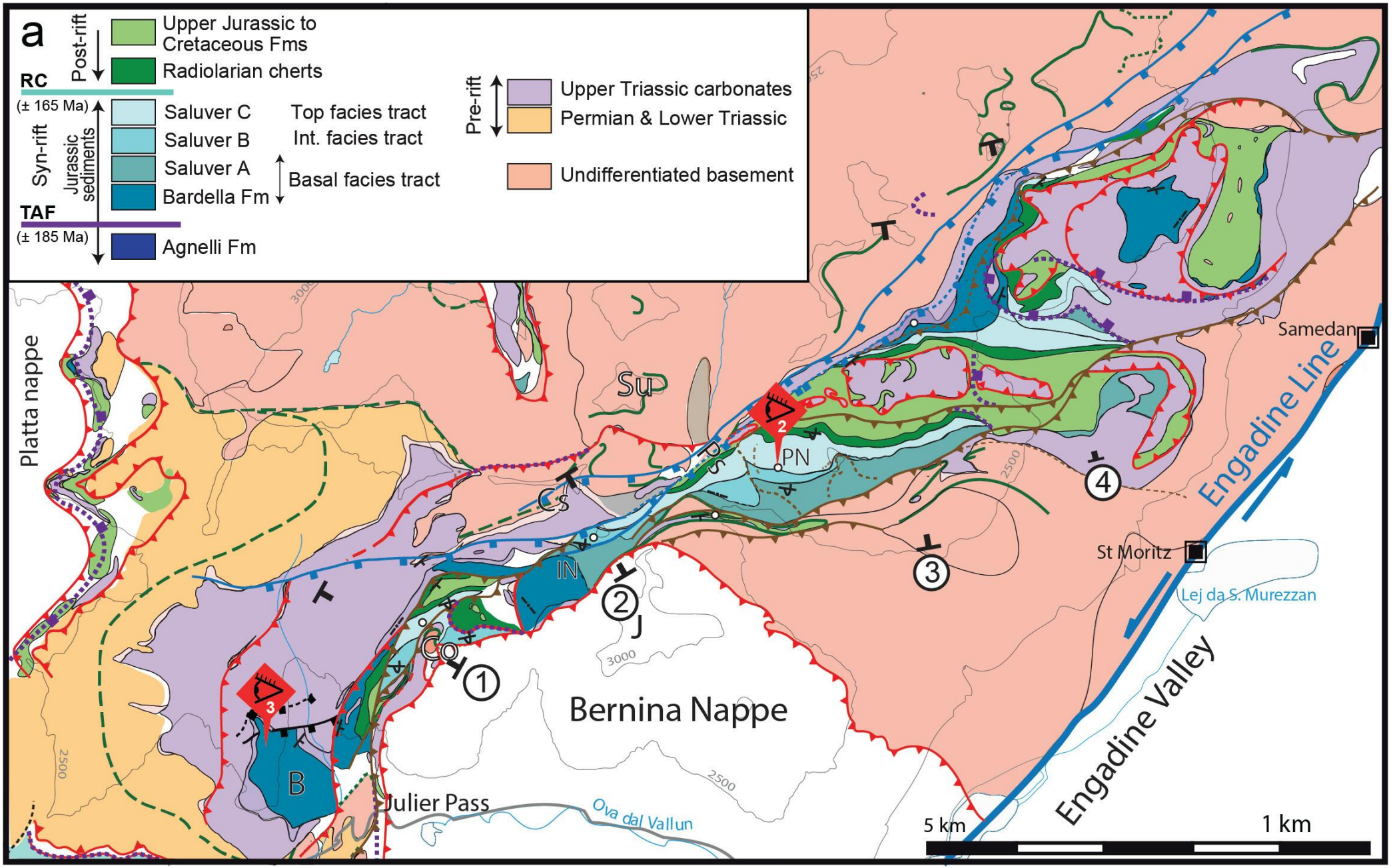

Fig. II.C.11 (modified from Masini et al., 2011) – a) Geological map of the Err Nappe including the Samedan Basin.

https://doi.org/10.3301/GFT.2023.02

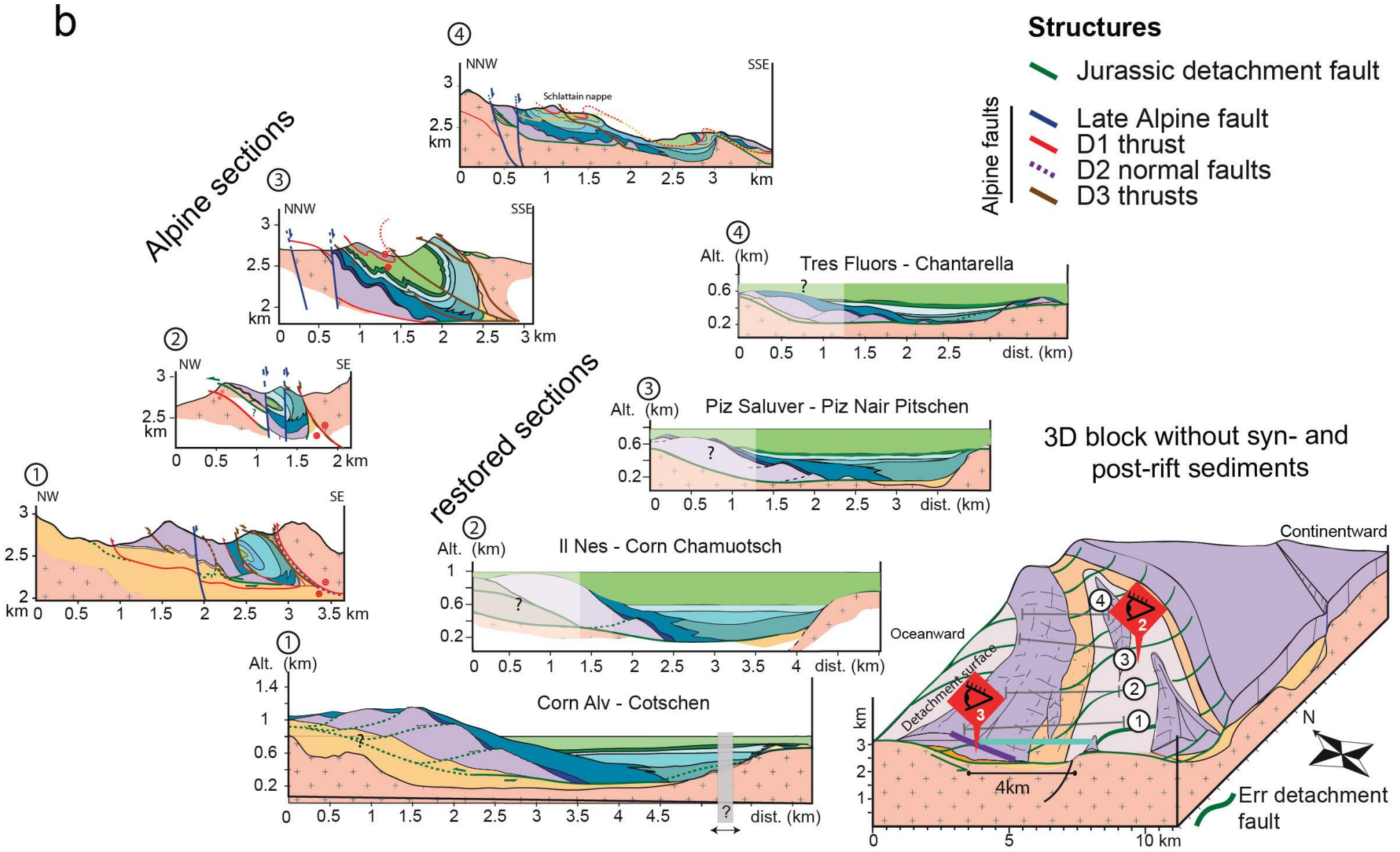

Fig. II.C.11 (modified from Masini et al., 2011) - b) present-day transects, their pre-Alpine restoration and a three-dimensional restoration of the supra-detachment Samedan Basin. Abbreviations: B, Piz Bardella; Co, Fuorcla Cotschna; Cs,Corn Suvretta; IN, Il Nes; Int. : Intermediate J, Piz Julier; Pn, Piz Nair; Ps, Pass Suvretta; RC: Radiolarian Cherts; sed.: sediments; Su, Piz Suvretta ; TAF : Top of the Agnelli Fm.

https://doi.org/10.3301/GFT.2023.02

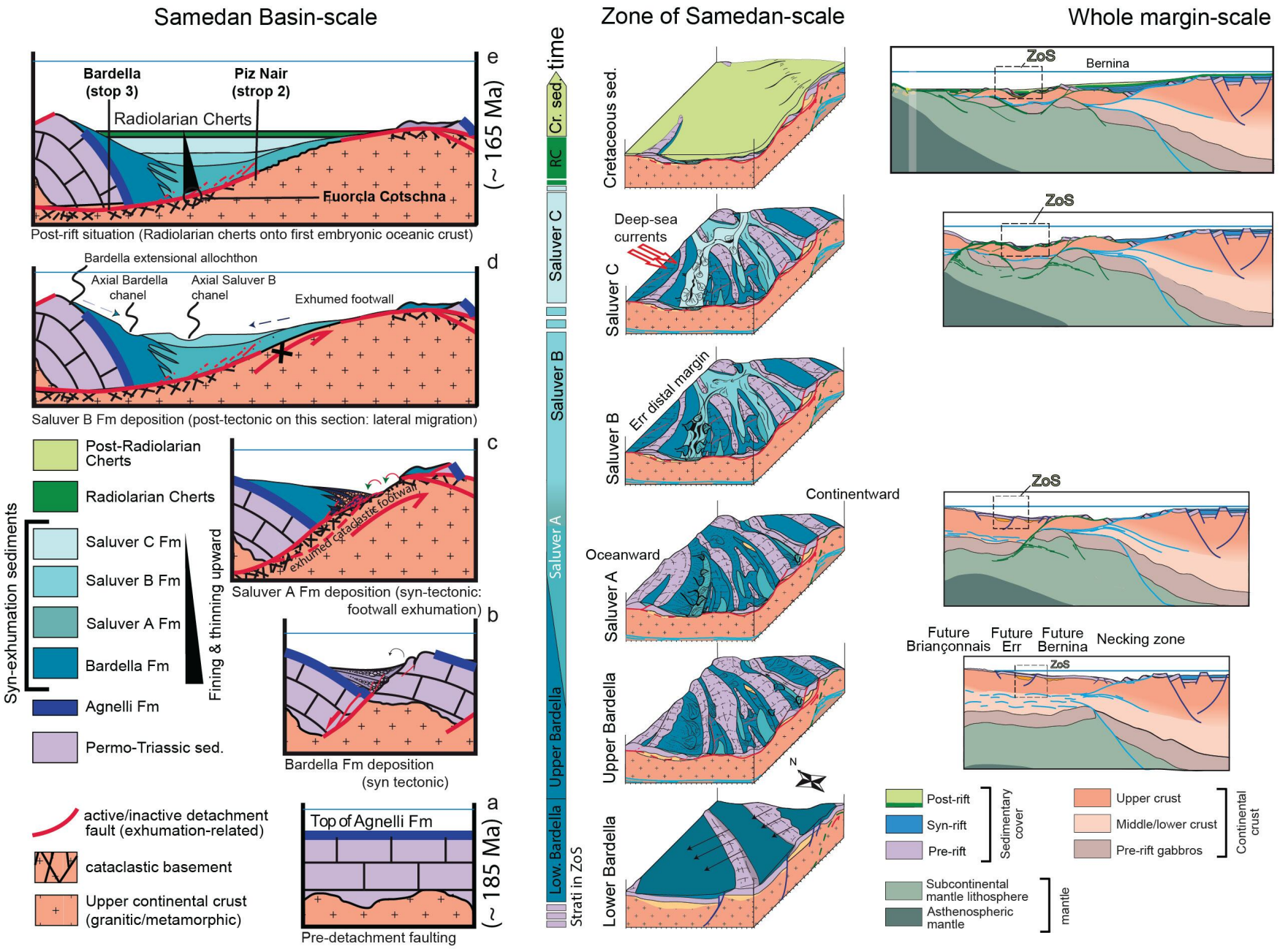

Fig. II.C.12 - Schematic evolution of the Samedan supra-detachment basin in 2D, 3D and its location within a margin-wide framework (modified from Masini et al., 2011). Abbreviations: Cr. Cretaceous; RC: Radiolarian Cherts; sed.: sediments; ZoS: Zone of Samedan.

https://doi.org/10.3301/GFT.2023.02

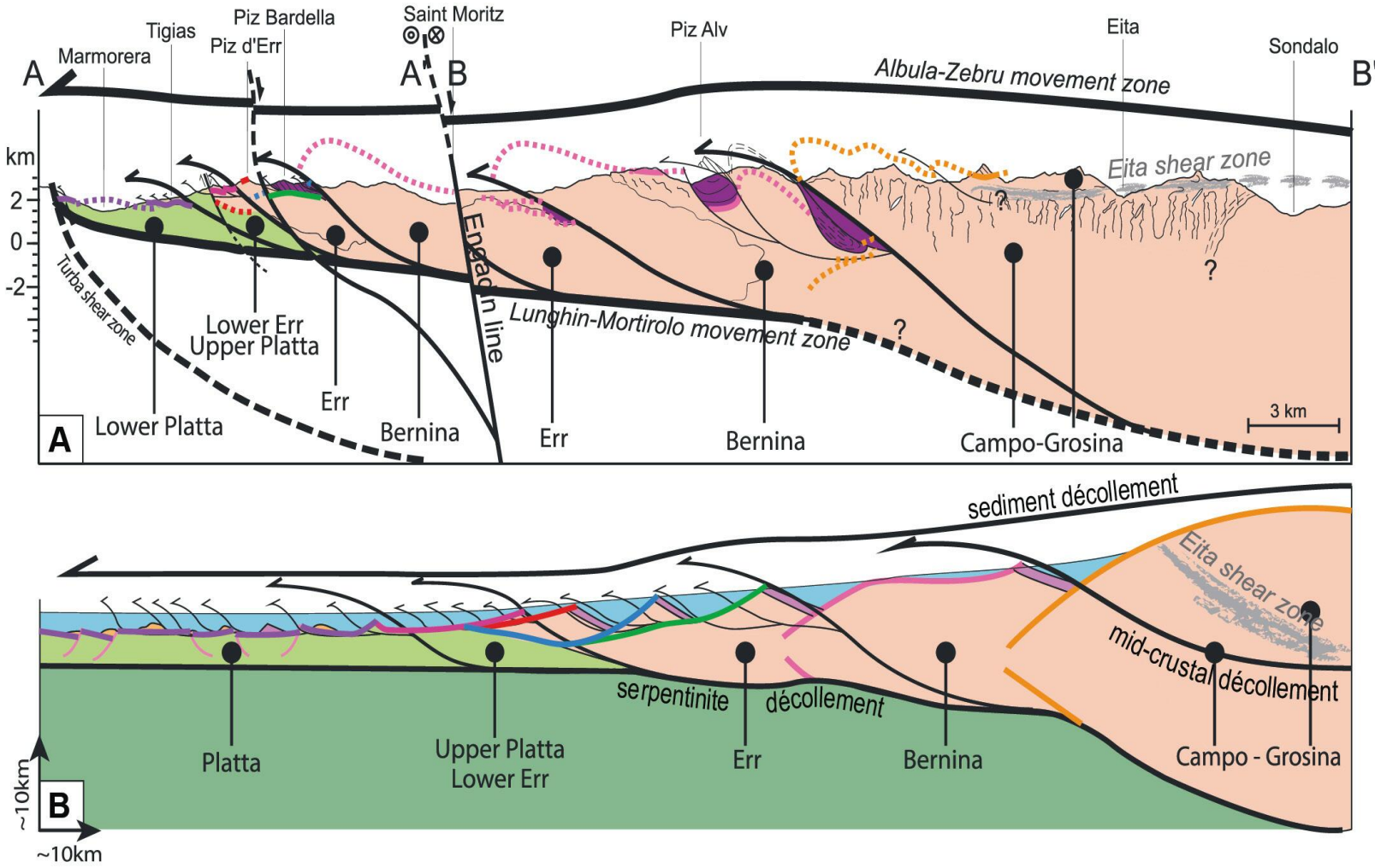

Cover
- basalt
- syn- and post-rift sediments
- pre-rift sediments

Basement
- continental crust
- serpentinised mantle
- mantle

Alpine structures
- D1 first and second order thrusts
- D1 third order thrust

Jurassic rift structures
younger
- Upper Platta detachment
- Agnel detachment
- Jenatsch detachment
- Err detachment
- Bernina detachment
- Grosina detachment

Normal faults

Fig. II.C.13 (modified from Epin et al., 2017) - Schematic sections through (a) the present-day Alpine nappe stack; and (b) the former distal Adriatic margin. Note how the architecture of the former Adriatic margin controlled the architecture of the Alpine nappe stack.

https://doi.org/10.3301/GFT.2023.02

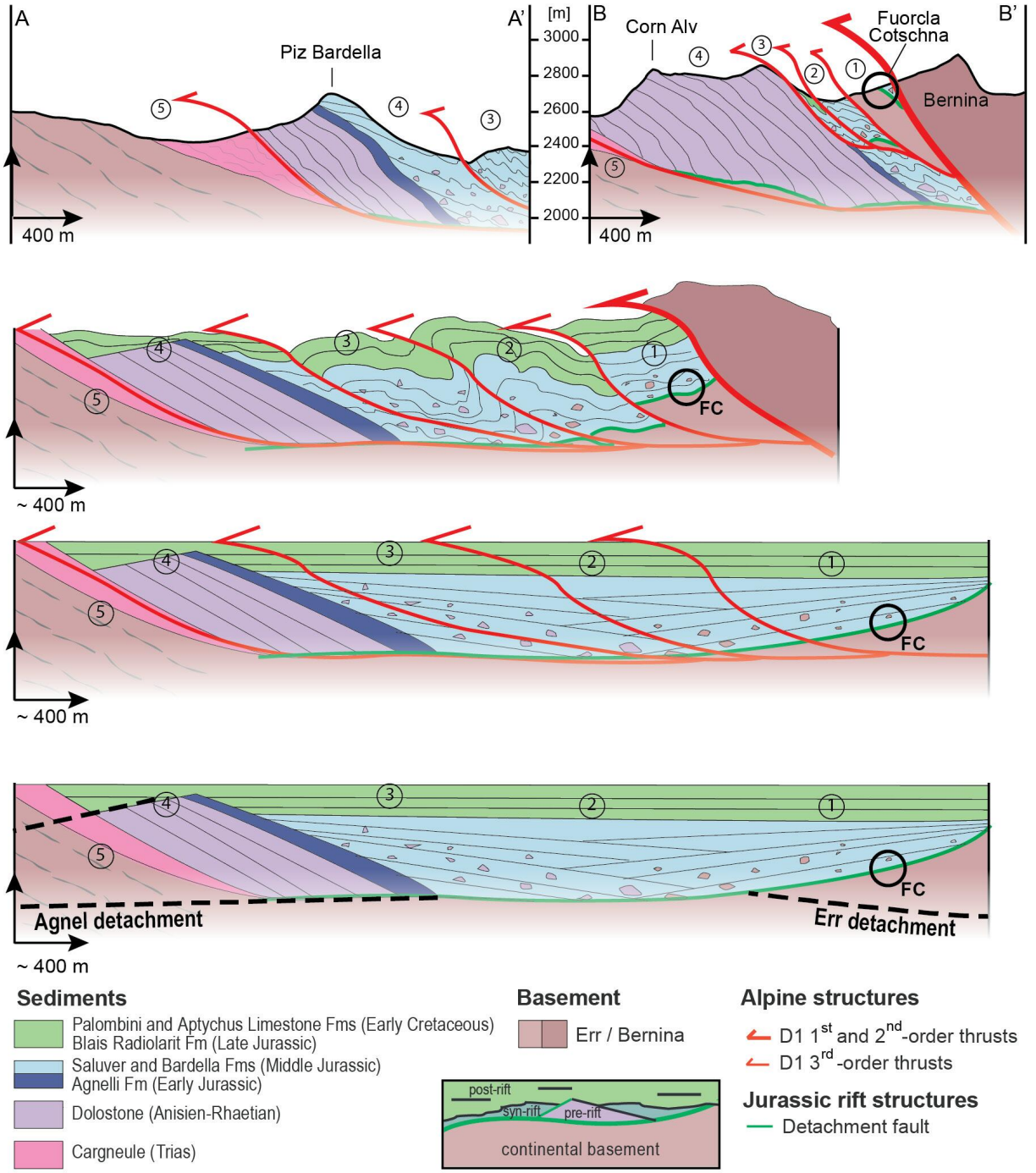

Fig. II.C.14 (modified from Epin et al., 2017) - Restoration of the present-day geological section A-A' and B-B' in Fig. II.C.2 back to their position at the end of rifting in late Middle Jurassic time. Note the link between D1 thrusts and inherited Jurassic detachment structures. Abbreviation: FC: Fuorcla Cotschna.

https://doi.org/10.3301/GFT.2023.02

On a local scale, the kinematics of the Jurassic and Alpine fault systems were approximately co-linear in the Piz Bardella-Fuorcla Cotschna area, both trending E-W to SE-NW. This enabled Epin et al. (2017) to propose a qualitative restoration of a section parallel to the transport direction (Fig. II.C.14). They identified 5 sub-units stacked one on top of each other and noticed that thrusts partly reactivated the inherited Jurassic detachment, which was used as a decollement level (Fig. II.C.14).

FURTHER READING

Froitzheim and Eberli (1990); Manatschal and Nievergelt (1997); Masini et al. (2011, 2012, 2013); Epin et al. (2017, 2019); Epin and Manatschal (2018); Ribes et al. (2019a).
About fluids: Manatschal (1999); Manatschal et al. (2000); Pinto et al. (2015); Incerpi et al. (2017, 2018, 2020a).
Ph.D. theses: Epin (2017); Incerpi (2017); Masini (2011); Pinto (2014).

https://doi.org/10.3301/GFT.2023.02

EXCURSION D
The exhumed mantle domain of the Adriatic margin: Falotta-Marmorera-Val da Natons-Bivio (Platta Nappe, southeast Switzerland)

ABSTRACT

The Platta Nappe in south-eastern Switzerland samples the exhumed mantle domain of the former Adriatic margin. The Platta Nappe can be subdivided into two units based on their lithology and tectonic position, namely the Upper- and Lower Platta units: the Upper Platta Unit corresponds to the most proximal part of the exhumed mantle domain. It is comprised of an inherited subcontinental lithospheric mantle with minor magmatic additions and a few continental allochthons. The more distal Lower Platta Unit is comprised of (re-)fertilized mantle with an increasing number and volume of intrusive and extrusive magmatic bodies oceanward. It also preserves remnants of a proto-Oceanic Core Complex (OCC). The exhumed mantle domain is characterized by intense hydrothermal fluid activity and Cu-Fe-Ni-Co-Zn-rich mineralizations linked to serpentinization.

This excursion aims to display: (1) the general architecture of the exhumed mantle domain; (2) the tectono-sedimentary sequences and structures associated with mantle exhumation; (3) the nature of fluid-rock interactions and associated mineralizations; (4) the characteristics of the magmatic intrusions affecting the exhumed mantle domain; (5) the evidence for a proto-OCC; and (6) how rift-related structures controlled the style and location of subsequent Alpine deformation.

MAIN TAKE-AWAY OF THE EXCURSION

- **Age of rift-related deformation:** latest Middle Jurassic (Callovian; ca. 161 Ma).
- **Deformation style:** essentially controlled by detachment faults affected by later normal faulting; minor magmatic activity and intense hydrothermalism.
- **Paleogeographic framework:** Ocean-Continent Transition (OCT) of the southeast Alpine Tethys margin.
- **Onset of Alpine reactivation:** Late Cretaceous (Santonian/Campanian).
- **Reactivation style:** thin-skinned tectonics; controlled by local buttresses and decoupling levels at the top and within the serpentinized mantle.
- **Main remaining questions:** what is the nature and age of the contact between the Upper- and Lower Platta units? A primary lithological transition or a major Jurassic shear zone?

INTRODUCTION

The Platta Nappe belongs to the Upper Penninic Unit. It preserves remnants of the most distal part of the northern Adriatic margin, namely the exhumed mantle domain. The mechanisms of mantle exhumation are well-constrained for the Platta Nappe (Epin et al., 2019). Seismic

https://doi.org/10.3301/GFT.2023.02

imaging of exhumed mantle domains at present-day rifted margins highlights complex architectures with pronounced top basement topography. However, only a few drill holes have been performed in such distal settings and drilling was limited to basement highs, leaving a lot of uncertainty on the nature of the basement and the processes at play in exhumed mantle domains. In this framework, the study of a field analogue like the one preserved in the Platta Nappe is of great interest. The Platta Nappe is presumably the best exposed and investigated rift-related exhumed mantle domain worldwide.

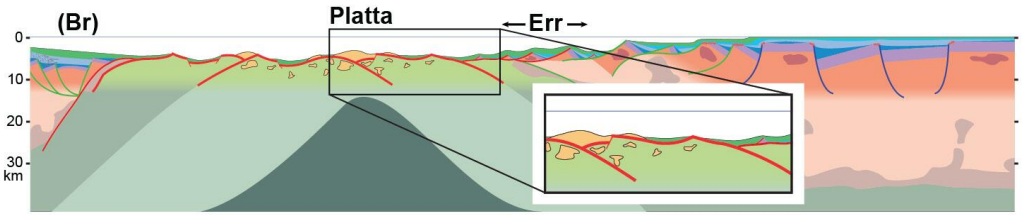

Fig. II.D.0 - Schematic section across the Alpine Tethys rift system showing the position of the Briançonnais (Br), Err and Platta domains during the Middle Jurassic mantle exhumation phase (modified from Manatschal et al., 2022).

ITINERARY

This excursion takes place in the Val Surses in southeast Switzerland. Main localities visited are Alp Flix/Falotta; the Marmorera Lake area, and outcrops/panoramas close to the village of Bivio (Fig. II.D.1).

Stop 1 (Viewpoint 1 in Fig. II.D.1): From Bivio, drive north on road 3. Approximatively 2 km beyond the Marmorera Lake, turn right into the village of Sur. Drive up 2.3 km and then turn right to reach the Alp Flix parking place (P1 on Fig. II.D.1; GPS: 46°31'21.9"N 9°38'36.7"E, i.e., 46.522745, 9.643513). Look north in the direction of Falotta.
Stop 2 (Outcrop 2): From the P1 parking place, walk on the road track ca. 1.5 km up to the café/farm. Then, take the smaller road track on the right, which evolves into a hiking path. Walk north up to Falotta (46°32'47.9"N 9°39'55.7"E, i.e., 46.546650, 9.665474; see the path on Fig. II.D.1).
Stop 3 (Outcrop 3): Park the car on the northern end of the Marmorera Lake (P3 on Fig. II.D.1; GPS: 46°30'37.5"N 9°38'03.0"E, i.e., 46.510421, 9.634153). Take the path heading southwest along the lake up to its end at the foot of a cliff (ca. 800 m; Outcrop 3 in Fig. II.D.1; GPS: 46°30'19.3"N 9°37'41.1"E, i.e., 46.505361, 9.628077).
Stop 4 (Viewpoint 4 in Fig. II.D.1): From P3 drive 3.7 km south on road 3 and park the car on P4 at Stalveder (GPS: 46°28'55.6"N 9°38'29.4"E, i.e., 46.482102, 9.641499); look into the NNE toward the outcropping gabbro bodies cropping out in Val da Natons.
Stop 5 (Viewpoint 5 in Fig. II.D.1): From P4 drive 2.7 km south on road 3 and park the car on P5 at the Tua ski lift station (GPS: 46°27'46.8"N 9°39'22.9"E, i.e., 46.463007, 9.656362); look into the NE toward the cliff above the road.

https://doi.org/10.3301/GFT.2023.02

Stop 1: Alp Flix (46°31'21.9" N - 9°38'36.7" E)

The Platta Nappe can be subdivided into two units based on mantle lithology and Alpine tectonic position, namely the Upper- and Lower Platta units (Fig. II.D.2). Each one of these units is up to 400 m thick. The Upper Platta Unit corresponds to the more proximal part of the OCT. It overlies the Lower Platta Unit along an Alpine tectonic contact. The basement of the Upper Platta Unit is comprised of serpentinized subcontinental lithospheric mantle (Mantle type 1a of Picazo et al. 2016; cf. section 2 of the Petrology thematic sheet). It is affected by rare late Middle Jurassic magmatic additions and overlain by a few extensional allochthons made of continental crust and pre-rift sediments.

The Lower Platta Unit corresponds to the more distal domain in the OCT. It is comprised of infiltrated serpentinized subcontinental lithospheric mantle (Mantle type 2 of Picazo et al. 2016; cf. section 2 of the Petrology thematic sheet). It displays an increasing number of MORB-type gabbroic intrusive- and basaltic extrusive rocks oceanward. These magmatic bodies are interpreted as the first products of an embryonic spreading system (section 3 of the Petrology thematic sheet). The magmatic bodies of the Platta Nappe were emplaced over a short period of time at 161±1 Ma (Schaltegger et al., 2002).

Mylonitic shear zones can be found within the mantle peridotites (e.g., the Muttariel mylonitic shear zone). Müntener et al. (2010) reckoned their formation temperature to 700-900 °C and suggested that these

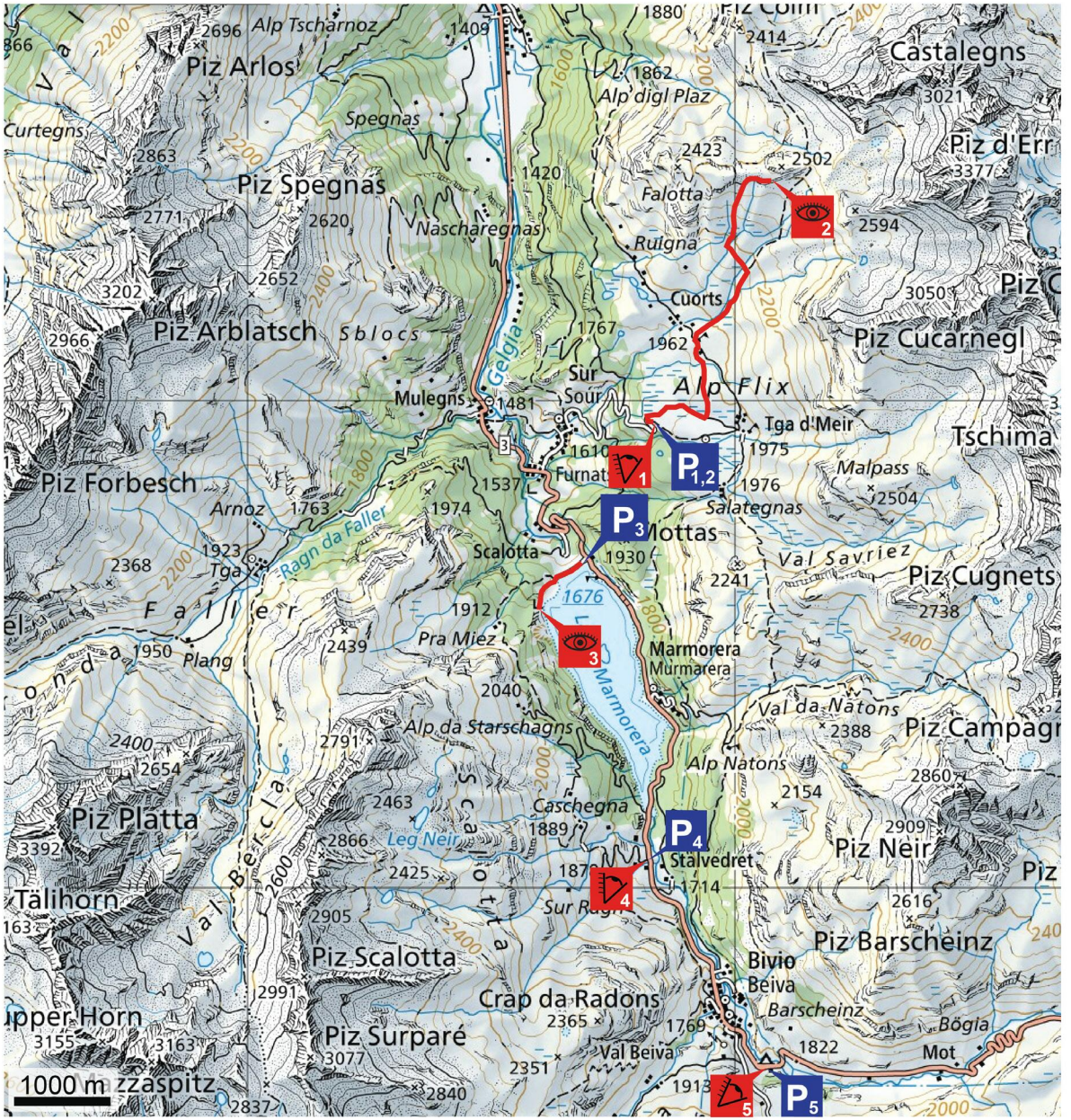

Itinerary: by foot | P parking place | viewpoint | outcrop

Fig. II.D.1 - Map of the Platta Nappe area and route to the outcrops and viewpoints (background map from https://map.geo.admin.ch/).

https://doi.org/10.3301/GFT.2023.02

mylonitic shear zones separated the infiltrated/(re-)fertilized mantle of the Lower Platta (Mantle type 2) from the inherited subcontinental lithospheric mantle of the Upper Platta (Mantle type 1). Mylonitic shear zones may have acted as permeability barriers.

Stop 2: Falotta (46°32'47.9" N - 9°39'55.7" E)

The Falotta outcrop (Fig. II.D.3b) displays a succession from "undeformed" serpentinized and re-fertilized mantle to intensively, brittlely deformed fault rocks overlain by a volcano-sedimentary sequence (basalts/breccias/ophicalcites; Fig. II.D.4 and log 1 of Fig. II.D.5). Hydrothermal activity was intense during mantle exhumation since almost all rocks have been altered and or chemically modified (Coltat et al., 2020).

The extensional structures found at Falotta are comparable to those observed in the Err Nappe, despite the fact they affect different types of lithologies. Extensional structures are marked by serpentinite cataclasites and black gouges topped by ophicalcites and overlain by tectono-sedimentary breccias, which are typical fingerprints of Jurassic detachment faults (Pinto et al., 2016; Epin et al., 2019; Coltat et al., 2020; Fig. II.D.4). Thus, the Platta extensional detachment may be interpreted as the oceanward continuation of the Err detachment system (cf. Excursion C; see also Epin et al., 2017).

An idealized section through the footwall of the Platta detachment fault includes, from base to top (Fig. II.D.4c):

- foliated massive serpentinized peridotite or gabbro;
- serpentinized peridotite or gabbro cataclasites marked by fractures and veins filled with syn-kinematic chlorite and serpentinite; the intensity of cataclastic deformation increases upward, passing into;
- serpentinite gouges (core zone).

A recent study by Coltat et al. (2020) investigated the contact between the basalts and the mantle rocks at Falotta and showed that the deformation of the basalts is pre-Alpine and occurred under seafloor conditions, suggesting that the basalts were emplaced during mantle exhumation.

The first sediments overlying the detachment surface are carbonate-rich tectono-sedimentary breccias named ophicalcites (Fig. II.D.4c). These formed in a syn-tectonic setting, either at low- or high temperatures depending on the presence or absence of overlying basalts (Coltat et al., 2019a; cf. section 5 of the Fluids thematic sheet). From bottom up, two types of ophicalcites can be identified:

- Type 1 ophicalcites are characterized by penetrative impregnation and replacement of serpentinite cataclasites and gouges by calcite;
- Type 2 ophicalcites are calcitic matrix-supported tectono-sedimentary breccias that rework serpentinized mantle.

https://doi.org/10.3301/GFT.2023.02

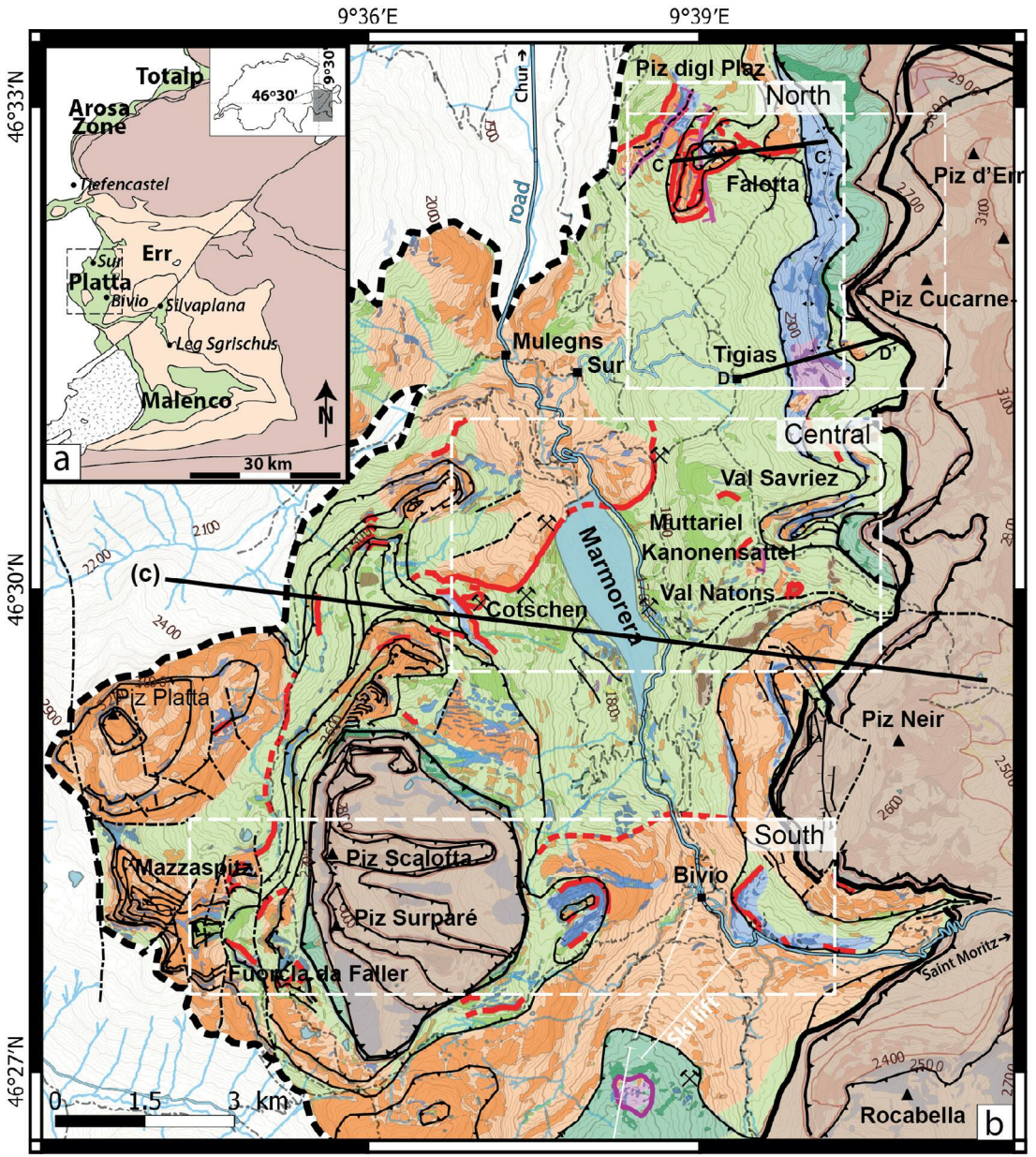

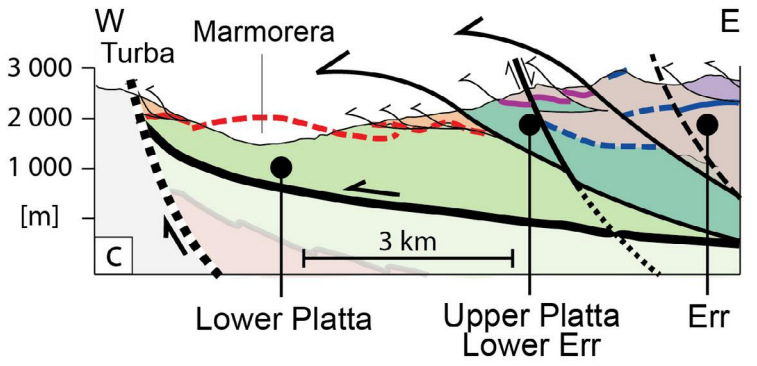

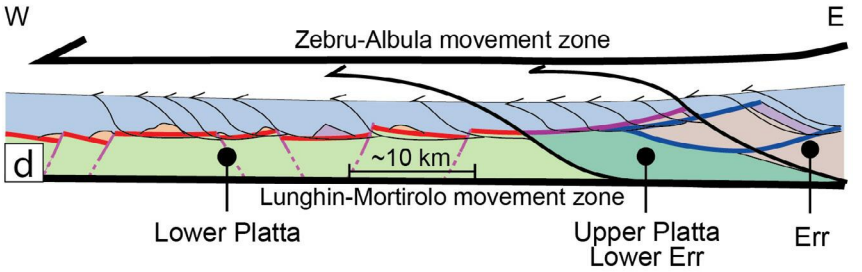

General units (inset map a)
- Cenozoic or Neogene intrusion (Bregaglia)
- Upper Austroalpine and Southalpine
- Lower Austroalpine
- South Penninic
- Middle - Northpenninic

Alpine structures
- Late normal faults
- Turba normal fault
- D2 normal fault
- D1 thrust

Oberved / Inferred lithologies (map b)
- Syn- and post-rift sediments
- Pre-rift sediments
- Continental basement
- Basalts
- Gabbro
- Refertilized mantle (Lower Platta)
- Subcontinental mantle (Upper Platta)

Pre-Alpine structures
- Jurassic Err detachment
- Jurassic Upper Platta det.
- Jurassic Lower Platta det.
- Jurassic Lower Platta normal faults

- Mines (in sediments and in peridotites)

Fig. II.D.2 (modified from Epin et al., 2019) - a) Geologic map of the Central Grisons area showing the distribution of the Austroalpine units and South Penninic ophiolites derived from the Adriatic OCT; b) geological map of the Platta Nappe; c) section through the Platta and Err nappes showing main Alpine units and Alpine D1 structures; d) restored section at Late Jurassic time across the Platta and Err domains. Black lines mark the location of major Alpine first-, second-, and third-order D1 thrust faults. Abbreviation:det.: detachment.

https://doi.org/10.3301/GFT.2023.02

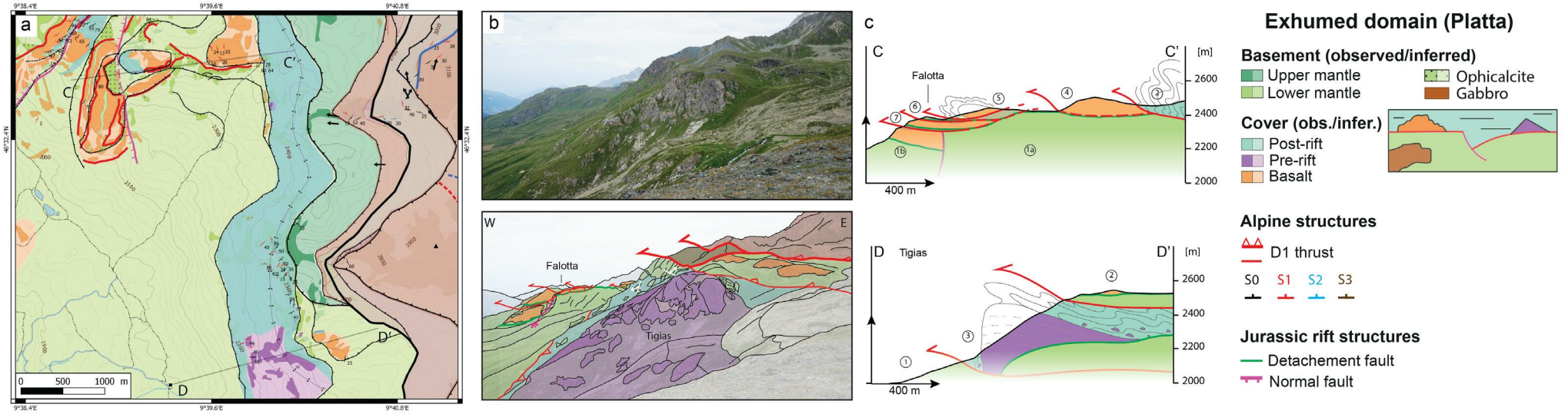

Fig. II.D.3 (modified from Epin et al., 2017) – a) Geological map of the Falotta region; b) photograph and line drawing of the panoramic view of the Tigias-Falotta area (view from the south); c) constructed sections C-C' and D-D' across the Falotta-Tigias area (for location see Fig. II.D.2 and II.D.3a). Abbreviations: obs./infer.: observed/inferred.

Stop 3: Marmorera Lake (46°30'19.3" N - 9°37'41.1" E)

The outcrop east of the Marmorera Lake (outcrop 3 in Fig. II.D.1) displays a contact between the serpentinized mantle in the footwall and basalts in the hanging wall (Fig. II.D.6). Close to the contact, the serpentinized mantle in the footwall is affected by rodingitized mafic dykes. These dykes are generally parallel to the contact between the mantle and overlying basalts. They were interpreted as feeders of the overlying basalts. The contact between the mantle and the basalts is made of ophicalcites reworking serpentine and intensively deformed rocks, which suggests that it is a detachment fault linked to mantle exhumation. A pre-Alpine age is further supported by the observation that the fault rocks are crosscut by carbonate veins. Carbonate veins in a comparable position further west, near Cotschen, were dated 144±13 Ma using the U/Pb method on carbonate (Coltat et al., 2019b).

The base of the basalts overlying the contact is strongly deformed, similar to what can be observed at Falotta. Epin et al. (2019) suggested that these basalts were emplaced during mantle exhumation, in the hanging wall of a detachment system.

In a detailed study, Coltat et al. (2019b) described an ultramafic-hosted Cu-Fe-Ni-Co-Zn-rich mineralization well exposed at Cotschen, west of the Marmorera Lake (Fig. II.D.6a and II.D.6b). Along the cliff east of the Marmorera Lake, mineralization occurs as sporadic thin oxidized reddish corridors and patches of Fe-Ca-silicates, semi-massive sulphides and/or Cu-rich massive sulphides. Some of these patches were mined (e.g., Cotschen mine on Fig. II.D.6a). Coltat et al. (2019b) suggested that hot (>350 °C) hydrothermal fluids were drained along sills

https://doi.org/10.3301/GFT.2023.02

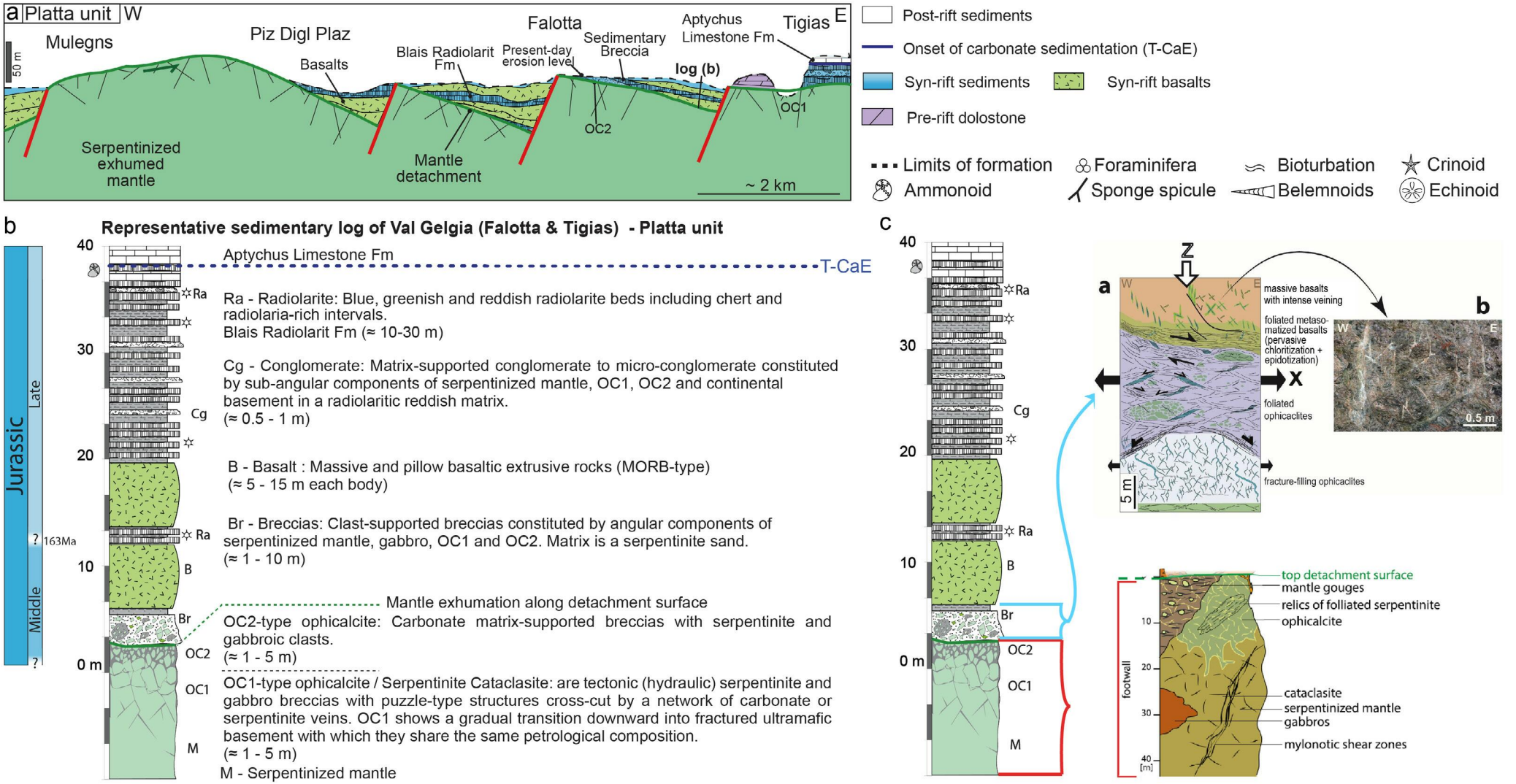

Fig. II.D.4 - a) Palinspastic reconstructions across the northern Platta Nappe by Ribes et al. (2019a). Note that the scale for syn-rift sediments is different from that for pre-rift sediments and basement; b) representative sedimentary successions of the Platta Nappe from Ribes et al. (2019a); c) structural and petrologic details showing the nature of the deformation at the top of the exhumed mantle and the overlying basalts (from Epin et al., 2019 and Coltat et al., 2020). Abbreviation: T-CaE: Tithonian Carbonate Event.

and dykes toward the surface. They compared these mineralizations to those related to the high-temperature black smokers of the North Atlantic Ridge. This implies that processes comparable to those taking place at mid-oceanic ridges can take place during the formation of OCTs and prompt us to reconsider the potential metal resources available in such settings.

https://doi.org/10.3301/GFT.2023.02

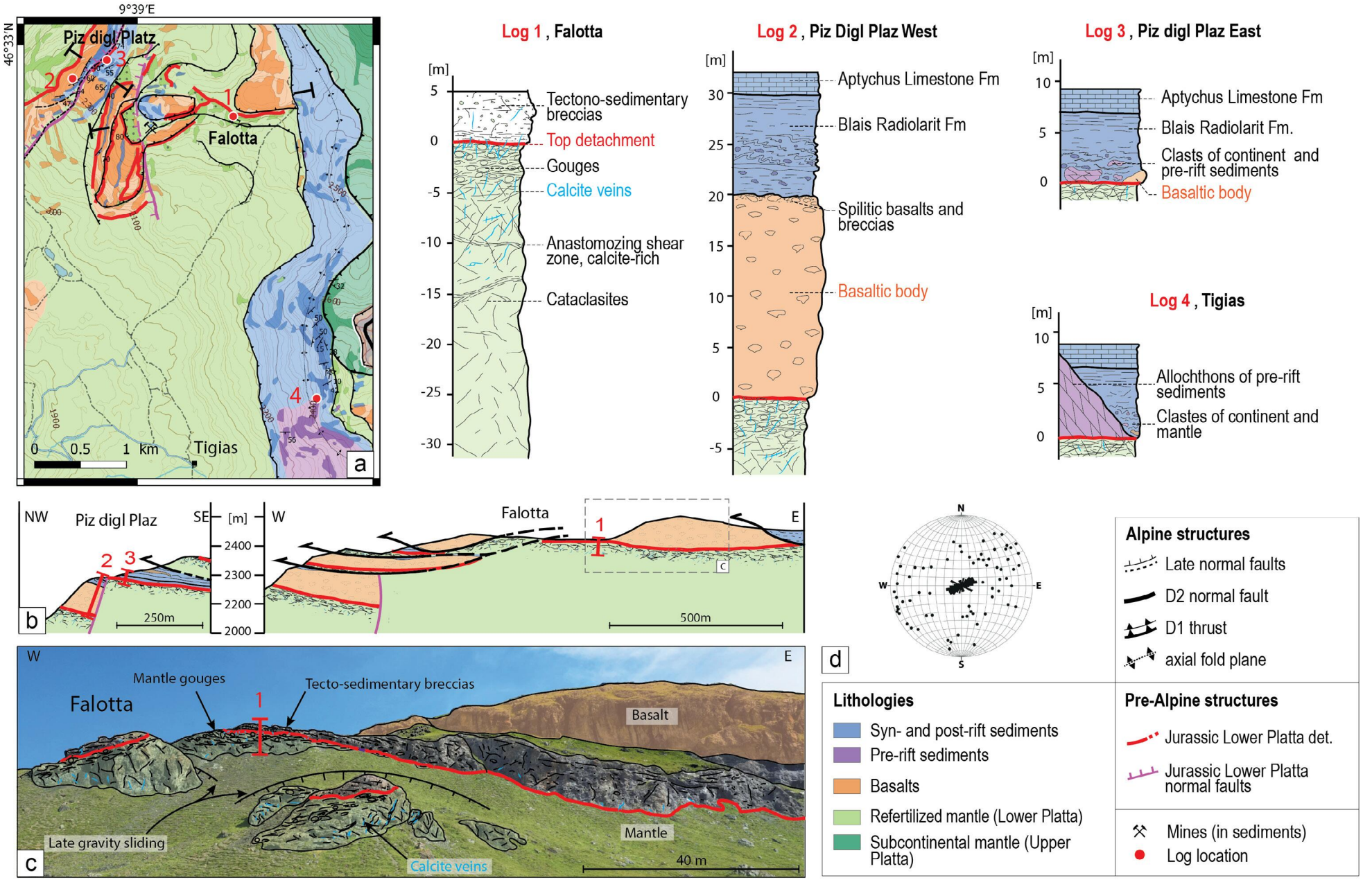

Fig. II.D.5 (modified from Epin et al., 2019) - a) Geological map of the northern part of the Platta Nappe and associated logs (1-4); b) section through the Falotta ridge (see panel (a) for location); c) panorama of the Falotta area; d) stereo-plot in lower hemisphere showing a rose diagram and poles to planes of calcite veins. Abbreviation: det.: detachment.

https://doi.org/10.3301/GFT.2023.02

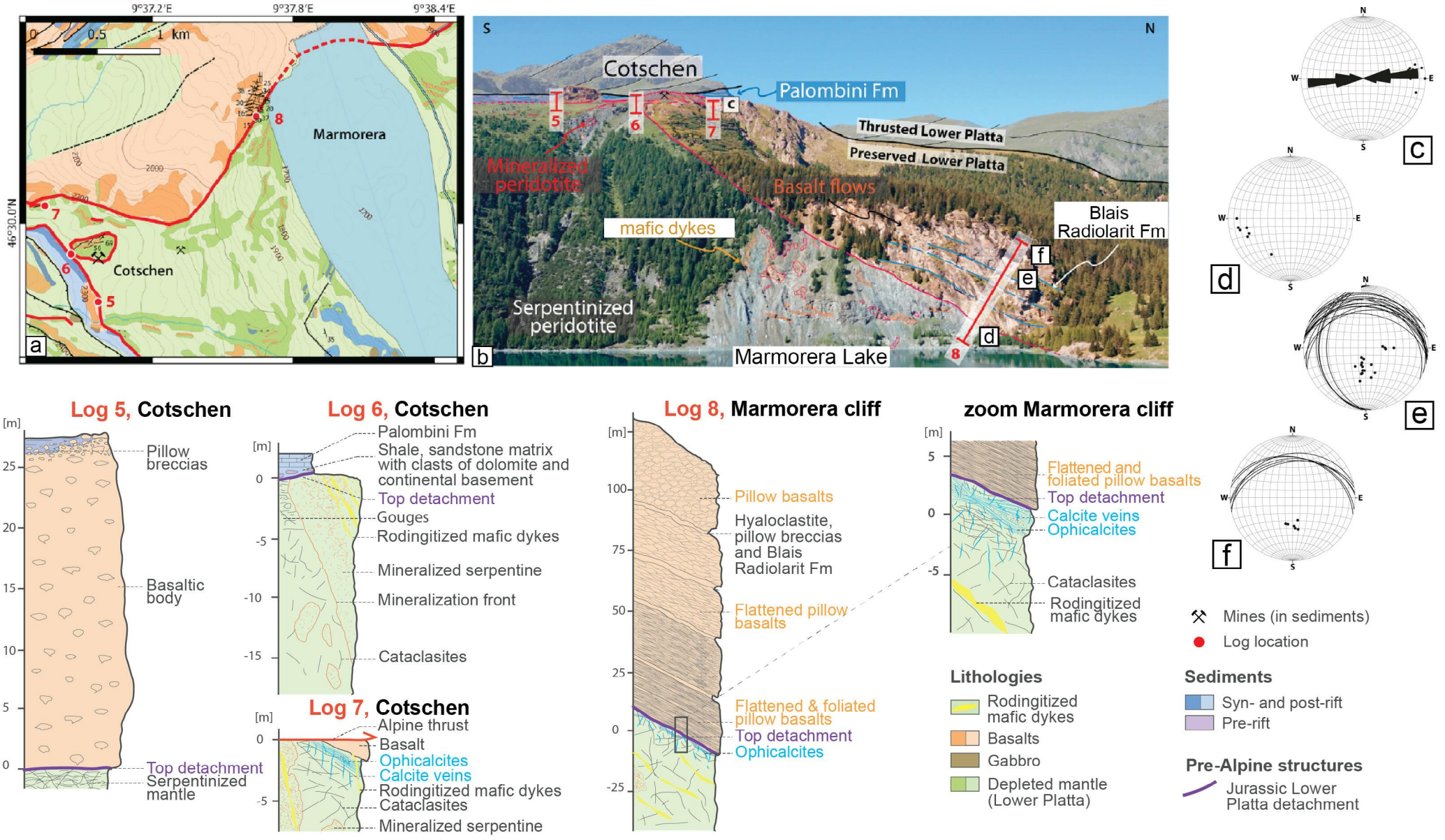

Fig. II.D.6 (modified from Epin et al., 2019) - a) Geological map of the central part of the Platta Nappe (see Fig. II.D.2 for location) and associated logs (5-8); b) panorama of the eastern side of the Marmorera Lake; c) stereo-plot in lower hemisphere showing a rose diagram and poles to planes of calcite veins; (d) paleo direction of basaltic flows; (e) orientation of hyaloclastite and Radiolarit Fm (poles to planes); and (f) extensional detachment fault orientation at the base of the Marmorera cliff (poles to planes).

https://doi.org/10.3301/GFT.2023.02

Carbonatation (ophicalcite formation; Coltat et al., 2019a) close to the paleo-seafloor and along extensional detachment faults marks the end of hydrothermal activity.

Stop 4: Stalvedret/Val da Natons (46°28'55.6" N - 9°38'29.4" E)

Two types of gabbros occur in the Val da Natons:

- a first group of sheet-shaped bodies whose extent can be mapped over a few kilometres;
- a second group of sphere-shaped bodies with diameters <100 m (Fig. II.D.7b).

The sheet-shaped bodies are mainly made of Mg-gabbros, although a high compositional diversity can be observed, ranging from primitive olivine gabbros to highly differentiated Fe-Ti-P gabbros that indicate fractional crystallization. The sphere-shaped bodies originate from a Transitional MORB (T-MORB)-type source and are very homogenous (Desmurs et al., 2002).
Evidence for contact metamorphism at the interface between the serpentinized mantle and the intrusive gabbros suggests that gabbros intruded into the already serpentinized mantle (Desmurs et al., 2001). It implies that they were emplaced at or above the serpentinization front, i.e., at 4 to 6 km below the seafloor (Fig. II.D.8), consistent with seismic observations at present-day margins (Gillard et al., 2019). Val da Natons gabbros were emplaced at 161±1 Ma, during a very short-lived magmatic event (Desmurs et al., 2001; Schaltegger et al., 2002).
Gabbro bodies underwent different deformation phases. The first one is recognized as syn-magmatic. It is overprinted by later mylonitic shear zones that presumably formed under lower amphibolite- to greenschist facies conditions. Finally, cataclastic deformation truncated the shear zones, testifying to deformation in the brittle regime (Fig. II.D.7c).
Gabbros are stratigraphically (primary contact) overlain by sedimentary- and pillow breccias that contain gabbro clasts, which implies that these gabbros were exhumed to the seafloor.
The petrology of the basaltic flows is described in section 4 of the Petrology thematic sheet (for further details see Amann et al., 2020).

Stop 5: Tua ski lift station (46°27'46.8" N - 9°39'22.9" E)

The village of Bivio lies at the edge of a glacial lake that was filled by Quaternary, post-glacial sediments. A drill hole penetrating the basement flooring of the village of Bivio (Log 16 in Fig. II.D.8) penetrated a sequence of Upper Jurassic Aptychus limestones and pillow basalts interleaved with radiolarian cherts. These formations overlie cataclastic serpentinized peridotites that show a decrease in deformation downhole. This succession is similar to that observed in the Falotta section. Thus, Bivio sits on exhumed mantle covered with Jurassic deep-water sediments and magmatic products, comparable to sequences described from magma-poor OCTs. East of Bivio, the sedimentary sequence is well

https://doi.org/10.3301/GFT.2023.02

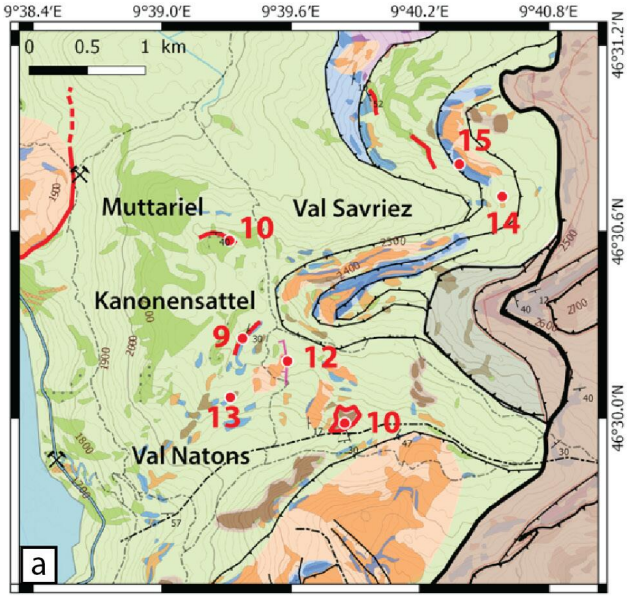

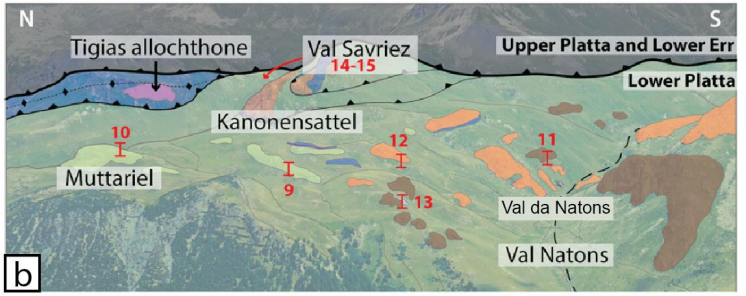

Lithologies

- Syn- and post-rift sediments
- Pre-rift sediments
- Basalts
- Gabbro
- Refertilized mantle (Lower Platta)

Alpine structures

- Late normal faults
- D1 thrust

Pre-Alpine structures

- Jurassic Lower Platta detachment

Others

- Log location
- Mines in peridotite

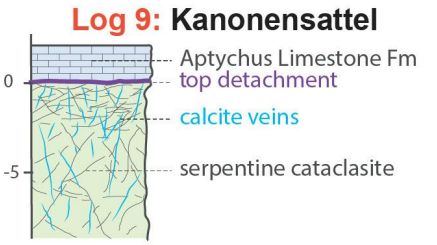

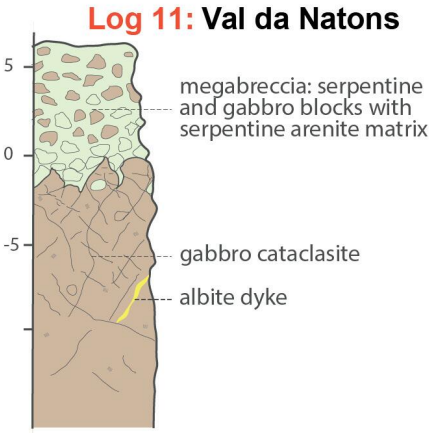

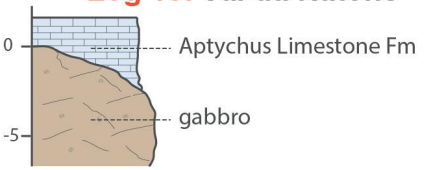

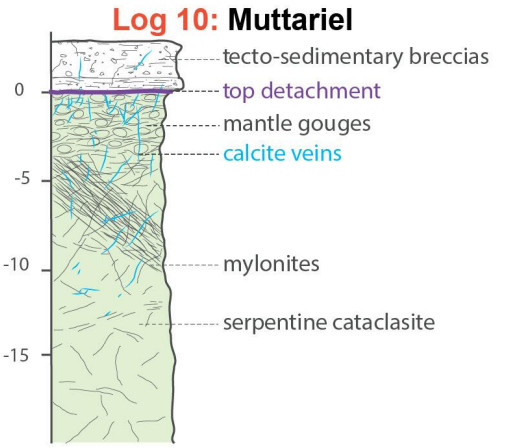

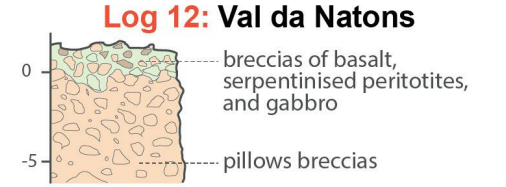

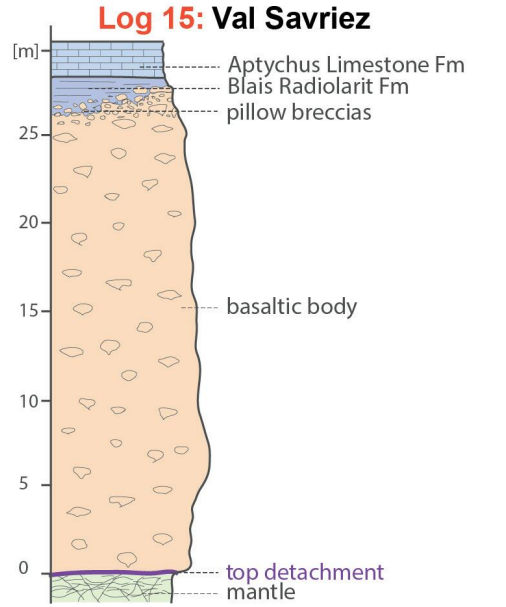

Fig. II.D.7 (from Epin et al., 2019) – a) Geological map of the southern part of the Platta Nappe (see Fig. II.D.2 for location) and associated logs (9-15); b) panorama of the Val da Natons area.

https://doi.org/10.3301/GFT.2023.02

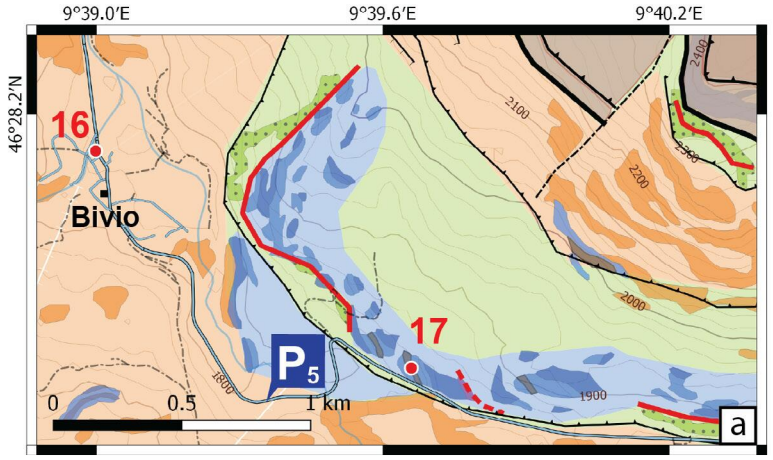

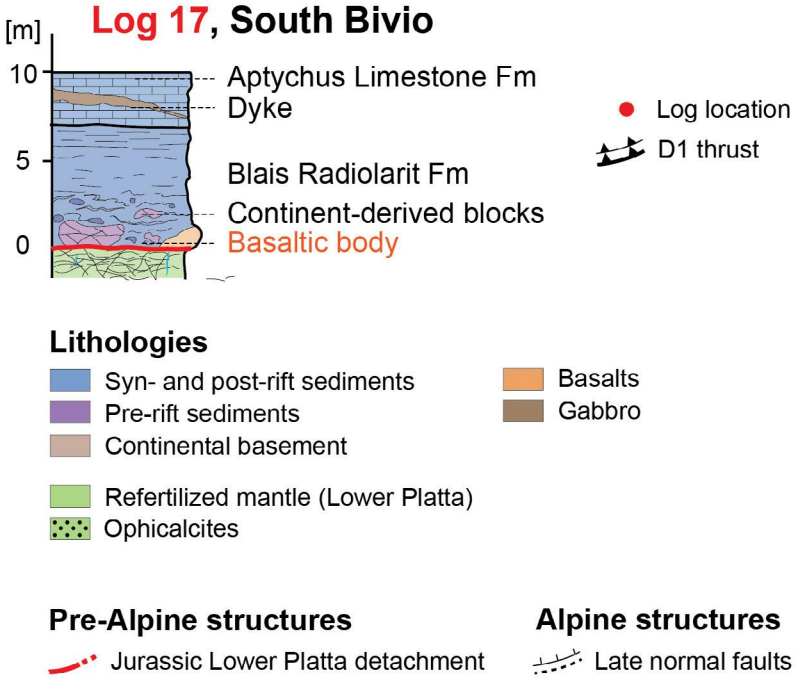

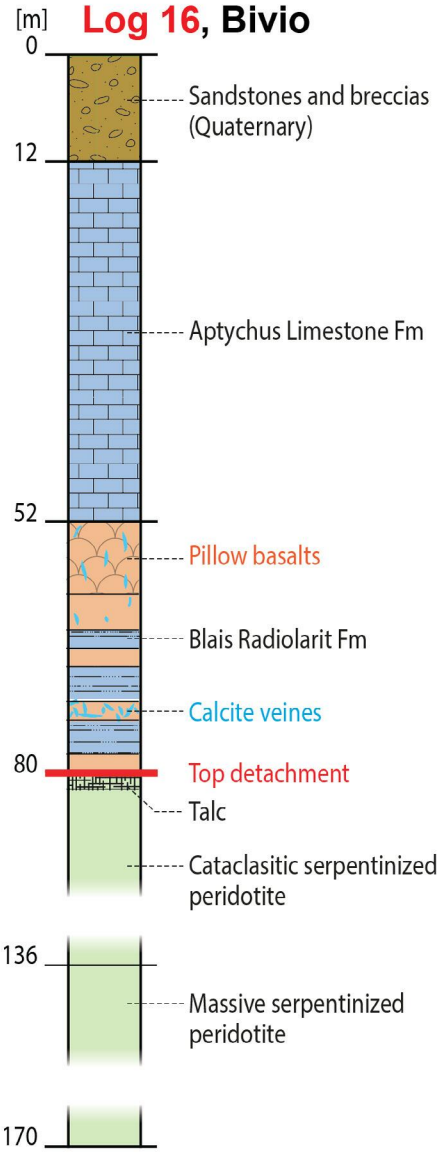

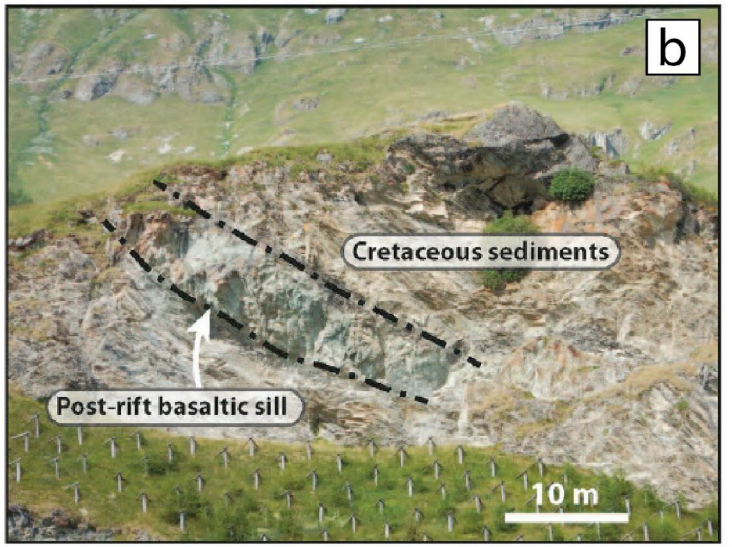

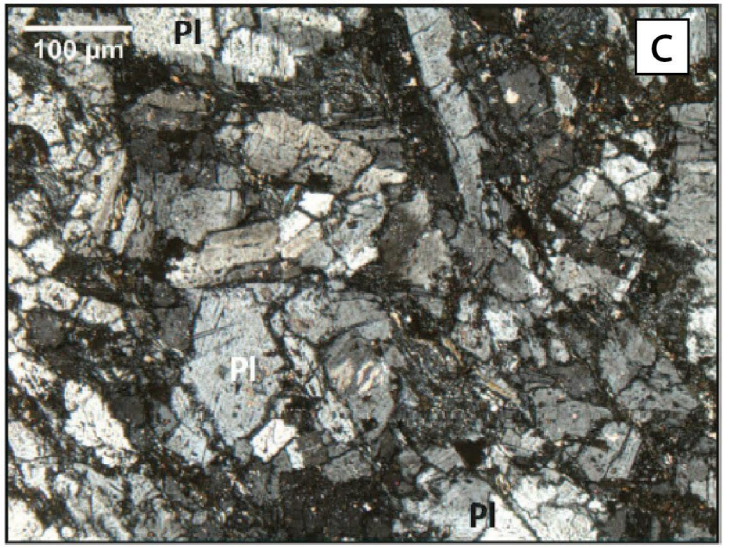

Fig. II.D.8 - a) Geological map of the area southeast of Bivio and log drawn from a drilled core (from Epin et al., 2019); b) Early Cretaceous basaltic sill intruding post-rift sediments; c) photomicrograph of a Cretaceous basaltic sill showing subhedral granular albitite (doleritic texture).Pl, plagioclase (from Amann et al., 2020).

https://doi.org/10.3301/GFT.2023.02

exposed and exhumed mantle floors the skiing area of Bivio. The hills surrounding the village are made of heavily hydrated and deformed pillow breccias and hyaloclastites.
Looking into the east from the parking of the Tua ski lift (P5 in Fig. II.D.2), one can see a cliff a few tens of meters above the Julier road (Fig. II.D.8b). This outcrop shows post-rift sediments belonging to the Upper Jurassic Aptychus Limestone Fm, which are intruded by a magmatic sill of alkaline basalts (see description in Amann et al., 2020). These relationships indicate that magmatic activity continued after mantle exhumation in the Platta OCT, similar to what has been described from the present-day Newfoundland margin (see ODP Site 1276; Péron-Pinvidic et al., 2010).

DISCUSSION

3D architecture of a proto-Oceanic Core Complex (proto-OCC)

The OCCs in exhumed mantle domains are capped by exhumation faults that are characterized by a trilogy of fault rocks, namely cataclasites, gouges, and ophicalcites. This rocks association can be mapped throughout the Platta Nappe, which provides an overview of the paleo-top of the exhumed mantle. The exhumed mantle was dome-shaped in the Lower Platta Unit, as shown on sections striking from the north of the Marmorera Lake to Bivio (Fig. II.D.9c) and from the toe of Piz Platta to Val da Natons (Fig. II.D.9b). The paleo-top of the exhumed mantle is often truncated by later normal faults (Figs. II.D.9a and II.D.9b). The observed offset of these normal faults locally reaches 200 m. The fact that basalts become thicker toward normal faults suggests that basalts were emplaced during fault activity. All mantle rocks linked to the OCC are serpentinized, chloritized and/or carbonatized, while mafic rocks (basalt and gabbro) are spilitized and rodingitized. Hydration reactions occurred both during mantle exhumation and during the emplacement of the mafic intrusive and extrusive rocks.
The widespread basalts of the Platta Nappe become generally thicker “oceanward”, which suggests an increase in magmatic budget with time. Basalts are also thicker on either side of the exhumed mantle dome compared to the dome itself. Indeed, on the top of the dome, Upper Jurassic limestones directly overlie the exhumed mantle, indicating that both basalts and sediments of the Blais Radiolarit Fm are locally lacking.

Comparison with present-day OCC

Comparing to present-day Oceanic Core Complexes (OCC), the Lower Platta exhumed mantle domain displays:

- similar lithologies (exhumed mantle, basalts, gabbros, breccias);
- similar dome size (ca. 15x20 km);
- comparable hydrothermal activity (see next paragraph).

https://doi.org/10.3301/GFT.2023.02

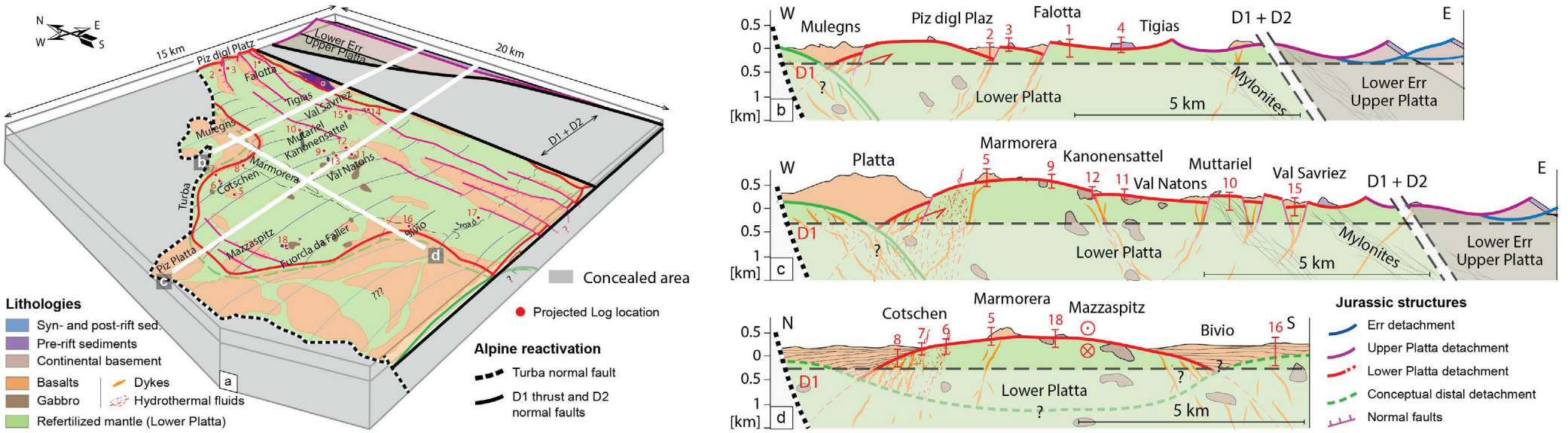

Fig. II.D.9 (from Epin et al., 2019) – a) 3D paleogeographic restoration of Platta units and (b-d) sections across the OCC preserved in the Lower Platta Unit.

However, the Lower Platta exhumed mantle domain differs from classical OCC by:

- the nature of the exhumed mantle, namely is subcontinental (mantle type 1 and 2) in Platta while it is depleted oceanic (mantle type 3) in classical OCC;
- existence of continent-derived blocks in the Lower Platta not observed in present-day OCCs;
- evidence for polyphase tectono-magmatic activity in the Lower Platta, while either tectonic- or magmatic activity/segments at mature ultra-slow spreading ridges;
- basalt chemistry in the Lower Platta differs from that of classical N-MORB observed at mature ridges and were defined as OCT basalts (Amann et al., 2020).

Mantle exhumation at rifted margins has first been described in the pioneering work of Decandia and Elter (1972) in the Alps before it was proven at slow-spreading ridges and present-day rifted margins (Boillot et al. 1987). The processes of mantle exhumation have been described in the meantime by many authors at many places, in particular at magma-poor, slow-spreading ridges (e.g., Sauter et al., 2013). Imaging of present-day mid-oceanic ridges enabled to recognize detachment faults capping so-called Oceanic Core Complexes (OCC), along which mantle rocks are exhumed at the seafloor (MacLeod et al. 2009). These OCC are complex, km-scale structures linked to magmatic and

https://doi.org/10.3301/GFT.2023.02

hydrothermal processes. They show the interaction of high-angle normal faults and long-offset exhumation faults. Detailed mapping of the Lower Platta Unit enabled to restore such an OCC, namely the Platta OCC that is exposed over ca. 5 km both in the strike- and dip directions along the Julier valley, between the Marmorera Lake and the village of Bivio (Fig. II.D.9; Epin et al., 2019).

Intense hydrothermal activity occurred along the Platta OCC, in particular at the interface between the mafic extrusives (pillow breccias, hyaloclastites, and basalt flows) interleaved with deep-water sediments, and the ultramafic exhumed serpentinized mantle. Products of hydrothermalism include local patches of Cu-Fe-Ni-Co-Zn-rich mineralizations (Coltat et al., 2019b).

The existence of continent-derived allochthonous blocks in the Lower Platta Unit is difficult to explain if we consider that the Lower Platta OCC was formed in a steady-state, ultra-slow spreading system. The subcontinental nature of the mantle does not support this theory either, since the mantle of ultra-slow spreading systems displays classically depleted oceanic chemistry (Mantle type 3 of Picazo et al., 2016). Allochthonous blocks were possibly "delaminated" from the conjugate margin at the same time as mantle exhumation (e.g., Nirrengarten et al., 2016). In this case, the exhumed subcontinental mantle underlying the continental allochthon would originate from beneath the conjugate margin (Fig. II.D.10b).

Alpine reactivation

The base of the Platta Nappe is juxtaposed against Eocene flysch sediments along the late Eocene Turba normal fault (e.g., Nievergelt et al., 1996; black dashed line in Figs. II.D.2b and II.D.2c). The contact between the Platta Nappe and the overlying Err Nappe corresponds to a polyphase contact including a pre-Alpine detachment system that has been reactivated by an Alpine D1 thrust and truncated by an Alpine D2 normal fault (Figs. II.D.2c and II.D.2d). More recent studies suggest that the contact between the Upper Platta Unit and the Err Nappe could be affected only by minor Alpine convergence (for details see Epin et al., 2017 and Epin and Manatschal, 2018). Epin et al. (2017) interpreted the contact between the Upper- and Lower Platta Units as a Late Cretaceous Alpine thrust, which may have seeded on the primary mylonitic shear zone that separates the Upper- and Lower Platta units.

Thrust faults did essentially root at the top of the massive serpentinized mantle, while the overlying material was scrapped off (Fig. II.D.11). The resulting duplexes are thus essentially comprised of basalts, continent-derived remnants, and sediments. Basement topography largely controlled the style of reactivation: positive topographies acted as buttresses (for instance volcanoes, continental allochthons, or normal faults), so that ramps were usually located along their borders. In contrast, flats seeded at former detachment faults, at the top of the exhumed mantle (Figs. II.D.11).

Alpine metamorphism ranged from prehnite-pumpellyite to greenschist facies (Trommsdorff, 1983). However, to what extent Alpine metamorphism has overprinted pre-Alpine events is a matter of ongoing debate. For instance, while Bernoulli and Weissert (2021) argue that the metamorphic facies record only the Alpine orogeny, Coltat et al. (2021) claim that the rocks of the Platta Nappe preserve the record of pre-Alpine, rift-related thermal events.

https://doi.org/10.3301/GFT.2023.02

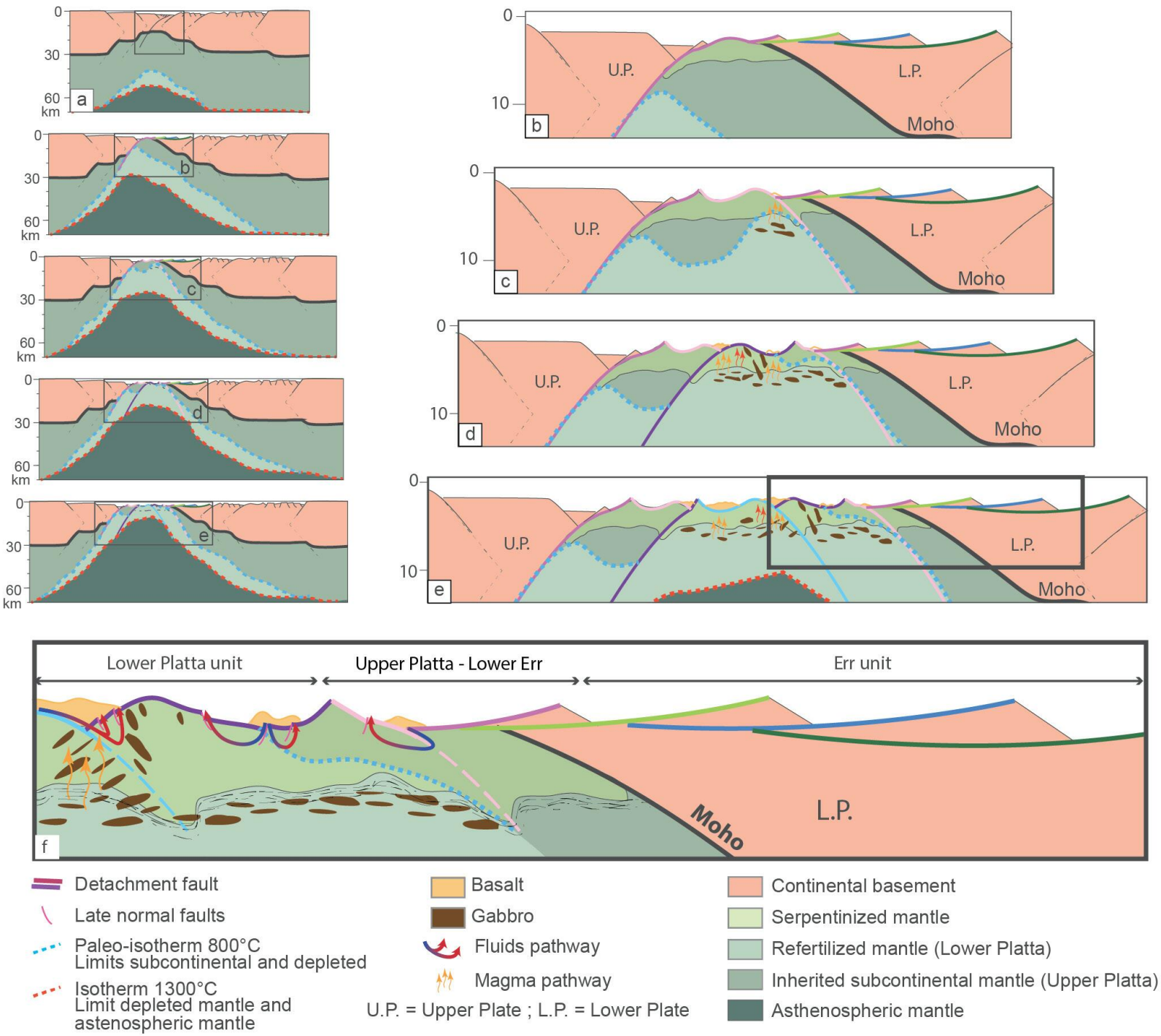

Fig. II.D.10 (modified from Epin et al., 2019) - Conceptual model showing the evolution of the OCT and its implication in the structural, thermal, and magmatic evolution. a) Conceptual model showing the large-scale evolution of the OCT and related mantle, the evolution of the 800 °C isotherm (brittle–ductile transition in lithospheric mantle) and the evolution of the 1300 °C isotherm (base lithosphere) during final rifting; b) first exhumation of subcontinental mantle; c) onset of exhumation of infiltrated mantle and first gabbro emplacement; d) exhumation of infiltrated mantle exhumation, formation of gabbros and emplacement of basalts; e) out-of-sequence fault evolution and increase in ascend of lithosphere-asthenosphere boundary and associated magmatic rock emplacement; f) conceptual model showing location of fluids and magma pathways across exhumed mantle linked to detachment faults evolution.

https://doi.org/10.3301/GFT.2023.02

FURTHER READING

Desmurs et al. (2001, 2002); Müntener et al. (2009); Epin et al. (2017, 2019); Amann et al. (2020); Coltat et al. (2019a, 2019b, 2020).

Ph.D. theses: Coltat (2020); Desmurs (2001); Epin (2017).

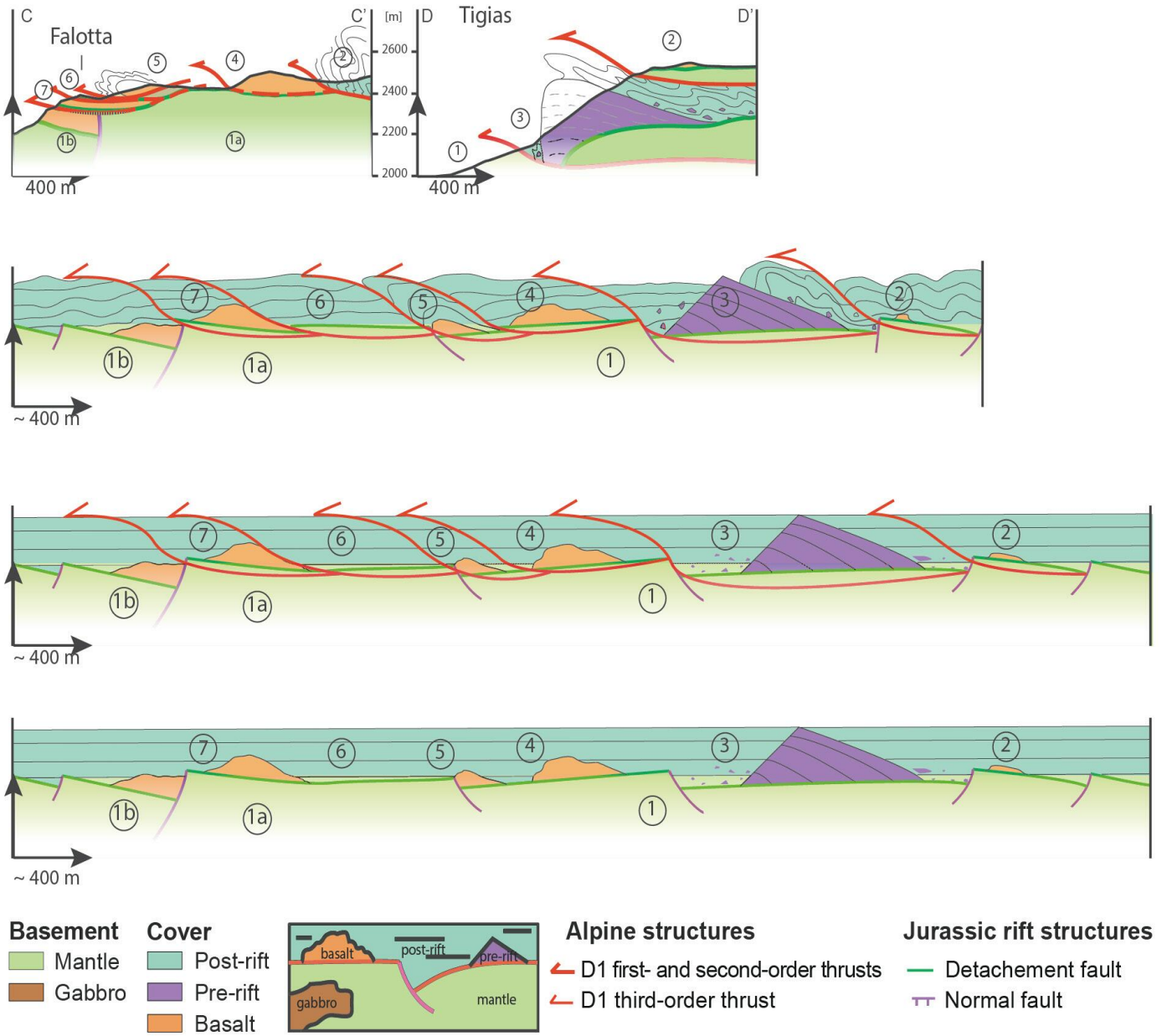

Fig. II.D.11 (modified from Epin et al., 2017) - Alpine sections through the Falotta and Tigias regions and their restoration to the pre-Alpine stage.

https://doi.org/10.3301/GFT.2023.02

EXCURSION E
The European-Briançonnais Ocean-Continent Transition: Tasna (Tasna Nappe, southeast Switzerland)

ABSTRACT

The Tasna Nappe in south-eastern Switzerland preserves a quasi-intact fragment of the Ocean-Continent Transition (OCT) between the former European-Briançonnais margin and the Valais Basin floored with exhumed mantle. The Tasna Nappe displays a wedge of continental crust adjacent to exhumed subcontinental mantle. Field evidence indicates two major detachment faults, namely the Upper Tasna Detachment (UTD) at the top of the crust, and the Lower Tasna Detachment (LTD) that extends from the base of the crust to the top of the exhumed mantle. This excursion aims to display: (1) the general architecture of an OCT; (2) the nature of crustal and mantle rocks involved; (3) the main deformation structures and their role; (4) the nature, origin, and architecture of the sedimentary deposits found in this OCT; (5) the paleogeography of the Alpine Tethys rift system; and (6) the architecture of the nappe stack associated with the reactivation of the Tasna OCT.

MAIN TAKE-AWAY OF THE EXCURSION

- **Age of rift-related deformation:** prior to the deposition of the Tithonian Falknis breccias (Late Jurassic); mantle exhumation was presumably coeval throughout the Ligurian-Piemonte-Valais domain and occurred after 170 Ma (post-Bathonian).
- **Deformation style:** essentially controlled by extensional detachment faults with minor subsequent normal faulting; intense hydrothermal activity.
- **Paleogeographic framework:** OCT between the Briançonnais continental ribbon and the distal European margin, forming a V-shaped basin referred to as the Valais Basin.
- **Onset of Alpine reactivation:** Post-Tasna flysch (Eocene).
- **Reactivation style:** thick-skinned tectonics (minor Alpine overprint within the Tasna Sliver).
- **Main remaining questions:** Where and how did the crust thin prior to final detachment faulting?

INTRODUCTION

The Tasna Nappe in south-eastern Switzerland belongs to the Penninic domain of the Alpine nappe stack. It displays a unique example of a quasi-undeformed OCT, well exposed along an SSW-NNE trending mountain ridge between Muot da l'Hom and Piz Tasna (Figs. II.E.1 and

https://doi.org/10.3301/GFT.2023.02

II.E.2). This former OCT was linked to the Briançonnais continental ribbon and was part of the Valais exhumed mantle domain (Fig. II.E.3). The Tasna OCT has been largely used as a field analogue for the most distal part of magma-poor rifted margins (e.g., Hölker et al., 2002; Manatschal, 2004; Reston and McDermott, 2011). In the past, most studies focused on the relationship between the tip of the continental wedge and the adjacent exhumed mantle (Florineth et al., 1994; Froitzheim et al., 1998; Manatschal et al., 2006). More recently, Ribes et al. (2019c) undertook a more comprehensive study, including the surroundings of the Tasna Nappe. From these new observations, they proposed a new stratigraphic framework for the Tasna OCT.

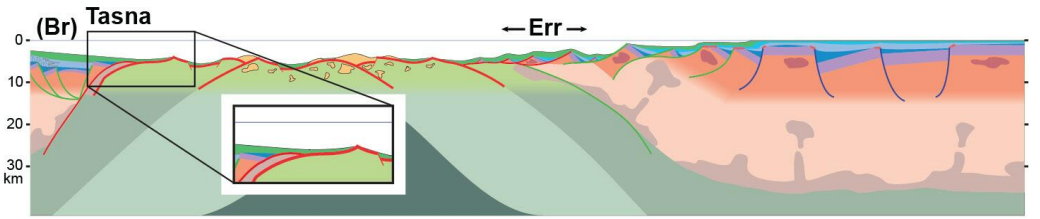

Fig. II.E.0 - Schematic section across the Alpine Tethys rift system showing the position of the Briançonnais (Br), Err and Tasna domains during the Middle Jurassic mantle exhumation phase (modified from Manatschal et al., 2022).

ITINERARY

This excursion takes place north of the villages of Ftan and Scuol, in the ski resort of Motta Naluns (Fig. II.E.1).

Stop 1 (viewpoint 1): From the north of Ftan, drive up on a mountain road (driving permission is needed). Bypass the cable car stations of Prui and Motta Naluns and park at the next intersection (P1 on Fig. II.E.1; GPS: 46°49'10.1"N 10°16'02.7"E, i.e., 46.819470, 10.267409). Look into the northwest between Piz Minschun and Piz Nair.

Stop 2: From P1, drive on ca. 550 m on the road track to the northwest and park at the restaurant (P2 on Fig. II.E.1; GPS: 46°49'02.0"N 10°15'45.5"E, i.e., 46.817210, 10.262644). From P2, walk ca. 75m to the west and turn right at the intersection. Follow the road track on ca. 800 m. Stop just before the creek bed (outcrop 2 on Fig. II.E.1; GPS: 46°49'21.1"N 10°15'11.0"E, i.e., 46.822514, 10.253041). Look at the rocks on the left-hand side of the track road.

Stop 3: From stop 2, keep walking up on the road track until the Mot da Ri ski lift station (GPS: 46°49'35.3"N 10°15'10.8"E, i.e., 46.826468, 10.253012). Outcrop 3 (Fig. II.E.1) is a few tens of meters up to the west (Moho-Lower Tasna Detachment outcrop).

Stop 4: From the Mot da Ri ski-lift station walk toward the north along the slope (do not follow the road to Champatsch but take the path to Fuorcla Champatsch that goes west of P. 2461 on Fig. II.E.1). Along the slope there are blocks of sedimentary and of mantle rocks derived from the contact between the exhumed mantle and overlying sediments.

Stop 5: Outcrop 5 in Fig. II.E.1 is located ca. 300 m west of the path to Fuorcla Champatsch, along the small creek in the Champatsch area (GPS: 46°50'24.4"N 10°15'38.3"E, i.e., 46.840112, 10.260629).

Stop 6: Ardez and surroundings.

https://doi.org/10.3301/GFT.2023.02

Stop 1: Tasna Panorama (46°49'10.1" N - 10°16'02.7" E)

The Tasna Nappe s.l. (Fig. II.E.2) was emplaced during Eocene-Oligocene Alpine convergence within a north verging nappe stack. This nappe stack comprises, from base to top (Fig. II.E.3b): (1) the Bündnerschiefer Nappe, which represents the infill of the Valais Basin; (2) the Tasna Nappe s.l., which includes remnants of continental crust, exhumed mantle, Mesozoic sediments, and flysch; (3) the Arosa Nappe, which preserves remnants of the southeastern OCT of the Piemonte-Ligurian Basin; and (4) the Austroalpine Nappe Complex, which preserves remnants of the Adriatic margin.

The Tasna Nappe s.l. comprised of 3 main tectonic units (Fig. II.E.2):

- the Upper Tasna Unit lies around the village of Ardez. It is made of continental crust covered with remnants of autochthonous Triassic to Lower Jurassic sediments, and then by upper Mesozoic to lower Cenozoic sediments;
- the Middle Tasna Unit lies north of the Upper Tasna Unit, between Muot da l'Hom and Piz Tasna. It represents the OCT itself, where lower continental crust and subcontinental lithospheric mantle were exposed next to each other to the seafloor and overlain by Early Cretaceous to Eocene sediments;
- the Lower Tasna Unit lies beneath the Middle Tasa Unit, in the Champatsch area. It comprises serpentinized mantle peridotites, basalts, and continent-derived allochthonous blocks covered with undated shales and Tithonian calcareous siltstones with breccia layers.

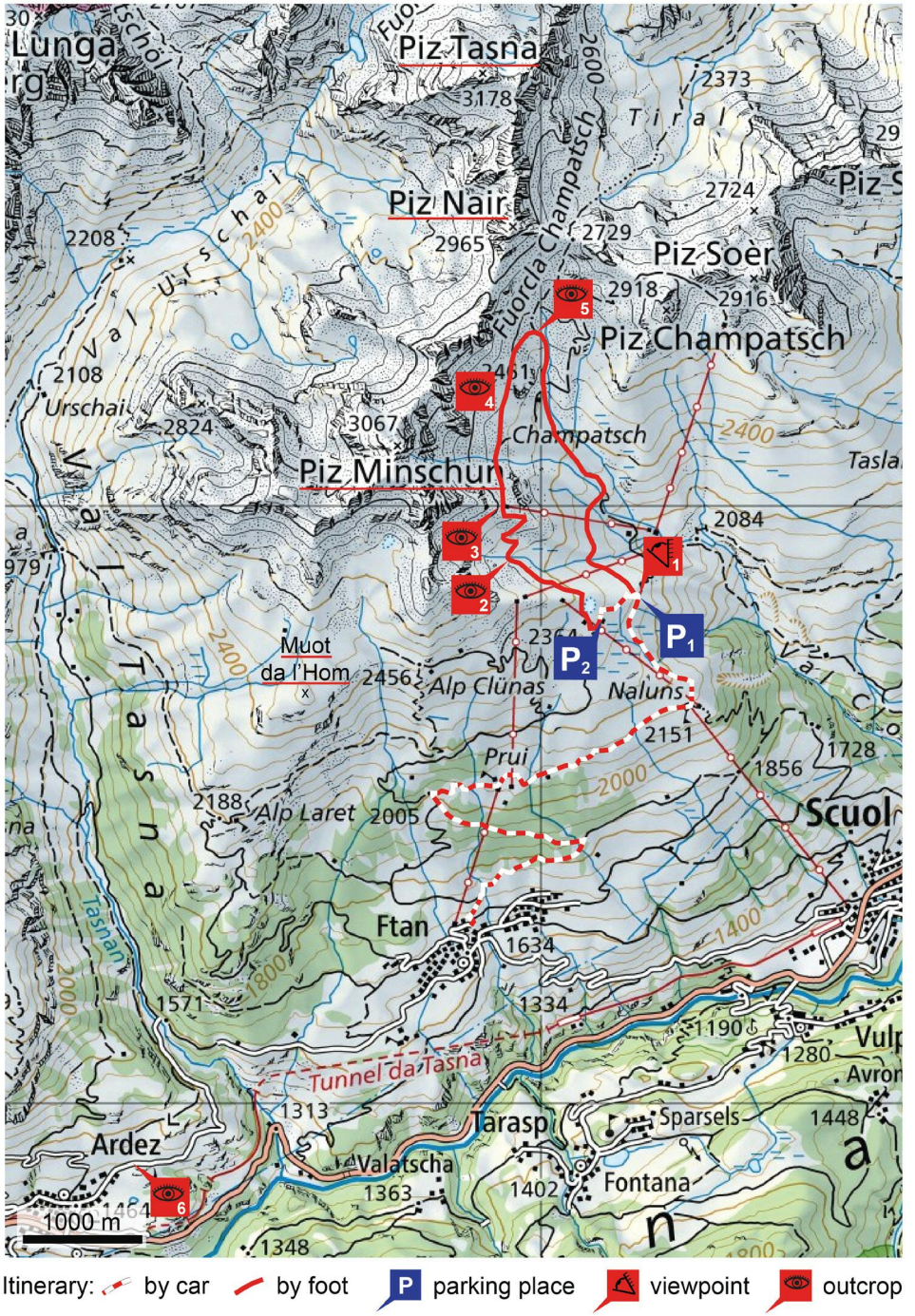

Fig. II.E.1 - Map of the Tasna area and route to the viewpoints and outcrops (background map from https://map.geo.admin.ch/).

https://doi.org/10.3301/GFT.2023.02

The present-day structure of the Tasna Nappe was described by Froitzheim and Rubatto (1998) as a wedge of continental crust next to exhumed subcontinental mantle, both covered by sediments. The crustal wedge is bounded by two detachment faults (Fig. II.E.4): the Upper Tasna Detachment (UTD) above separates continental crust from overlying sediments. The Lower Tasna Detachment (LTD) below separates the subcontinental mantle from the overlying continental crust in the southern part of the Middle Tasna Unit, and exhumed mantle from the overlying sediments in the northern part. Thus, the LTD truncates the UTD (Ribes et al., 2019c), contrary to what Manatschal et al. (2006) suggested.

Hölker et al. (2002) investigated the seismic expression of such an OCT. They highlighted that, on a synthetic Tasna-type seismic section, only lithological contacts stand out, while no fault is visible (Fig. II.E.5). Thus, the relatively flat-lying exhumed mantle can easily be misinterpreted as pre-rift basement in seismic sections.

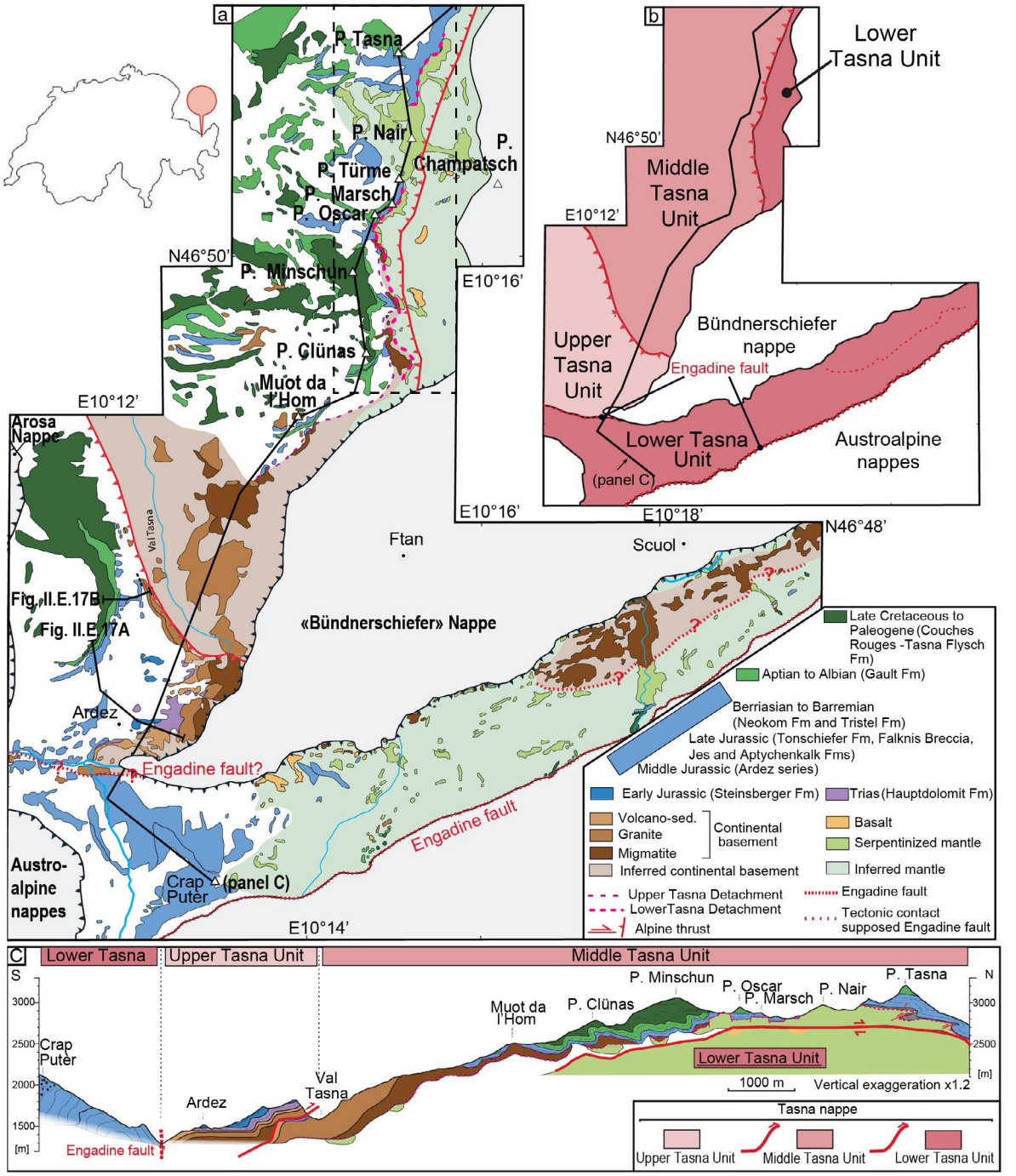

Fig. II.E.2 (modified from Ribes et al. 2019c) - a) Geological map of the Tasna Nappe in eastern Switzerland; b) map showing the upper-, middle-, and lower tectonic units constituting the Tasna Nappe s.l. (Upper-, Middle-, and Lower Tasna units), which were stacked as a result of north-directed convergence; c) cross-section along a S-N transect across the Tasna Nappe s.l. (see panel (a) for location). Abbreviations: P.:Piz; volcano-sed.: volcano-sedimentary.

https://doi.org/10.3301/GFT.2023.02

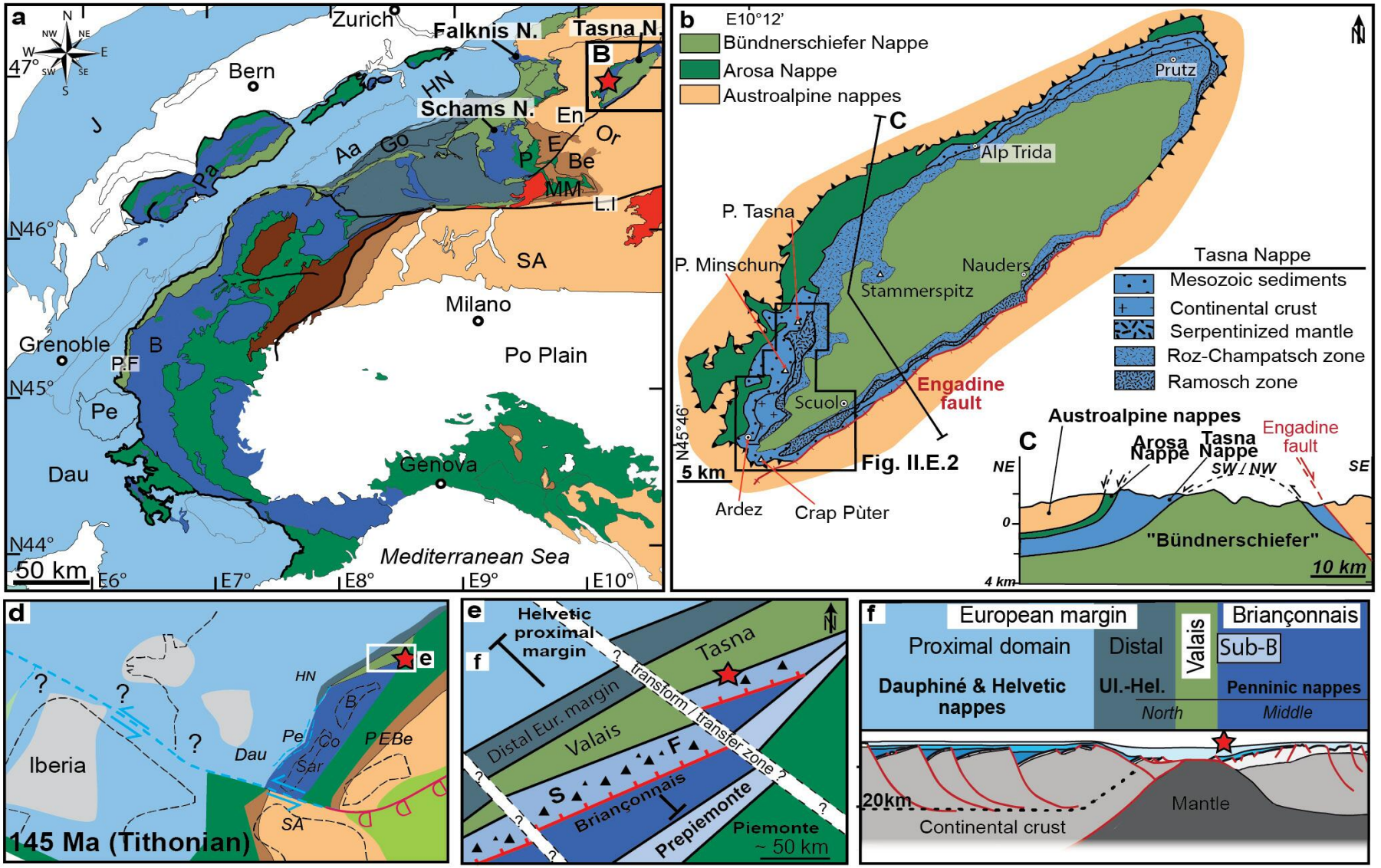

Fig. II.E.3 (from Ribes et al., 2019c) - Geological setting of the Tasna Nappe and its position in the former Alpine Tethys rift system. a) Tectonic map of the western- and central Alps; b) tectonic map and (c) cross-section through the Engadine window; d-e) paleogeographic reconstruction showing the Alpine realm at the end of Jurassic; f) cross-section through the Alpine Tethys margins at the end of rifting and before onset of Alpine convergence in Late Cretaceous time (no scale intended). The red star marks the location of the Tasna Nappe (see panel (e) for location of the cross-section). Abbreviations: Aa: Aar massif; B: Briançonnais nappes; Be: Bernina Nappe; Co: Corsica; Dau: Dauphiné nappes; E: Err Nappe; En: Engadine fault; F: Falknis domain; Go: Gothard massif; HN: Helvetic nappes; J: Jura; MM: Malenco-Margna nappes; Or: Ortler; P: Platta; Pa: Prealps; Pe: Pelvoux massif; SA: Southern Adria; Sar: Sardinia; L.I.: Insubric Line; N.: nappe; P.F.: Penninic Front; S: Schams domain; SubB: Subbriançonnais; Ul.-Hel.: Ultra-Helvetic. Colours of units refer to the paleogeographic domains.

https://doi.org/10.3301/GFT.2023.02

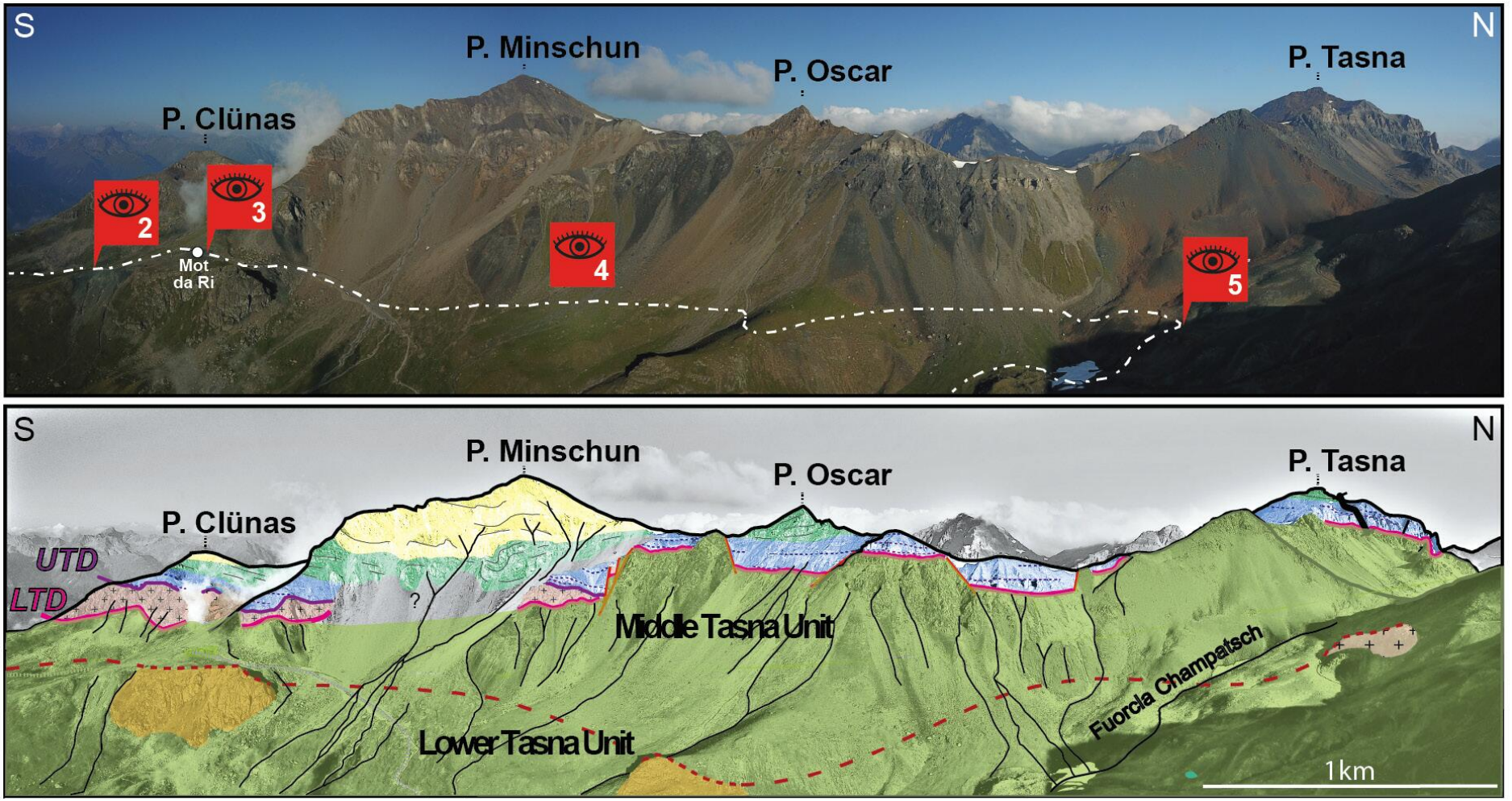

Fig. II.E.4 (modified from Ribes et al. 2019c) - Photograph and interpretation from the Middle Tasna Unit between Piz Clünas and Piz Tasna. The large-scale architecture viewed from the east shows the relationship between sediments and basement rocks, including migmatite rocks and exhumed mantle. For location of the photograph, see Fig. II.E.2. Abbreviations: UTD (purple): Upper Tasna Detachment; LTD (magenta): Lower Tasna Detachment; P.: Piz; sed.: sediments.

https://doi.org/10.3301/GFT.2023.02

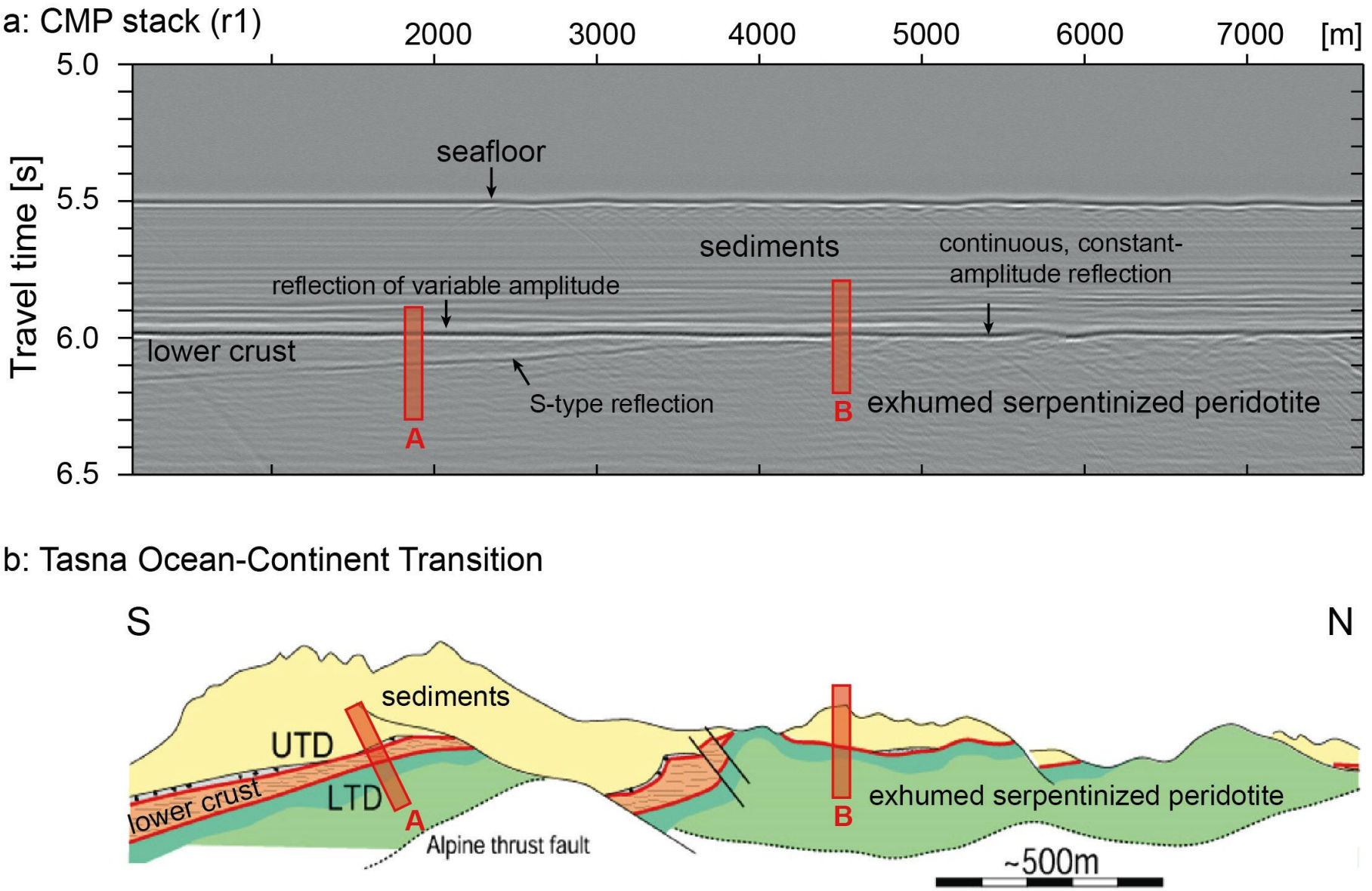

Fig. II.E.5 – a) Synthetic seismic section of the Tasna outcrop where velocities/densities were reckoned from log data from ODP Sites at the Iberia OCT (Hölker et al. 2002); b) geological profile of the Tasna OCT outcrop (modified from Florineth and Froitzheim 1994 and Manatschal et al., 2006).

https://doi.org/10.3301/GFT.2023.02

Stop 2: Characteristics of crustal and mantle rocks (46°49'21.1" N - 10°15'11.0" E)

In the Middle Tasna Unit, the continental basement is made of migmatites, gabbros, and diorites (Ribes et al., 2019c). Pressure-Temperature-time (P-T-t) estimates on these rocks indicate that they were emplaced at ca. 500 °C and 4-8 kbar during late Carboniferous to Permian time (Manatschal et al., 2006; Fig.II.E.7a and II.E.7b). These conditions testify to a pre-rift lower crust origin.
In contrast, the Upper Tasna Unit displays relics of upper crustal units, either made of granite or of Permian volcano sediments interpreted as the infill of a Permian basin (Ribes et al., 2019c; see Stop 6: village of Ardez and surroundings).
Both basement relics largely preserve their pre-rift magmatic textures, which suggests a lack of distributed syn-rift deformation in both the upper- and lower crust. No evidence for a pre-rift middle crust was found in the Tasna Nappe.
From these observations, Ribes et al. (2019c) deduced that crustal thinning was achieved via middle crust deformation during necking, rather than by lower crustal flow during hyperextension. Petri et al. (2019) found evidence of localized shear zones in basement rocks of the conjugate Adriatic margin and hypothesized a comparable mechanism for crustal thinning in the Briançonnais-European margin.
The mantle exhumed in the Tasna Nappe is made of highly serpentinized (>90%) spinel lherzolite derived from the subcontinental lithospheric mantle (Mantle type 1a of Picazo et al., 2016; Fig. II.E.6d). It equilibrated at a temperature of 900±50 °C, consistent with other subcontinental mantle peridotites exhumed close to the continent during Jurassic rifting (Fig. II.E.7c). These peridotites largely preserve their pre-rift high-temperature texture, which suggests that they did not undergo pervasive shearing during its exhumation to the seafloor. $^{40}Ar/^{39}Ar$ dating on mantle-derived phlogopite provides a cooling age of ca. 170 Ma (Bajocian time; Manatschal et al., 2006; Fig. II.E.7d). Exhumed mantle rocks are capped by ophicarbonates (cf. the Fluids thematic sheet) and tectono-sedimentary breccias.

Stop 3: Extensional structures (46°49'35.3" N - 10°15'10.8" E)

The Middle Tasna Unit displays two major extensional detachment structures: (1) the UTD at the top of the continental crustal wedge separates lower crust migmatites from a Jurassic sedimentary cover; and (2) the LTD at the base of the crustal wedge separates lower crust migmatites, gabbros, and diorites from mantle rocks. Both are planar structures, and both record a comparable extension displacement top to the NW in present-day coordinates.
The core zone of the UTD is formed by gouges and/or foliated cataclasites (Fig. II.E.6e) preceded by a less than 10 m-thick damage zone (Fig. II.E.6g). In the Upper Tasna Unit, the UTD manifests as a strongly tectonized top granitic basement and the pre-rift sequence is not preserved. The first sediment over the tectonized basement is a 5-m-thick clast- to matrix-supported breccia with gravel-sized clasts of Triassic dolomites, granites, and Carboniferous to Permian volcano-sedimentary sequences and gneisses (i.e., "Lias breccie" of Gruner, 1981; Fig. II.E.6a).

https://doi.org/10.3301/GFT.2023.02

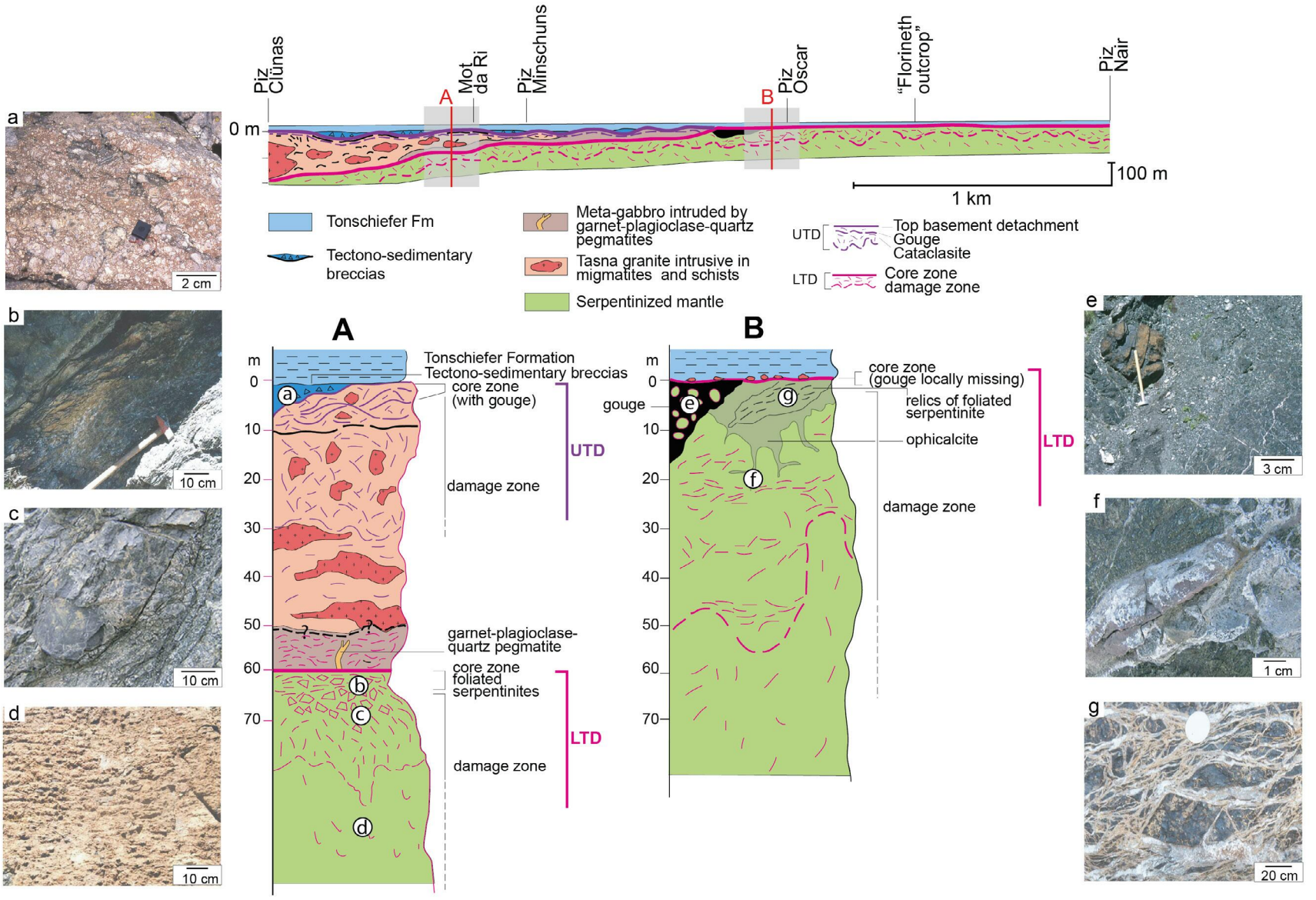

Fig. II.E.6 (modified from Manatschal et al., 2006) - Lithologies and low-temperature deformation structures in the Tasna OCT. Logs A and B show the relationships between structures and lithologies in a continental section (A) and in an exhumed mantle section (B). a-g) Deformation structures and fault rock types observed in the exhumed mantle rocks in the Tasna OCT. a) tectono-sedimentary breccia overlying the UTD; b) foliated serpentinite in the core zone of the LTD; c) serpentinite cataclasite, ca. 50 m below LTD; d) spinel foliation ca. 100 m below the LTD; e) serpentinite gouge ca. 15 m below the UTD; f) red microsparitic calcite vein, ca. 20 m below the LTD; g) foliated serpentinite cataclasite 0.3 m below LTD. Abbreviations: : UTD Upper Tasna Detachment; LTD: Lower Tasna Detachment.

https://doi.org/10.3301/GFT.2023.02

The LTD fault core is made of foliated cataclasites preceded by a >100 m-thick damage zone (Figs. II.E.6b-d). Deformation along this detachment occurred under greenschist facies to seafloor conditions and within the serpentine stability field.

Note that, because both the UTD and LTD display only evidence for deformation in the brittle field, they cannot account by themselves for the upper- and lower-crust juxtaposition.

Where prolate-shaped clasts exist in the gouges of the UTD and LTD, they define an NW-SE-directed lineation (Fig. II.E.8a). Relying on this lineation and on the asymmetry of the clasts in the gouge, a top-to-the northwest transport direction can be determined for both detachments. Structural measurements also indicate a planar sub-horizontal fault architecture for both detachments that is sub-parallel to the overlying sediments (i.e., sub-horizontal at the time of sediment deposition; Fig. II.E.8b).

Because the damage zone of both detachments is located in the footwall only and does not affect the overlying pre-Alpine sediments (Fig. II.E.9a),

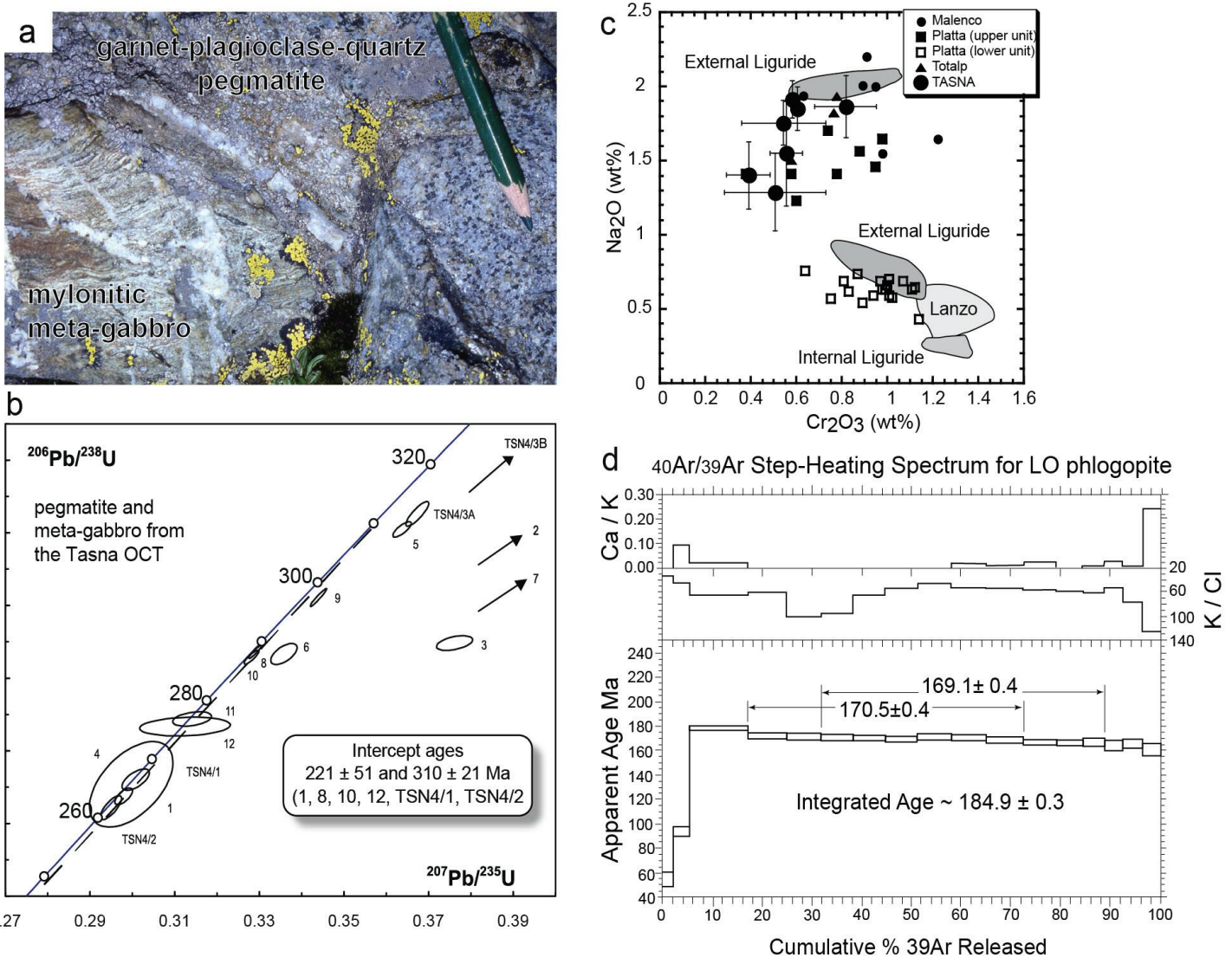

Fig. II.E.7 (from Manatschal et al., 2006) - a) Continental basement in the Tasna OCT at Mot da Ri showing a garnet-plagioclase-quartz pegmatite cutting foliated meta-gabbro; b) concordia plot of U/Pb zircon analyses of pegmatite and meta-gabbro from the Tasna OCT; c) comparison of the clinopyroxene composition of the spinel lherzolite from the Tasna OCT (Na vs. Cr) with those of other ultramafic units in the Alps and the Northern Apennines. For references and locations see Müntener et al. (2004). Clinopyroxenes from the Tasna OCT are similar to the Malenco and Totalp units and the Upper Unit in the Platta Nappe. All these units are interpreted as subcontinental mantle peridotites exhumed next to the continent in a former OCT (Müntener et al., 2004); d) $^{40}Ar/^{39}Ar$ ages on phlogopite derived from a spinel websterite sampled at the Tasna OCT.

https://doi.org/10.3301/GFT.2023.02

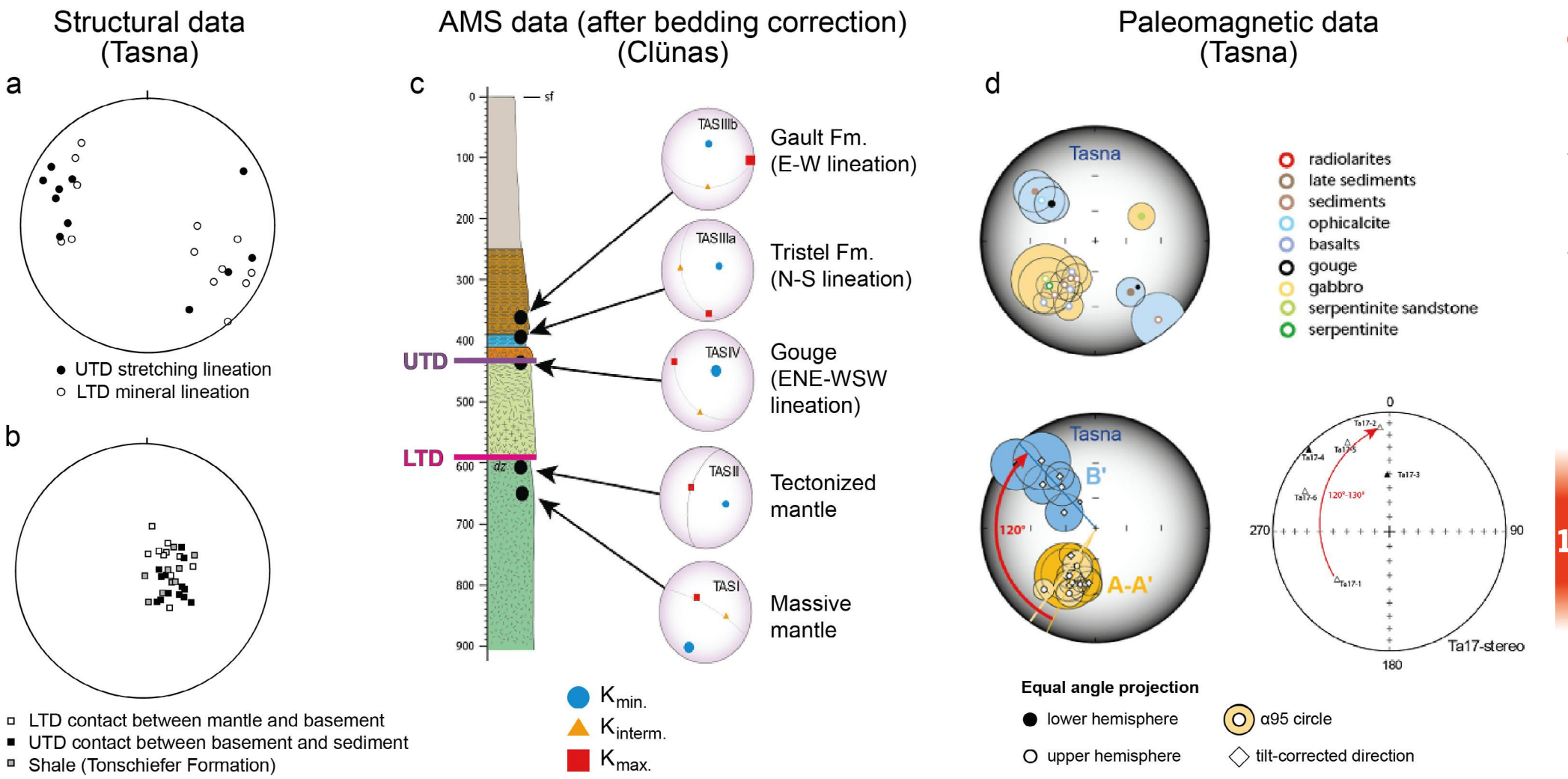

Fig. II.E.8 - a-b) Stereonet showing an equal area lower hemisphere projection (from Manatschal et al. 2007); a) elongated clasts in gouges along the UTD defining stretching lineations and mineral lineations in foliated serpentinites and continental rocks along the LTD; b) pole to plane representation of the UTD and LTD surfaces displayed together with measurements of bedding within the overlying sediments sealing the OCT; c) Anisotropy of Magnetic Susceptibility (AMS) data from Piz Clünas; K_{min}, K_{interm} and K_{max} represent the three axis of the magnetic susceptibility ellipsoid (Jean-Bernard Edel; unpublished); d) paleomagnetic data from the Tasna Nappe (Jean-Bernard Edel; unpublished). Abbreviations: UTD Upper Tasna Detachment; LTD: Lower Tasna Detachment.

https://doi.org/10.3301/GFT.2023.02

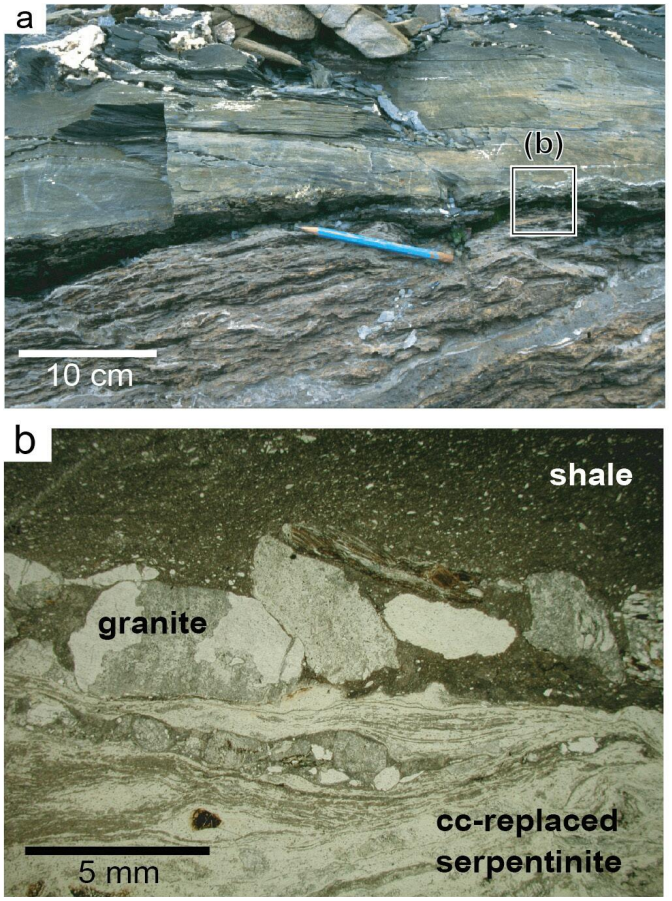

Fig. II.E.9 (from Manatschal et al., 2006) - Deformation structures in the continental basement and exhumed mantle associated with the UTD. A) Basement-cover contact in the Tasna OCT showing exhumed foliated mantle rocks, stratigraphically overlain by undeformed shales; b) thin section in plane polarized light of the basement-cover contact shown in (a). The section shows undeformed shales overlying a foliated serpentinite replaced by calcite. Note the imbricated and rounded clasts at the interface between sediments and exhumed mantle. All clasts are continent-derived detritus. In the exhumed mantle, chlorite and serpentine minerals define the foliation. The latter are almost completely replaced by calcite (cc). Remnants of core-and-mantle structures and σ-type porphyroclasts occur in these rocks.

both structures are considered as pre-Alpine. However, paleomagnetic data (Fig. II.E.8d) show that Tasna underwent a clockwise rotation between the time of mantle exhumation and the present, and thus none of the directions measured in the field can be interpreted as a reliable direction preserved from the former Alpine Tethys framework.

Stop 4: Sediments (46°50'08.1" N - 10°15'08.1" E)

In the Middle Tasna Unit, Jurassic sediments onlap directly onto the Upper- and Lower Tasna detachments over ca. 6 km (i.e., at the top of exhumed continental lower crust and exhumed mantle).

The first sediments onto exhumed mantle are lime-free, dark shaly sediments with a high proportion of clay minerals and pyrite known as the Tonschiefer Fm (Figs. II.E.10, II.E.11 and II.E.13; Florineth and Froitzheim, 1994). Although this formation was not formerly dated, it is reckoned to be of Late Jurassic age (Ribes et al. 2019c). The thickness of the Tonschiefer Fm varies largely along the Middle Tasna Unit, from <1 m in the southern part (Muot da l'Hom; Fig. II.E.12) to more than 25 m in the northern part (Piz Tasna; Fig. II.E.12; Ribes et al., 2019c). It contains local clasts of migmatite and mantle material, as well as a few manganese and phosphate nodules.

The overlying Falknis Breccia Fm is up to 40 m thick (Fig. II.E.14). It also onlaps onto the exhumed lower crust. The basal part of the Falknis Breccia Fm is comprised of poorly graded, clast-supported breccias. Clasts are mainly of continental origin (granite, granodiorite, diorite, migmatite and volcano sediments), but also semi-lithified clasts of late Jurassic limestones from the Briançonnais domain. Above, Falknis breccias become matrix-supported, and the contact with the underlying clast-supported breccias may be locally erosive.

The following sedimentary deposits are made of shales and marls (Neokom Fm), which become interbedded with calcarenite (Tristel Fm). The overlying Gault Fm is made of turbiditic, siliciclastic deposits. The sedimentary succession ends with the Couches Rouges and Tasna Flysch Fms, which are both characteristic of Alpine convergence.

Anomaly of Magnetic Susceptibility (AMS) data highlight that transport direction in the trurbidites of the Gault Fm was along strike of the paleo-margin (i.e., axial sedimentation), while the underlying debris flows of the Tristel and Falknis Fms were along dip (Fig. II.E.8b).

https://doi.org/10.3301/GFT.2023.02

Detrital zircon provenance analysis (Ribes et al. 2019c) showed that the source of the sandstones interbedded within the Falknis Breccia Fm (samples CR-T-03H and CR-T- 03G in Fig. II.E.15) is distinct from that of the Tonschiefer Fm. This means that both formations are not derived from the erosion of a unique local Penninic basement. A distinct source, or at least the contribution of one (or several) other source(s), must be considered.

Stop 5: Lower Tasna Unit (46°50'24.4"N - 10°15'38.3"E)

The basement of the Lower Tasna Unit consists of serpentinized peridotites. These are crosscut by rodingitized mafic dykes and locally overlain by basaltic bodies of MORB affinity (Amann, 2017). A magmatic vein in the mantle was dated 167.3±2.7 Ma using U-Pb on zircon, and ca. 161 Ma using $^{40}Ar/^{39}Ar$ on phlogopite (Hauser, 2011). Sediments locally occur directly on the exhumed mantle and are sometimes either overlain or interbedded with pillow basalts (Fig. II.E.16; Ribes et al. 2019c). These sediments consist of a decimetre-thick layer of greenish

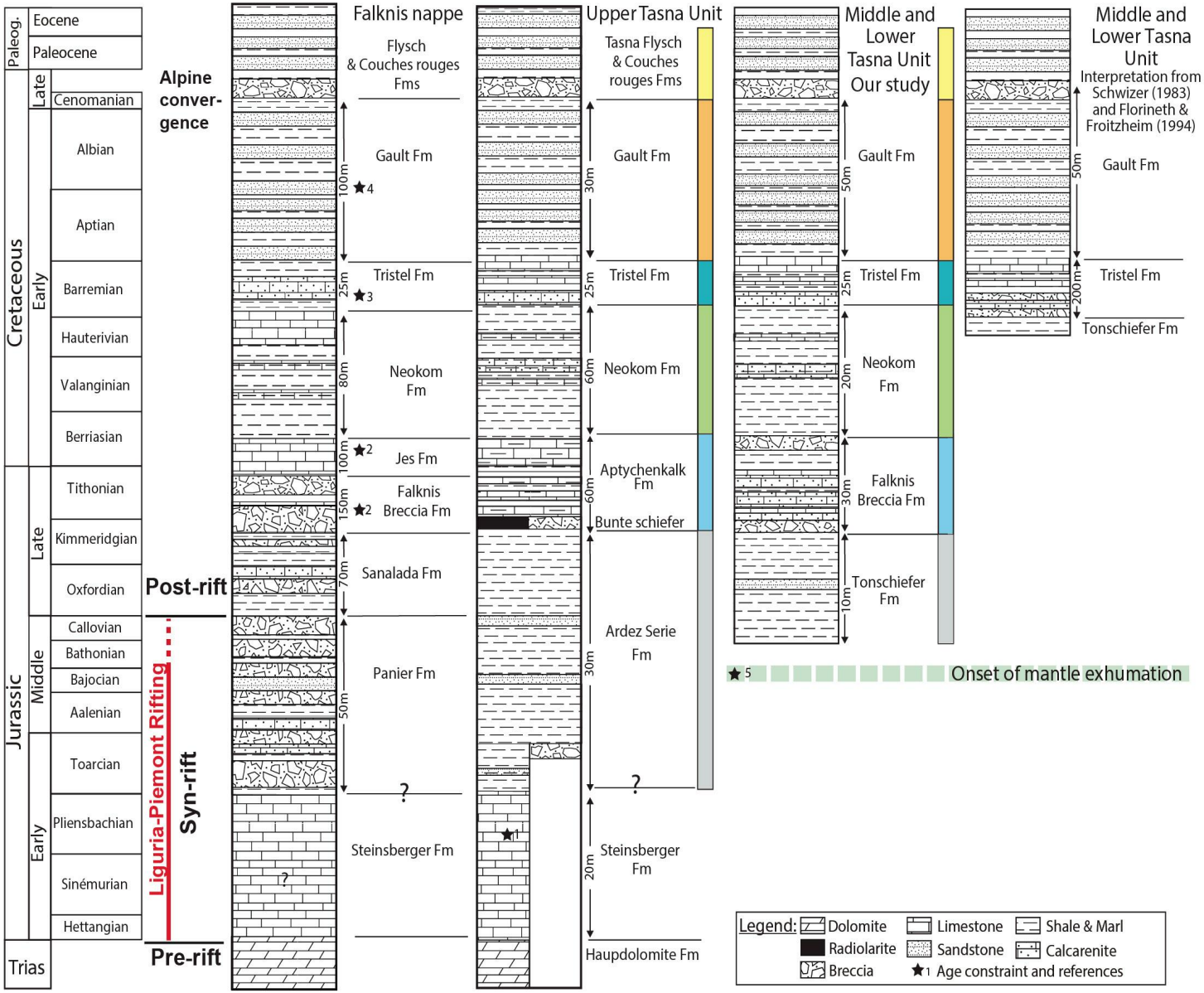

Fig. II.E.10 (from Ribes et al. 2019c, cum ref.) - Simplified stratigraphic columns of Tasna and Falknis nappes, Middle Penninic nappes. Black stars represent age-constrained references: 1 - Dommergues et al. (2012); 2 - Gruner (1981); 3 - Grüler (1995); 4 - Allemann (1957), Hesse (1974); 5 - Manatschal et al. (2006). Abbreviations: Trias: Triassic; Paleog.: Paleogene.

https://doi.org/10.3301/GFT.2023.02

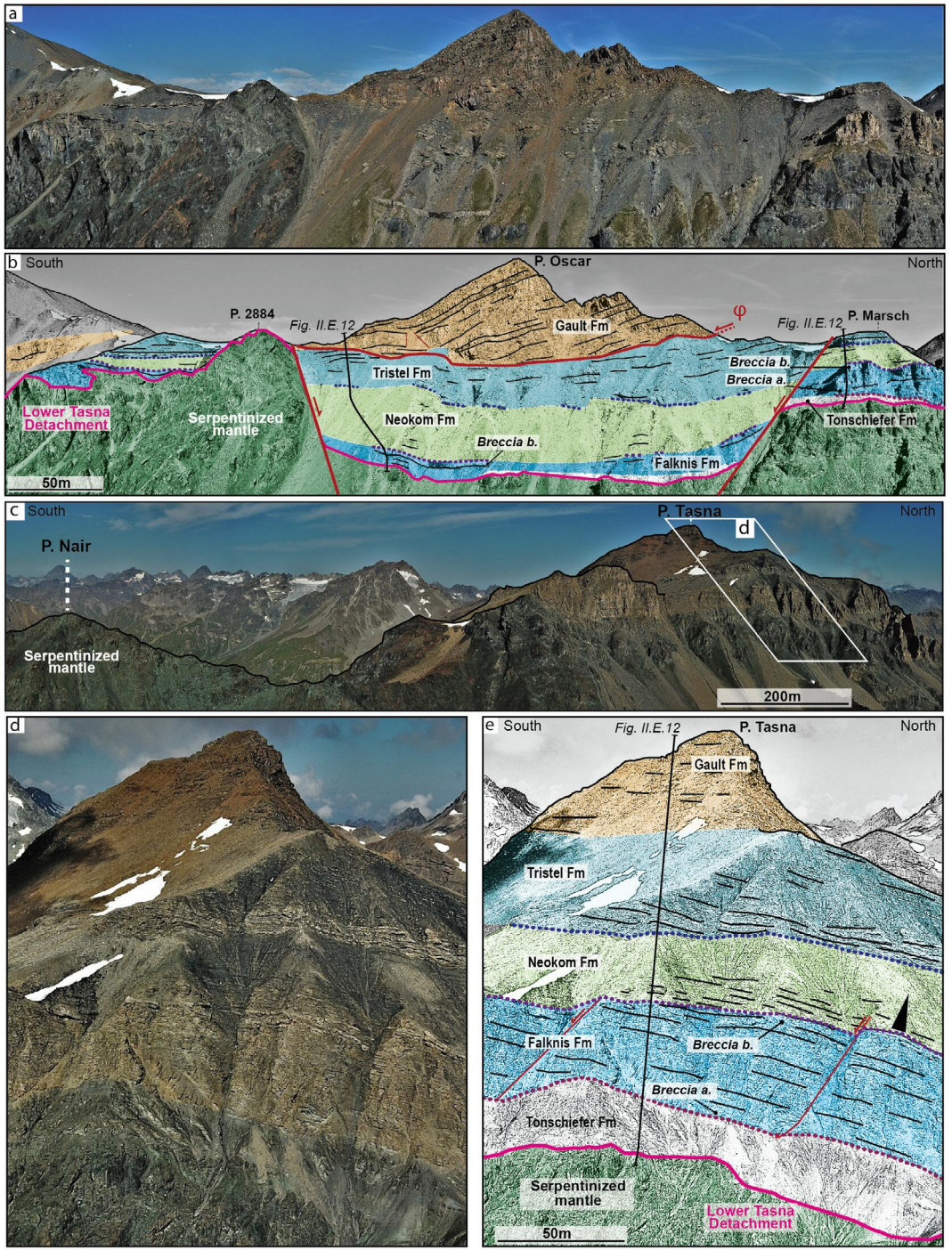

fine-grained sand overlain by either pillow basalts (Fig. II.E.16B) or beige immature sediments including reworked feldspar and amphibole grains (Fig. II.E.16A). Locally, isolated blocks of Triassic Hauptdolomit Fm occur directly on the exhumed mantle. They represent remnants of the former hanging wall stranded on the exhumed mantle (e.g., Tigias area in Excursion D; Epin et al., 2017). Up-section, sedimentary deposits evolve into a 3 m-thick package of medium-bedded, fine- to medium-grained siliciclastic turbidites interbedded with dark shale intervals (Fig. II.E.16). One of the dark shale intervals contains a thin basaltic lava flow (Fig. II.E.16; Ribes et al. 2019c). In the basal layer, Mg-chlorite is likely the result of submarine alteration and reworking of mafic and ultramafic rocks (e.g., Bracciali et al., 2014). Upward, the dark shales and quartz-dominated beds are erosional products of the continental basement. The latter deposits are attributed to the Tonschiefer Fm, given the lithological similarity with sandstone beds and dark shales of the Tonschiefer Fm in the Middle Tasna Unit (Fig. II.E.11).

Stop 6: Upper Tasna Unit (Ardez village and surroundings)

The village of Ardez is overlooked by the Steinsberg Castel, which sits on the late Sinemurian carbonates of the Steinsberger Fm (Dommergues et al., 2012). The Steinsberger Fm contains coarse

Fig. II.E.11 (modified from from Ribes et al. 2019c) - Photograph and interpretation across the Middle Tasna Unit illustrating the relation between the exhumed serpentinized mantle and sediments. a–b) Panorama of Piz Oscar area (WGS 84 coordinates: 46°50′19″N, 10°14′49″E); the red lines represent post-exhumation high-angle normal faults and décollement (ϕ); c) panorama from Piz Nair to Piz Tasna (WGS 84 coordinates: 46°50′51″N, 10°15′18″E); d-e) photograph and interpretation of Piz Tasna area (WGS 84 coordinates: 46°51′34″N, 10°15′09″E). Abbreviation: P.: Piz.

https://doi.org/10.3301/GFT.2023.02

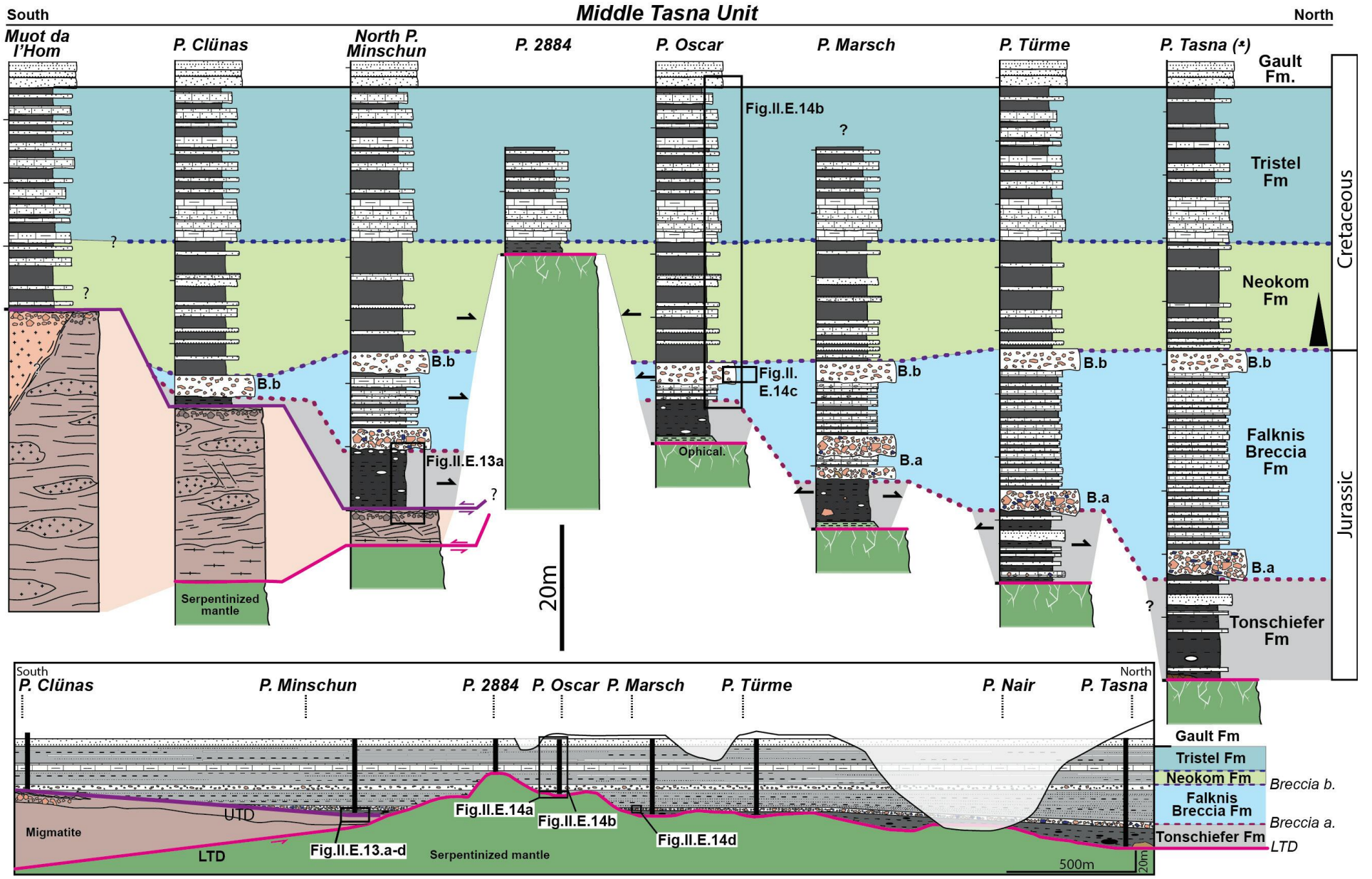

Fig. II.E.12 (modified from Ribes et al., 2019c) - Representative sedimentary successions across the Middle Tasna Unit and south-north section correlation along the basin depot axis correlation (i.e., in transport direction of the detachment fault). Lines correspond to correlations (i.e., correlative beds or facies tract boundaries). Abbreviations: UTD (purple): Upper Tasna Detachments; LTD (magenta): Lower Tasna Detachments; P.: Piz.

https://doi.org/10.3301/GFT.2023.02

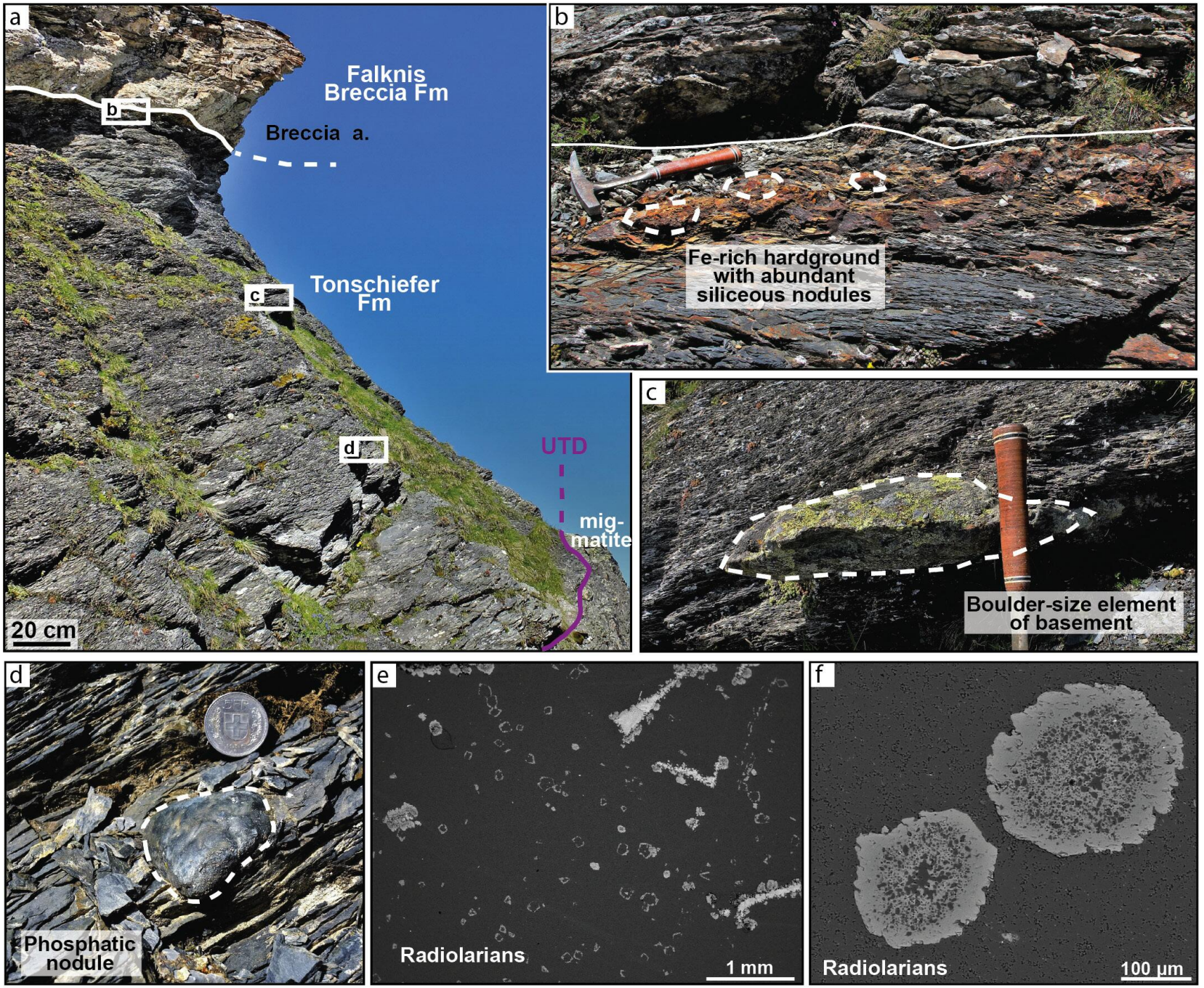

Fig. II.E.13 (from Ribes et al., 2019c) - Outcrop photographs and Scanning Electron Microscopy (SEM) images of representative sedimentary facies of the Tonschiefer Formation from the Middle Tasna Unit. a) Panoramic view of the migmatite basement overlain by the Tonschiefer and Falknis Formations in the northern Piz Minschun section (UTD-Upper Tasna Detachment); b) Fe-rich hardground, partly pyritized and containing abundant siliceous nodules with radiolarians observed at the top of the Tonschiefer Formation; c) isolated boulder-size element derived from the migmatitic gneiss basement in the Tonschiefer Formation; d) silica-rich phosphatic nodule with radiolarian microfossils in the Tonschiefer Fm; e-f) SEM images from siliceous nodules, containing radiolarians and *Calpionella*(?) fossils.

https://doi.org/10.3301/GFT.2023.02

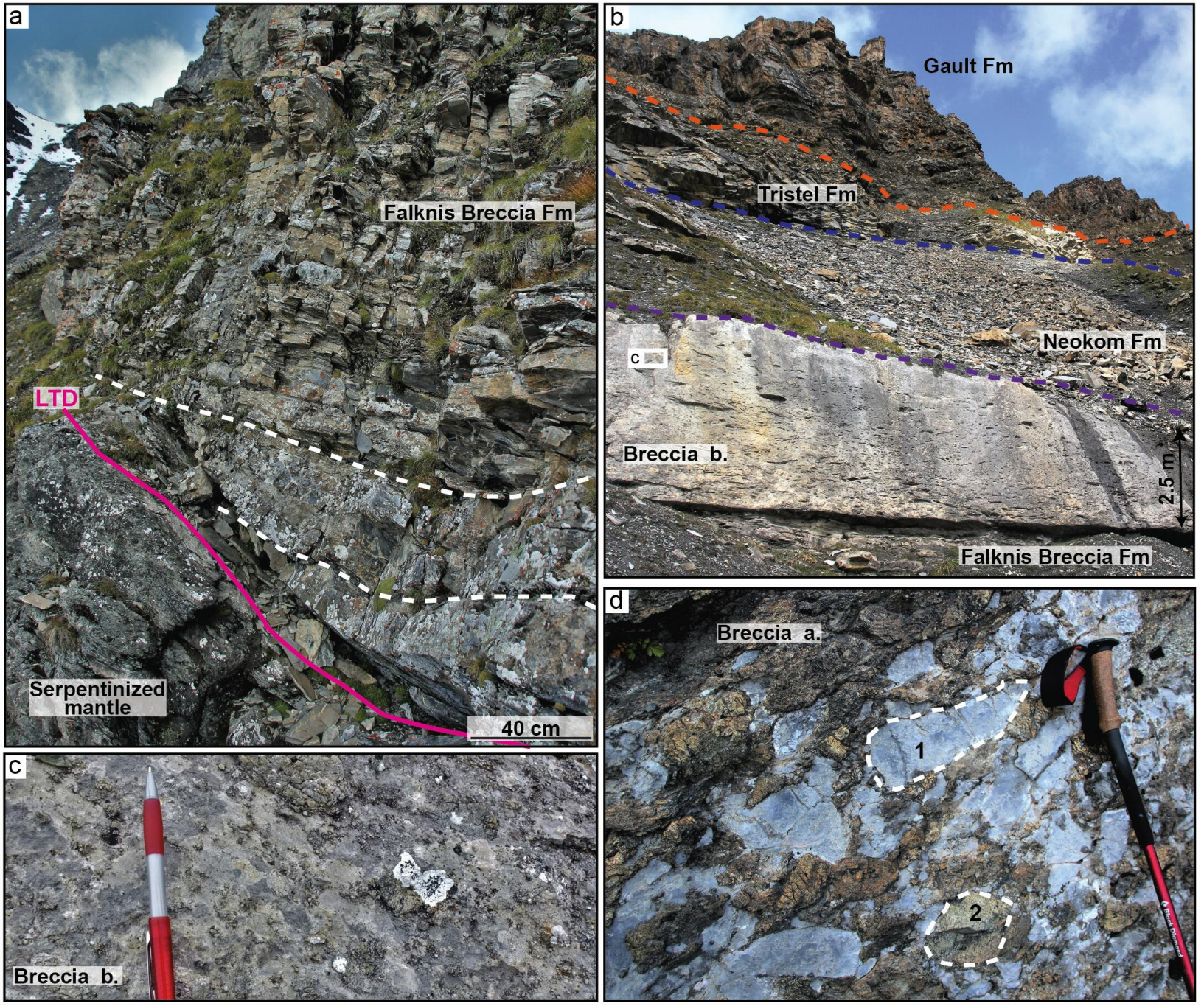

Fig. II.E.14 (from Ribes et al., 2019c) - Outcrop photographs of representative sedimentary facies of Middle Tasna Unit. a) Panoramic view of the serpentinized mantle basement (LTD-Lower Tasna Detachment) onlapped by thin- to medium-bedded calcarenites of the Falknis Breccia Formation in the Piz Oscar section; b) panoramic view of the breccia-prone, shale-rich, and the calcarenite-rich packages reinterpreted as the Falknis, Neokom, and Tristel Formations. Uppermost section corresponds to the Gault Formation. The dashed lines represent the formation limits; c) Breccia b of the breccia-prone package interpreted as the uppermost Falknis Formation. Breccia b consists of unsorted matrix-supported breccias with a light grey to bluish limestone matrix. The size of the clasts ranges from a few centimetres up to 30 cm, and the clasts are derived from the continental crystalline basement; d) image of the breccia-prone package interpreted as the basal Falknis Formation (Breccia a). This breccia is poorly graded, mostly made of pebble- to boulder-sized clast-supported breccias composed of (1) semi-consolidated clasts of marly limestones, and (2) angular to subrounded continental basement clasts, in a calcareous matrix.

https://doi.org/10.3301/GFT.2023.02

breccias with angular clasts derived from the Triassic Hauptdolomit Fm (Gürler, 1995). These limestones overlie thin, Upper Triassic dolostones, late Carboniferous to Permian volcano-sedimentary sequences, and Tasna granite (Cadisch, 1932; Grüler, 1995). Ribes et al. (2019c) interpreted this succession with preserved pre-rift strata above the basement as remnants of an allochthonous block.

Toward the northwest (Fig. II.E.2a), the top of the granitic basement is strongly tectonized, and the pre-rift sequence is not preserved. The first sediments occurring directly on the tectonized basement are clast- to matrix-supported breccias with gravel-sized clasts of Triassic dolostones, granites, and late Carboniferous to Permian volcano-sedimentary sequences and gneisses (i.e., "Lias breccie" of Gruner, 1981; Fig. II.E.17d). The matrix of this breccia consists of strongly transformed greenish schists and silica (Gürler, 1995). Ribes et al. (2019c) interpreted the top of the basement as a detachment fault that was exhumed to the seafloor (Fig. II.E.17c). The late Lower- to Upper Jurassic Ardez Fm, which overlies both the Steinsberger Fm and the allochthonous

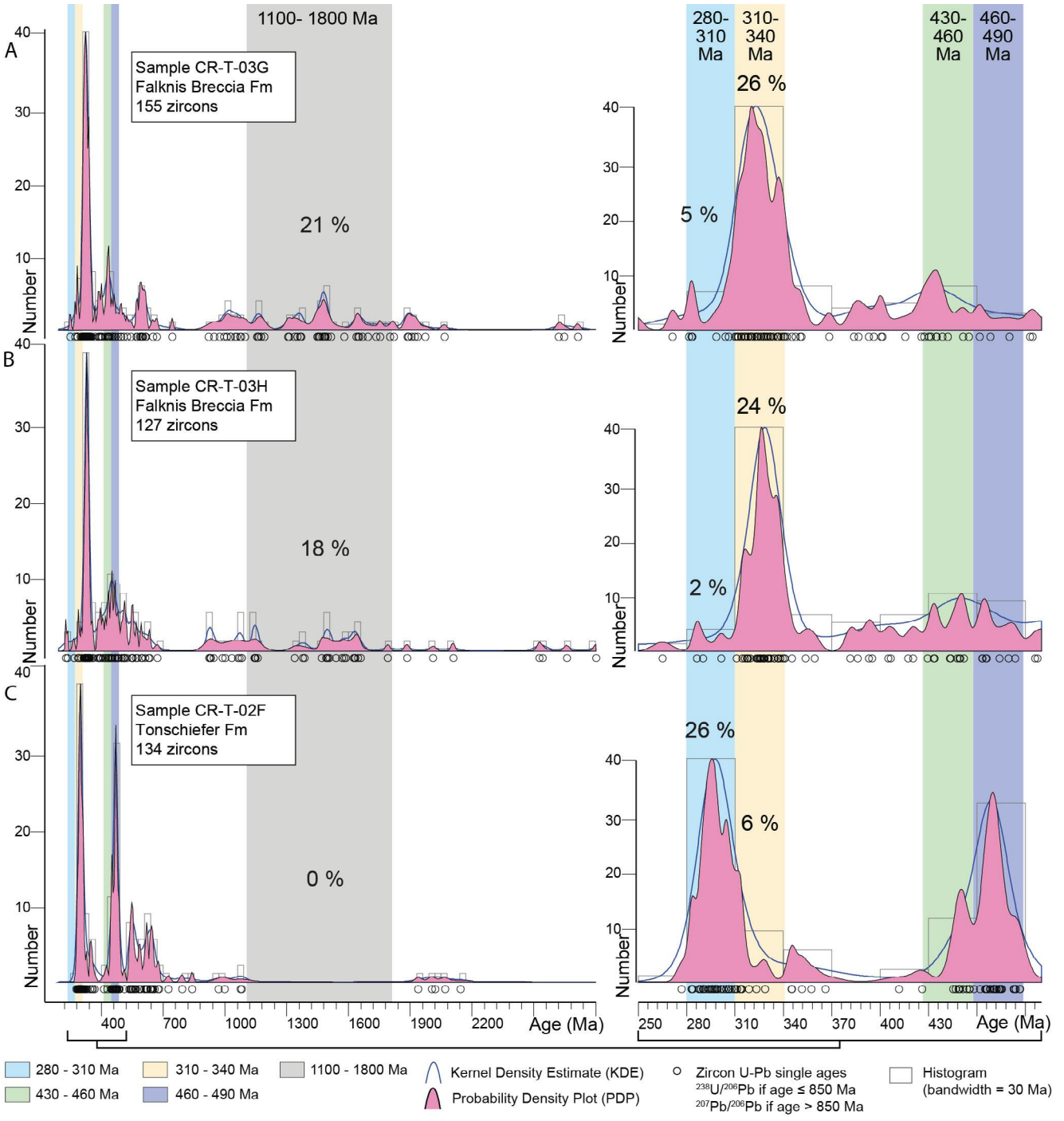

Fig. II.E.15 (from Ribes et al., 2019c) - Detrital zircon $^{206}Pb/^{238}U$ Laser Ablation–Inductively Coupled Plasma–Mass Spectrometry (LA-ICP-MS) age distributions measured in Late Jurassic Falknis sandstones from the Tasna Nappe. Time scale from Ogg et al. (2016).

https://doi.org/10.3301/GFT.2023.02

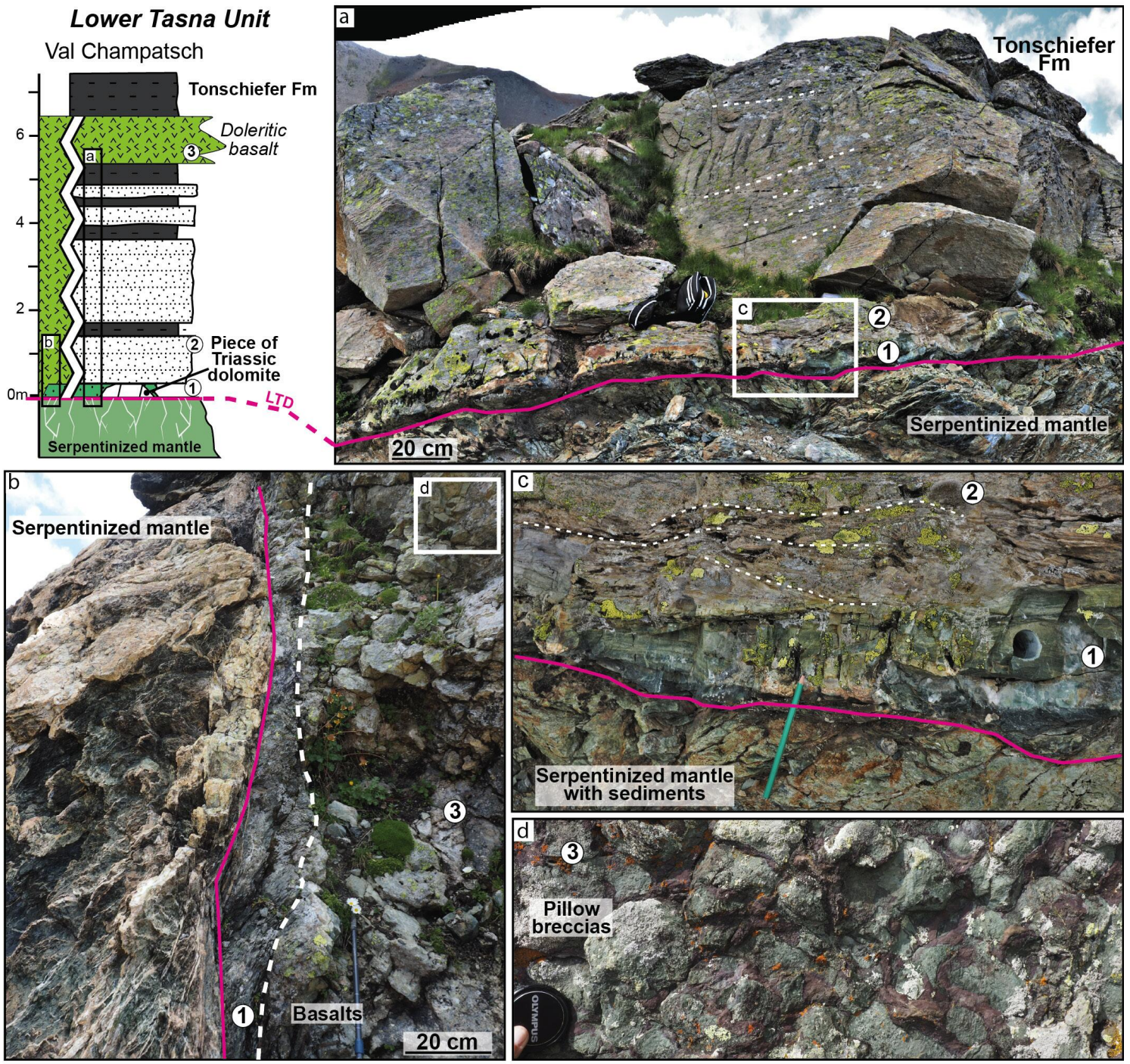

block, seals the basement-derived breccia (Fig. II.E.17a and b). The Ardez Fm consists of dark shales, 5-30 m in thickness, with thin sandstone beds (Gruner, 1981). Up-section, it grades into the greenish-reddish siliceous shales of the Bunte Schiefer Fm, within which ghosts of radiolarians have been identified. The transition from lime-free sedimentation, including the Ardez and Bunte Schiefer Fms, to carbonate sedimentation is sharp: it is marked by the deposition of the Aptychenkalk Fm and then the Neokom Fm (Fig. II.E.10). The base of the overlying Tristel Fm is locally characterized by fine-grained breccias with dolomitic components, up to 3 cm in diameter, alternating with decimetre-thick grey shales and

Fig. II.E.16 (modified from Ribes et al. 2019c) - Representative sedimentary succession and photographs illustrating the Lower Tasna Unit (WGS 84 coordinates: 46°50′25″N, 10°15′39″E). a, c) Exhumed serpentinite overlain by (1) greenish fine-grained sediments mainly composed of Mg-chlorite, passing up section to (2) medium-bedded, fine- to medium-grained siliciclastic turbidites made of quartz and plagioclase grains interbedded with dark shale intervals; b, d) vertical contact between serpentinite (1) greenish fine-grained sediments mainly composed of Mg-chlorite and (3) MORB–type pillow breccias.

https://doi.org/10.3301/GFT.2023.02

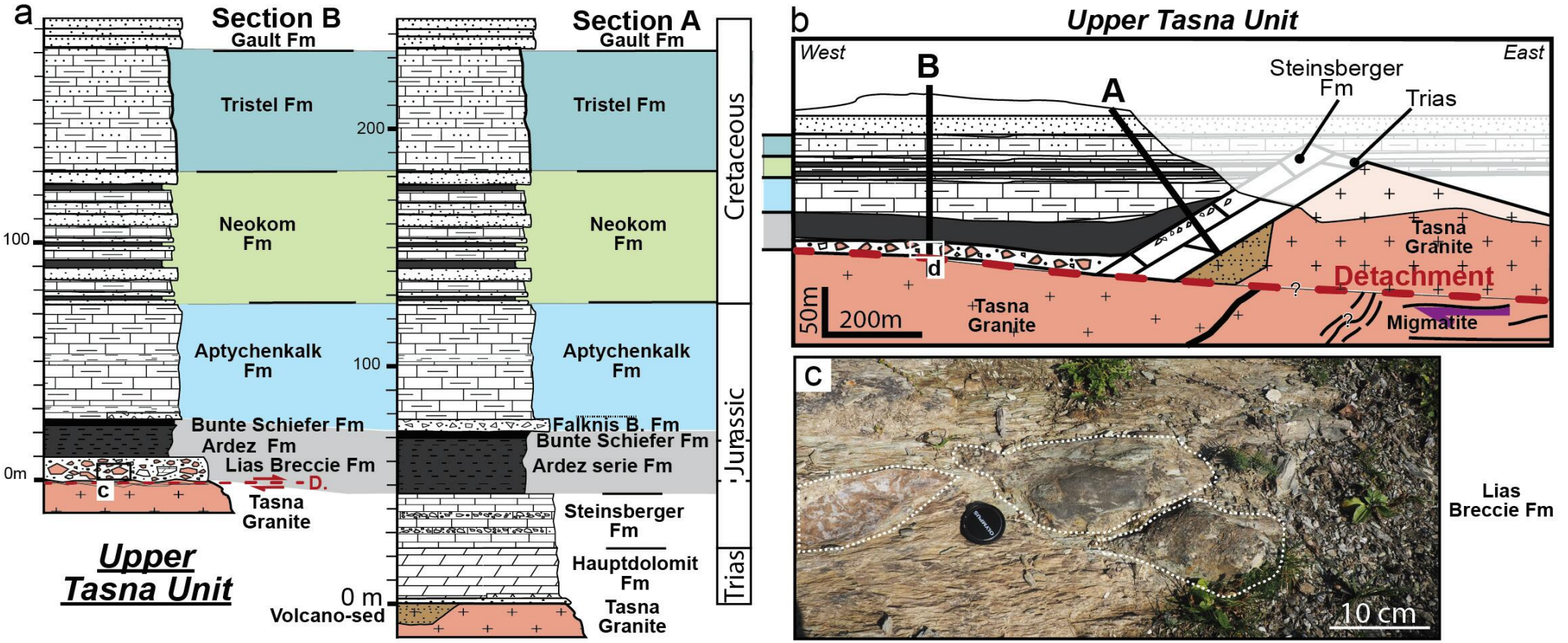

Fig. II.E.17 (modified from Ribes et al., 2019c) – a) Representative sedimentary successions of the Upper Tasna Unit based on Cadisch (1932), Gürler (1995), and own observations. See Fig. II.E.2 for location; b) palinspastic reconstructions across Upper Tasna Unit. The cross-sections summarize the sediment architecture and the fault geometry; c) photograph of the Lias Breccie Fm, which corresponds to first sediments of section B occurring directly onto the tectonized basement (detachment surface). White dashed lines highlight gravel-sized clasts of Triassic dolostone, granites, and Carboniferous to Permian volcano-sedimentary sequences. Abbreviations: B.: Breccia; D.: detachment; Fm: Formation; Trias: Triassic.

calciturbidite beds (Cadisch, 1932; Schwizer, 1983). Up-section the Tristel Fm passes into the glauconitic-bearing turbidites of the Gault Fm, and finally into the Couches Rouges and Tasna Flysch Fms.

These observations, which can be made in the surroundings of the village of Ardez within dispersed, not very well-exposed outcrops, allow us to interpret the Upper Tasna Unit as a pre-Alpine block preserving rift-related structures. This allochthonous block sealed by the Jurassic Ardez Fm is used to override an exhumed detachment fault.

https://doi.org/10.3301/GFT.2023.02

DISCUSSION

Sedimentary systems

Ribes et al. (2019c) suggested that basin sedimentation at the Tasna OCT was fed both by downdip-transported platform material and axial siliciclastic sediments. Pre- and early syn-exhumation sediments derived from the continental platform were presumably trapped into basins of the intervening hyperextended domain (Fig. II.E.18A), while the first sedimentary deposits onto exhumed mantle were emplaced via axial sedimentation from further sedimentary sources.

Later, during Tithonian time, widespread continent-derived breccias were deposited in the exhumed mantle domain (Fig. II.E.18B). Ribes et al. (2019c) concluded that most of the local topography in the Sub-Briançonnais domain was attenuated, most likely due to the filling of the hyperextended basins with Jurassic sediments.

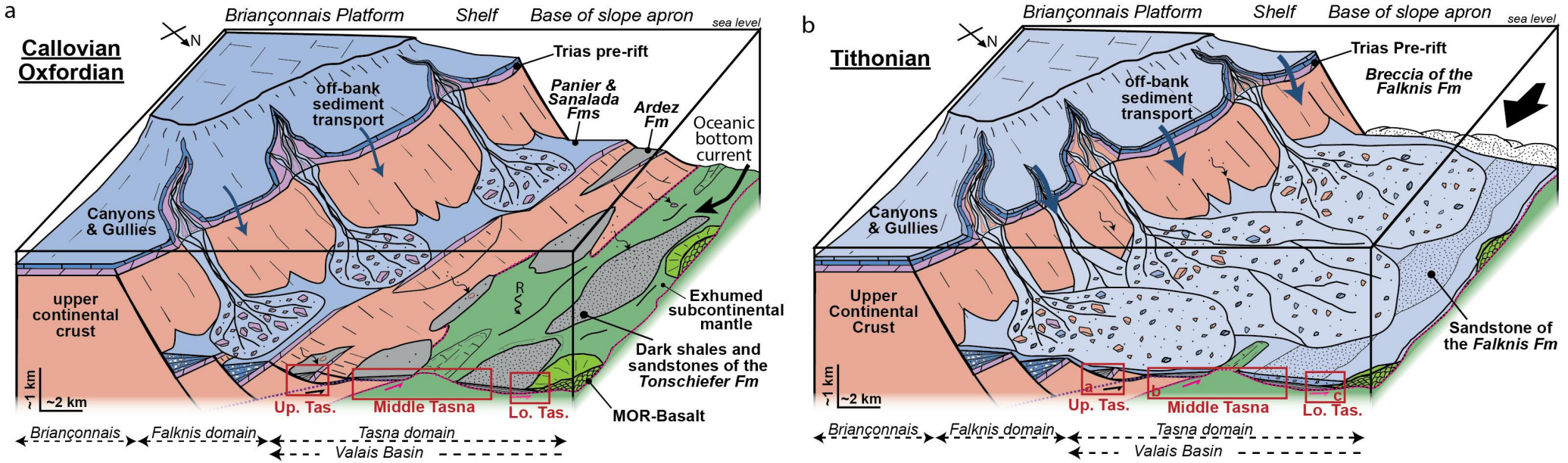

Fig. II.E.18 (modified from Ribes et al., 2019c) - Three-dimensional paleogeographic and tectono-stratigraphic diagrams of the Sub-Briançonnais domain (a) during the Callovian–Oxfordian (sediment distribution across this area is dominated by rockfall and debris flows derived from the long-lived mega-fault scarp in the Falknis domain and dark shales and sandstones derived from erosion of local basement source) and (b) during the Tithonian (the Falknis Breccia Fm interfingered with axial clastic systems). Abbreviations: Lo.: Lower; Tas.: Tasna; MOR: Mid-Ocean Ridge; R: radiolarians; Up: Upper.

https://doi.org/10.3301/GFT.2023.02

Crustal architecture

Based on field and petrological data, Ribes et al. (2019c) showed that the basement rocks of the Tasna Nappe are derived from at least three pre-rift lithospheric levels that became laterally juxtaposed during rifting (Fig. II.E.19B). The Carboniferous to Permian volcano-sedimentary sequence and underlying granite were part of the pre-rift upper crust. In contrast, pressure-temperature estimates performed on the Permian mafic intrusives indicate a pre-rift lower crustal origin. Finally, Picazo et al. (2016) interpreted the mantle peridotites of the Tasna Nappe to be derived from the sub-continental lithospheric mantle (Mantle type 1a).

The pre-rift lower crustal and mantle rocks were exhumed at or close to the seafloor during rifting, as evidenced by: (1) their stratigraphic relationship with syn- to post-rift sediments; (2) the 170-167 Ma $^{40}Ar/^{39}Ar$ ages on phlogopite from pyroxenites within the mantle (Manatschal et al., 2006); and (3) the strong retrogression of feldspar in both the granites and the migmatites. Manatschal et al. (2006) emphasized the role of the Upper- and Lower Tasna detachments in exhuming rocks at or close to the seafloor. However, these two structures only present brittle deformation (<300 °C) and do neither explain how the migmatites and mantle rocks were exhumed from deep- to shallow levels, nor the absence of a middle crust (Ribes et al. 2019c).

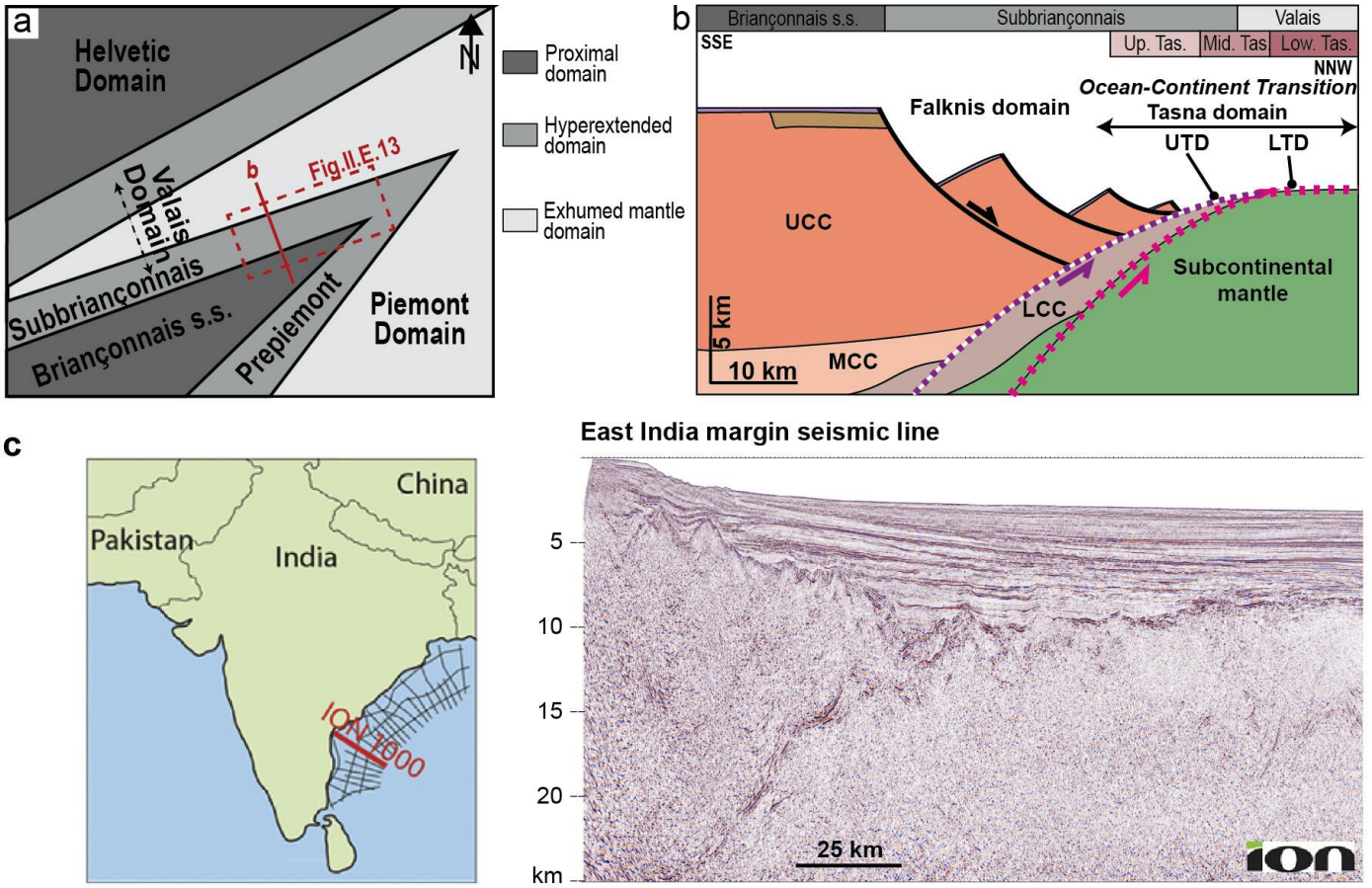

Fig. II.E.19 (modified from Ribes et al. 2019) – a) Paleogeographic reconstruction of the rift domain showing the situation in the Late Jurassic (modified from Mohn et al., 2010); b) tentative palinspastic reconstruction of the margin across the Briançonnais (s.s.-sensu stricto), Sub-Briançonnais, and Valais domains; c) seismic section in depth along dip of the East India margin (from ION; location map from Haupert et al. 2016). Abbreviations: Tas.: Tasna; UTD: Upper Tasna Detachment; LTD: Lower Tasna Detachment; UCC: Upper Continental Cust; MCC: Middle Continental Crust; LCC: Lower Continental Crust; Low.: Lower; Mid.: Middle; Up.: Upper.

https://doi.org/10.3301/GFT.2023.02

The preservation of most of the pre-rift fabric in the migmatites and mantle rocks conflicts with models suggesting a pervasive lower crustal flow to explain extreme crustal thinning (e.g., Huismans and Beaumont, 2008; Sibuet and Tucholke, 2013; Jolivet et al., 2015). A possible alternative mechanism to account for the exhumation of deep crustal- and/or upper mantle rocks to less than 10 km is shearing along high-strain localized shear zones, as documented in the basement of the conjugate Adriatic margin (Petri et al., 2019) and modeled by Lavier and Manatschal (2006), however, such structures are not observed in the Tasna Nappe. Deformation responsible for the exhumation and juxtaposition of the lower crust against the upper crust was presumably localized in the middle crust, which is lacking in the present-day Tasna Nappe.
The Tasna OCT displays (indirect) morphological evidence for an upper-plate affinity, namely (Chenin et al., 2022): (1) the presence of extensional detachment faults exhuming lower crustal rocks to the seafloor; and (2) the presence of mega-breccias (Falknis Fm), which may be related to a mega-fault scarp (Ribes et al., 2019b). A present-day analogue of the upper-plate margin is the East India margin (Fig. II.E.19C).

Paleogeography

The paleogeographic position of the Tasna Nappe was a matter of debate for a long time. It was initially considered as the termination of the Adriatic margin (Staub et al., 1921), before Trümpy (1972, 1980) suggested that it was part of the Briançonnais domain, a hypothesis that is at present largely accepted. Another matter of controversy was the age of the Valais domain and its relationships with both the Alpine Tethys realm and the Bay of Biscay. Frisch (1979), Stampfli (1993), and Handy et al. (2010) considered the Valais as an oceanic domain that propagated from the Bay of Biscay between Europe and Iberia/Briançonnais during the Early Cretaceous. More recently, several authors argued that the Valais (Fig. II.E.19A): (1) was not a true oceanic domain (Masson et al., 2008); (2) was not linked to the Bay of Biscay but was part of the Piemonte-Ligurian rift system (e.g., Manatschal et al., 2006); and (3) opened during the Early to Middle Jurassic, contemporaneously with the Piemonte-Ligurian Basin (Manatschal et al., 2006, 2022; Ribes et al., 2019c).
Fig. II.E.20 shows our preferred interpretation for the Tasna OCT. In this interpretation, we localize the Upper (U), Middle (M), and Lower (L) Tasna units in the northern margin of the Briançonnais continental ribbon, i.e., at the southern margin of the Valais V-shaped basin. The preserved stratigraphic record is compatible with such an interpretation, explaining two main sedimentary sources: (1) those derived from the Briançonnais, including the Falknis Breccia Fm, which were sourced perpendicular to the basin; and (2) axial deposits (e.g., Gault Fm) that were sourced from the European margin. The interpreted locations of the units are also in line with their observed stacking during a N-directed episode of shortening.

Alpine reactivation

The Tasna Nappe lies within the Engadine window in the Central Alps, which forms a fault-bounded, late Alpine, NE-SW-trending antiform exposing Penninic units in south-eastern Switzerland (Figs. II.E.3A and II.E.3B). In the Engadine window, the stack of thrust sheets includes, from bottom to top (Figs. II.E.3C and II.E.3D):

https://doi.org/10.3301/GFT.2023.02

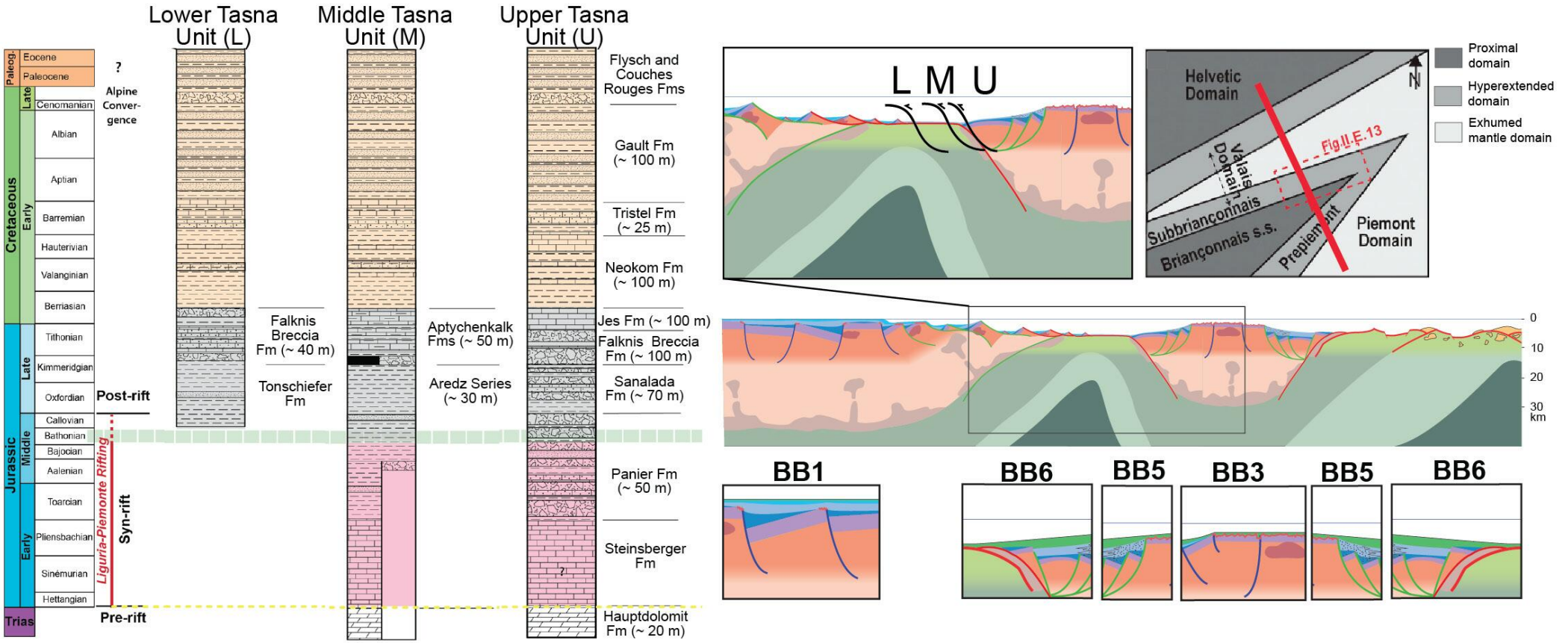

Fig. II.E.20 - Stratigraphic record of the Upper-, Middle- and Lower Tasna units and their position in the framework of the Alpine Tethys rift system (modified from Manatschal et al., 2022).

- the "Bündnerschiefer," a several-kilometre thick assemblage of highly deformed calcschists containing meta-basalt bodies (e.g., Cadisch et al., 1968; Dürr et al., 1993; Bousquet et al., 1998). This nappe is classically interpreted as representing the sedimentary fill of the Valais Basin (Trümpy, 1972; Stampfli, 1993);
- the Tasna Nappe s.l. derived from a complex assemblage of crustal and exhumed mantle units with an overlying Mesozoic sedimentary succession (e.g., Waibel and Frisch, 1989), which are interpreted as the easternmost remnants of the Briançonnais continental ribbon (e.g., Trümpy, 1980);
- the south Penninic Arosa zone, consisting of strongly tectonized pelagic sediments and ophiolitic material, interpreted as the Mesozoic remnants of the south Penninic Piemonte Basin (Weissert and Bernoulli, 1985; Ring et al., 1990);

https://doi.org/10.3301/GFT.2023.02

- the Austroalpine units, derived from the Adriatic rifted margin, i.e., the south-eastern continental margin of the Piemonte-Liguria branch of the Alpine Tethys (Trümpy, 1980).

This north- to northwest-vergent nappe stack (Fig. II.E.20) was emplaced during Eocene to Oligocene Alpine convergence (Hitz, 1996; Springhorn, 2007). Early Cenozoic thrusting was followed by late Oligocene post-stack, east-west extension, and large-scale open folding (Froitzheim et al., 1994). Contemporaneous or subsequent local uplift and erosion, together with faulting along the Engadine fault (Schmid et al., 1993), generated the present-day shape of the Engadine window (Fig. II.E.3).

FURTHER READING

Florineth and Froitzheim (1994); Froitzheim and Rubatto (1998); Manatschal et al. (2006); Ribes et al. (2019b, 2019c).
Ph.D. theses: Engström (2006); Hölker (2001).
Three-dimensional model of the Tasna OCT: https://sketchfab.com/3d-models/05b270df7e424f7a8c86138aa10ef8c4 (Betlem et al., 2023)

https://doi.org/10.3301/GFT.2023.02

THEMATIC SHEETS

In the following thematic sheets, we briefly develop some specific concepts related to rifting or rifted margins. We illustrate how this knowledge can be applied to the understanding of the Alpine Tethys rift system.

The following themes are developed:

https://doi.org/10.3301/GFT.2023.02

A. PETROLOGY THEMATIC SHEET
Crust, mantle, and magma characteristics across the former Alpine Tethys

INTRODUCTION

Rifting exhumes rocks of various crustal and mantle positions to the seafloor so that lithospheric levels that were initially on top of each other become exposed next to each other (see coloured stars in Fig. III.A.1). Magma-poor rifted margins are thus ideal places to characterize the initial architecture, lithology, and thermal conditions of a pre-rift lithosphere. Based on Pressure-Temperature-time (P-T-t) paths deduced from preserved mineral assemblages and cooling ages, it is possible to identify the pre-rift position and thermal conditions of rocks and gain insights into their exhumation history. In the Alps, the pre-rift (Variscan) magmatic intrusions are particularly well suited for such analyses.

ARCHITECTURE AND LITHOLOGY OF THE ALPINE TETHYS PRE-RIFT CRUST

The pre-rift upper crust (red star in Fig. III.A.1) is made of a polymetamorphic basement affected by late Carboniferous to early Permian felsic intrusive and extrusive rocks. Such rocks occur in the Err, Bernina, Sella, Margna, and Grosina nappes (Fig. III.A.2d) and were related to the Variscan orogeny and post-Variscan orogenic collapse. The P-T conditions deduced from the mineral assemblages preserved in these rocks (Fig. III.A.2a) as well as their contacts with Permian sedimentary deposits indicate very shallow intrusion depths (<3 km; Peters, 2007, 2005). Pre-rift mid-crustal rocks (orange star in Fig. III.A.1) have only been recognized in the basement of the Campo nappe. Campo's basement consists essentially of metapelites that equilibrated within the amphibolite facies during pre-Permian and/or Permian time (the timing of peak metamorphism remains ill-constrained). Mafic intrusions such as the Sondalo gabbro (Fig. III.A.2d) were emplaced within these rocks by 300 to 270 Ma (Tribuzio et al., 1999; Petri et al., 2017, 2016). Based on P-T estimates from the rocks encompassing the Sondalo gabbro (Fig. III.A.2b) and the relationship between the intrusion and the country rock, Tribuzio et al. (1999); Braga et al., (2003, 2001), and Petri et al. (2017, 2016) concluded that the Sondalo intrusion resided at mid-crustal levels (0.6±0.2 GPa, 900 °C) during the Permian. Its exhumation occurred during the necking phase of the Alpine Tethys rifting (ca. 185 Ma; Mohn et al., 2012).
Pre-rift lower crustal rocks (yellow star in Fig. III.A.1) have only been recognized in the Margna and Malenco nappes (Fig. III.A.2d). The Malenco nappe preserves a former crust-mantle boundary welded by early Permian gabbroic rocks dated 281±19 Ma by U/Pb on zircons (Hansmann et al., 2001). The country rocks affected by gabbroic intrusion and underplating are meta-pelites and meta-carbonates that underwent granulite-facies intrusion-related contact metamorphism (Appendix 4). Müntener et al. (2000) demonstrated that, after the intrusion of gabbros in Permian time, the mantle and lower crustal rocks cooled more or less isobarically over 50 Ma (Fig. III.A.2c). They calculated that, at the crust-mantle boundary, the temperature was ca. 550 °C and pressure ranged between 0.9 and 1 GPa at the onset of rifting. Such conditions are expected at the base of

https://doi.org/10.3301/GFT.2023.02

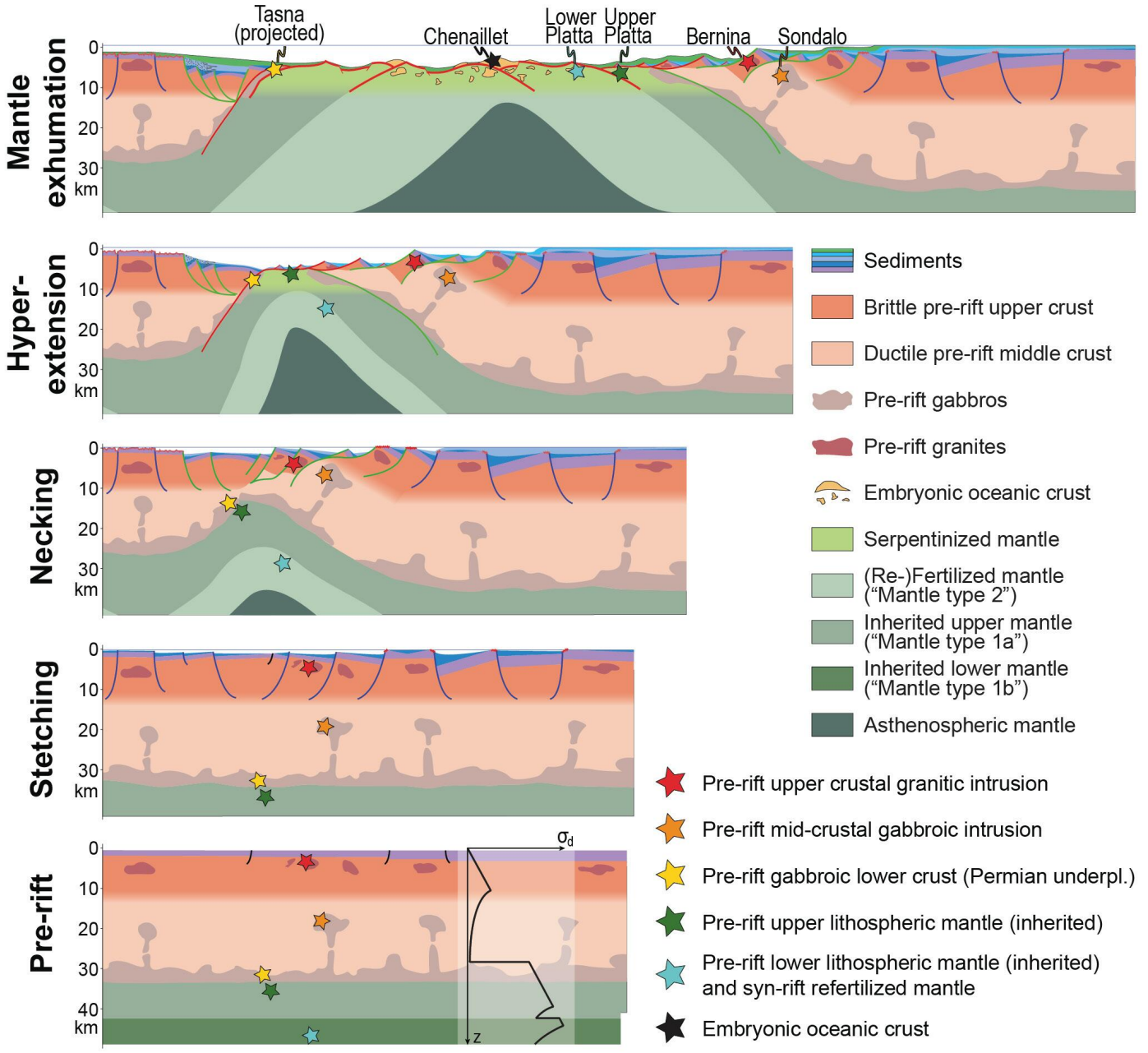

Fig. III.A.1 - Schematic evolution of the Alpine Tethys rift system with tracing of specific crustal and mantle positions (coloured stars). Abbreviation: underpl.: underplate.

a ca. 30 km-thick crust. The Malenco lower crustal gabbro was exhumed to the seafloor by 160-165 Ma (Fig. III.A.2c).

Based on these petrological and thermochronological data, a rheological model with a brittle upper crust, a ductile middle crust, a mafic/gabbroic strong lower crust, a brittle upper mantle, and a plastic lower mantle can be proposed for the pre-rift lithosphere (lower panel of Fig. III.A.1). Pre-existing Variscan and Permian structures, local pre-rift volcanic activity and underplated gabbros along the crust-mantle boundary resulted in rheological heterogeneities (Handy, 1989), which may have strongly controlled the distribution of rift structures at the onset of rifting (Chenin et al., 2015, 2019a; Manatschal et al., 2015).

MANTLE COMPOSITION ACROSS THE ALPINE TETHYS RIFT SYSTEM

Picazo et al. (2016) identified three types of mantle peridotites based on their bulk composition and on the chemistry of their clinopyroxene and spinel, namely: (1) inherited subcontinental, (2) refertilized subcontinental and (3) depleted oceanic mantle (Fig. III.A.3).

https://doi.org/10.3301/GFT.2023.02

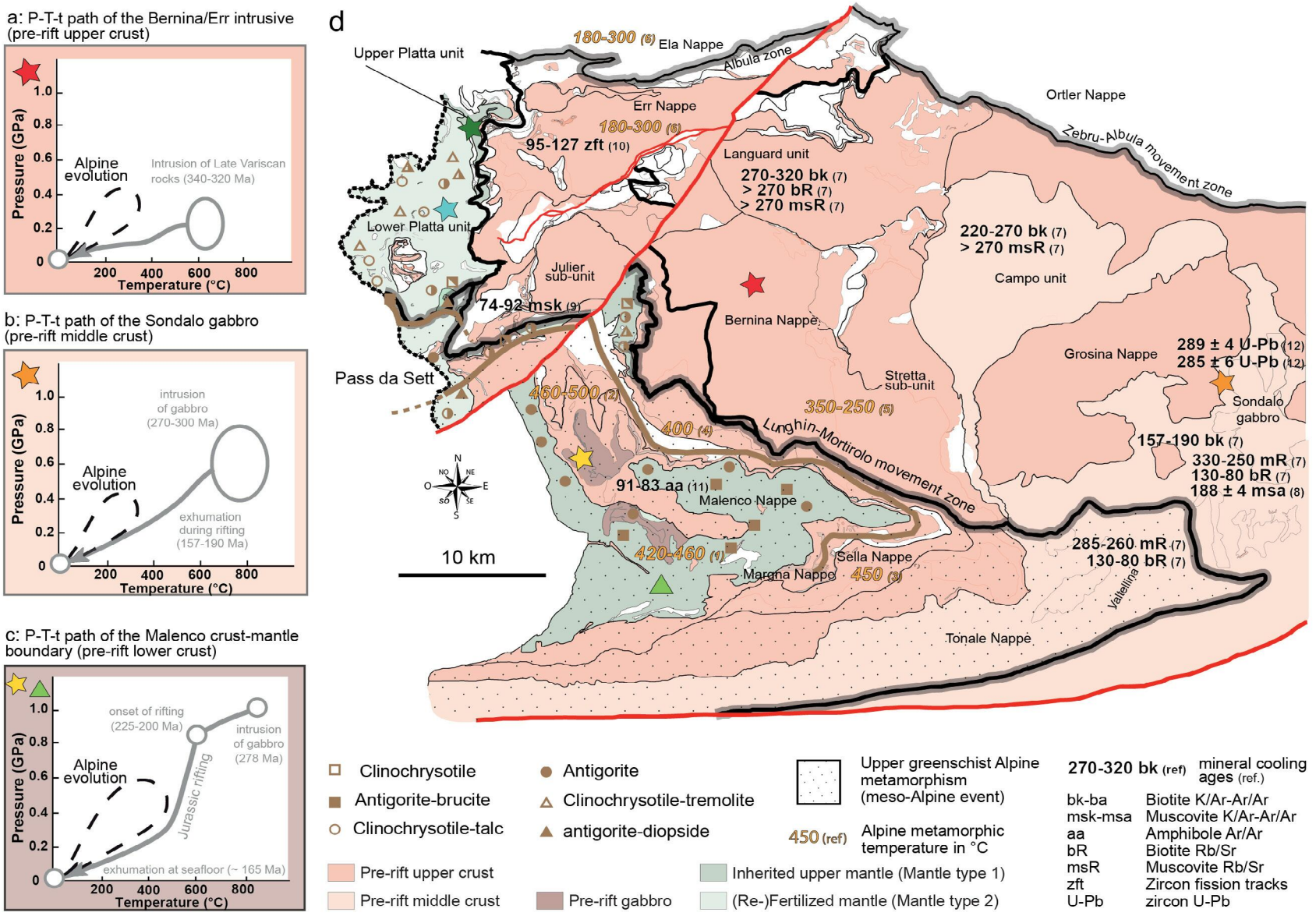

Fig. III.A.2 (modified from Mohn et al., 2011) - Pressure-Temperature-time (PTt) path of specific magmatic bodies: a) pre-rift upper crustal Bernina and Err intrusive granitoids (Peters, 2007, 2005); b) pre-rift middle crustal Sondalo gabbro (Braga et al., 2003, 2001; Tribuzio et al., 1999); c) pre-rift lower crustal rocks from the Malenco crust–mantle boundary (Müntener et al., 2000; Villa et al., 2000);d) map of the Grison region showing the distribution of cooling ages and Alpine metamorphic temperatures. References: (1) Hermann and Müntener (1992); (2-3) Liniger (1992); (4-5) Spillmann (1993); (6) Mählmann (1996); (7) Thöni (1981); (8) Meier (2003); (9) Handy et al. (1996); (10) Eggenberger (1990); (11) Villa et al. (2000); (12) Petri et al. (2017).

https://doi.org/10.3301/GFT.2023.02

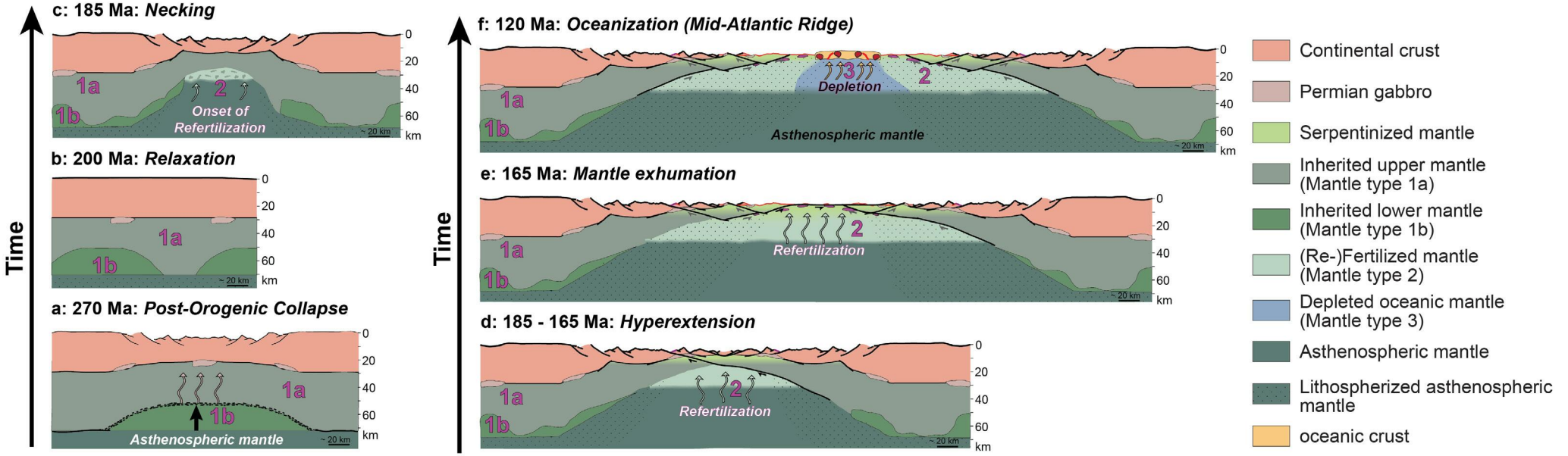

Fig. III.A.3 - The different mantle types and their location in the framework of a Wilson Cycle (modified from Picazo et al., 2016). a) Depletion of the uppermost asthenospheric mantle due to post-orogenic magmatism; b) incorporation of the depleted asthenospheric mantle in the lithosphere due to thermal relaxation; c-e) subcontinental mantle refertilization as a result of extension-related asthenosphere partial melting; f) depletion of the uppermost asthenosphere as a result of MORB accretion.

Mantle type 1: Inherited mantle

Mantle type 1 corresponds to the pre-rift subcontinental lithospheric mantle. Because the upper part and lower part of the subcontinental lithospheric mantle underwent different tectono-magmatic evolutions, and thus display different geochemical signatures, Picazo et al. (2016) made a distinction between them (Mantle type 1a and 1b in Fig. III.A.3):

- Mantle type 1a (green star in Fig. III.A.1) corresponds to the upper part of the pre-rift subcontinental lithospheric mantle (see also Figs. III.A.3a and III.A.3b). Remnants of this type of mantle are found in Malenco, Totalp, Tasna and Upper Platta (Fig. III.A.2d), as well as in the proximal part of the Iberia-Newfoundland OCTs.

  Mantle type 1a is characterized by an important heterogeneity: it may be comprised of lherzolite (dominant), dunite, harzburgite and/or pyroxenites (Fig. III.A.4). The variability in clinopyroxenes and spinel chemistry reflects the record of several former magmatic depletion and/or impregnation events (chemical overprint of the different events). Mineral assemblages have usually equilibrated in the spinel stability field, which implies long-time rest at depths >30-40 km (Fig. III.A.5).

https://doi.org/10.3301/GFT.2023.02

- Mantle type 1b (turquoise star in the lower panel of Fig. III.A.1) corresponds to the lower part of the pre-rift subcontinental lithospheric mantle (see also Figs. III.A.3a and III.A.3b). It used to belong to the uppermost part of the asthenosphere, which was strongly depleted during the Permian large-scale magmatic event that followed the orogenic collapse of the Variscan range. The uppermost part of the asthenosphere became progressively part of the lithospheric mantle due to the thermal relaxation that followed the end of the post-orogenic collapse. Remnants of Mantle type 1b are found in Civrari, ca. 20 km NW or Torino (Picazo et al., 2016).
  Compared with inherited mantle type 1a, depleted mantle type 1b is more homogeneous. It is mainly comprised of pyroxene-bearing spinel harzburgites (Fig. III.A.4) whose pyroxenes are extremely depleted in Na_2O and TiO_2.

Mantle type 2: Refertilized mantle

Mantle type 2 (turquoise star in the middle and top panels of Fig. III.A.1) corresponds to a relatively deep subcontinental lithospheric mantle (formerly Mantle type 1b) that was refertilized by syn-rift asthenosphere-derived partial melts (Figs. III.A.3 and III.A.4). Indeed, rift-related lithospheric thinning induces partial melting of the rising asthenosphere. The resulting magmatic fluids move upward due to their lower density compared to the encompassing mantle. These melts then react with and "impregnate" the subcontinental mantle as they percolate through it, forming plagioclase and pyroxene (Figs. III.A.3c-III.A.3e and III.A.5). Remnants of Mantle type 2 are found in Lower Platta, Lanzo Central and South, Chenaillet (Fig. III.A.2d) and in the distal part of the Iberia OCT.

Mantle type 2 is mainly comprised of plagioclase-lherzolites. During melt percolation, melt-rock reactions form orthopyroxene at the expense of olivine on the one hand, and orthopyroxene and plagioclase at the expense of clinopyroxene on the other hand (Fig. III.A.4). TiO_2 content and Cr of spinel become higher with increasing fertilization. Based on this observation, Picazo et al. (2016) noticed an increase in the importance of melt-rock reaction oceanward.

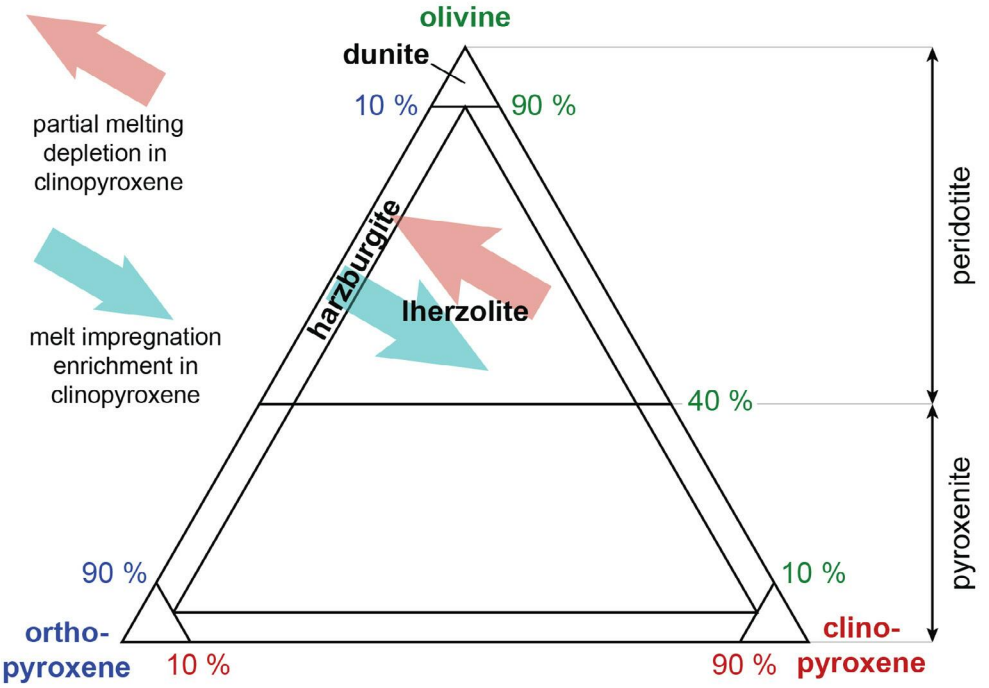

Fig. III.A.4 - Triangular diagram displaying the composition of the main types of peridotites in % of olivine, clinopyroxene and orthopyroxene. The blue and red arrows represent the shift in composition of the peridotite affected by melt impregnation and partial melting, respectively (modified from Chenin et al., 2020b).

https://doi.org/10.3301/GFT.2023.02

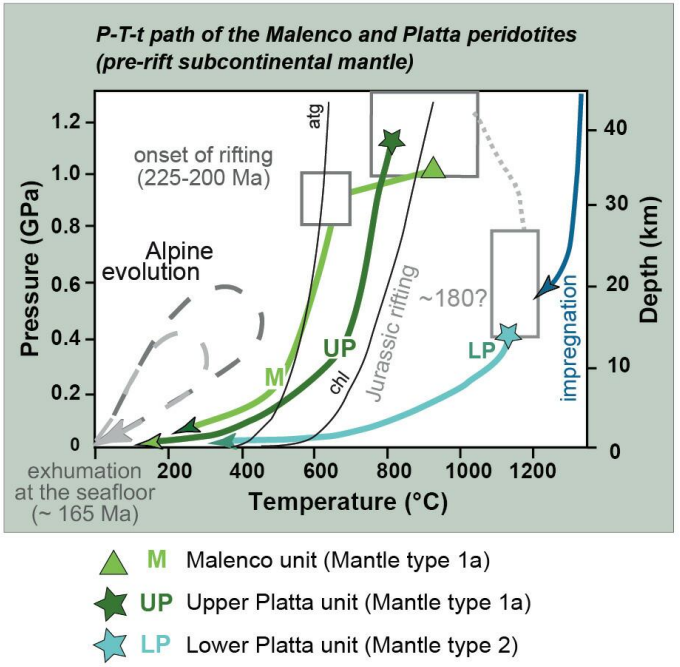

Fig. III.A.5 - Pressure-Temperature-time (PTt) path of subcontinental mantle rocks (modified from Müntener et al., 2010); see the triangle and stars symbols on Figure III.A.2d for location. Abbreviations: M: Malenco; LP: Lower Platta; UP: Upper Platta; chl: chlorite; atg: antigorite.

Mantle type 3: Depleted oceanic mantle (not evidenced in the Alps)

At slow or ultra-slow spreading ridges, the depleted mantle is typically exhumed by detachment faults. This type of oceanic mantle is dominantly comprised of harzburgite together with rare dunite and lherzolite (Fig. III.A.4). Clinopyroxenes in harzburgite are extremely depleted in Na_2O and TiO_2, consistent with high degrees of partial melting (15-20 %). At present, no evidence for Mantle type 3 has been found in the former Alpine Tethys realm, which questions the existence of a mature accretion system between Adria and Europe (Fig. III.A.6). Whether or not there was a true ocean remains to date a matter of debate.

MAGMATIC BODIES OF THE EMBRYONIC SEAFLOOR SPREADING SYSTEM

The embryonic seafloor spreading system of the Alpine Tethys formed two types of magmatic bodies, namely basalts, and gabbros. A description of the latter is provided in Excursion D (Stop 4 at Stalvedret/Val da Natons). Below we provide a short overview of the rift-related basalts. Only scattered remnants of “oceanic” basalts (black star in Fig. III.A.1) have been found so far in the Lower Platta and Lower Tasna nappes (Fig. III.A.2d), which sample the ocean-continent transition of the former Alpine Tethys. These basalts formed during late stages of rifting (167-161 Ma extrusive rocks in the Platta and Tasna nappes; Lower Cretaceous sills in the Platta Nappe) and overly exhumed subcontinental lithospheric mantle. Their chemical signature differs from that of classical MORB. Amann et al. (2020) identified two types of basalts based on their geochemical signature (Fig. III.A.7). Both basalts are related to 15-20 % melting of a mantle source that differs from the standard asthenospheric Depleted Mantle (DMM):

- Type 1 basalts were all formed during the Jurassic mantle exhumation phase (i.e., they are syn-tectonic). They display a depletion in Light Rare Earth Elements (LREE) comparable to that of Normal-MORB (N-MORB). However, Type 1 basalts differ from N-MORB by their lower Nb/La ratio and their higher (Sm/Nb)N ratio. Such a high (Sm/Nb)N ratio is typically related to a garnet component in the MORB source. Type 1 basalts were interpreted to result from relatively low degree partial melting (<15 %) of refertilized subcontinental lithospheric mantle in the spinel stability field (i.e., relatively shallow; Fig. III.A.7a). Partial melting of the subcontinental lithospheric mantle at shallow depths was presumably enabled by high geothermal gradients caused by both asthenosphere upwelling and melt percolation.

https://doi.org/10.3301/GFT.2023.02

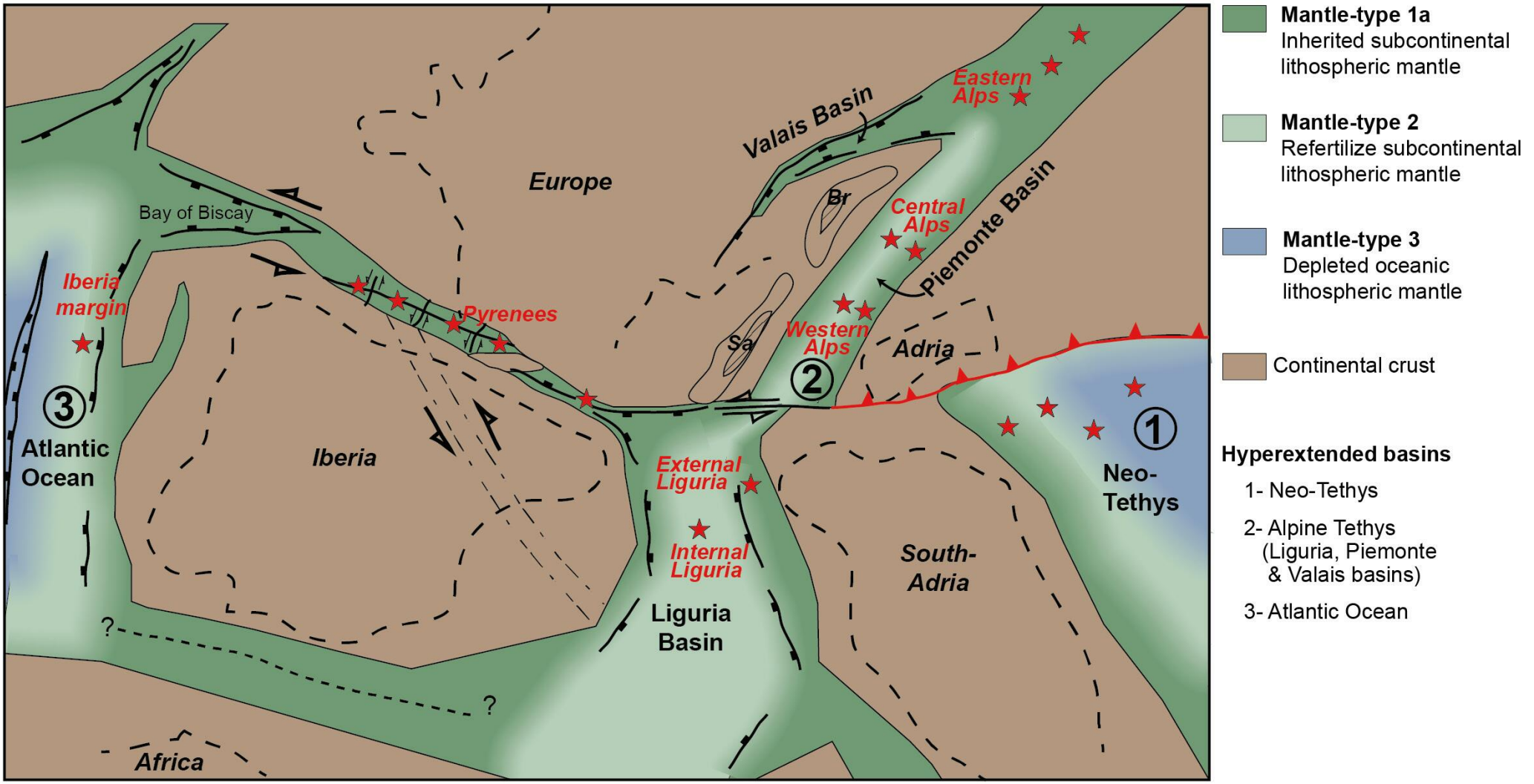

Fig. III.A.6 (from Picazo et al., 2016) - Distribution of the different types of mantle flooring the Neo-Tethys, Alpine Tethys and southern North Atlantic systems (restoration at late Aptian time, ~110 Ma). Abbreviations: Br.: Briançonnais; Sa: Sardinia.

- Type 2 basalts were emplaced either during the Jurassic, or the Cretaceous, simultaneously with and/or after the mantle exhumation phase. They are similar to present-day Enriched MORB (E-MORB): they are enriched in incompatible elements and High Field Strength Elements (HFSE) and display high (La/Sm)N and (Sm/Yb)N ratios.

https://doi.org/10.3301/GFT.2023.02

Type 2 basalts were interpreted as a mix between 80-90 % of standard DMM partial melts and 10-20 % of garnet-pyroxenite-derived melts (Fig. III.A.7b). Garnet-pyroxenite source may derive from high degrees batch melting of a recycled oceanic crust (e.g., Variscan-derived eclogite?).

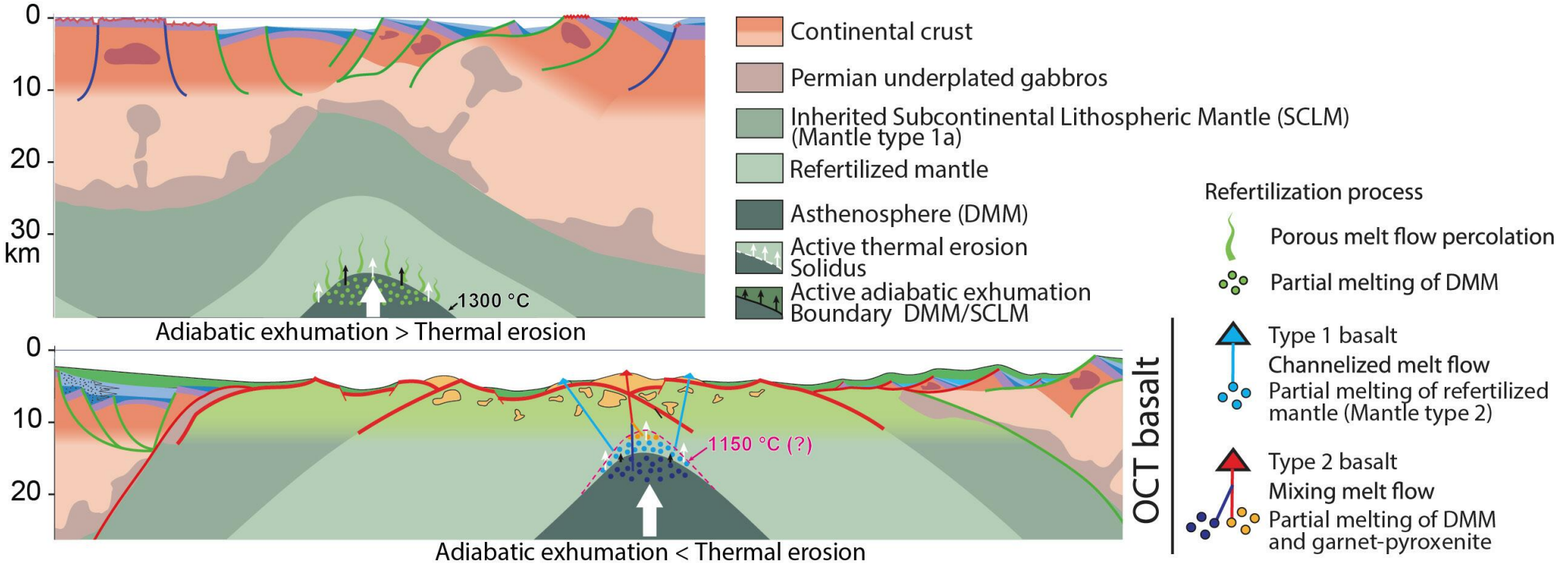

Fig. III.A.7 - Conceptual model for the formation of OCT-basalts (inspired from Amann et al., 2020). a) Near-adiabatic upwelling of the asthenosphere (DMM) and onset of DMM partial melting (apple green circles) during necking and/or hyperextension phase; initial percolation of melts towards the subcontinental lithospheric mantle (SCLM) inducing its refertilization; the distal SCLM is melt-impregnated by up to 12%; b) thermal advection enhanced by porous-flow melt percolation moves the solidus upwards allowing for melting of the refertilized SCLM (light blue circles) forming the Type-1 basalts (light blue pipes and volcanoes). Mixing of partial melts from the DMM (dark blue circles) and garnet-pyroxenite (black dashes, orange circles) creates type-2 basalts (red pipes and volcanoes).

https://doi.org/10.3301/GFT.2023.02

B. TECTONO-STRATIGRAPHY THEMATIC SHEET
Migration of rift activity and related depocenters with time: the multistage and polyphase nature of the Tethyan-Atlantic rifting during the Mesozoic

INTRODUCTION

The tectono-stratigraphic record of a rift system is controlled by the migration of deformation with time. Here we unravel the two main - and not mutually exclusive - types of rifting, namely multistage and polyphase rifting.

MULTISTAGE RIFTING

Definition

During multistage rifting, several successive extensional events take place under various plate kinematic directions. The different extensional phases may or may not overlap in space. In the Tethyan-Atlantic realm, at least three extensional phases occurred: The first was the Triassic Meliata-Vardar rifting to the east of the Adria microcontinent and Central Atlantic rifting southwest of Iberia (violet rifting in Fig. III.B.1a). The second was the Jurassic rifting of the Alpine Tethys within the proximal domain of the western Meliata-Vardar margin (blue rifting in Fig. III.B.1a; the violet stripped pattern represents the domain where it overprints the Meliata-Vardar rift system). The third occurred during the Early Cretaceous when the southern North-Atlantic Ocean started to propagate northward from the Central Atlantic and eastward in the Bay of Biscay.

Multistage rifting is common in Earth's history and may even be the standard rift evolution. For instance, Cadenas et al. (2020) evidenced at least three successive rift events at the northern

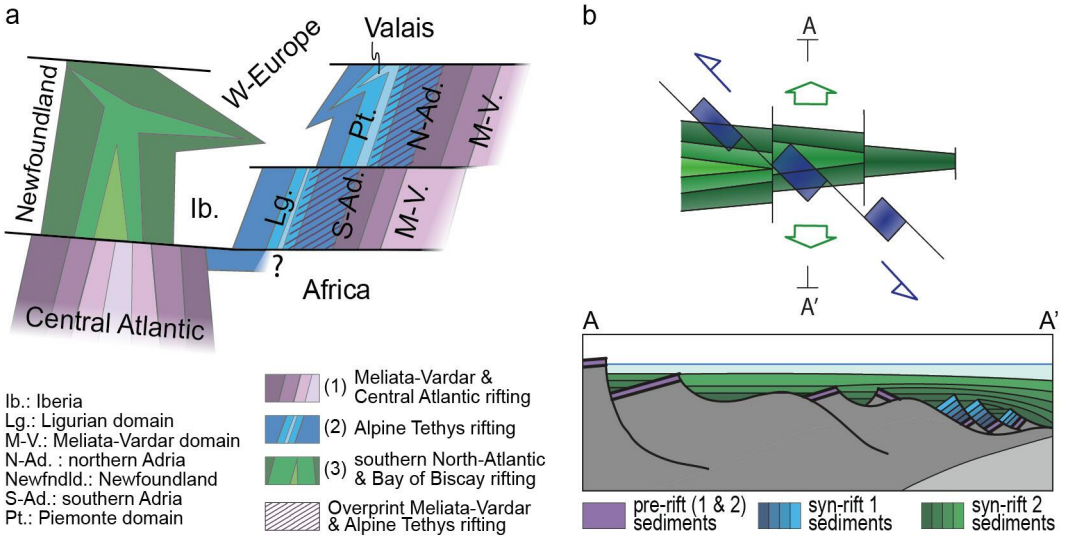

Fig. III.B.1 – a) Schematic view of the successive rifting events that took place in Western Europe. Lighter colours represent more distal domains; b) illustration of the stratigraphic complexity in a multistage rift system: the local presence of blue sediments unrelated to the green rift event in the distal margin may be misinterpreted when the multistage nature of the rift is not recognized (Chenin et al., 2022, modified from Miró et al., 2021).

https://doi.org/10.3301/GFT.2023.02

Iberian margin. Lovecchio et al. (2018) identified three independent extension phases at the Argentinian margin of the South Atlantic. Bergh et al. (2007) recognized three extensional phases with various plate kinematics at the Norwegian margin. Sang Chan et al. (2010) identified three extension phases with different plate kinematics during the opening of the South China Sea in the Pearl River Delta region. Senkans et al. (2019) described three extensional phases with various plate kinematics at the Mozambique margin.

When two rift systems (or more) overlap during multistage rifting, the sedimentary record is necessarily complex in the area of overprint (Fig. III.B.1b). Indeed, sediments related to different rifting episodes may locally be incorporated into the sedimentary record of a given margin. These may be erroneously interpreted when not recognized as resulting from multistage rifting.

Overview of the pre-Alpine Tethys rift setting

Triassic sediment thickness and depositional environments changed across the future Alpine realm (violet sediments in Fig. III.B.2b). They testify to relatively deep-water environments to the east and southeast and evolve into platform carbonates, sabkha environments, and continental siliciclastic systems to the west and northwest (Fig. III.B.2a). The sedimentary sequence is generally thicker in the east and south (future Upper Austroalpine and Southern Alps; 1 to 5 km) and is locally only a few tens of meters in the future proximal European margin (Fig. III.B.2b). The distribution and thickness of Triassic sediments in between is complex and poorly constrained due to the pervasive tectonic overprint from both the Jurassic Alpine Tethys rifting and subsequent Alpine convergence.

The thicker Triassic sequences in the eastern and south-eastern parts of the Alpine realm

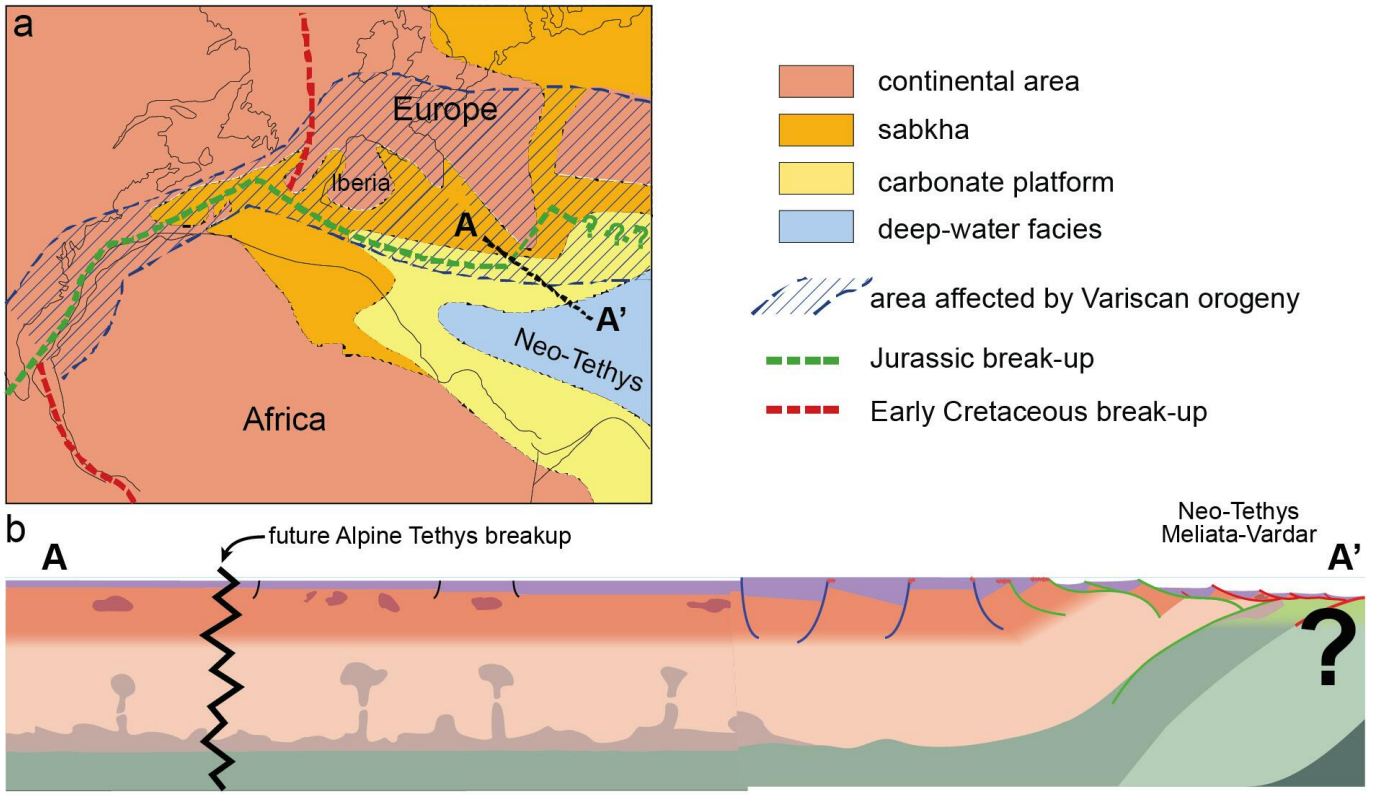

Fig. III.B.2 – a) Late Triassic restoration of the Alpine and central Atlantic realm showing the pre-rift depositional settings and the location of the future Alpine Tethys (modified from Bosellini, 1973 and Laubscher and Bernoulli, 1977); b) schematic section across the Meliata-Vardar margin and future Alpine Tethys realm during the Late Triassic.

https://doi.org/10.3301/GFT.2023.02

can be explained by their proximity to the Triassic Meliata-Vardar domain and the thermal subsidence following its Carnian (ca. 220 Ma) rifting (Fig. III.B.2a; Dercourt et al., 1986; Channell and Kozur, 1997; Robertson, 2004). To the west (future European margin), the presence of shallow-marine deposits and the lack of subsidence during the Triassic suggest that the pre-rift continental crust and lithosphere were in isostatic equilibrium and were approximately 30 and 120 km thick, respectively.

POLYPHASE RIFTING

Definition

Polyphase rifting corresponds to the succession of different deformation phases (namely stretching, necking, hyperextension, and mantle exhumation; see section 2 of the excursion notes) during continuous extension under one and the same kinematic setting. The polyphase nature of the Alpine Tethys rifting was first evidenced by Froitzheim and Eberli (1990) using stratigraphy. They recognized a first extensional event with minor to moderate subsidence in the former proximal domain of the Alpine Tethys; and they identified a second extensional event with larger subsidence in the former distal part of the margin. A few years later, Lavier and Manatschal (2006) suggested that the first extensional event was largely distributed over the entire Alpine Tethys realm (the stretching phase), while the second extensional phase was expressed by the focusing of deformation over a narrower domain (the necking, hyperextension and mantle exhumations phases). More recently, Ribes et al. (2019a) provided a detailed review of the tectono-stratigraphic evolution of the Alpine Tethys rifting using absolute time markers.

In the following, we use the term Tectonic Sequence (TS) to refer to all the sediments deposited during a given rift-related deformation phase. We describe the characteristics of the TS corresponding to each one of the successive deformation phases at play during an ideal, polyphase, magma-poor rifting event. By ideal we mean that the six following hypotheses are fulfilled: (1) rifting is achieved via four distinct and successive extension phases that are the stretching, necking, hyperextension and mantle exhumation phases; (2) these extension phases do not overlap in time, therefore each one is associated with one single ST, namely the stretching, necking, hyperextension and mantle exhumation ST; (3) each extension phase is controlled by a single deformation mode, namely the stretching, necking, hyperextension and mantle exhumation deformation mode; (4) the structures formed during a deformation phase are characteristic and specific to the corresponding deformation mode; (5) each deformation mode is spatially restricted to the rift domain(s) it affects, and when a rift domain is affected by a deformation mode, its entire width is affected; and (6) rifting is a localizing process during which the successive deformation modes affect an ever narrower region (see Chenin et al., 2022, for a more comprehensive review).

This record compares well with that of the Alpine Tethys described in the different excursions of this field guide (see Manatschal et al. (2022) for a more comprehensive review).

https://doi.org/10.3301/GFT.2023.02

Tectono-stratigraphic evolution of an ideal magma-poor polyphase rifting

The stretching ST

The stretching TS records the stretching phase, a low-β pure shear extension of the lithosphere that is manifested by broadly distributed high-angle (60°) normal faulting in the brittle layers and plastic deformation in the ductile ones. The corresponding half-graben basins are distributed over the entire rift domain (Fig. I.4b of the excursion notes). Thus, the stretching TS displays comparable depositional characteristics in the proximal, necking, and hyperextended domains (fifth line of Fig. III.B.3b), although it is increasingly overprinted/ dismembered by subsequent extensional events in distal domains (fifth line of Fig. III.B.3c). In contrast, the stretching TS is lacking in the exhumed mantle domain, as well as overall new real estate domains since neither crustal nor mantle basement is exhumed to the seafloor at the stretching stage.

The stretching TS is characterized by wedge-shaped sedimentary deposits that thicken toward the normal fault bounding the depocenter (Fig. III.B.3a5 and fifth

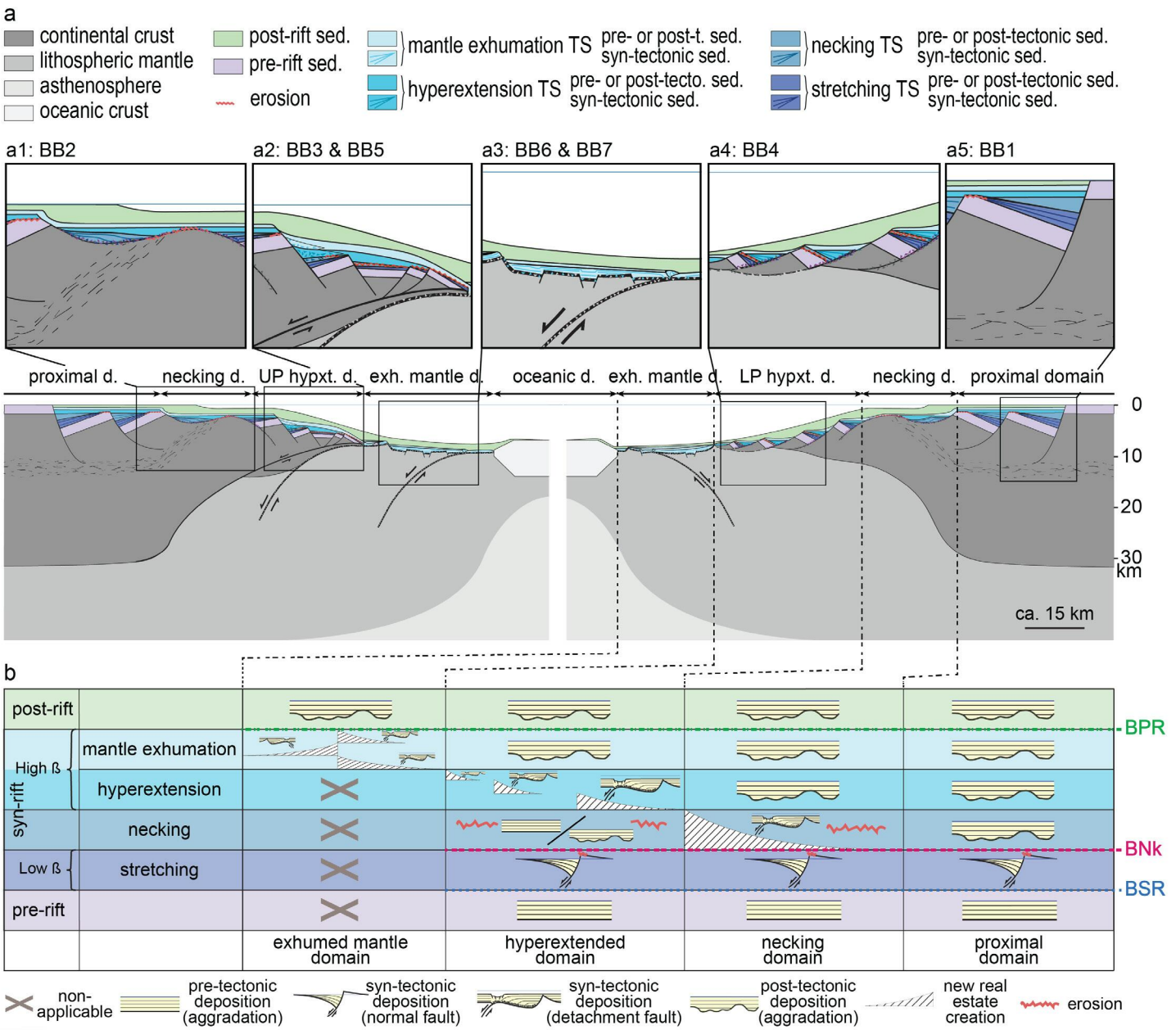

Fig. III.B.3 (modified from Chenin et al., 2022) - Tables summarizing the main characteristics of each Tectonic Sequence in the different rift domains of an idealized magma-poor polyphase rifting. a) Margin architecture at the end of rifting with close-up on the stratigraphy.

https://doi.org/10.3301/GFT.2023.02

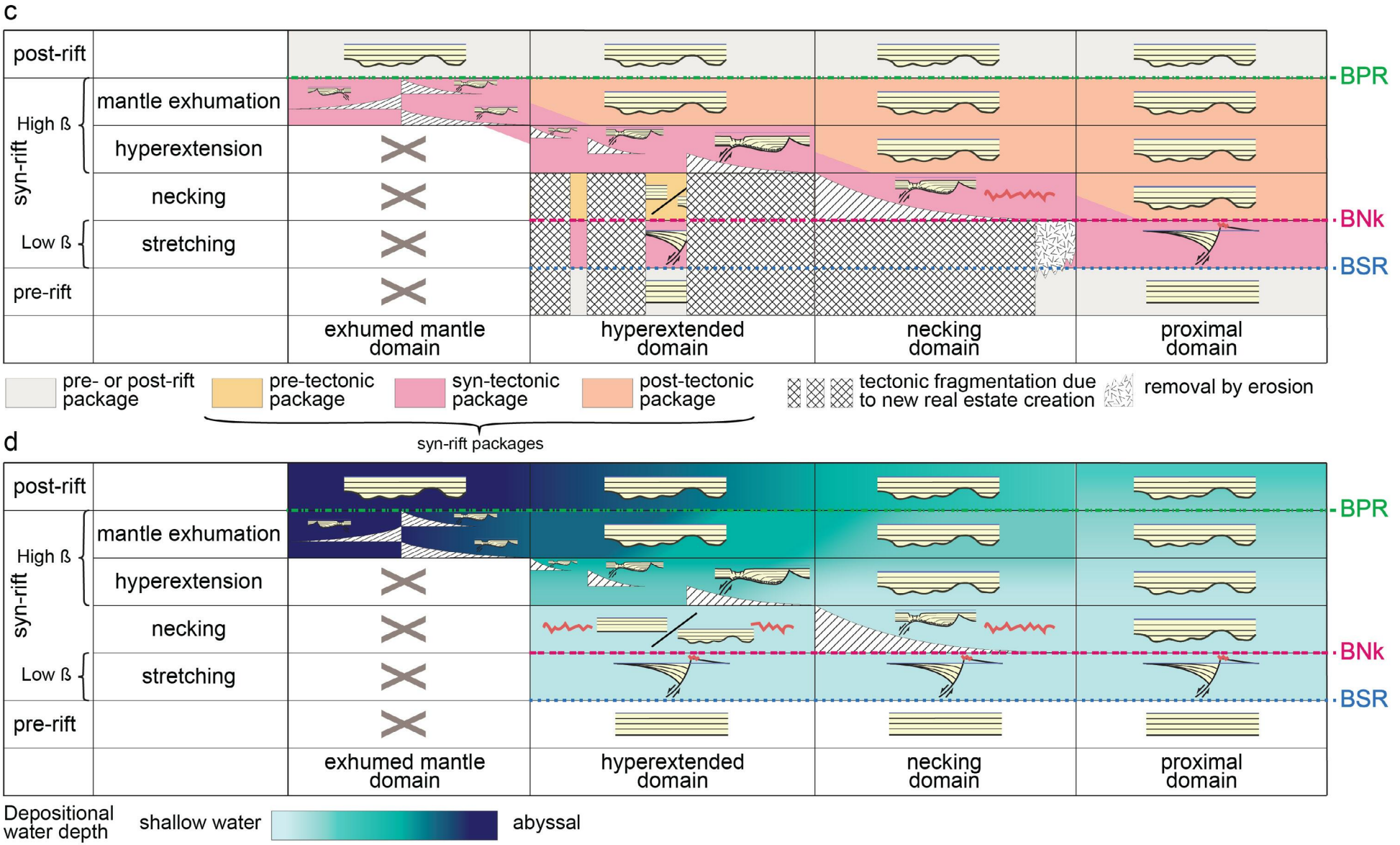

Fig. III.B.3 (modified from Chenin et al., 2022) - Tables summarizing the main characteristics of each Tectonic Sequence in the different rift domains of an idealized magma-poor polyphase rifting. b) main structures and related stratigraphic architecture with time in the different rift domains; c) spatio-temporal distribution of pre-, syn- and post-tectonic sedimentation and tectonic fragmentation; d) spatio-temporal evolution of the depositional water depth. Abbreviations: BNk: Base of the Necking tectonic sequence; BPR: Base of the Post-Rift megasequence; BSR: Base of the SynRift megasequence; d.: domain; exh.: exhumed; hypertext.: hyperextended; LP: lower plate; UP: upper plate; sed.: sediments; TS: Tectonic Sequence.

https://doi.org/10.3301/GFT.2023.02

line of Fig. III.B.3b). Related deposits often include breccias derived from the adjacent footwall crest and/or fault plane. Indeed, the activity of a normal fault is usually associated with footwall uplift and erosion due to the rotation of the fault block (Yielding, 1990) and/or to the flexural response of the lithosphere (Kusznir and Ziegler, 1992). Most of the infill is, however, linked to axial sedimentation (Leeder et al., 1987).
No significant lithospheric thinning occurs during the stretching phase, which results in only limited creation of accommodation space outside the basins, and minor subsequent thermal subsidence across the future proximal domain. Moreover, the high ratio between the rates of sedimentation and accommodation space creation hampers the formation of significant bathymetry during the stretching phase (fifth line of Fig. III.B.3d).
The stretching TS is best preserved in the proximal domain of rifted margins, where the stretching phase is at the origin of BB1 (Figs. III.B.3a5 and III.B.4a). Examples include the Bourg d'Oisans area in SE France (former European proximal margin), and the Il Motto (Excursion A) and Monte Generoso (southern Switzerland) areas (former Adriatic proximal margin). In more distal settings, the stretching TS is largely overprinted by subsequent deformation phases (necking and hyperextension).

The necking ST

The necking TS records the necking phase, which corresponds to the onset of significant crustal thinning via only a few active faults on either side of a largely undeformed crustal keystone (called H-block in Lavier and Manatschal, 2006; Fig. I.4c). These major crustal-scale extensional detachment faults are specific and characteristic structures of the future necking domains.
At the same time, most normal faults that were formed during the stretching phase are abandoned outside the necking domain. As a result, the necking TS outside the necking domain is characterized by the sealing of the older half-graben depocenters by post-tectonic, passively infilling sediments (Fig. III.B.3a5 fourth line of Fig. III.B.3b).
The onset of crustal necking is linked to the yield of the strongest lithospheric layer, which is usually the upper mantle in a thermally equilibrated lithosphere. When the upper crust is mechanically decoupled from the mantle, the yielding of the upper mantle is followed by a flexural rebound that accounts for the shallow-water depth, or even the uplift and local erosion of the keystone (i.e., the future necking and hyperextended domains) during the necking phase (see erosional unconformity in Figs. III.B.3a1, III.B.3a2 and III.B.3a4; Chenin et al., 2019b, 2020a). Uplift of the keystone may be further increased by the thermal erosion related to the upwelling of the underlying asthenosphere.
The necking phase is linked to significant crustal and lithospheric thinning, which will eventually counterbalance the flexural rebound and thermal erosion of the lithosphere and cause rapid and significant subsidence. The timing of uplift vs subsidence depends strongly on the rheology of the lithosphere (Chenin et al., 2020a). Subsidence might be further enhanced by a large sediment supply and by subsequent thermal relaxation of the rift system.
In summary, in the necking domain of the final margin, the necking TS is expressed by (fourth line of Figs. III.B.3b-III.B.3d): (1) creation of new real estate due to the exhumation of upper- to middle crustal rocks to the seafloor via extensional detachment faulting; (2) supra-

https://doi.org/10.3301/GFT.2023.02

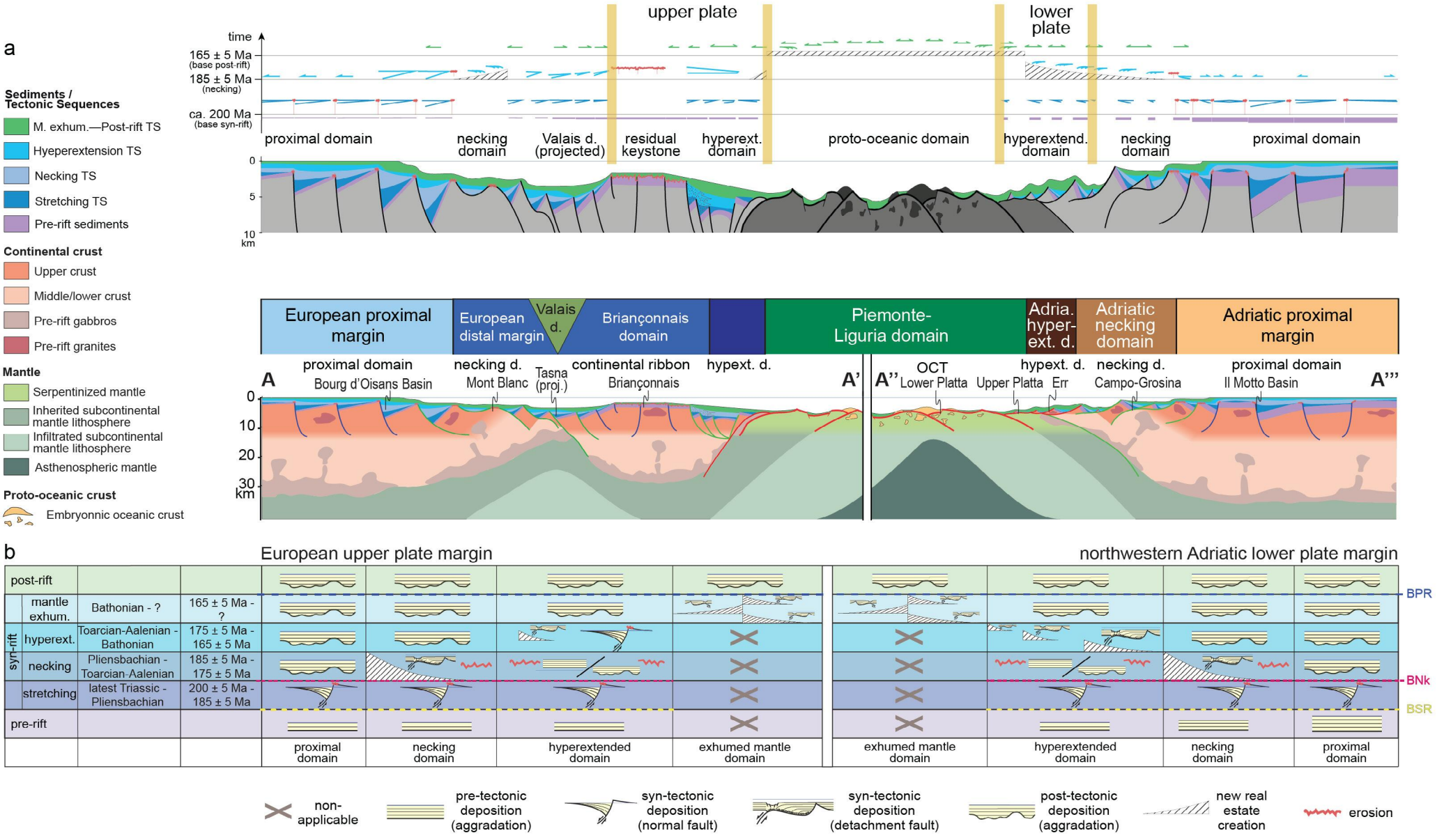

Fig. III.B.4 (modified from Chenin et al. 2022 and Manatschal et al. 2022) – a) Wheeler diagram for the Alpine Tethys conjugate margins; and (b) table summarizing corresponding main structures and related stratigraphic architecture. Abbreviations:BNk: Base of the Necking tectonic sequence; BPR: Base of the Post-Rift megasequence; BSR: Base of the SynRift megasequence; d.: domain; hypertext., hypext: hyperextended; M. exhume.: mantle exhumation; OCT: Ocean-Continent Transition; TS: Tectonic Sequence.

https://doi.org/10.3301/GFT.2023.02

detachment wedge-shaped sedimentary deposits of necking phase age emplaced directly onto exhumed basement; (3) uplift and erosion of exhumed basement and pre-necking sediments potentially visible in both the necking and hyperextended domains; and (4) contemporaneous deposition of basement-derived material (e.g. sandstones) in adjacent regions. These sediments may be "cannibalized" (i.e., reworked, and re-deposited) during the necking phase owing to the progressive exhumation/uplift/rollover of the detachment fault on which the sandstones were deposited.

The necking phase is at the origin of BB2 in the necking domain of rifted margins and BB3 in the hyperextended domain. In the Alps, BB2 is best preserved in the Mont Blanc region (former European margin) and in the Cusio-Biellese region (former Adriatic margin), and BB3 in the Briançonnais domain (Figs. III.B.3a2 and III.B.4a). The Alpine Tethys necking TS displays different characteristics along dip (Fig. III.B.4b): it expresses as passive infill in the proximal domain (e.g., Excursion A), as basement exhumation in the necking domain (e.g., Mont Blanc; Ribes et al., 2020) and as shallow-water deposition and/or erosion in the future hyperextended domain (e.g., shallow-water facies of the Agnelli Fm; Decarlis et al., 2015).

The hyperextension ST

The hyperextension TS records the hyperextension phase, which corresponds to the localized dismembering of fully brittle continental crust. Hyperextension is the first deformation stage that displays a marked asymmetry: on the one hand, the future lower-plate margin is extended via in-sequence detachment faulting, while on the other hand, the future conjugate upper-plate margin is delaminated by the play of the underlying detachment fault (Fig. I.4e).

During hyperextension, the proximal and necking domains are tectonically inactive, which results in continued passive infill in the proximal domain and the sealing of syn-tectonic structures/deposits in the necking domain (third line of Fig. III.B.3b). Thus, in the proximal and necking domains of the future margin, the hyperextension TS is characterized by post-tectonic deposits. In the exhumed mantle domain, the hyperextension TS is lacking since no mantle is exhumed to the seafloor at the hyperextension stage.

The hyperextension phase is associated with rapid subsidence in both the necking and hyperextended domains (third line of Fig. III.B.3d). Subsidence is related to significant crustal thinning (crustal thickness between 10 and 0 km in the hyperextended domain) above a mechanically weak mantle (mechanical breakup achieved during the previous necking phase). In the necking domain, subsidence is at this stage essentially driven by thermal relaxation.

In the lower plate hyperextended domain, each successive in-sequence detachment fault crosscuts the former one, resulting in the typical BB4 in-sequence architecture illustrated in Fig. III.B.3a4 (Ranero and Pérez-Gussinyé, 2010). These detachment faults create new real estate via the exhumation of the basement to the seafloor. The exhumed basement is typically pre-rift upper- to the middle crust. Each detachment fault is associated with a supra-detachment sedimentary basin floored by tectono-sedimentary breccias. These basins are filled with supra-detachment wedge-shaped syn-tectonic sediments emplaced directly onto the detachment surface, getting younger toward the

https://doi.org/10.3301/GFT.2023.02

detachment exhumation point (third line of Fig. III.B.3b). As the successive in-sequence detachment faults play one after another, syn-tectonic sedimentary deposits are getting younger oceanward. Therefore, sedimentary deposits of given age that are syn-tectonic in one supra-detachment basin are post-tectonic in supra-detachment basins located more continent-ward.

In summary, in the hyperextended domain of the final lower-plate margin, the hyperextension TS is expressed by (third line of Figs. III.B.3b-III.B.3d): (1) creation of new real estate due to the exhumation of upper- to middle crustal rocks to the seafloor via in-sequence detachment faults that dip exclusively oceanward; (2) tectono-sedimentary breccias and overlying supra-detachment wedge-shaped sedimentary deposits of hyperextension phase age emplaced directly onto exhumed basement, and (3) a progressive younging of supra-detachment basins fill oceanward.

The hyperextended domain of upper plate margins represents the residual part of the initial keystone block (Haupert et al., 2016; Fig. III.B.3a2). It preserves therefore much more of the stretching and necking-related structures and deposits compared to its conjugate, namely high-angle normal faults that can dip continent- or oceanward. The base of the outer part of the hyperextended domain is an extensional detachment fault that may exhume both subcontinental mantle and lower crustal rocks to the seafloor (e.g., Excursion E).

The individualization of the upper plate hyperextended domain is often associated with the formation of mega-fault scarps at its boundary with the adjacent necking domain, and thus with the emplacement of breccias at its toe, over a wide part of the hyperextended domain (Fig. III.B.3a2; Ribes et al., 2019b).

In summary, in the hyperextended domain of the final upper-plate margin, the hyperextension TS is expressed by: (1) the creation of a mega-fault scarp and associated mega-breccias at the boundary between the necking and hyperextended domain; (2) good preservation of earlier sedimentary structures due to the lack of significant new real estate creation; and (3) possible exhumation of lower crustal rocks to the seafloor at the outer edge of the hyperextended domain.

The hyperextension phase is at the origin of BB4 and BB6 at the lower-plate margin and BB5 & BB6 at the upper-plate margins. In the Alps (Figs. III.B.3a2 III.B.4), BB4 is best preserved in the Err Nappe (Excursion C), BB5 in the Falknis Nappe and Nappe de Brèches (Ribes et al., 2019b) and BB6 in the Upper Platta (Excursion D; Epin and Manatschal, 2018) and Tasna Nappe (Excursion E; Ribes et al., 2019c).

The mantle exhumation ST

The mantle exhumation TS records the phase of subcontinental mantle exhumation to the seafloor (Fig. I.4f). Mantle exhumation occurs while tectonic activity has ceased in the continental domains of the future margin, therefore the mantle exhumation TS in the proximal, necking and hyperextended domains of the final margin is characterized by post-tectonic sedimentation (second line of Fig. III.B.3b). The entire margin keeps on subsiding during the mantle exhumation phase.

The exhumed mantle domain is entirely comprised of new real estate (except from few potential allochthonous blocks of continental crust and/or pre- to syn-rift sediments). Subcontinental mantle exhumation is achieved via flip-flop (out-of-sequence) detachment faults that develop

https://doi.org/10.3301/GFT.2023.02

successively on either side of the future spreading centre, generating a relatively symmetrical pattern (Epin et al., 2019; Gillard et al., 2016b; Fig. I.4g and second line of Fig. III.B.3b). The play of a mantle exhumation fault is associated with the formation of a topographic high at the detachment fault breakaway and thus characterized by over-tilted sedimentary sequences (see to the very right of Fig. III.B.3a3). As tectonic activity continuously steps toward the locus of the future breakup, the age of the over-tilted sequences decreases oceanward.

The first sediments overlying the exhumed mantle are tectono-sedimentary breccias that are mixed and/or overlain with either pelagic, detritic, or chemical (e.g., cherts or brines precipitated from SiO_2-oversaturated fluids) sediments depending on the available sources (e.g., in transform margins this domain may be directly fed by the adjacent continent). In the case of high sedimentation rates, these sediments form supra-detachment wedge-shaped architectures directly onto the detachment surface.

The exhumation phase often displays incipient magmatic activity, which results in discontinuous magmatic intrusions and lava flows. Magmatic flows are syn-tectonic, and thus they are interbedded with sediments of exhumation phase age.

In summary, in the exhumed mantle domain of the final margin, the mantle exhumation TS is expressed by (second line of Figs. III.B.3b and III.B.3c): (1) exclusively new real estate basement comprised of subcontinental lithospheric mantle exhumed to the seafloor via out-of-sequence detachment faulting; (2) tectono-sedimentary breccias and overlying supra-detachment wedge-shaped sedimentary deposits of mantle exhumation phase age emplaced directly onto exhumed mantle; (3) over-tilted sedimentary packages at detachment faults breakaway; and (4) a progressive younging of supra-detachment basins fill oceanward.

The mantle exhumation phase is at the origin of BB7 in the exhumed mantle domain. In the Alps (Fig. III.B.4), BB7 is best preserved in the Lower Platta Nappe (Excursion D, Epin et al., 2019) and at the Chenaillet (Manatschal et al., 2011).

https://doi.org/10.3301/GFT.2023.02

C. FLUIDS THEMATIC SHEET
Signature of syn-rift fluids: the example of the former Alpine Tethys

INTRODUCTION

In a general way, “magma-poor” rifting can be regarded as a succession of deformation phases with specific characteristics that affect an ever-narrower domain as extension progresses, namely the stretching, necking, hyperextension, mantle exhumation, and seafloor spreading phases (Fig. III.C.1; see also section 2 of the excursion notes). Over the last twenty years, several researchers attempted to link these different deformation phases to specific geochemical and petrological signatures of syn-rift neo-formed minerals and/or sediments (e.g., Manatschal, 1999; Manatschal et al., 2000; Pinto et al., 2015; Incerpi et al., 2020a, 2020b; see also https://convergent-margins.com/fluids/).
A few years ago, Pinto et al. (2015) evidenced specific chemical signatures of syn-tectonic detachment fault minerals from the time the crust and mantle are mechanically coupled. More recently, Incerpi et al. (2020a) achieved a detailed tracing of fluid signature in time and space within the sedimentary deposits of the Alpine Tethys rift system.

FLUID SIGNATURE IN SYN-TECTONIC DETACHMENT FAULT ROCKS/MINERALS

Fluid signature prior to crust-mantle coupling: the Bernina and Grosina detachments

The Bernina and Grosina detachment faults are two of the oldest detachment faults found in the Adriatic margin of the former Alpine Tethys. They formed during the necking- and early hyperextension phases (fluid event 2 in Fig. III.C.1c). Fluid-continental rock reactions were recorded along the Grosina and Bernina detachment faults at 190 and 185 Ma, respectively (Pinto et al., 2015). Both detachments show syn-tectonic clay minerals, which display little chemical variations compared with the composition of the protolith. Sr isotopes indicate interactions with continental crust (Incerpi et al. 2020a).

Fluid signature after crust-mantle coupling: the Err detachment system

The Err detachment system belongs to the distal Adriatic margin of the Alpine Tethys. It is younger than both the Bernina and Grosina detachment faults. The Err detachment system formed during the hyperextension phase of rifting (fluid event 3 in Fig. III.C.1d). Evidence for fluids circulation along the Err extensional detachment system includes:

- quartz and albite veins produced by saussuritization processes (i.e., alteration of feldspar);
- precipitation of iron oxides in cataclastic foliations as a result of biotite alteration syn-tectonic phyllosilicates enriched in Cr, Ni, V, and Fe along the detachment fault zone.

https://doi.org/10.3301/GFT.2023.02

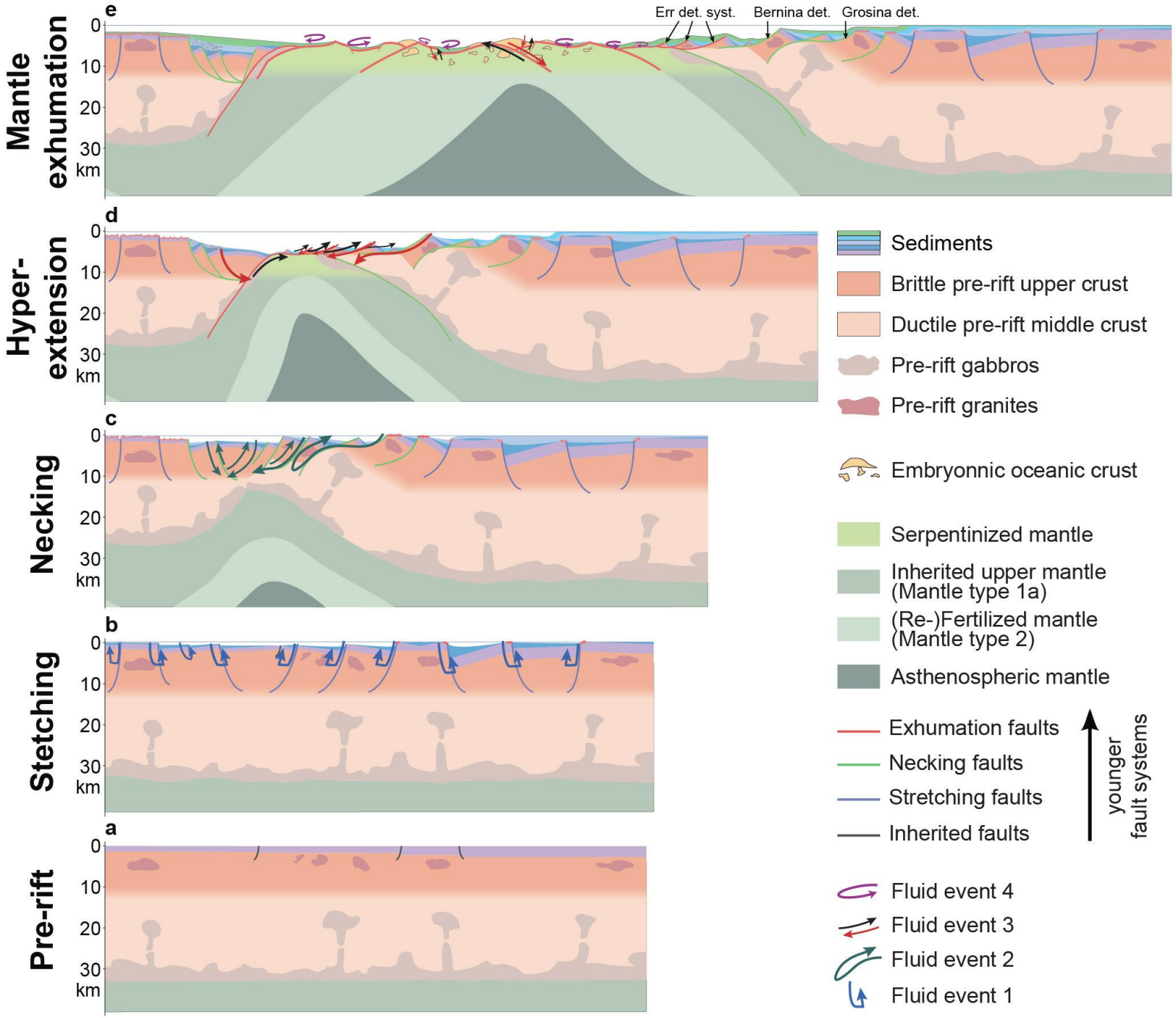

Fig. III.C.1 - Schematic evolution of the Alpine Tethys rift system. a) Pre-rift settings; b) carbonate-rich event affect pre-rift sediments during the stretching phase; c) fluid-rock interactions during the necking phase are evidenced in both syn-tectonic fault minerals and in overlying sedimentary deposits; d) mantle-reacted fluid-rock reactions during the hyperextension phase are evidenced in both syn-tectonic fault minerals and in overlying and adjacent sedimentary deposits; e) mantle-reacted fluid-rock reactions continue during the mantle exhumation phases. At the same time, syn- to post-tectonic carbonatation of exhumed mantle takes place. Abbreviations: det.: s=detachment; syst.: system.

https://doi.org/10.3301/GFT.2023.02

Pinto et al. (2015) interpreted the enrichment of syn-tectonic neo-formed minerals in Cr, Ni, V, and Fe to result from the circulation of mantle-reacted hydrothermal fluids along extensional detachment faults (Figs. III.C.2a). Indeed, crust-mantle mechanical coupling allows the percolation of marine fluids down into the mantle, where they are heated. These hydrothermal fluids trigger efficient mantle serpentinization, which is characterized by a depletion of peridotites in Cr, Ni, V, and Fe. These elements enrich the hydrothermal fluids, which migrate back up along the active part of extensional detachment faults and enrich seawater where tectonic activity is responsible for dynamic permeability (Fig. III.C.2a). Consequently, syn-tectonic neo-formed minerals within these fault zones (as well as sedimentary deposits above them) are enriched in mantle-derived elements (Fig. III.C.2b). Fluid circulation is maximal in the active portion of detachment faults (i.e., prior to their exhumation to the seafloor) due to intense tectonic fracturing and high geothermal gradient. Once exhumed to the seafloor, the detachment becomes inactive, and thus its porosity decreases rapidly.

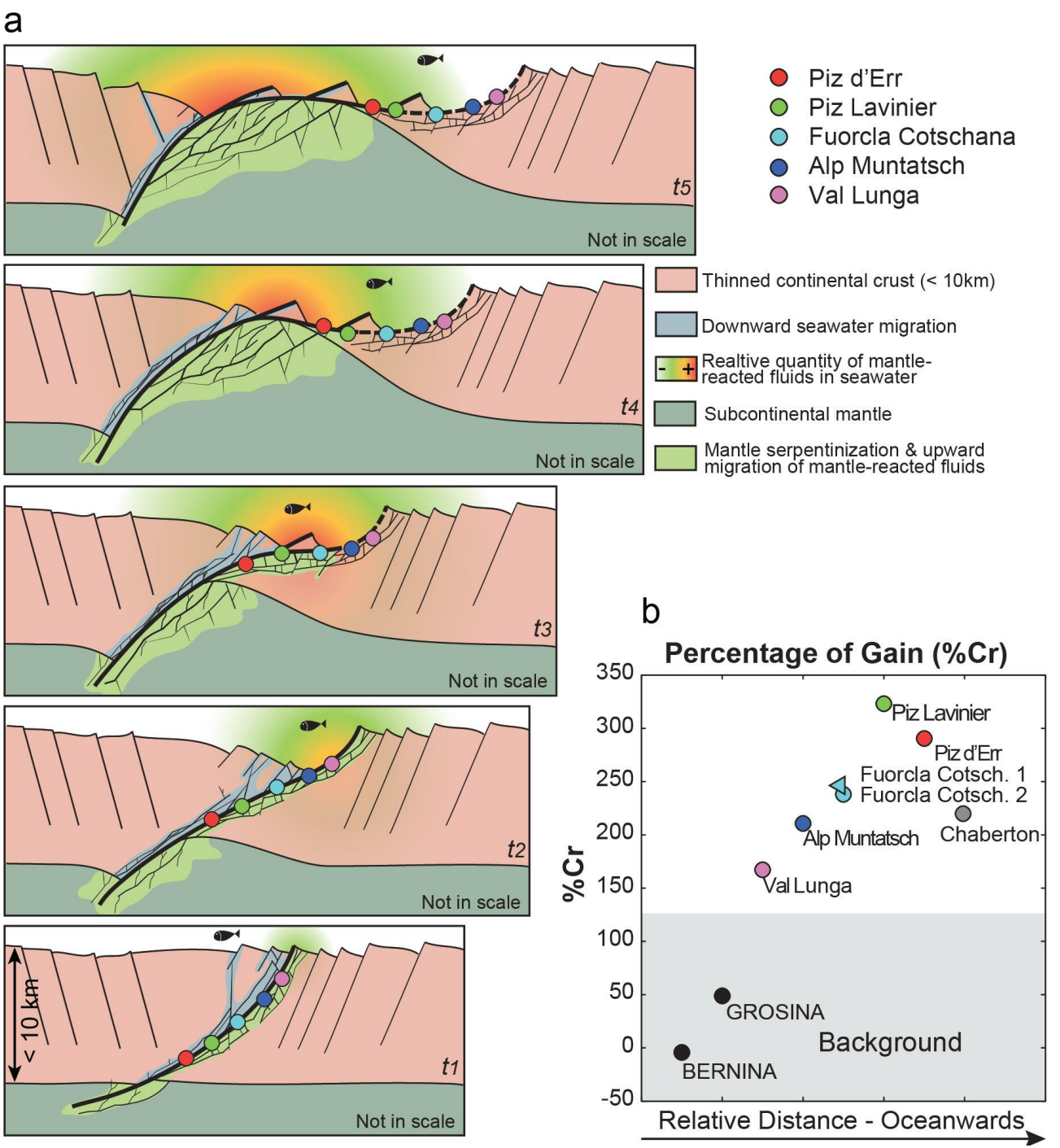

Fig. III.C.2 (from Pinto et al., 2015) – a) Conceptual model of mantle-reacted fluids migration during active detachment faulting (modified from Pinto et al., 2015); b) graph displaying the percentage of Cr as a function of the sample position with respect to the exhumation point.

https://doi.org/10.3301/GFT.2023.02

Pinto et al. (2015) observed a progressive enrichment in Ni, Cr, and V of syn-tectonic sediments and neo-formed minerals from 185 Ma onward. They suggested that this enrichment marks the onset of mantle serpentinization beneath hyperextended continental crust.
Pinto et al. (2015) also noticed a peak in Ni, Cr, and V concentration in the syn-tectonic sediments of the distal margin towards the end of the 185-165 Ma interval (i.e., member C of the Saluver Fm; see Excursion C). They interpreted it as evidence for efficient serpentinization, most likely related to the exhumation of the mantle to the seafloor. They emphasized that member C of the Saluver Fm is more enriched in Cr, Ni, and V than overlying radiolarian cherts. They suggested that hydrothermal activity had largely decreased and/or moved further outboard (i.e., in the proto-oceanic domain) by this time.

Interpretation

The absence of mantle fluid signature in the syn-tectonic fault rocks of the Grosina and Bernina detachments indicates that continental crust was not mechanically coupled to the subcontinental lithospheric mantle until 185 Ma (Pinto et al., 2015). In contrast, mantle fluids signature within the syn-tectonic minerals of the Err detachment fault rocks as well as in the overlying syn-tectonic sediments testify to crust-mantle mechanical coupling during the hyperextension stage, from approximately 185 Ma onward.

FLUID SIGNATURE IN SEDIMENTARY DEPOSITS

Fluid signature in sediments during the stretching phase

Incerpi et al. (2020a) recognized a first carbonate-rich stage along the entire Adriatic margin from Rhaetian to Pliensbachian (latest Triassic to Early Jurassic; Fluid event 1 in Fig. III.C.1b). It consists of of dolomitization of the Late Triassic Hauptdolomit and Kössen Fms before their reworking within syn-tectonic breccias (Alv, Bardella, and Saluver Fms). Precipitation of dolomite, calcite, and minor quartz occurred as passive infill of open cracks, which suggests tectonically static conditions.
The dolomitization process began once the Triassic carbonate platform started to be fragmented, which occurred during the so-called stretching phase of rifting. Seawater percolated down into the thick pre-rift sediments via high-angle normal faults, was heated and chemically modified by exchanges with Triassic sediments on its way down and dolomitized the carbonate platform on its way up (hydrothermal loop represented in Fig. III.C.3).

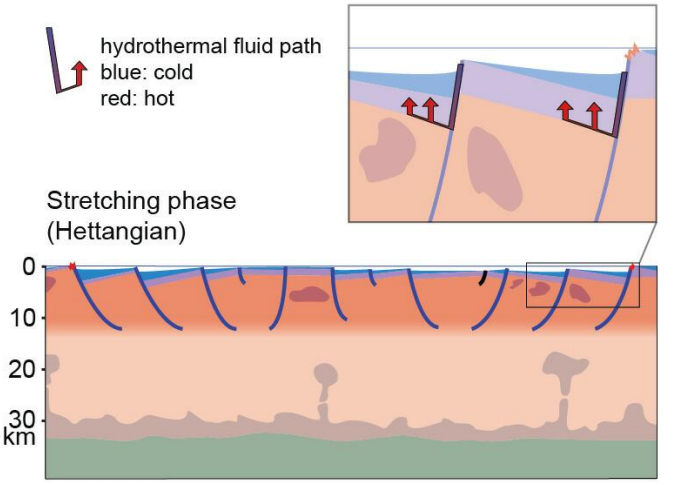

Fig. III.C.3 - Conceptual model of fluid circulation within the Triassic carbonate platform during the stretching phase.

https://doi.org/10.3301/GFT.2023.02

Fluid signature in sediments during the necking phase

Incerpi et al. (2020a) observed a second set of events that are recorded only in the distal part of the margin from the late Pliensbachian to the Toarcian (Fluid event 2 in Fig. III.C.1c). It includes dolomitization, dedolomitization, hydrofracturing and calcite cementation of hydraulic breccias. These events are related to detachment faulting and crustal thinning.

Evidence for both hydrothermal and more superficial fluids suggests a mix between surface fluids flowing along detachment faults with fluids flowing up from deeper fracture basement. Surface fluids may be at the origin of the patchy dedolomitization observed along brittle faults.

Fluid signature in sediments during the hyperextension and mantle exhumation phases

Incerpi et al. (2020a) recognized a third set of events after Toarcian time (Fluid event 3 in Fig. III.C.1d). It affected the entire pre- and syn-rift sedimentary pile of the distal margin, although it is more marked in the syn- to early post-tectonic sequences. This fluid event manifests as quartz precipitation both in veins and as cement, as well as local septarian-like concretions in fine-grained syn-rift sediments. Such concretions were formed close to the seafloor, where they were often reworked (Incerpi et al., 2017, 2018; Fig. III.C.4b).

The existence of Fe and Mn oxides within debris flow deposits in the outermost part of the margin suggests a contribution of mantle fluids (Fig. III.C.4a).

In the exhumed serpentinized mantle domain of the Platta Nappe, Coltat et al. (2019b) noticed Fe-Ca-silicates, semi-massive sulphides, Cu-rich massive sulphides (Cu-rich MS), which occur as sporadic thin

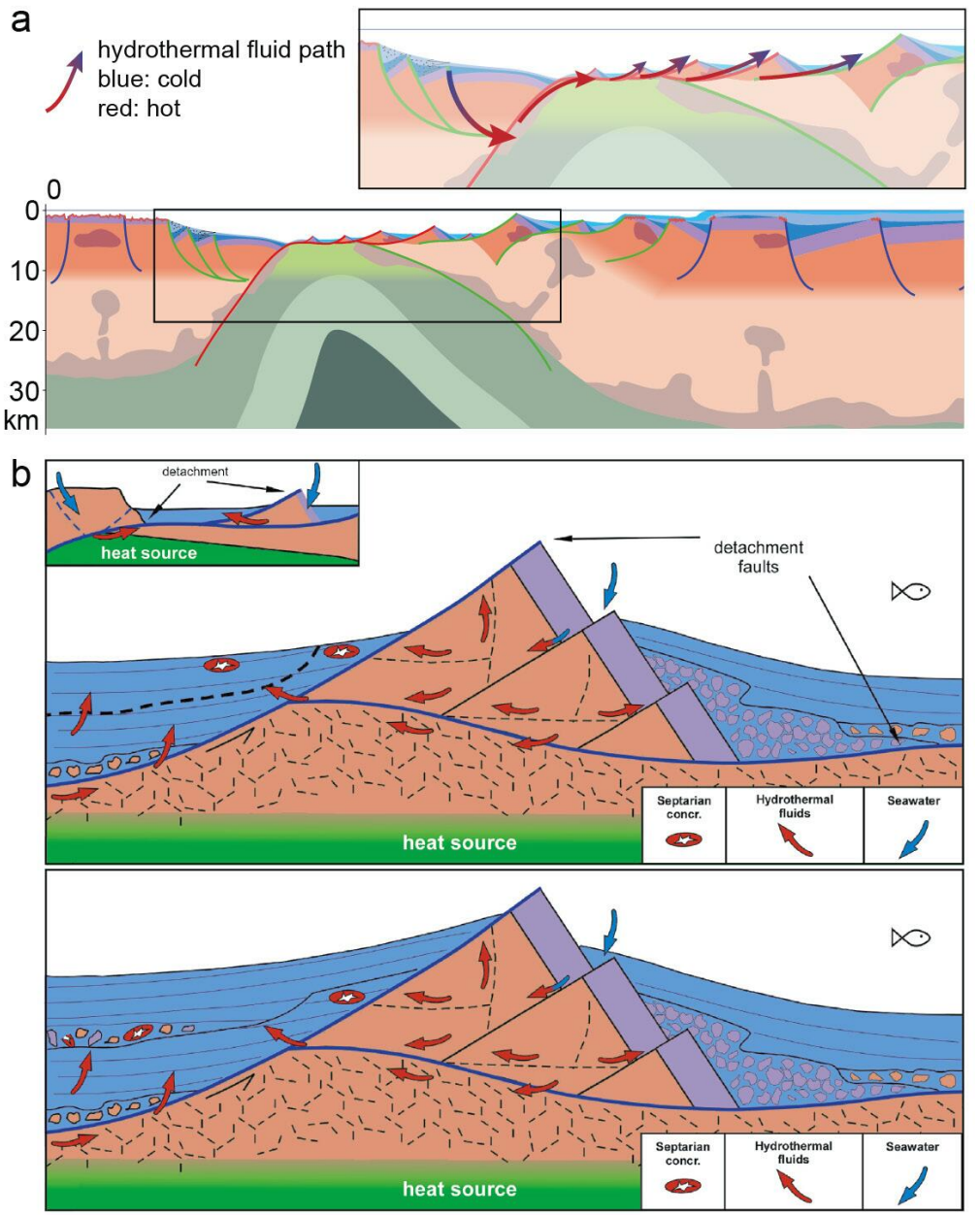

Fig. III.C.4 - a) Schematic fluid path during the hyperextension stage; b) fluid path within and around an allochthon during crustal detachment faulting (modified from Incerpi et al., 2018). Abbreviation: concr.: concretion.

https://doi.org/10.3301/GFT.2023.02

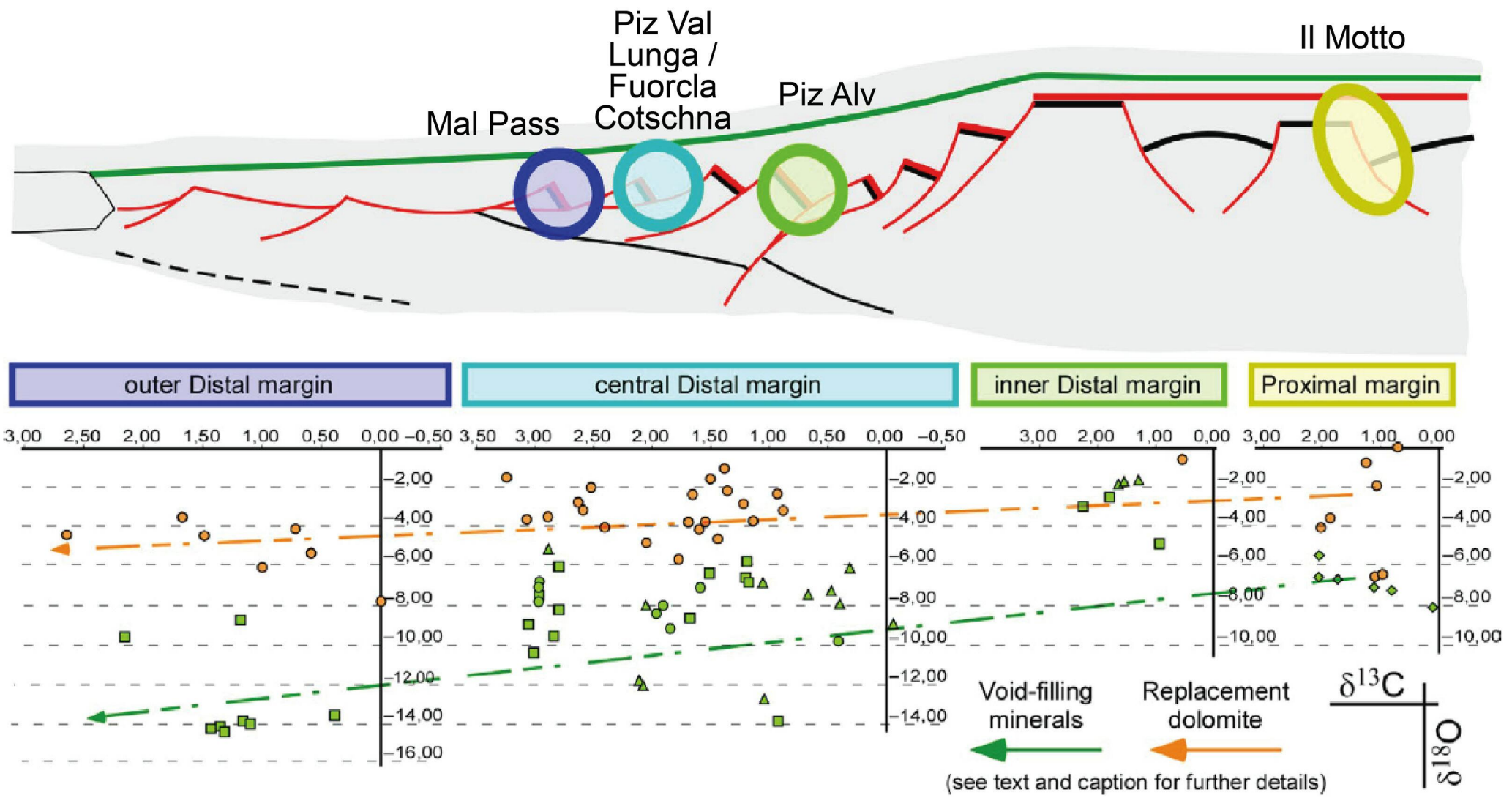

Fig. III.C.5 (modified from Incerpi et al., 2020b) - Stable isotope data: $\delta^{18}O$ versus $\delta^{13}C$ cross-plot for dolomite and calcite minerals from the five studied areas along the Adriatic margin; values are given relative to VPDB (Vienna Pee Dee Belemnite) standard. The orange circles represent the replacement dolomite affecting the Hauptdolomit Fm. The green colour is for those minerals occurring as void-filling phases: rhombs (dolomite cement in hydraulic breccias), squares (dolomite veins), circles (calcite veins), triangles (calcite cement in hydraulic breccias and dedolomitization).

https://doi.org/10.3301/GFT.2023.02

oxidized reddish corridors and patches. They interpreted the metalliferous deposits as a result of black smoker-type hydrothermal structures comparable to those observed at present-day slow-spreading ridges.

Oxygen and Carbon isotopes along the Adriatic margin

Oxygen and carbon isotope analyses on different carbonate phases display very homogeneous C isotope values along the entire Adriatic margin (Fig. III.C.5), with values ranging between 0 and 3‰ of the Vienna Pee Dee Belemnite standard (VPDB). Conversely, O isotope values vary significantly both among the different paleogeographic domains and within a given domain (Fig. III.C.5). $\delta^{18}O$ value becomes increasingly negative oceanward, with values ranging from 0 to -16‰ VPDB.

CARBONATATION OF EXHUMED MANTLE

Picazo et al. (2013) highlighted that the top ~20 m of the mantle exhumed to the paleo-seafloor is intensively replaced by carbonates. The fact that carbonatized serpentines are crosscut by neptunian dykes filled with Jurassic sediments testifies to the pre-Alpine origin of the carbonatation process.

Picazo et al. (2013) interpreted the carbonatation of the top of the exhumed mantle as the result of paleo-seafloor

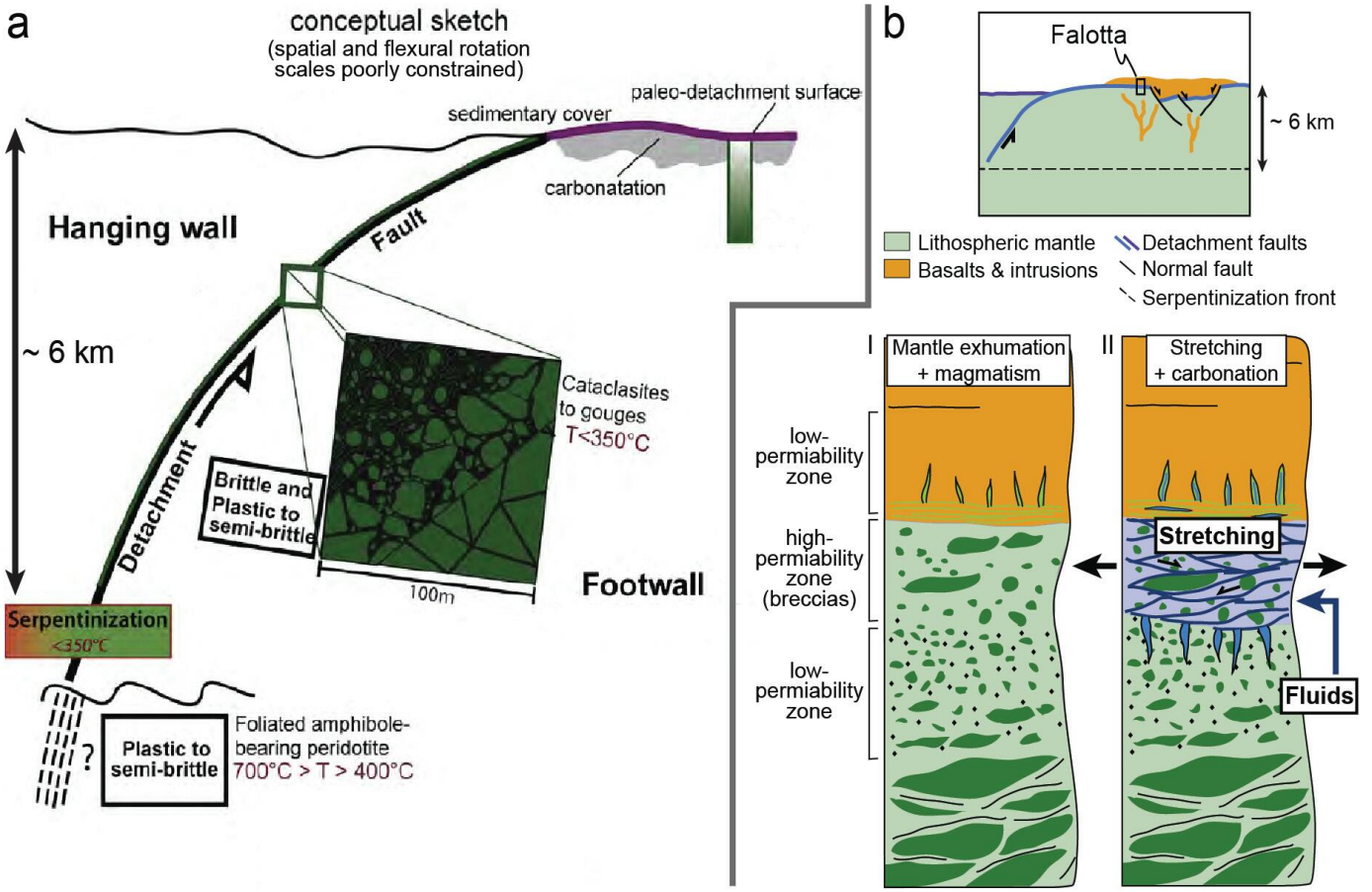

Fig. III.C.6 – a) Conceptual sketch (modified from Picazo et al., 2013) illustrating the formation of ophicalcites. Serpentinite cataclasites and gouges observed up to 100 m away from the paleo-seafloor are interpreted to reflect deformation in the ultramafic footwall next to Jurassic mantle exhumation faults. This deformation postdates mantle serpentinization. When the detachment fault reaches the seafloor, carbonation affects the exhumed mantle rocks and sediments are deposited; b) (modified from Coltat et al., 2019b): model of carbonation (sketches I and II) in context of magma-assisted mantle exhumation (top sketch). Carbonation is represented in blue (veins).

https://doi.org/10.3301/GFT.2023.02

alteration in post-tectonic settings (fluid event 4 on Fig. III.C.1e; see also Fig. III.C.6a). Carbonatation was linked to hydrothermal fluid circulation at relatively low temperatures (<100-150 °C; Früh-Green et al., 1990).

More recently, based on field studies in the Lower Platta Nappe (Excursion D), Coltat et al. (2019a) evidenced that carbonatation may also be syn-tectonic, occurring during late stages of syn-magmatic mantle exhumation (Fig. III.C.6b). In this case, carbonatation takes place along the detachment fault plane, in the high-permeability zone between serpentine and basalts. The remarkable homogeneity of the carbonate isotopic signature suggests that they formed during a single and short seawater-derived carbonatation event at relatively low temperatures (ca. 100 °C).

Picazo et al. (2013) noted that carbonates are sometimes reworked into tectono-sedimentary breccias. They concluded that mantle exhumation was associated with the formation of topographic highs in the footwall of active detachment faults. This hypothesis is also supported by the study of Epin et al. (2019) in the Lower Platta Nappe (Excursion D). Footwall-derived products could subsequently be deposited onto active tectonic surfaces.

https://doi.org/10.3301/GFT.2023.02

D. TECTONO-STRUCTURAL THEMATIC SHEET
3D architecture of the former Alpine Tethys margins and its impact on the present-day Alpine orogenic structure

INTRODUCTION

The present-day architecture of the Alpine collisional orogen is strongly controlled by that of the former Alpine Tethys rift system. Therefore, our understanding of the Alpine Tethys rift system is intimately linked to our understanding of the Alpine orogen, and vice versa. In the following, we characterize the architecture of both magma-poor rift systems and collisional orogens and highlight their relationships.

TECTONO-STRUCTURAL EVOLUTION OF RIFT SYSTEMS

Three-dimensional-large-scale rift structure and evolution

Rifting often initiates with a phase of distributed extension characterized by the formation of numerous half-graben basins over a wide region (Fig. III.D.1a, e.g., Ball et al., 2013; Withjack et al., 2012). During this so-called stretching phase, extensional basins are mostly oriented perpendicular to the main extension direction (Nirrengarten et al., 2018), although further complexity may arise due to structural inheritance (Zwaan et al., 2021). In the Alpine Tethys realm, the stretching phase started in the latest Triassic-earliest Hettangian (Fig. III.D.1e) and formed, amongst others, the Il Motto (Excursion A), Monte Generoso and Bourg d'Oisans basins (cf. Manatschal et al., 2022, for a review).

During the subsequent necking and hyperextension phases, deformation focalizes in different rift segments (Nirrengarten et al., 2018). These rift segments are either limited by transform faults or set up as overlapping en-échelon systems comprised of individual disconnected rift basins (Fig. III.D.1b). In the Alpine Tethys realm, three independent segments developed from Sinemurian-Pliensbachian time onward, namely the Piemonte, Ligurian, and Valais basins (Fig. III.D.1f).

Brune et al. (2016) noticed that this stage commonly displays a sudden acceleration of extension within the rift system. They related this acceleration to the yielding of the lithosphere (i.e., upper mantle and/or crustal necking) under a constant force extensional setting. Considering a tectonic system submitted to a constant bulk extension rate leads to a comparable acceleration in extension at the switch from distributed to localized extension (i.e., during the necking phase; Chenin et al., 2018a). However, based on the plate kinematic reconstruction of the southern North Atlantic rifting, Nirrengarten et al., (2018) suggested that this phase of acceleration started contemporaneously with the onset of hyperextension, implying that mechanical weakening of the lithosphere occurred already during the preceding necking phase.

https://doi.org/10.3301/GFT.2023.02

During the following mantle exhumation and proto-oceanic phases, the individual rift basins merge into a single rift system (Nirrengarten et al., 2018). At this stage, non-segmented V-shape propagation may dominate rifting (Fig. III.D.1c), which suggests that inheritance does not control extension anymore (Manatschal et al., 2015; Nirrengarten et al., 2018).
In the Alpine Tethys realm, the Piemonte, Ligurian, and Valais basins became connected during Callovian-Bathonian time (Fig. III.D.1g; Baumgartner, 2013).

Two-dimensional architecture of rifted margins

The first-order architecture and lithology of magma-poor rifted margins are described in section 2.1 of the excursion notes. In the following, we focus on the aspects important for subsequent compressional reactivation.
The proximal and necking domains of rifted margins are comprised of thick (35-10 km), buoyant, and little altered continental crust that tapers oceanward (Fig. III.D.2a). The underlying mantle is not hydrated, and thus much denser and stronger compared to the overlying crust. In these domains, the crust and mantle are mechanically decoupled by a ductile middle and/or lower crust. The proximal domain is almost exclusively structured by high-angle normal faults, while the necking domain displays both high-angle normal faults and extensional detachment faults.
In contrast, the basement in the hyperextended and exhumed mantle domains is highly fractured and its top six kilometres are intensively hydrated

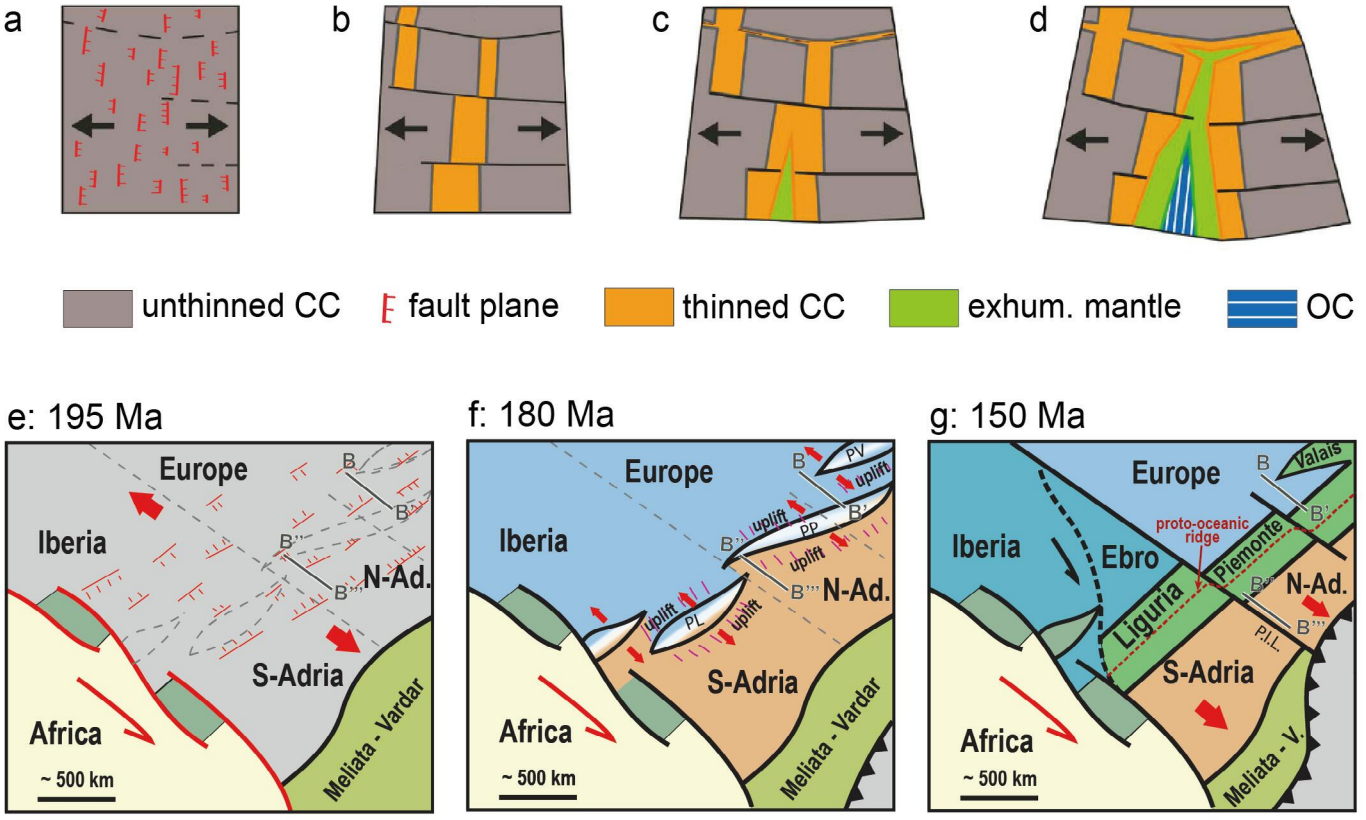

Fig. III.D.1 - 3D sketch of a magma-poor rifting (modified from Nirrengarten et al., 2018). a) The stretching phase is characterized by broadly distributed half graben basins generally perpendicular to the extension direction; b) during the necking and hyperextension phases, a few rift basins separated by transfer faults/zones individualize; c-d) at the stage of mantle exhumation and proto-oceanic accretion, individual rift basins are connected and extension continues into a non-segmented V-shape propagator; e-g) schematic paleogeographic evolution of the Alpine Tethys rift system (from Manatschal et al., 2022; see legend of Figure I.12).

https://doi.org/10.3301/GFT.2023.02

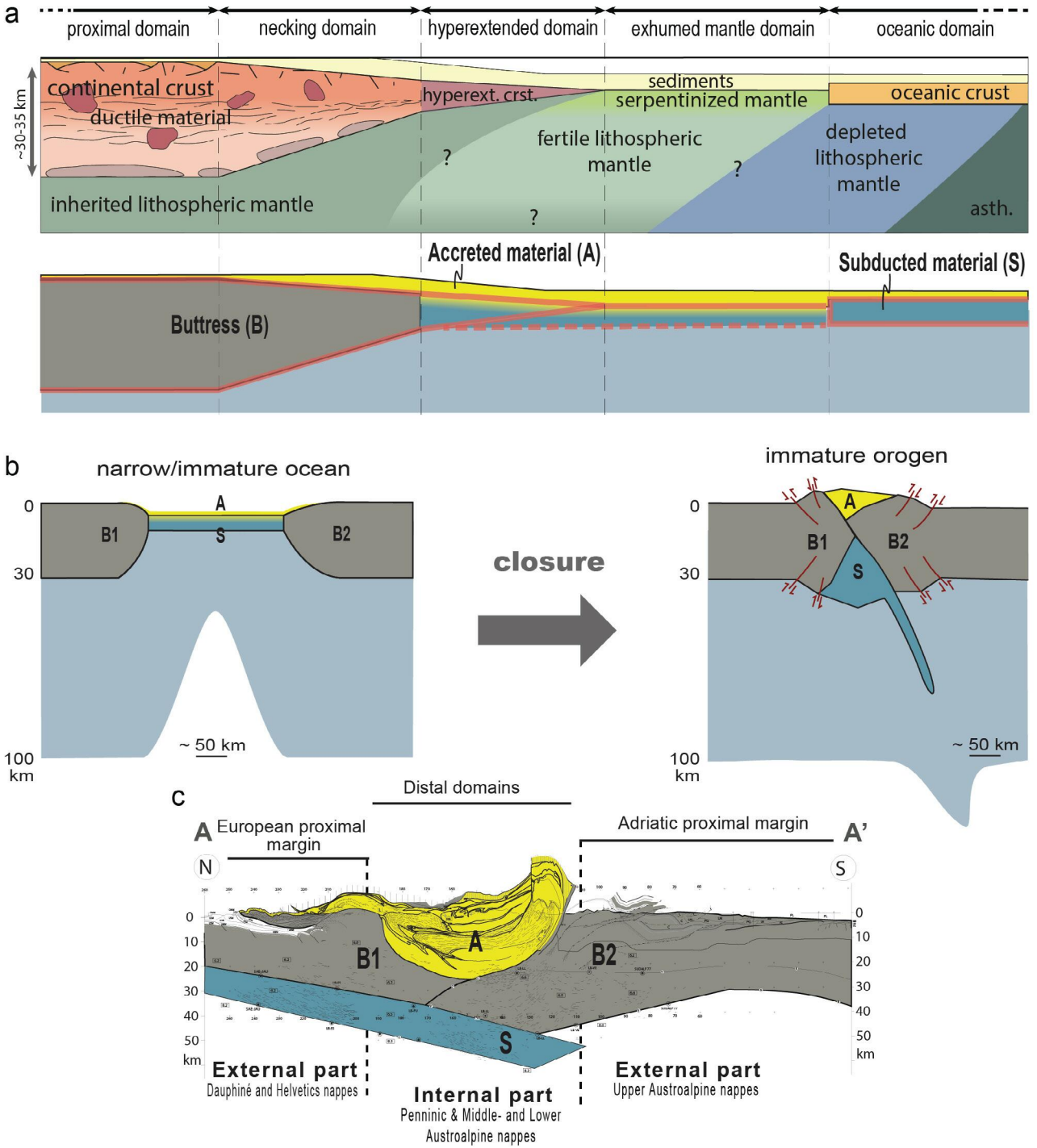

(Fig. III.D.2a; Manatschal, 1999): feldspars in the residual/allochthonous continental crust are altered into clay minerals, and mantle peridotites are serpentinized. Both the residual crust and uppermost mantle are largely weakened and deform in a frictional way (Nirrengarten et al., 2016). Within the serpentinized mantle, a major rheological interface at ca. 3 km below the top basement marks a sharp limit between weak material above and significantly stronger material below (Gillard et al., 2019). Both domains are essentially structured by extensional detachment faults that dip at a low angle.

Further outboard, in the oceanic domain, the Penrose-type oceanic crust and underlying mantle represent a stronger, mechanically coupled, and globally denser domain (Fig. III.D.2a). The oceanic crust is often fractured by high-angle normal faults.

Fig. III.D.2 – a) Schematic view of a rifted margin displaying the first-order morphology of magma-poor rifted margins and their main lithological interfaces (modified from Chenin et al., 2017); b) sketch illustrating the fate of the different components of an immature "ocean" during orogeny upon its closure (from Chenin et al., 2017); c) representation of the buttresses, accreted material and subducted material on the seismic cross section through the Alps (from Schmid et al., 1996; see transect A-A' in Figure I.0a for location and abbreviations).

https://doi.org/10.3301/GFT.2023.02

TECTONO-STRUCTURAL EVOLUTION IN COMPRESSIONAL SETTINGS

Two-dimensional/regional-scale architecture of a magma-poor collisional orogen

Collisional orogens can be regarded primarily as three-part systems comprising: (1) two buttresses, (2) an accretionary wedge, and (3) a subducted part (respectively B, A, and S in Figs. III.D.2b and III.D.2c). In the case of hyperextended rift systems and narrow/immature "oceans" like the Alpine Tethys or the Pyrenean rift system, no long-lasting subduction of oceanic lithosphere occurs, and thus there is no significant arc-related magmatic overprint. As a result, the closure of the rift system is essentially controlled by mechanical processes (Chenin et al., 2017).

During the closure of a hyperextended rift system, the oceanic lithosphere tends to be efficiently subducted due to its high density (Fig. III.D.3). According to Stern (2004), most of the ophiolites

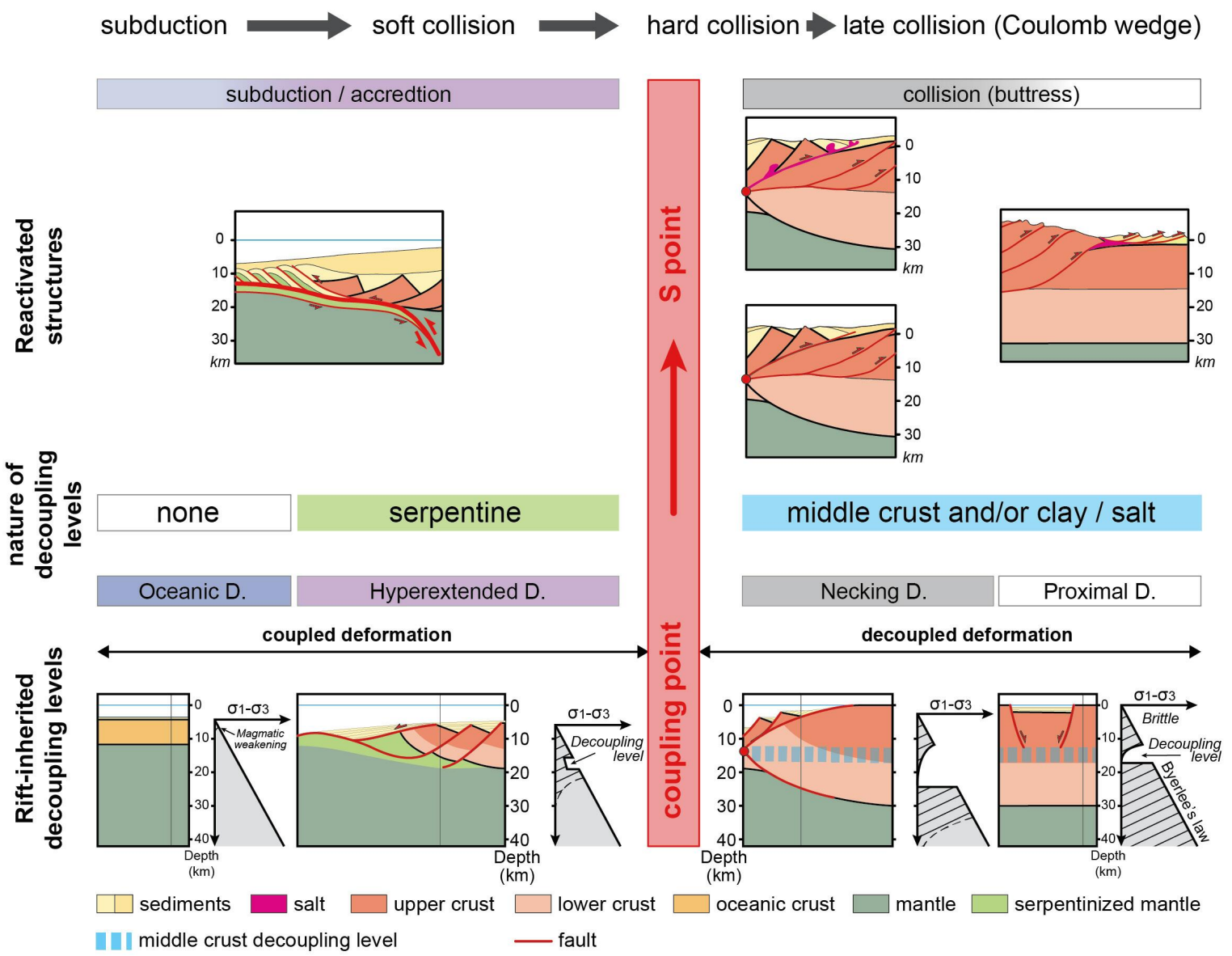

Fig. III.D.3 (modified from Lescoutre and Manatschal, 2020) - Conceptual model explaining the in-sequence reactivation of rift-inherited decoupling levels at a segment centre and the transition from subduction to soft collision, to hard collision and finally to late collision. Abbreviation: D.: Domain.

https://doi.org/10.3301/GFT.2023.02

preserved within orogens correspond to remnants of buoyant oceanic crust from small and young oceanic basins, usually former forearcs or back-arcs, rather than mature oceanic crust. A large part of sediments is also usually subducted, while the remaining part accumulates in the accretionary prism (e.g., Clift and Vannucchi, 2004; Stern, 2011). A significant proportion of the subducted material must be integrated into the orogenic root in order to account for the isostasy of collisional orogens; however, the deep architecture of collisional orogens is very poorly constrained (Butler, 2013), as illustrated by the diversity in the interpretation of the deep part of the ECORS-CROP seismic section (Mohn et al., 2014).

Both the Alpine and the Pyrenean orogens display a similar first-order architecture, where the external domain is made of a little-deformed continental basement and the internal part of a complex stacking of material originating from the former distal margin (e.g., De Graciansky et al., 2011), with the difference that the Pyrenees do not show subduction- or orogenic-related metamorphic overprints. Recent studies (Mohn et al., 2014; Tugend et al., 2015) show consistently that the external parts of orogens (the buttresses, B, in Fig. III.D.2b) correspond to the little deformed necking zones of the former continental margins. In contrast, the internal part corresponds to the accretionary prism (A in Fig. III.D.2b), which is composed of the thinned continental basement (remnants of the hyperextended domain), ophiolites and/or exhumed mantle, and thick sequences of highly deformed sediments (see Beltrando et al., 2014, for a review).

The distribution of accreted versus subducted material may be largely controlled by decoupling horizons like salt layers and the rheological boundary within the serpentinized mantle described in section 1b (Fig. III.D.3; Gillard et al., 2019; Manatschal et al., 2021).

Manatschal et al. (2021, cum ref.) suggested that, in a hyperextended rift system or immature ocean, subduction initiates in the exhumed mantle domain. The exhumed mantle- and adjacent hyperextended domain are usually subducted during this initial, so-called “soft-collision stage”. However, when the necking zone enters the subduction zone, a major change in the collision style occurs, switching from “soft-” to “hard collision”. At this stage, the necking zone starts to act as a buttress. Subsequent shortening reactivates either ductile levels within the residual continental crust, resulting in a thick-skinned reactivation, or continuous low friction levels in the sedimentary section (e.g., salt), resulting in a thin-skinned reactivation. Thin-skinned deformation forms a nappe stack that consists of supra-salt units only. In contrast, thick-skinned reactivation results in the stacking of crustal nappes, which induces crustal thickening, the creation of orogenic topography, erosion, and exhumation. Combinations of thick- and thin-skinned reactivation are commonly observed in collisional orogens.

The architecture of mature collisional orogens can be described with the Coulomb Wedge Theory, which indicates that rift inheritance plays an increasingly subordinate role as compression progresses (Manatschal et al., 2021).

Large-scale tectonic evolution during the closure of a segmented rift system

The three-dimensional reactivation of segmented rift systems has been little investigated so far, except from the study by Lescoutre and Manatschal (2020) in the Pyrenean system. These authors suggest that, away from the edges of rift segments, the closure of a rift basin follows the two-step evolution described in the previous section, namely (1) thin-skinned reactivation of the exhumed mantle and hyperextended domain; and (2) thick-skinned deformation once the necking zone reaches the subduction zone.

https://doi.org/10.3301/GFT.2023.02

In contrast, at the edges of two overstepping rift segments separated by a block of thicker continental crust (Fig. III.D.4), thick-skinned deformation may affect the exhumed mantle and hyperextended domains already during early stages of convergence due to the formation of shortcutting thrust faults at the V-shaped termination of both rift segments. This may lead to the excellent preservation of pre-Alpine structures and integration of the subcontinental mantle in the orogenic wedge.
This situation may account for the preservation of lower crustal rocks and exhumed mantle domain in Ivrea and in the Grischun (Malenco). Indeed, both used to lie along the transfer zone separating Northern- and Southern Adria, which now corresponds to the Insubric line (Fig. III.D.1g).
This model may also explain the preservation of the Briançonnais domain, which may have been a ribbon of thick continental crust between two rift systems, in a comparable situation as the Basque Massif in Fig. III.D.4

MULTISTAGE OROGENY: THE CASE OF THE ALPINE TETHYS

As described in section 3.3 of the excursion notes, the Alpine orogen is the result of the closure of three (proto-)oceanic rift basins, namely the Meliata-Vardar, the Alpine Tethys, and the East-Mediterranean through three successive and non-coaxial phases of convergence, namely the Eoalpine, Mesoalpine, and Neoalpine orogenic phases (Figs. I.9 and III.D.5). As a consequence, the Alpine nappe stack differs from that of classical orogens described in the previous section.
During the Eoapline phase, the Grischun region was in the footwall of the closing Meliata-Vardar domain located between Northern Adria and the Dacia-Rhodopes microcontinent (Fig. III.D.5a; Schmid et al., 2020). During the final stages of continental collision, the Albula-Zebru movement zone juxtaposed the Ela and Ortler upper Austroalpine nappes against the Campo and Grosina middle Austroalpine nappes and the Bernina, Err, and Platta Lower Austroalpine nappes in the Grischun region (Fig. III.D.5b; Mohn et al., 2011, cum ref.).
Contemporaneously or shortly later, the Alpine Tethys proto-oceanic domain started to be subducted beneath Northern Adria, marking the onset of the Mesoalpine phase. In the Grischun region, deformation was essentially controlled by the Lunghin-Mortirolo movement zone, which juxtaposed the northern Platta, Err, and Bernina nappes over the southern Platta and Sella nappes (Fig. III.D.5b; Mohn et al., 2011).
Following the conclusions from Lescoutre and Manatschal (2020) in the Pyrenees, we suggest that, in the necking and proximal domains, the Lunghin-Mortirolo movement zone continued within the mid-crustal decoupling level (equivalent to the blue dashed line in the bottom right of Fig. III.D.3). At present, the Lunghin-Mortirolo movement zone delimits the low-grade metamorphic nappe stack above (i.e., the northern Platta, Err, and Bernina nappes) from a nappe stack affected by pressure-dominated, upper greenschist- to epidote-amphibolite-facies conditions below (i.e., the southern Platta and Sella nappes). On a smaller scale, the Grischun region was affected by numerous second-order thrust faults. Related folding mostly affected post-rift sediments.
Following the closure of the Alpine Tethys, active subduction has finally initiated in the Eastern Mediterranean. During the resulting Neoalpine phase, the nappe stack of the Adriatic margin was thrust more or less “en bloc” over the Middle- and Lower Penninic units along the Pre-Piemonte Front (Fig. III.D.5a; Haupert, 2015).

https://doi.org/10.3301/GFT.2023.02

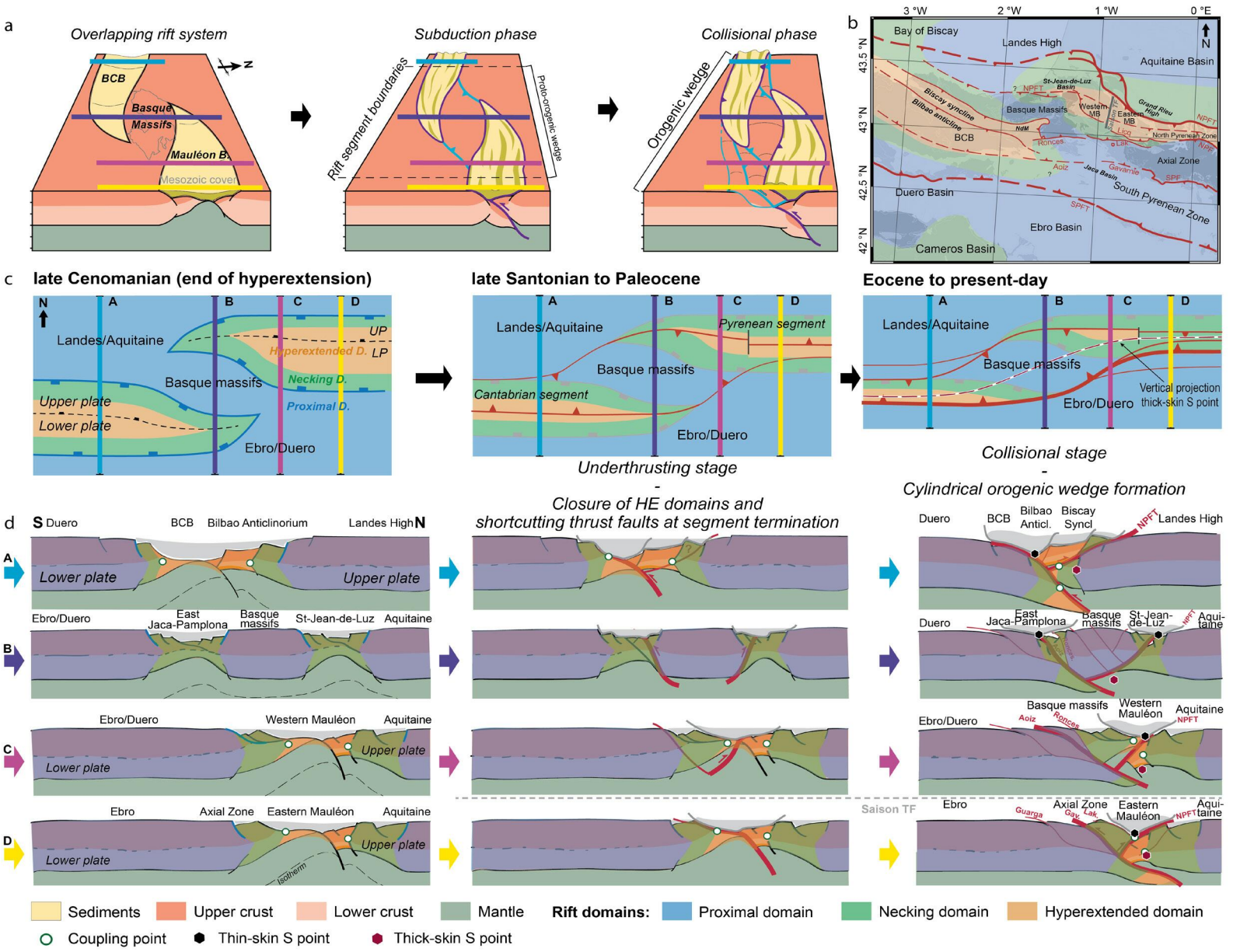

Fig. III.D.4 (modified from Lescoutre and Manatschal, 2020) – a) schematic 3D representation of the reactivation of overstepping, en-échelon rift segments; b) map of the Basque Massifs region displaying the remnants of the proximal (blue), necking (green) and hyperextended (orange) domains; c) paleogeographic reconstruction of the Pyrenean phase of convergence in the Basque Massifs region; d) tectonic restoration of transects A-D shown in panel c. Abbreviations: anticl.: anticlinal; B.: Basin; BCB: Basque-Cantabrian Basin; Gav.: Gavarnie; Lak: Lakora fault; LP: Lower Plate; MB: Mauléon Basin; NdM: Nappe des Marbres; Ronces: Roncesvalles fault NPFT: North Pyrenean Frontal Thrust; NPF: North Pyrenean Fault; SPF: South Pyrenean Fault; ; SPFT: South Pyrenean Frontal Thrust; syncl.: synclinal; TF: Transfer Fault; UP: Upper Plate.

https://doi.org/10.3301/GFT.2023.02

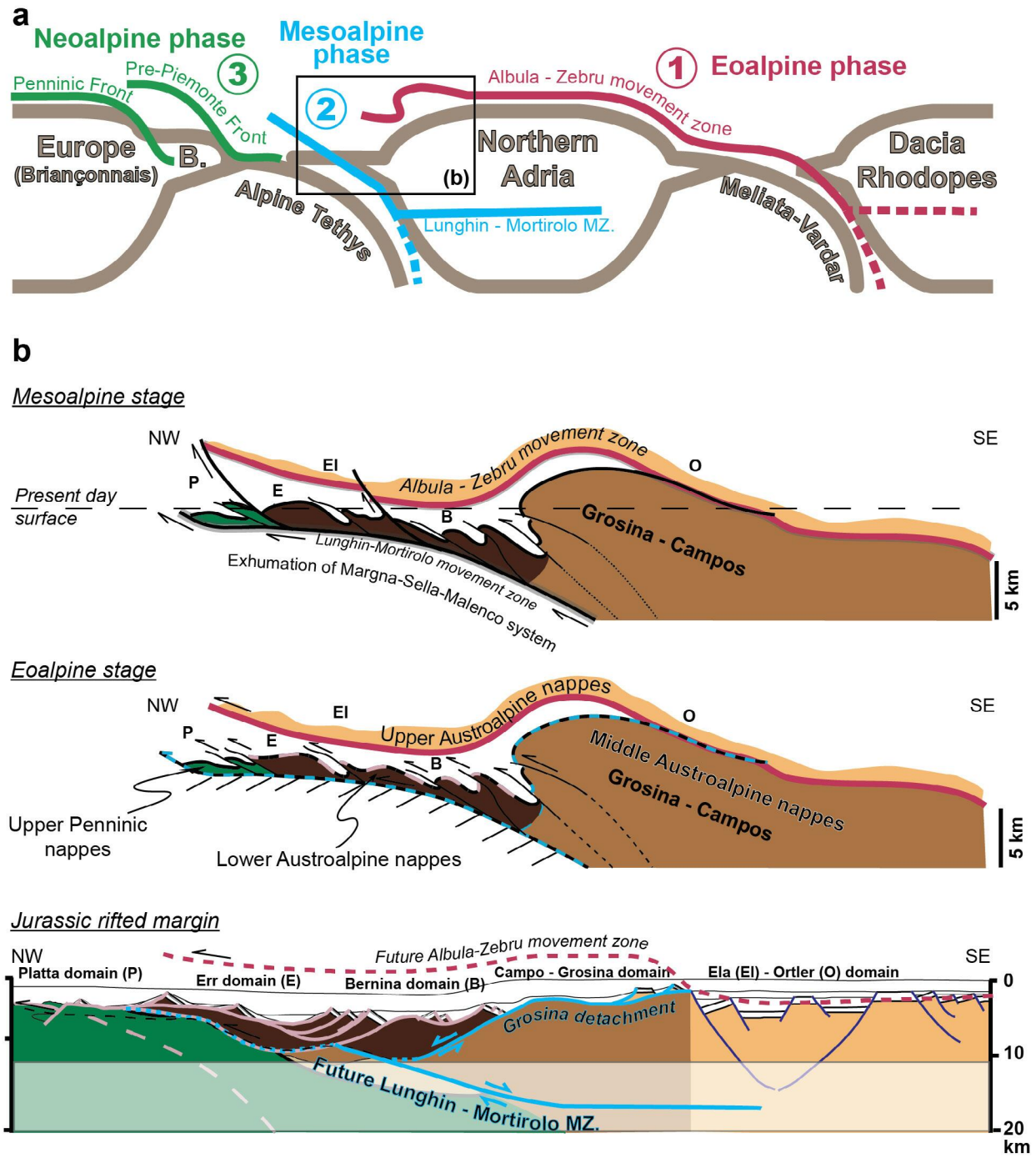

Fig. III.D.5 – a) Simplified crustal cross-section displaying the succession of the Eo-, Meso- and Neoalpine convergence phases during the Alpine orogeny; b) position of the tectonic domains inherited from the Alpine Tethys rifting (bottom panel) during the Eoalpine (middle panel) and Neoalpine (top panel) orogenic phases (from Mohn et al., 2011). Abbreviation: B.: Briançonnais domain; MZ: Movement Zone.

https://doi.org/10.3301/GFT.2023.02

E .INHERITANCE THEMATIC SHEET
The impact of inheritance during rifting and orogeny

INTRODUCTION

All tectonic systems, except maybe oceanic systems, build on inheritance that is controlled by their specific and unique geological history. Recognizing the legacy of previous tectonic events and determining the initial conditions prevailing at the onset of rifting or orogeny is fundamental to understanding and predicting the evolution of geological systems.

DEFINITION

To unravel the role of inheritance during tectonic events, we first need to define what is inheritance and determine which and under what circumstances it may be reactivated. We distinguish between the transient topographic and thermal conditions, which we refer to as interface shape inheritance and persisting inheritance that survives tectonic events.

Transient initial conditions: Interface shape inheritance

In the framework of a Wilson Cycle, a tectonic system evolves through convergent and divergent stages, during which its thermal state and gravitational potential energy are changing (Fig. III.E.1a, b; Manatschal et al., 2021). The gravitational potential energy and thermal state of a geological system can be approximated by the three main interfaces defining the lithosphere, namely the Earth's surface, the Moho, and the base of the lithosphere. Therefore, we name the transient gravitational and thermal state prevailing at the onset of a tectonic event interface shape inheritance.
In the convergent part of a Wilson Cycle, gravitational potential energy increases as a consequence of crustal and lithospheric thickening (slabs, crustal thickening, and orogenic topography), while in the divergent part of the cycle, the gravitational potential energy decreases due to crustal/lithospheric thinning (Fig. III.E.1b). This decrease in gravitational potential energy is associated with an increase in the geothermal gradient, which is linked to the thinning of the lithosphere. Thus, while the surface topography and base of the lithosphere interfaces diverge during the convergent part of a Wilson Cycle, they converge during its divergent part. The only stage at which a tectonic system may reach a gravitational and thermal equilibrium (i.e., all interfaces are approximately sub-horizontal) is the transition between a convergent and a divergent stage when this transition is slow enough. Indeed, it takes at least tens of millions of years to reach a gravitational and thermal equilibrium (Fig. III.E.1a, b).

https://doi.org/10.3301/GFT.2023.02

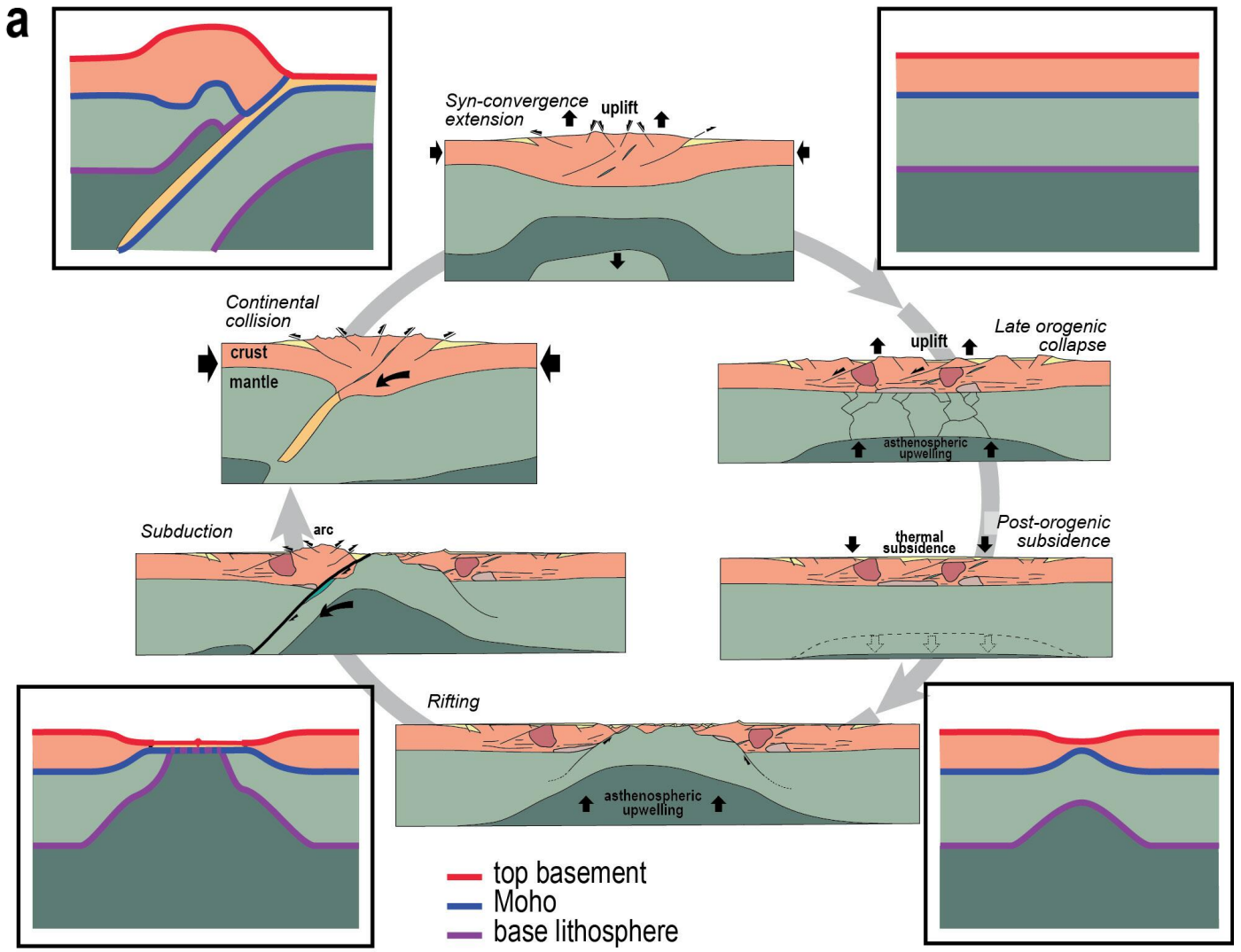

Fig. III.E.1 – a) Main stages of a Wilson Cycle (rifting, seafloor spreading, subduction, and late orogenic state) illustrated by the shapes of the three main interfaces, which are the top basement (red line), the Moho (blue line) and the base of the lithosphere (violet line). Modified from Manatschal et al. (2021) and Petri (2014).

Following the Permian Variscan post-orogenic collapse, surface topography was largely flat, as indicated by the widespread occurrence of Early Triassic fluvial sandstones (Buntsandstein) throughout Western Europe (Ziegler, 1988; Dercourt and Vrielynck, 1993). We can therefore suspect that at the onset of the Alpine Tethys rifting (latest Triassic), the lithosphere was largely thermally equilibrated. At the onset of convergence in the Alpine Tethys realm, the Alpine Tethys hyperextended rift system had reached the stage of mantle exhumation but presumably not the stage of steady-state seafloor spreading (Picazo et al., 2016).

Persisting inheritance

While gravitational and thermal states are transient and tend to equilibrate with time, structural and compositional heterogeneities last in lithospheric rocks (Fig. III.E.2). They may exert a major control on strain localization or distribution during subsequent tectonic events.

Compositional inheritance is often linked to igneous or metamorphic processes, or to hydration reactions. It results in the juxtaposition of rocks with different properties (density, velocity, permeability, radiogenic heat production, etc.), and thus rheologies. Yet the rheological architecture and composition of the lithosphere determine the distribution of weak vs. strong spots, including decoupling levels and dense vs. buoyant materials that are more or less easy to subduct.

https://doi.org/10.3301/GFT.2023.02

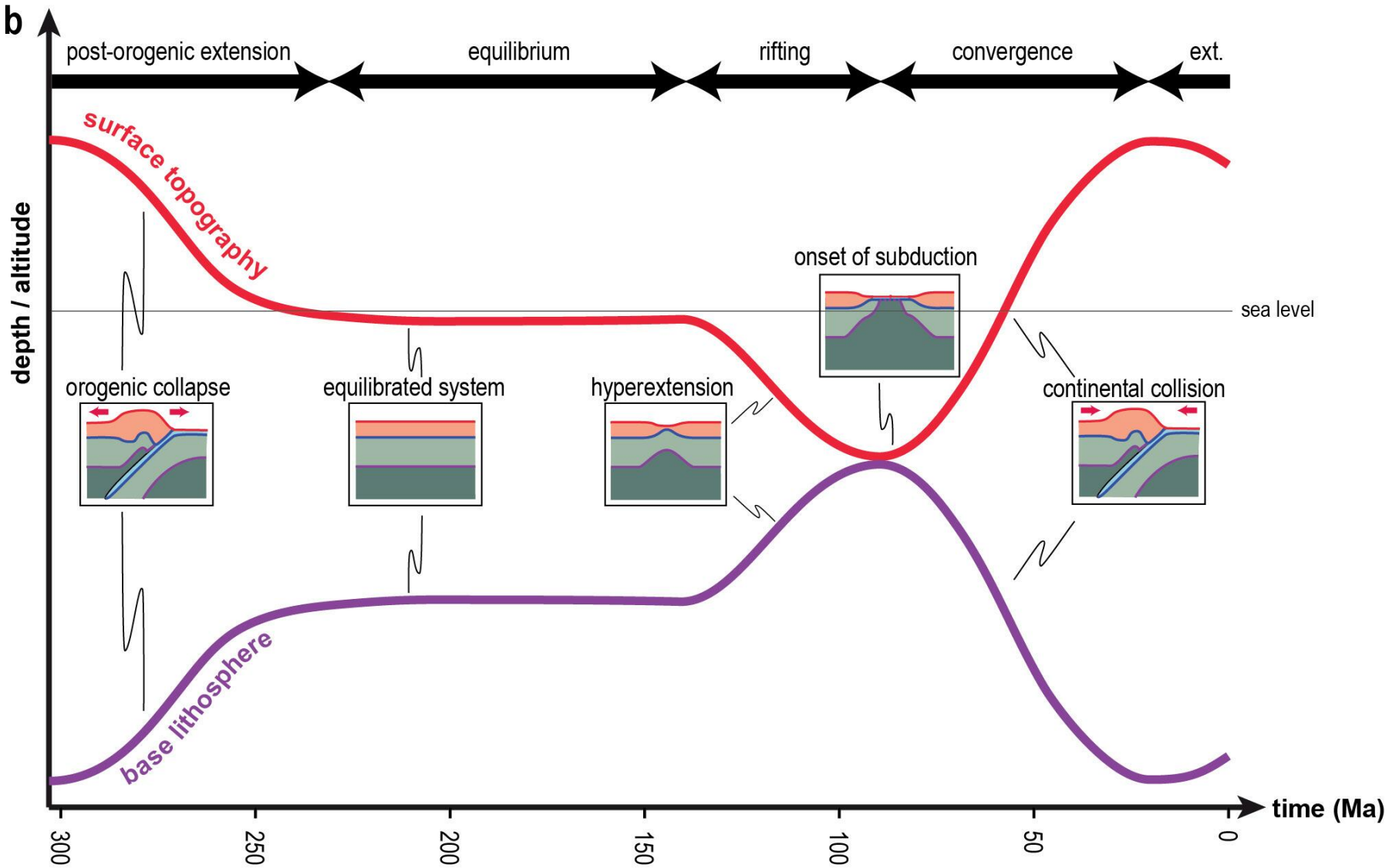

Fig. III.E.1 – b) idealized thermally equilibrated layer-cake lithosphere vs. "real" post-orogenic lithosphere comprising inherited structural and compositional complexities (modified from Manatschal et al., 2015); c) schematic evolution of the thermal state and gravitational potential energy depicted by the base of the lithosphere (1300°C isotherm) and the surface topography within a Wilson Cycle (modified from Manatschal et al., 2021).

https://doi.org/10.3301/GFT.2023.02

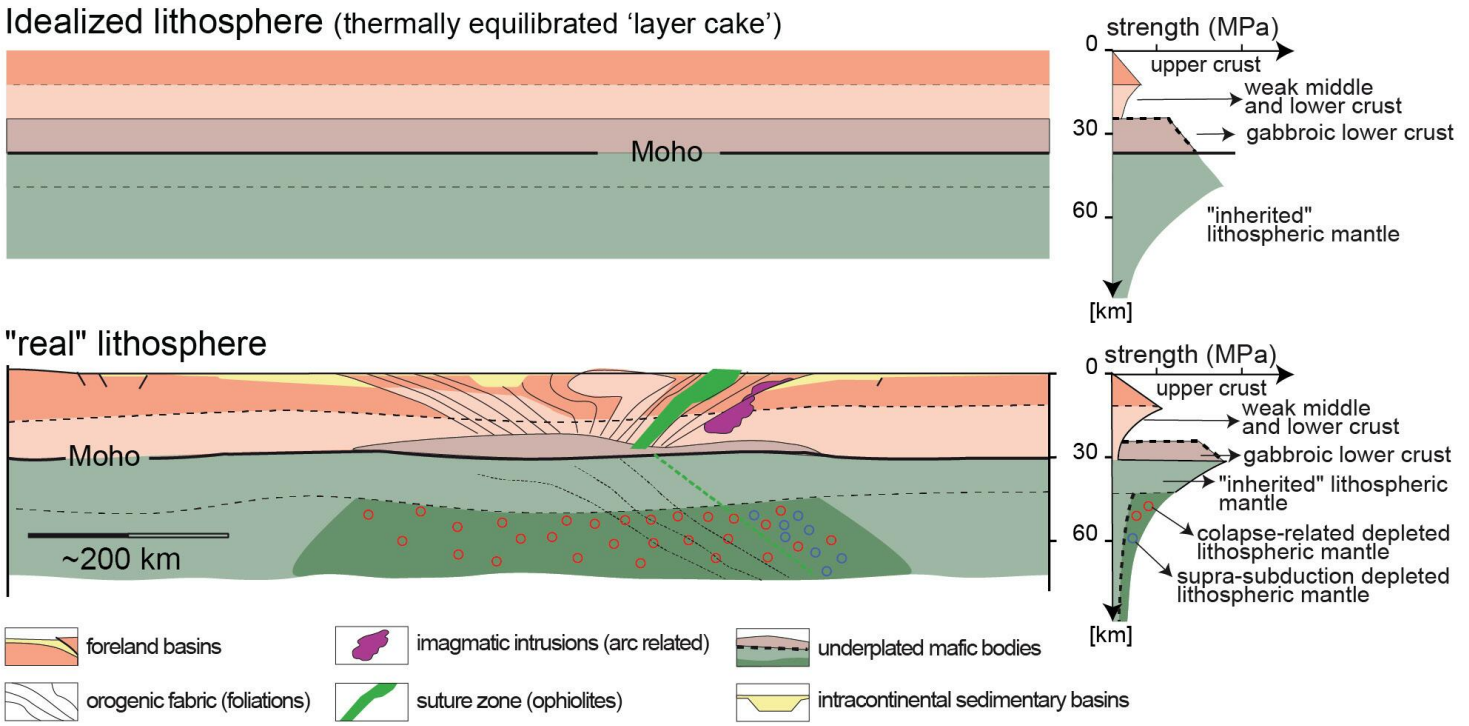

Fig. III.E.2 - Schematic evolution of the thermal state and gravitational potential energy depicted by the base of the lithosphere (1300°C isotherm) and the surface topography within a Wilson Cycle (modified from Manatschal et al., 2021).

Structural inheritance results either from a strong anisotropy linked to crystal-or shaped preferred orientations (e.g., foliation or alignments of grains or aggregates), or from mechanical discontinuities (e.g., faults). They may provide preferential slip-plans when appropriately oriented with respect to the stress direction (e.g., Ring 1994). Examples of systems leaving pervasive persisting inheritance (compositional and structural) in convergent systems are subduction systems with arcs/fore-arcs/back-arcs, and collisional orogens with suture zones, fold-and-thrust belts, and foreland basins (Fig. III.E.2). In divergent systems, igneous processes are often linked to mafic underplating, mantle depletion and/or enrichment, deposition and/or formation of low frictional materials (e.g., salt, clays, or serpentine), and deposition of thick sedimentary sequences. Structural and compositional inheritance cannot always be dissociated, and their efficiency may depend on the background/boundary conditions prevailing in the tectonic system (e.g., stress field, thermal state, pressure, etc.).

Under some circumstances, structural and/or compositional inheritance can be wiped out. Examples are prograde metamorphic events that can change mineralogical compositions (e.g., dehydration, metamorphism, metasomatism) and/or thermally anneal microstructures; Braun et al., 1999; Yamasaki et al., 2006). Processes like slab breakoff can result in efficient lithospheric thinning and induce intense magmatic activity, which strongly depletes the uppermost part of the asthenosphere (e.g., Permian evolution in W-Europe; Petri et al., 2017). Conversely, the percolation of asthenosphere-derived partial melts through overlying depleted subcontinental mantle lithosphere may refertilize it (Müntener et al., 2004, 2010). The composition of the subcontinental mantle lithosphere may exert a strong control on the magmatic budget related to different tectonic events through a Wilson Cycle (Chenin et al., 2018b).

https://doi.org/10.3301/GFT.2023.02

THE IMPACT OF OROGENIC INHERITANCE ON RIFTING

Large-scale/3D perspective

The North Atlantic region is particularly well-suited to analyse the impact of orogenic inheritance on rifting since two distinct orogenic domains with various geological histories, namely the Caledonides to the north and the Variscides to the south (Fig. III.E.3), were both affected by a same episode of rifting during the Mesozoic.

Comparing the distribution of orogenic inheritance and the characteristics of rifting between the southern- and northern part of the North Atlantic highlight major differences in rift architecture, rifting duration, and amount of breakup-related magmatism depending on whether it affected Caledonian or Variscan orogenic lithosphere (Fig. III.E.3; Chenin et al., 2015). Indeed, in the northern North Atlantic, the rift cut through the Caledonian orogenic lithosphere, rifting was protracted (> 80 Ma) and achieved via multiple extension phases, and the breakup was magma rich. In contrast in the southern North Atlantic, the rift circumvented the core of the Variscides of Western Europe, rifting was of relatively short duration (<50 Ma), and 'magma-poor' lithospheric breakup was achieved after one, apparently continuous, episode of extension. These observations support that orogenic inheritance impacts considerably subsequent rifting, and its influence may vary significantly depending on the characteristics of the orogenic lithosphere involved.

A first possible factor controlling the behaviour of the rift may be the thermal state of the lithosphere at the onset of rifting, which depends primarily on the time lag between the last orogenic event and the onset of rifting. In the North Atlantic region, ≥200 Ma elapsed between the end of the Caledonian orogeny and the onset of necking, whereas this time lag was only ≥100 Ma between the termination of the Variscides and the onset of necking in the southern North Atlantic. Yet, as horizontal thermal re-equilibration is usually achieved in less than 100 Ma (Jaupart et al., 2007), it is likely that no significant thermal heterogeneity existed in either of these orogenic lithospheres. This conclusion is consistent with the lack of significant topography in Western Europe and the hypothesis that both the Caledonian and Variscan orogenic systems were in a thermally and gravitationally equilibrated stage by the onset of North Atlantic rifting.

The magma-rich versus magma-poor nature of the post-orogenic collapse is another potential explanation for the difference in rift characteristics between the Caledonian and Variscan lithospheres in Western Europe. Indeed, while the collapse of the Caledonian range was essentially controlled by mechanical processes, the significant magmatic event associated with the collapse of the Variscan range resulted in the rejuvenation of the lower crust by mafic underplating (Rey, 1993; Costa and Rey, 1995). This event probably welded the different crustal blocks together and depleted the underlying mantle. As the Variscan lithosphere was presumably thermally equilibrated by the onset of the North Atlantic rifting (cf. previous paragraph), the mafic lower crust and underlying depleted mantle may have acted as strong regions compared to the encompassing lithosphere, preventing deformation to localize in the former orogenic area (Chenin et al., 2019a).

The magma-rich versus magma-poor nature of the northern- versus southern North Atlantic rifting was presumably controlled by the kinematics of rifting, rather than by the composition of the underlying mantle. Indeed, rifting in both the northern- and southern North Atlantic took place

https://doi.org/10.3301/GFT.2023.02

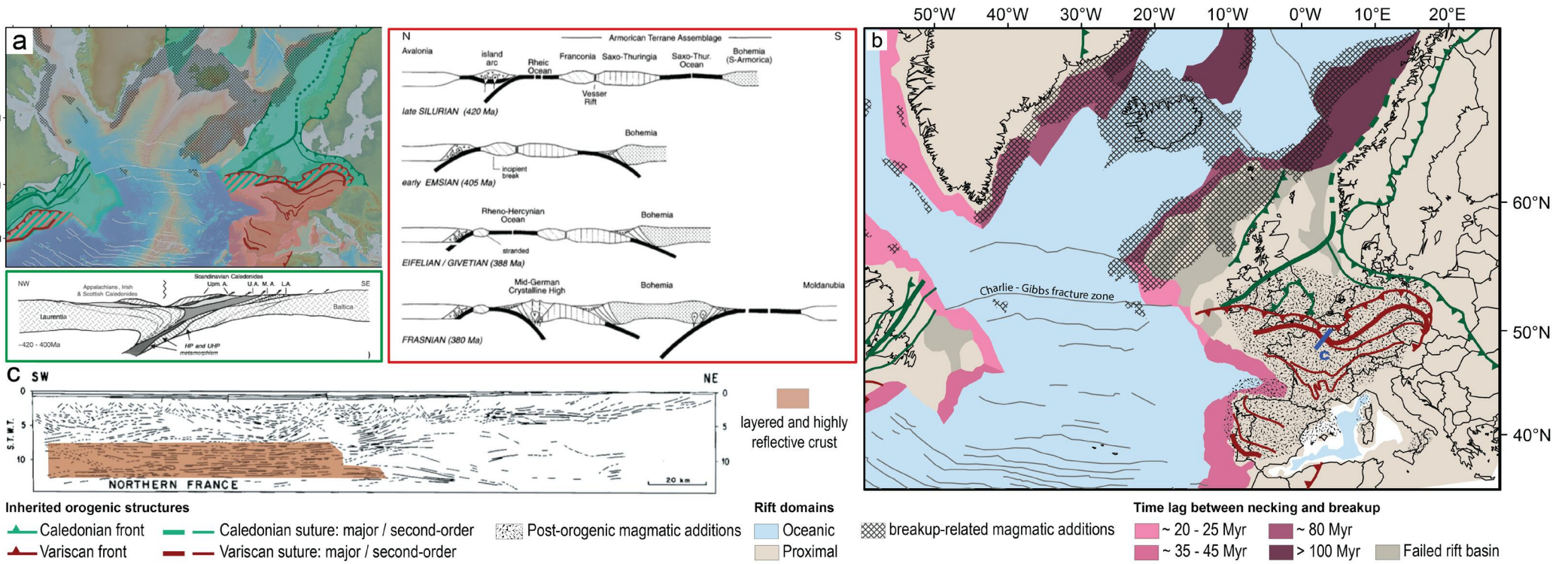

Fig. III.E.3 - a) Extent of the Caledonian (green) and Variscan (red) orogenic lithosphere (from Chenin et al., 2015); The top-right panel illustrates the unique, long-lasting subduction of the Iapetus Ocean at the origin of the Caledonides (from Roberts, 2003); the bottom-right panel illustrates the multiple subductions at the origin of the Variscides (from Franke, 2006); b) map displaying the main Caledonian and Variscan structures, the extent of post-orogenic magmatism, the location of rift domains, the extent of breakup-related magmatism and the duration of rifting in the North Atlantic (from Chenin, 2016); c) interpreted seismic section through the Variscan orogenic area (from Bois et al., 1989; see panel b for location). The brown shading highlights the layered and highly reflective lower crust interpreted as magmatic underplate or granulite-facies metamorphosed rocks.

over a subcontinental lithospheric mantle that was depleted, either due to subduction-related arc-magmatism during the closure of the Iapetus Ocean in the former case, or due to massive magmatism following the post-orogenic collapse of the Variscan range in the latter. Yet rifting in the northern North Atlantic was achieved via successive phases of hyperextension, during which the subcontinental lithospheric mantle was presumably efficiently refertilized as a result of melt impregnation (Müntener et al., 2004, 2010). In contrast, the single phase of the extension during rifting in the southern North Atlantic may not have refertilized the subcontinental mantle enough to generate significant magma at the breakup stage. Another possibility to explain the intense magmatic activity during the late rift stages in the northern North Atlantic is the presence of the Iceland plume. Although the presence of this plume is likely to have influenced the magmatic budget of the northern North Atlantic rifting, the fact that excess magma is observed along the entire length of the Norway-Greenland rifted margins, and not only around Iceland, questions the exclusivity of its contribution.

https://doi.org/10.3301/GFT.2023.02

Regional scale/2D perspective

The evolution of rift systems during extension is controlled by the interaction between extensional stresses, inheritance, rift-induced processes, and external factors (e.g., mantle plume). While inheritance corresponds to pre-existing transient or persisting heterogeneities (cf. section 2), rift-induced features/processes correspond to physical properties/processes acquired during or triggered by rifting. They include physical, chemical, compositional, and/or thermal modifications related to hydration and/or fracturation (e.g., serpentinization, feldspar breakdown) and magmatic activity, all of which impact the bulk rheology of the lithosphere.

In their review, Manatschal et al. (2015) concluded that the role of inheritance is maximal during the early stages of rifting and decreases as rifting progresses (Fig. III.E.4). For instance, in the early stages of rifting, the amount of inherited heat controls largely the mode of deformation (distributed when the geothermal gradient is hot, localized when it is cold, e.g., Buck et al., 1999). Structural and compositional inheritance are largely reactivated on a local scale throughout rifting when properly oriented with respect to the stress field (Ring, 1994).

In the Alps, Lemoine et al. (1986) suggested that most of the Early Jurassic rift structures exposed in the proximal domain may have been seeded either on Variscan orogenic structures or on former Meliata-Vardar rift structures. Recently, Epin and Manatschal (2018) highlighted that the architecture of the Err detachment system in the distal domain was also partially controlled by the presence of a pre-rift Permo-Carboniferous sedimentary basin and pre-rift Triassic salt (see Excursion C).

Conversely to inheritance, rift-induced processes have a minor influence during the early stages of rifting but become dominant during the hyperextension phase (Fig. III.E.4). Indeed, hydration and fracturing processes lead to the breakdown of continental crust feldspar (Manatschal et al., 1999). In the hyperextended domain, the less than 10 km-thick continental crust is entirely brittle, and thus largely hydrated. Nirrengarten et al. (2016) emphasized that most hyperextended rifted margins display a comparable dip angle and suggested that this consistency testifies to the disappearance of inheritance that is specific to each lithosphere. Subcontinental mantle impregnation by asthenosphere-derived partial melts during hyperextension tends also to erase the initial heterogeneity of inherited mantle (Picazo et al., 2016).

Finally, when passive extension gives way to active rifting as a result of adiabatic asthenosphere decompression (Huismans et al., 2001), the location of the final breakup is not controlled by lithospheric inheritance but by the rise of the asthenosphere (Manatschal et al., 2015).

THE IMPACT OF RIFT INHERITANCE ON OROGENY

Since the advent of plate tectonics and the understanding of primary subduction processes, collisional orogens have been usually regarded as the result of the telescoping of continental margins after long-lasting subduction of a wide oceanic domain (Uyeda, 1981; Willett et al., 1993; Ernst, 2005; Handy et al., 2010). Such orogens are characterized by paired metamorphic belts, namely a low-temperature-high-pressure belt corresponding to the accretionary wedge and a high-temperature-low-pressure belt related to arc metamorphism and/or magmatism

https://doi.org/10.3301/GFT.2023.02

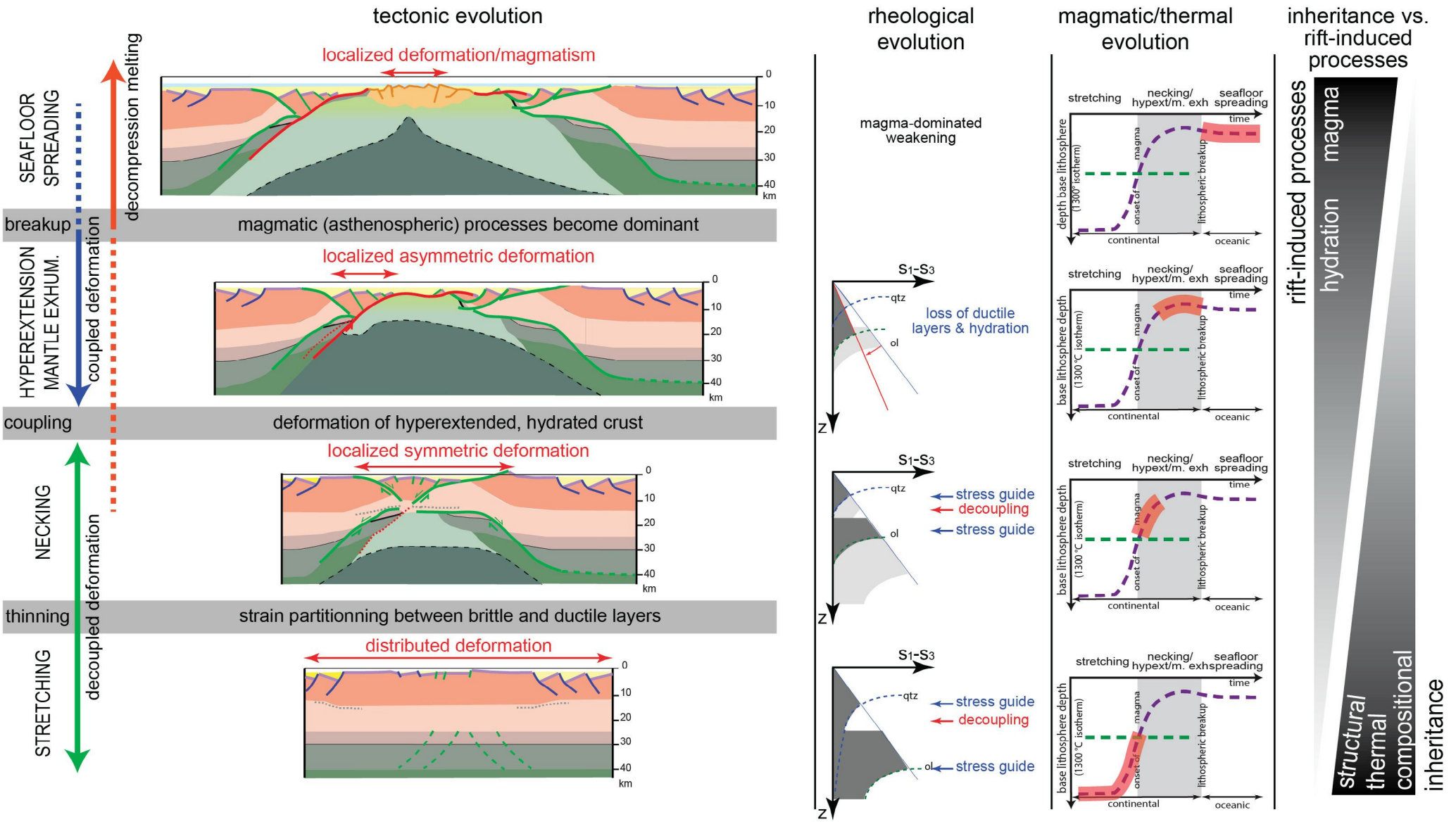

Fig. III.E.4 (modified from Manatschal et al., 2015) - Evolution of the contribution of inheritance vs rift-induced processes during rifting. Abbreviation: EXHUM., exh: exhumation; hypext.: hyperextension; m.: mantle; S1-S3: deviatoric stress; ol: olivine; qtz: quartz; z: depth.

https://doi.org/10.3301/GFT.2023.02

(Miyashiro, 1961; Dewey and Horsfield, 1970; Brown, 2009, cum ref.). However, several collisional orogens such as the Alps and the Pyrenees lack voluminous magmatism contemporaneous to subduction; that is, they are devoid of remnants of arcs, forearcs, and back-arcs and of high-temperature-low-pressure metamorphic assemblages in the upper plate. Yet both orogens result from the closure of relatively narrow (400-600 km for the Alpine Tethys, <200 km for the Pyrenean rift system), hyperextended rift basins (e.g., Pyrenees), or embryonic oceans (Alps; Lemoine et al., 1987; Rosenbaum et al., 2002; Rosenbaum and Lister, 2005; Mohn et al., 2010; McCarthy et al., 2020). This small width may be the main cause of the lack of significant magmatic products.

Narrow/immature hyperextended rift basin versus wide/mature oceanic domains

Chenin et al. (2017) highlighted that extensional systems narrower than 300 km are usually devoid of a mature, self-sustaining spreading system, and thus of normal oceanic crust. As a result, their seafloor is composed of thinned continental crust, exhumed mantle, and/or embryonic oceanic crust underlain by fertile/refertilized mantle (Mantle type 2 of Picazo et al., 2016) resulting from the impregnation by asthenospheric melts during hyperextension (Müntener et al., 2010). Conversely, mature oceanic systems are usually characterized by a homogeneous, Penrose-type oceanic crust underlain by a depleted oceanic mantle (Mantle type 3 of Picazo et al., 2016). As there is statistically no relationship between the size or maturity of a magma-poor hyperextended rift system and the architecture of its margins (Chenin et al., 2017), the main difference between narrow and wide oceans is the existence of a significant amount of oceanic crust and underlying depleted mantle (Figs. III.E.5a and III.E.5b).

The closure of narrow/immature hyperextended rift basin versus wide/mature oceanic domains

During short-lived subduction associated with the closure of narrow oceans, the small length of the slab may not allow for a significant amount of volatiles to reach the critical depth for entering the hot part of the mantle wedge (Rüpke et al., 2004; Grove et al., 2006). Indeed, significant dehydration of the basaltic crust and serpentinized mantle starts from a depth of only 100-200 km (Peacock et al., 1994; Rüpke et al., 2004). Chenin et al. (2017) estimated that the subduction of rift basins narrower than 300 km is unlikely to produce significant magmatic activity. In such circumstances: (1) the subsequent orogeny may be essentially controlled by mechanical processes, in which the structural and lithologic architecture of the intervening margins may be the dominant factor in controlling the architecture of the orogen; and (2) hydration and enrichment of the mantle wedge with subducted fluids and sediments may dominate over partial melting (Peacock et al., 1994), and thus the lithosphere underlying orogens resulting from the closure of narrow oceans is likely to be relatively fertile and hydrated (Fig. III.E.5c). In contrast, protracted subduction associated with the closure of wide oceans develops usually vigorous convection in the mantle wedge that efficiently transports volatiles derived from the dehydration of the slab to great depths (Peacock et al., 1994). The resulting partial melting creates thickened sialic crust at the surface (magmatic arcs), induces high-temperature metamorphism in the encompassing upper plate, and depletes the underlying mantle in fusible elements (Uyeda, 1981). Although vigorous convection within the mantle wedge tends to

https://doi.org/10.3301/GFT.2023.02

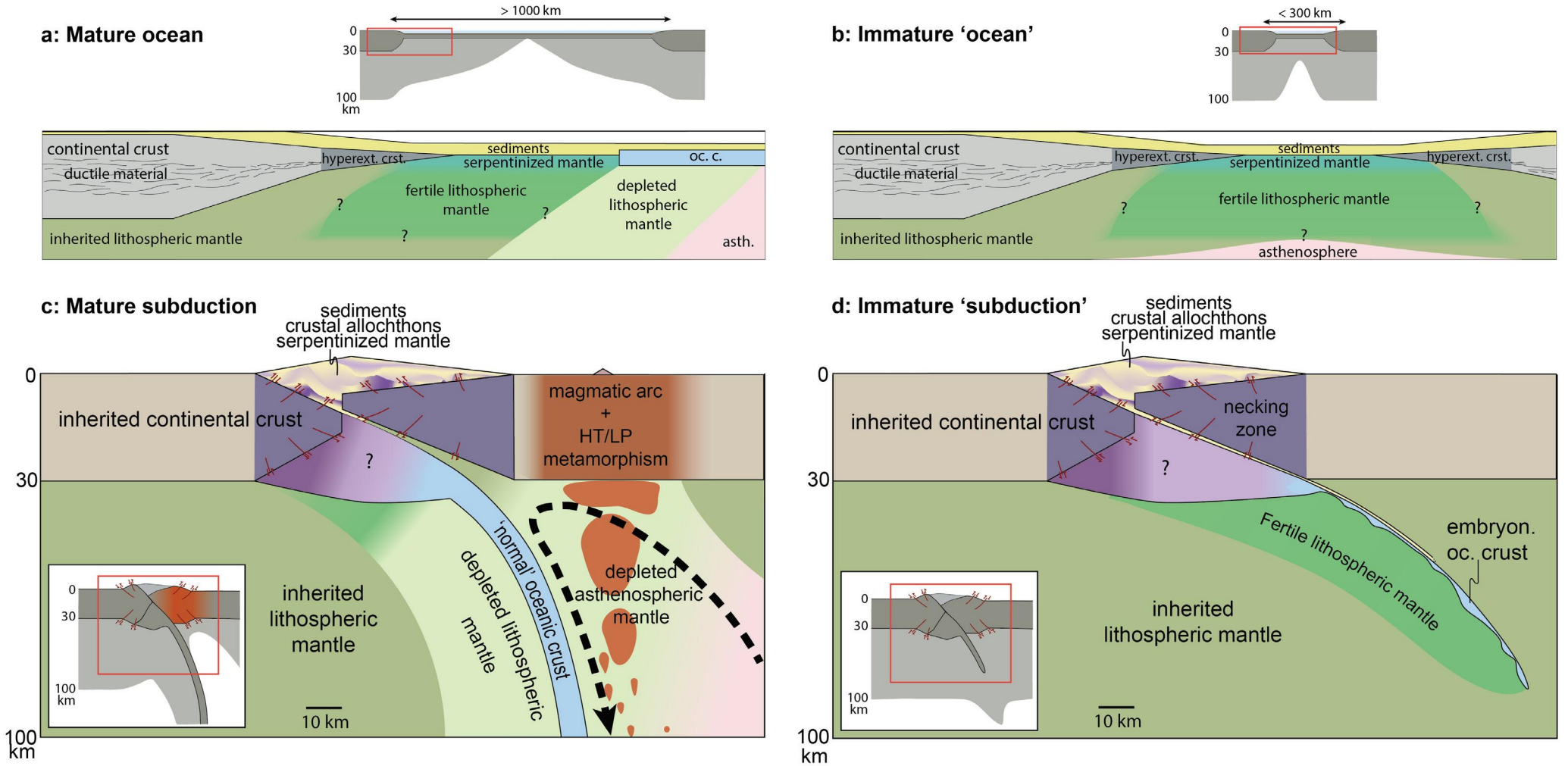

Fig. III.E.5 (from Chenin et al., 2017) – a-b) Primary architecture of a magma-poor rifted margin from (a) a wide/mature ocean and (b) a narrow, immature 'ocean'; c-d) architecture of a subduction system related to the closure of (c) a wide and mature ocean and (d) a narrow and immature ocean. The insets highlight the scale of the zones represented. Abbreviations: Abbreviations: asth.: asthenospheric mantle; hyperext. crst.: hyperextended continental crust; HT/LP: high temperature-low pressure; oc.: oceanic; c.: crust.

homogenize its composition, lower mantle fertility is still to be expected beneath an orogen resulting from the closure of a wide ocean. This assumption is supported by the depleted mantle wedge composition of the Pacific subduction compiled by Woodhead et al. (1993). The thermal and lithological architecture of orogens related to the closure of wide oceans may largely differ from the thermal and lithological architecture of their initial margins, as opposed to orogens consequent upon the closure of narrow oceans (cf. Figs. III.E.5c and III.E.5d).

https://doi.org/10.3301/GFT.2023.02

Impact on Subsequent Collapse or Rifting Magmatic Budget

The difference in mantle composition resulting from the closure of narrow and/or embryonic oceans versus wide oceans may dictate the magmatic budget of subsequent extensional events such as post-orogenic collapse or rifting. Indeed, the depleted mantle beneath orogens related to mature subduction systems may not allow for voluminous magma production, in contrast to the fertile mantle underlying orogens produced by the closure of narrow oceans. This hypothesis may account for both the amagmatic collapse of the Scandinavian Caledonides and the large amount of magmatism during the Variscan post-orogenic collapse.

The Variscides of western Europe result from the closure of several narrow oceans (Franke, 2006; McKerrow et al., 2000a), in addition to the suturing of the wide (Nance and Linnemann, 2008; Torsvik, 1998) Rheic Ocean. Only the closure of the Rheic Ocean presumably formed a significant magmatic arc (Franke, 2006). The post-orogenic collapse of the Variscan topography was followed by a significant magmatic activity, which resulted in widespread, more or less acidic intrusions within the crust, and formed a thick mafic crustal underplating across most of the orogenic area (Bois et al., 1989; Rey, 1993; Costa and Rey, 1995; Schaltegger, 1997; Petri et al., 2017).

In contrast, the Scandinavian Caledonides between Norway and Greenland resulted essentially from the closure of the wide (>2000 km; Van Staal and Barr, 2012) Iapetus Ocean. At this latitude, the two-sided subduction of this ocean formed at least one major volcanic arc, now exposed in Norway (Mac Niocaill et al., 1997; McKerrow et al., 2000b). The Caledonian topography underwent a phase of post-orogenic collapse, which was essentially achieved through mechanical deformation without significant magmatic activity north of the Elbe lineament (McClay et al., 1986; Andersen, 1998; Meissner, 1999; Fossen et al., 2014).

The importance of the magmatic event associated with a post-orogenic collapse has direct consequences on the characteristics of the lithosphere, since it may erase all the structural inheritance in the lower crust, introduce major compositional and thermal heterogeneities in the upper and middle crust, and significantly deplete the underlying mantle (see section 3).

Structural architecture of orogens: 2D and 3D perspectives

The impact of both the 2D/regional-scale and 3D/large-scale architecture of a hyperextended rift system on the structure of the orogen upon its closure is described in section 3 of the previous Tectono-Structural thematic sheet.

https://doi.org/10.3301/GFT.2023.02

F. ISOSTASY THEMATIC SHEET
Possible causes for transient syn-rift uplift and heat pulse at future distal margins

INTRODUCTION

To explain the subsidence and temperature evolutions of sedimentary basins formed in extensional settings, McKenzie (1978) developed a simple but robust model assuming that lithosphere thinning is instantaneous and uniform with depth (Fig. III.F.1a). In this so-called depth-uniform thinning (DUT) model, the extension of a lithosphere generates (black curves in Fig. III.F.1b and c): (1) immediate surface subsidence related to crustal thinning together with (2) instantaneous geothermal gradient increase without any material heating (the lithospheric material is simply advected upward); subsequently, thermal relaxation results in (3) progressive surface subsidence due to lithosphere cooling.
The DUT model has been successfully applied to describe the subsidence and thermal evolutions of rift basins that developed over a crust/lithosphere that underwent little thinning, for instance in the proximal domain of rifted margins where the ratio of initial to final crustal thickness β is less than 1.3 (White and McKenzie, 1989; Hendrie et al., 1993). However, growing evidence suggests that the distal part of rifted margins displays a more complex tectono-thermal evolution during the necking phase of rifting.

TOPOGRAPHIC EVOLUTION OF THE FUTURE DISTAL DOMAIN DURING RIFTING

The Tithonian shallow-water carbonates and clays drilled at ODP Sites 901, 1065 and 1069 offshore Iberia suggest that the distal domain of the Iberian margin remained at shallow water depths during advanced stages of rifting (Mohn et al., 2015). This subsidence evolution is schematically represented as the red curve in Fig. III.F.1b.
In some rift systems, distal domains show an initial phase of rift-related subsidence, which is followed by a phase of erosion and/or emersion, and subsequently a phase of renewed subsidence. For instance, the Briançonnais domain in the fossil distal European margin of the Alpine Tethys (e.g., Claudel and Dumont, 1999; Fig. III.F.1d), the Campos Basin offshore Brazil (Lewis et al., 2014), the South China Sea (e.g., Lin et al., 2003) and the East India margin (Haupert et al., 2016) show such a subsidence-uplift/emersion-subsidence evolution.
The width of the karstified/emerged domain in the Briançonnais can be roughly estimated to a few tens of kilometres based on present-day mapping of the corresponding formation (Fig. III.F.1e). Note however that the width of the karst varies largely along strike and its estimate depends on the assumptions made on the direction of Alpine convergence. The extent of the erosional unconformity is better constrained in the outer hinge of the Campos Basin, where it was mapped over a width of 10-30 km over 120 km along strike (Lewis et al., 2014). The subsidence-uplift/emersion-subsidence evolution recorded by these margins is schematically represented by the blue curve in Fig. III.F.1b.

https://doi.org/10.3301/GFT.2023.02

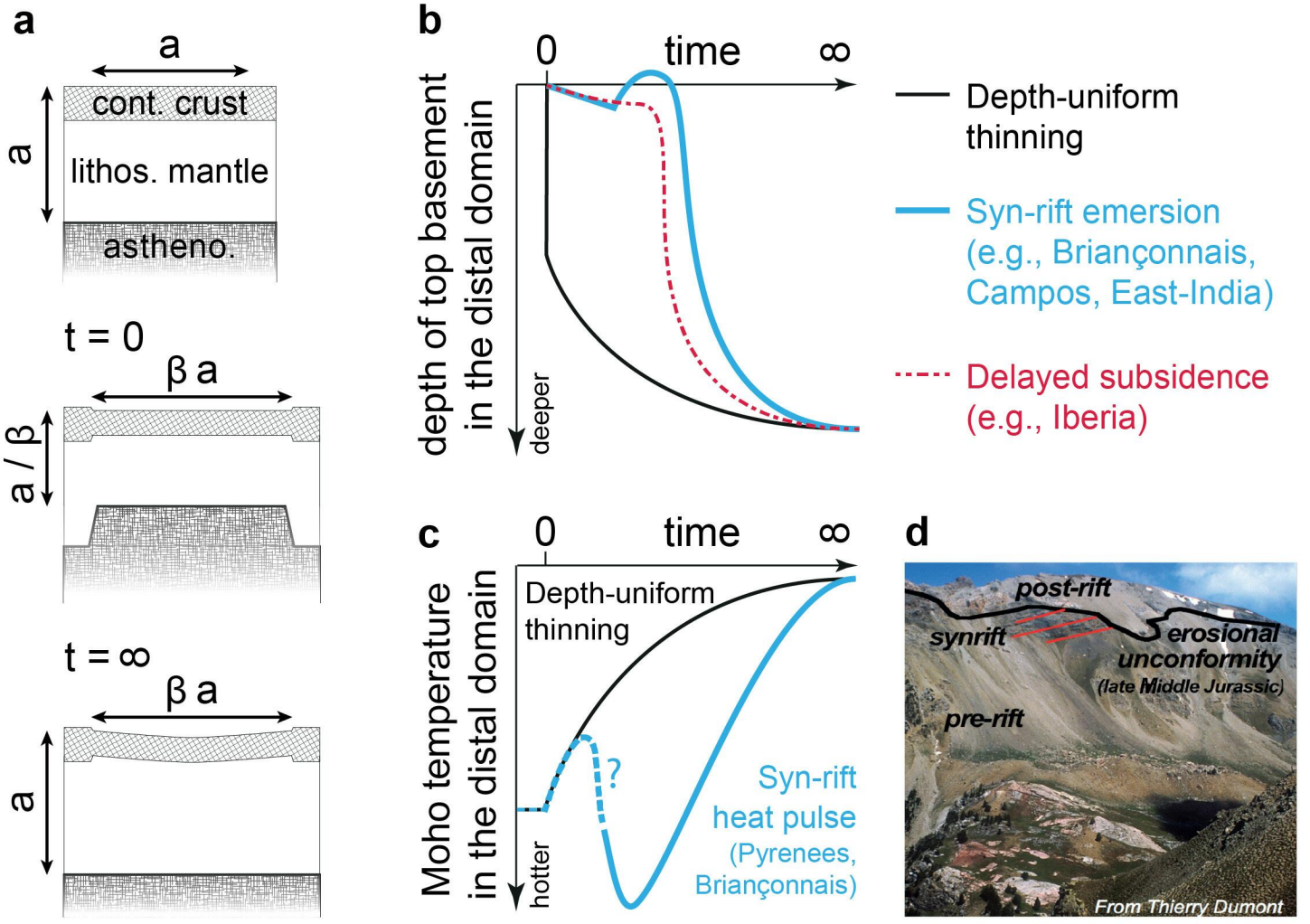

Fig. III.F.1 – a) Illustration of the depth-uniform thinning model of McKenzie (1978); abbreviations: cont.: continental; lithos.: lithospheric; astheno.: asthenospheric mantle; b) schematic graph showing the topographic evolution of the distal part of different types of rift systems (Chenin et al., 2020a); c) schematic graph showing the thermal evolution at the base of the crust in the distal part of different types of rift systems; d) annotated photograph showing the stratigraphic relationships in the Briançonnais unit (Alps of south-eastern France). The Briançonnais unit belonged to the distal European margin of the former Alpine Tethys rift system; e) (left) restored section across the Briançonnais domain showing the major unconformity affecting Permian to Jurassic sediment (modified from De Graciansky et al., 2011); (right) overview of the Briançonnais domain in the Alpine Tethys rift system (modified from Manatschal et al., 2022).

https://doi.org/10.3301/GFT.2023.02

THERMAL EVOLUTION OF THE FUTURE DISTAL DOMAIN DURING RIFTING

The thermal evolution of continental crust during rifting is difficult to assess due to the lack of access to deep crustal levels, especially at present-day rifted margins. Currently, the only clues are thermochronological data from fossil rifted margins exposed in the Alps and Pyrenees. In both cases, data indicate a transient but intense syn-rift heating event at the base of the continental crust (prograde metamorphism), which predates the phase of subcontinental mantle exhumation (Smye and Stockli, 2014; Seymour et al., 2016; Hart et al., 2017).
In the Alps, this thermal event was dated to 200-179 Ma (Beltrando et al., 2015), and thus was largely contemporaneous with the necking phase dated between 189 and 179 Ma by Mohn et al. (2012) and between 191 and 185 Ma by Ribes et al. (2019a). The thermal evolution recorded at the base of the crust in the distal domain of the Alpine and Pyrenean rift systems is schematically represented by the blue curve in Fig. 1c.

POSSIBLE CAUSES FOR NON-MCKENZIE-TYPE BEHAVIOURS

Several processes may account for delayed subsidence, emersion, and/or a heat pulse at the base of the crust during rifting. These include:

- the simple shear-dominated extension (e.g., Wernicke, 1985; Lemoine et al., 1987; Fig. III.F.2b), where one lithospheric-scale shear zone causes a lateral offset in crustal and mantle thinning. This process can account for both uplift and transient crustal heating at the distal upper plate margin of a rift system. However, this model implies highly localized, simple shear deformation across the lithosphere, which is incompatible with the distributed extension generally observed during the early stages of rifting (e.g., Withjack et al., 2012; Ball et al., 2013; Beltrando et al., 2015).

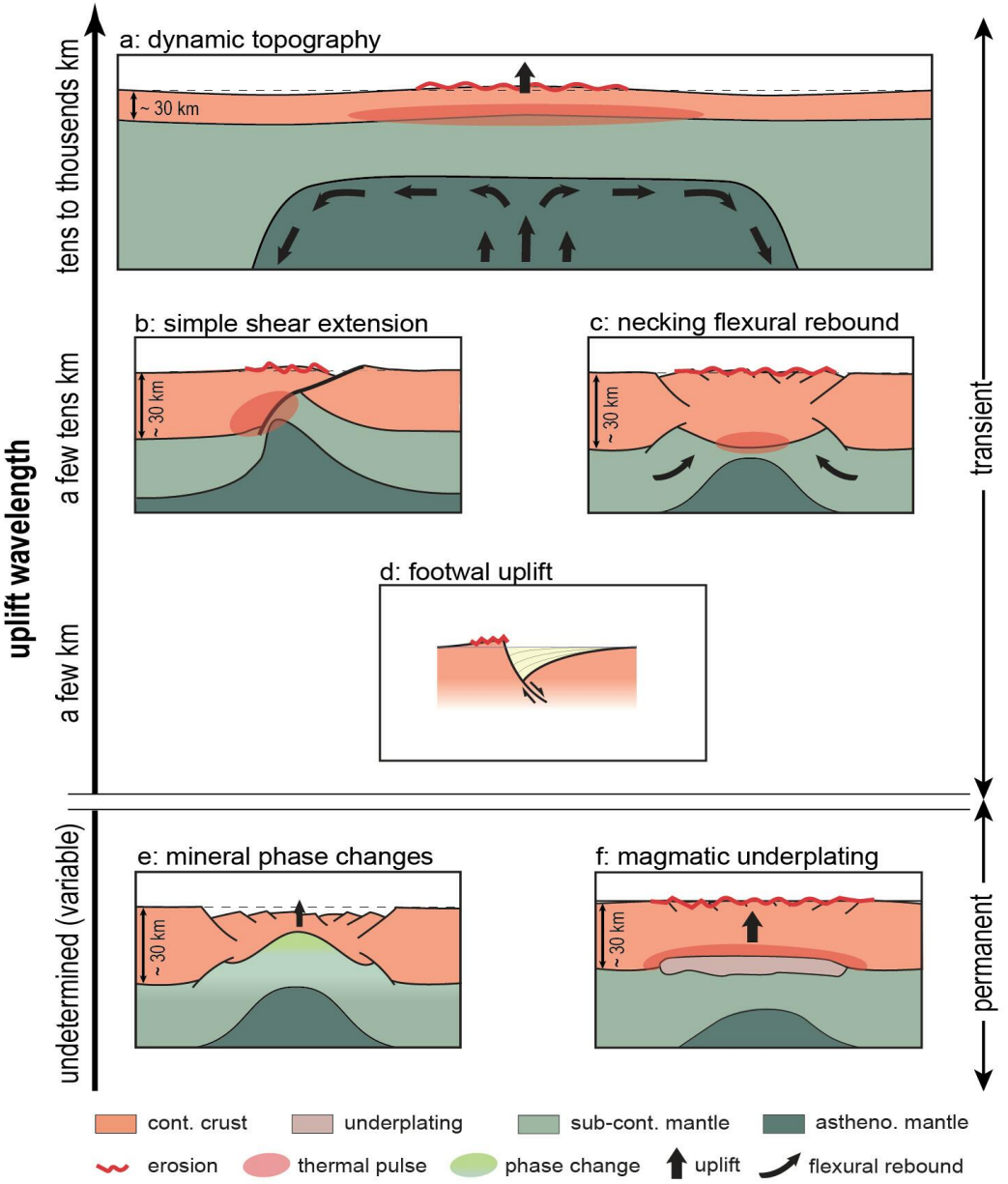

Fig. III.F.2 - Illustration of the different mechanisms that may cause either permanent, or transient uplift and/or a thermal pulse at the base of the crust as a function of their wavelength. Abbreviations: cont.: continental; astheno.: asthenospheric.

https://doi.org/10.3301/GFT.2023.02

- Magmatic underplating (e.g., White and McKenzie, 1989; Fig. III.F.2f), where the addition of hot and low-density material beneath the crust may result in local uplift and heating; This process may explain distal margin uplift but does not account for an only transient and local heating event. Besides, magmatic underplating is accompanied by extensive syn-rift magmatic activity, which is not observed during 'magma-poor' rifting.
- Flexural processes (Braun and Beaumont, 1989; Weissel and Karner, 1989; Kooi et al., 1992; Fig. III.F.2d), where the flexural response to the thinning of a lithosphere with a significant rigidity results in uplift (or subsidence) of parts of the margin. For instance, flexural rift shoulder uplift is important in numerical models with strain softening (e.g., Huismans and Beaumont, 2011; Svartman Dias et al., 2015). However, these uplifts are of short wavelength (ca. 5 km; Fig. III.F.2b) compared to that observed in the distal domain (several tens of kilometres at both the Briançonnais and Outer Campos Hinge; Fig. III.F.1e).
- Dynamic topography (e.g., White and McKenzie, 1989; Xie et al., 2006; Fig. III.F.2a) or removal of the continental mantle lithosphere (i.e., 'delamination') prior to continental breakup (e.g., Esedo et al., 2012), where a mantle plume or replacement of lithospheric mantle by lower density asthenospheric mantle, respectively results in uplift and heating of the lower crust. However, dynamic topography and delamination of the continental lithosphere induce typically a large-scale uplift (several hundred kilometres in diameter, e.g., Campbell, 2005; Esedo et al., 2012) and long-lasting heating event, which are incompatible with the much smaller (few tens of kilometres) region of erosion observed in the future distal domain.
- Mineral phase changes, where the density decrease associated with the transition from garnet- to plagioclase-peridotite at relatively low pressure and high temperature (e.g., Kaus et al., 2005; Simon and Podladchikov, 2008; Fig. III.F.2e) or the increased volume and lower density of serpentinized peridotite with respect to fresh peridotite causes uplift in the most distal part of the rift basin during advanced stages of crustal thinning (Reston et al., 2011). Although both processes can account for up to hundreds of meters of uplift of distal parts of a rift system, they are restricted to advanced stages of crustal thinning (i.e., when the crust is less than 10 km thick), and thus cannot account for uplift during the earlier necking phase of rifting.
- Flexural rebound following depth-dependent lithosphere necking (Chenin et al., 2019b, 2020a; Fig. III.F.2c): When the upper crust and upper mantle are mechanically decoupled by a weak lower crust and, in the absence of any prominent rheological heterogeneity, upper mantle, necking starts first because of the higher deviatoric stresses associated with its larger effective viscosity. Upper mantle necking causes a transient heat pulse at the base of the crust of the future distal margin. At the same time, ductile crustal material flows toward the necked mantle domain, delaying thinning of the overlying crust. Once the necked lithospheric mantle has locally lost most of its strength, the over-deepened Moho moves upward toward an isostatically compensated depth. This flexural rebound causes uplift and emersion of distal parts of the rift system that are composed of still relatively thick crust and triggers the necking of the overlying crust.

In conclusion, the hypothesis that best explains both the syn-rift heat pulse and transient, several tens kilometres wide uplift in the future distal domain of a rift system is the depth-dependent necking of a lithosphere where the upper crust is mechanically decoupled from the upper mantle by a weak lower crust.

https://doi.org/10.3301/GFT.2023.02

LEXICON

Cataclasite
Rock in which the fabric results from the fracture and breaking up of rocks along a fault plane or in a fault zone.

Depleted oceanic mantle
Peridotites made of dominant harzburgites and rare dunites and lherzolites (see Fig. A2b) crosscut by gabbroic bodies and basaltic rocks. Clinopyroxene in oceanic harzburgites are depleted, indicating a ca. 15-20% partial melting of the upper part of the asthenosphere.

Diabase (= **Diorite**)
Dark-coloured igneous rock compositionally equivalent to gabbro and basalt (see Fig. A2a) but texturally between them.

Distal domain
Oceanward part of the margin that is made of significantly thinned crust and, in some cases, of exhumed mantle (see Fig. I.5a).

External Massif
Mountain where crystalline rocks of the European plate crop out. All External Massifs are located North of the Penninic Front. They include, from south to north, the Argentera and Pelvoux massifs, the Belledonne range, the Aiguilles Rouges and Mont Blanc massifs, and the Aar and Gotthard massifs (Fig. I.0a).

Fixism
Theory of geology holding that the continents are fixed in position.

Granulite
Metamorphic rock formed under high temperature and moderate- to high-pressure conditions (see Fig. A4).

Inherited subcontinental mantle
Heterogeneous mantle lying close to the base of the continental crust and recording former partial melting and/or depletion events related to previous tectonic events. Inherited subcontinental mantle is typically comprised of different ultramafic rocks on a sub-meter scale, such as dunite, harzburgite, lherzolite, spinel pyroxenite, garnet pyroxenite and/or phlogopite-hornblende pyroxenite (see Fig. A2b).

https://doi.org/10.3301/GFT.2023.02

In-sequence (faulting)
Progression of deformation where each new fault develops in the hanging wall of the previous fault.

Keystone (in extensional settings; see also H-block in Lavier and Manatschal, 2006)
Block of little deformed material framed by two major high-angle normal faults or shear zones that merge at depth (Crosby and Crosby, 1925).

Mafic
Relating to or denoting a group of dark-coloured, mainly ferromagnesian minerals such as pyroxene and olivine.

Mobilism
Theory of geology holding that the continents are displaced over time, in opposition to fixism.

Mylonite
Rock in which the fabric results from intense ductile shearing of a pre-existing rock.

Nappe
Slab of Earth's surface that has been significantly displaced (i.e., allochthonous) in a horizontal or near horizontal direction through thrust faulting.

Necking
Necking (domain)
Domain of a rifted margin where the crust is thinned from its initial thickness (usually 35±5 km) to a thickness where it becomes fully brittle (usually ca. 10 km). See Fig. I.5a.
Necking (period of time)
Time during which the crust is thinned from its initial thickness (usually 30±5 km) to a thickness where it becomes fully brittle (usually ca. 10 km).

Necking (mechanical process)
Mode of tensile deformation where relatively large amounts of strain localize in a disproportionately small region of the material. The necking domain of rifted margins is thought to be mainly controlled by the viscoplastic necking of the lithosphere (Chenin et al., 2018a).

https://doi.org/10.3301/GFT.2023.02

Ocean-continent transition (OCT)
Domain located between unequivocal continental- and oceanic crusts, indicative of an embryonic seafloor spreading system.

Ophicalcite
Rock made of calcite and ultramafic material. Different origins are possible: hydrothermal or sedimentary (see the Fluids thematic sheet).

Out-of-sequence (faulting)
Backward progression of deformation where new faults develop in the footwall of the previous fault.

Pangea
Large continental landmass ("supercontinent") that encompassed most of the continental lithosphere between the latest Carboniferous (ca. 300 Ma) and latest Triassic (ca. 200 Ma). The present-day continents' configuration results from the breakup of Pangea.

Penrose-type oceanic crust
6-7 km thick layered oceanic crust comprised of, from top down: (i) ca. 1 km of pillow basalts; (ii) 1-2 km of basaltic sheeted dykes; (iii) several km of gabbros. Such mature oceanic crust develops only when the magmatic budget at the mid-ocean ridge is high enough.

Peridotite
Coarse-grained, dark-coloured, ultramafic igneous rock made of at least 40% olivine and comprising frequently a significant proportion of pyroxenes (see Fig. A2b).

Post-orogenic collapse
Loss of height and lateral spread out of mass of an orogen as a consequence of the cessation or overcoming of the tectonic forces at the origin of the orogeny.

Proximal domain
The most continentward part of the margin that is made of little thinned crust and where the top basement and Moho are largely horizontal and parallel (see Fig. I.5a).

https://doi.org/10.3301/GFT.2023.02

Radiolarite
Fine-grained, homogeneous, and relatively hard siliceous sedimentary rock formed mainly from the skeletal remains of radiolarians (i.e., single-celled aquatic animal that has a spherical amoeba-like body with a spiny skeleton of silica). Also: any sedimentary rock formed mainly from radiolarians. Radiolarites are characteristic of deep depositional settings, i.e., below the Carbonate Compensation Depth (CCD).

(Re-)Fertilized subcontinental mantle
Mantle lying close to the base of the continent, oceanward from inherited subcontinental mantle, and recording melt percolation and trapping from asthenosphere-derived partial melts. (Re)Fertilized subcontinental mantle is dominated by plagioclase lherzolites and subordinate harzburgites and dunites with trapped cm-scale gabbroic veins. The proportion of plagioclase mineral is important, with a modal composition locally exceeding 10%.

Unit
Volume of rock recognizable by its distinctive petrographic, lithologic and/or paleontological features.

Variscan orogeny
Late Palaeozoic mountain-building event resulting from the collision between Laurussia (North America + Europe), Gondwana (Africa), and a number of microcontinents (see Kröner and Romer, 2013 for a review).

https://doi.org/10.3301/GFT.2023.02

APPENDIX

A1: GEOLOGICAL TIME SCALE

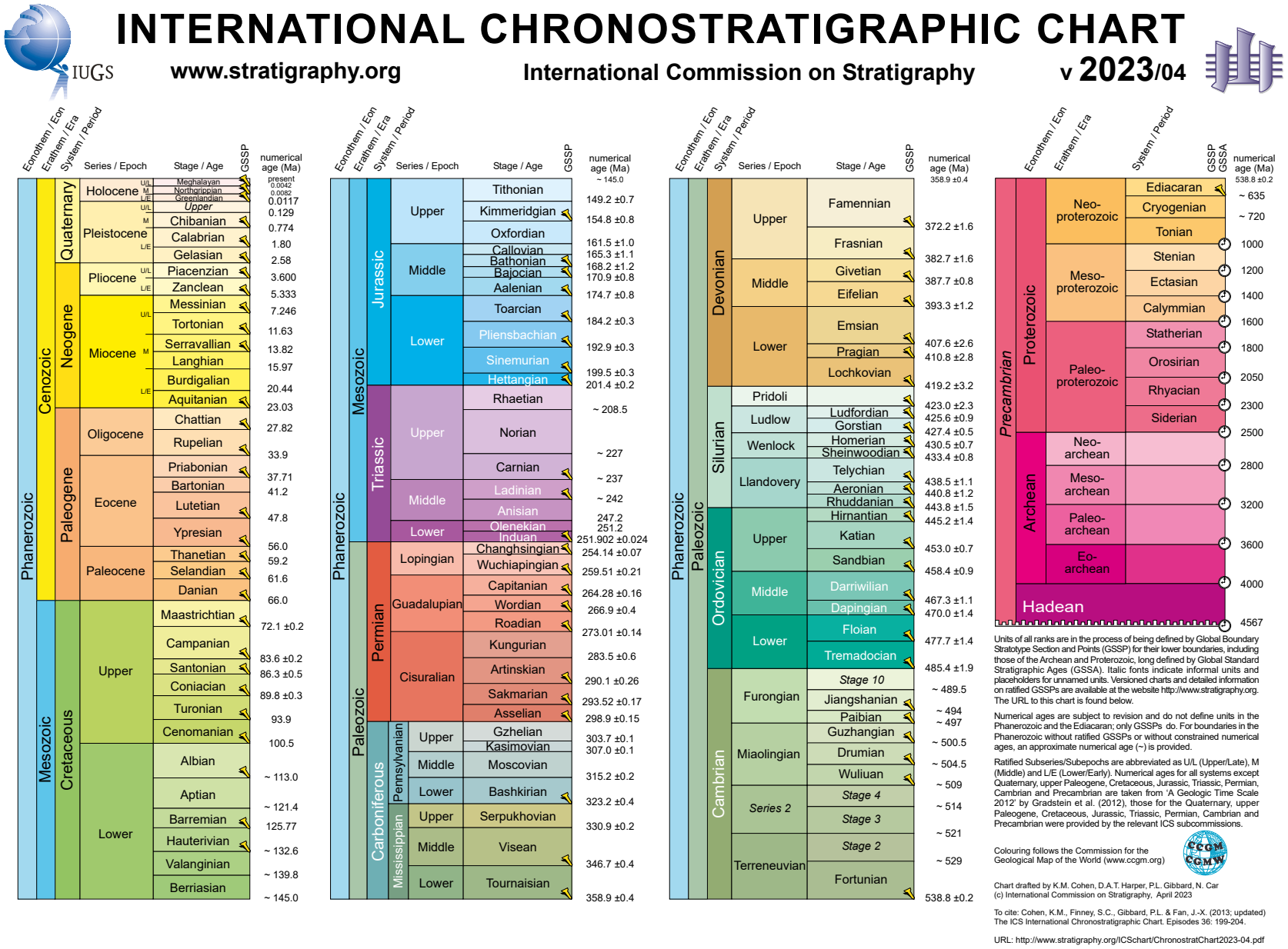

Fig. A1 - Geological time scale used in this field guide (from Cohen et al., 2013).

https://doi.org/10.3301/GFT.2023.02

A2: CLASSIFICATION FOR IGNEOUS AND ULTRAMAFIC ROCKS

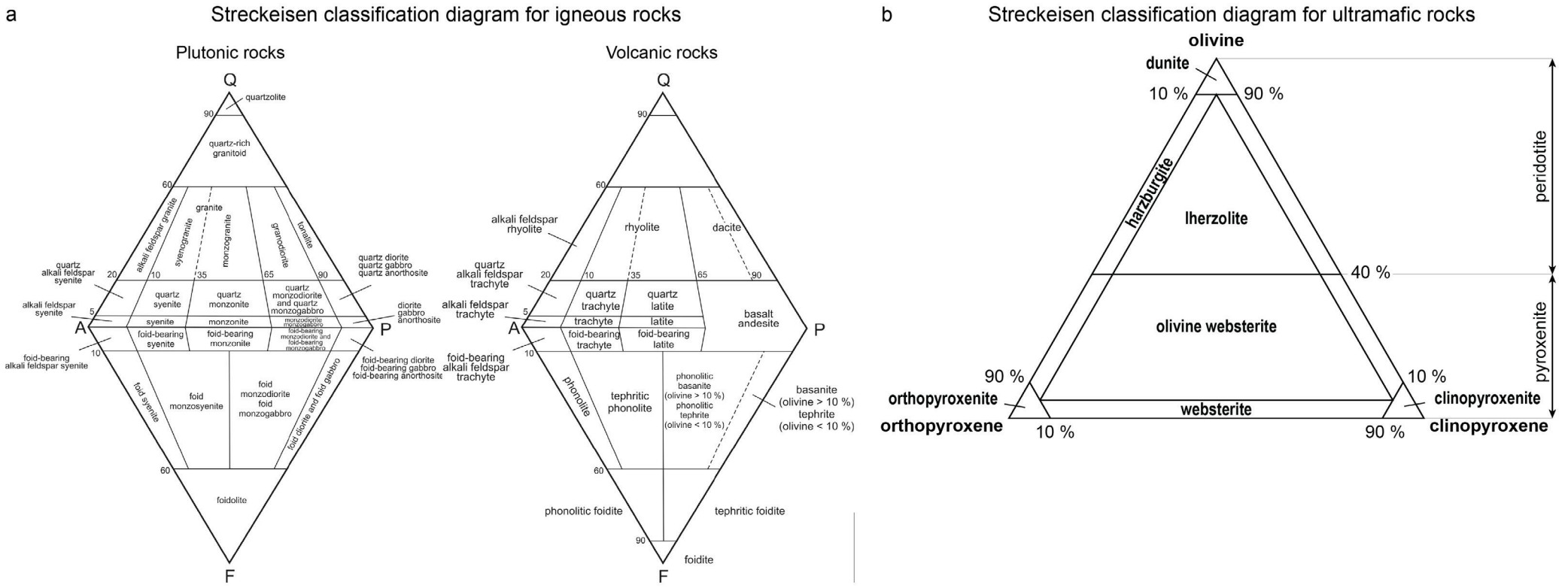

Fig. A2 - Streckeisen (1976) classification diagrams for (a) igneous plutonic (left-hand side) and volcanic (right-hand side) rocks whose mafic minerals modal content is less than 90%. The diagram consists of two ternary diagrams whose poles (100% modal composition) are: Q: Quartz pole; A: Alkali feldspar pole; P: Plagioclase feldspar pole; F: Feldspathoids (i.e., silica poor minerals) pole; b) ultramafic rocks whose mafic minerals modal content is more than 90%. The poles (100% modal composition) of this ternary diagram are olivine, orthopyroxene, and clinopyroxene.

A3: SERPENTINIZATION

Serpentinization reaction (many other reactions are possible):

Olivine (Fo90) + water → Serpentine + Brucite + Magnetite + Dihydrogene

$$3\ Mg_{1.8}Fe_{0.2}SiO_4 + 4.1\ H_2O \rightarrow 1.5\ Mg_3Si_2O_5(OH)_4 + 0.9\ Mg(OH)_2 + 0.2\ Fe_3O_4 + 0.2\ H_2$$

Serpentinization rates are highest at temperatures of 200-300°C and in high-permeability fault zones.

https://doi.org/10.3301/GFT.2023.02

Serpentinization produces:

- heat (ca. 250 J.kg^{-1})
- volume increase, and thus density decrease (from ca. 3.3 g.cm^{-3} for fresh peridotite down to 2.6 g.cm-3 for fully serpentinized peridotite) and seismic velocity decrease (from ca. 8 km.s^{-1} in fresh peridotite down to 5.5 km.s^{-1} in fully serpentinized peridotite)
- increase in natural remanent magnetization (NRM) at high serpentinization degrees
- increase in magnetic susceptibility (K) at high serpentinization degrees

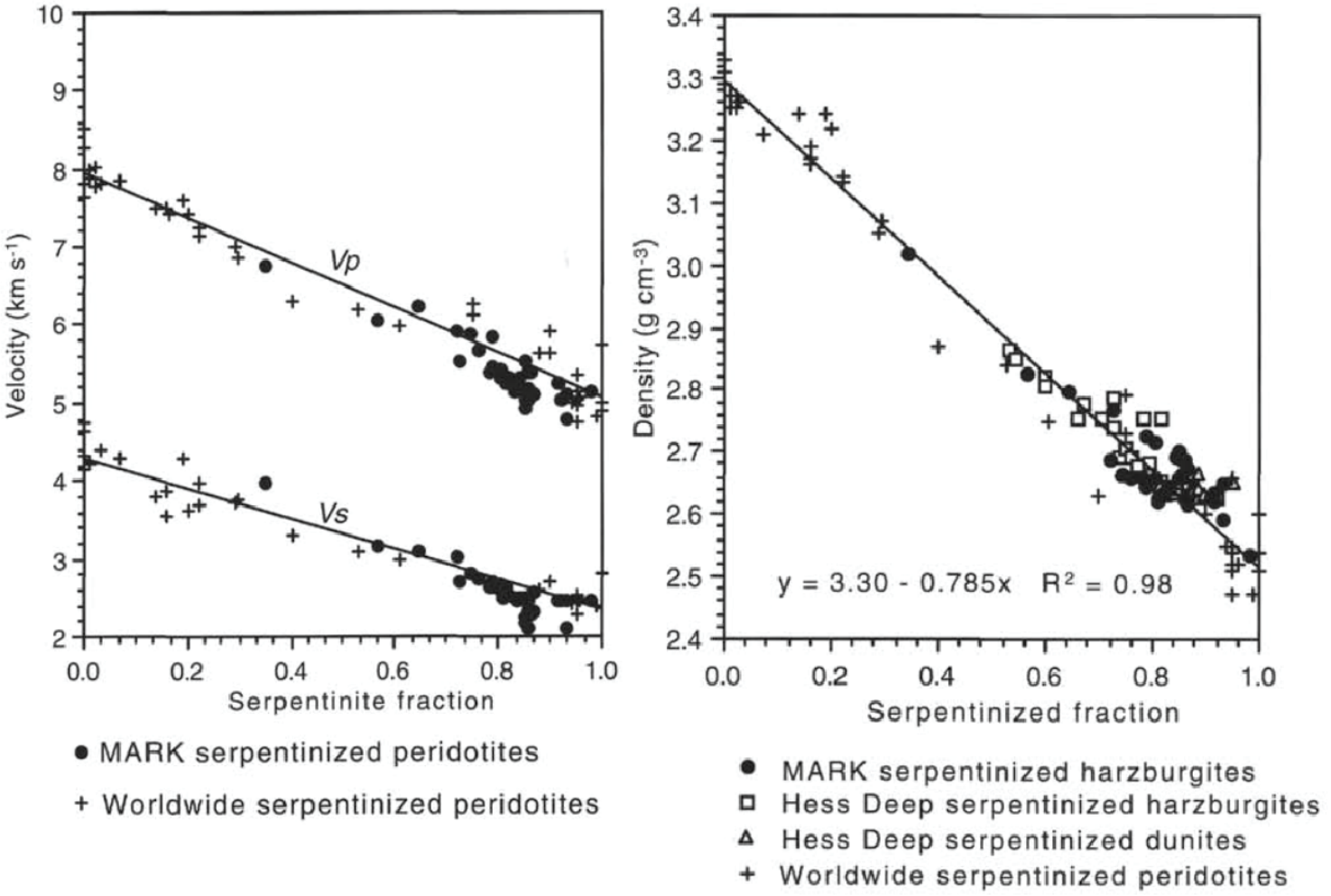

Fig. A3 - Left-hand side) Compressional-wave (Vp) and Shear-wave (Vs) seismic velocity within worldwide serpentinized peridotites relative to their degree of serpentinization; right-hand side) Density of worldwide serpentinized peridotites plotted relative to their degree of serpentinization. Both plots are from Miller and Christensen (1997).

https://doi.org/10.3301/GFT.2023.02

A4: METAMORPHIC FACIES

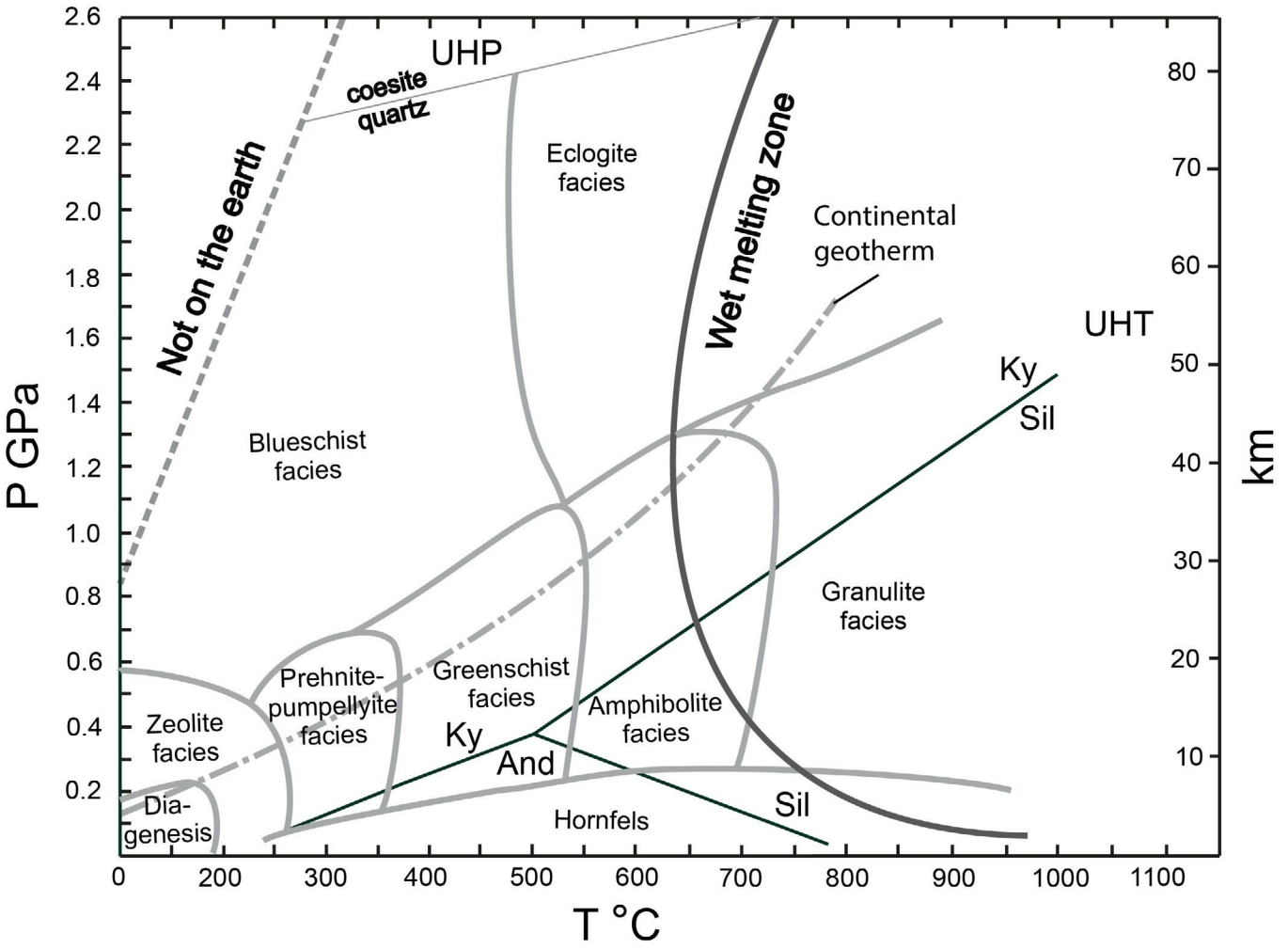

Fig. A4 - Pressure-temperature diagram regarding the metamorphic facies (from Hanžl et al., 2018). Abbreviations: And: andalusite; Ky: kyanite; Sil: sillimanite; UHP: ultra-high pressure; UHT: ultra-high temperature.

https://doi.org/10.3301/GFT.2023.02

REFERENCES

Allemann, F. (1957) - Geologie des Fürstentums Liechtenstein (Südwestlicher Teil) unter besonderer Berücksichtigung des Flyschproblems. Jahrb. der Hist. Vereinigung Lichtensteins 56, 1–244.

Amann M. (2017) - Evolution of magmatism and metasomatism in magma-poor rifted margin during the initiation of the seafloor spreading: Example of the fossil Platta Margin (Swiss Alps) and comparison with the present-day Iberia-Newfoundland Margin. Université de Strasbourg, France.

Amann M., Ulrich M., Manatschal G., Pelt E., Epin M.-E., Autin J., Sauter D. (2020) - Geochemical characteristics of basalts related to incipient oceanization: The example from the Alpine-Tethys OCTs. Terra Nova, 32, 75-88, https://doi.org10.1111/ter.12438.

Ampferer O. (1941) - Gedanken über das Bewegungsbild des atlantischen Raumes. Sitzungsberichten Der Akademie Der Wissenschaften, 150, 19-35. Retrieved from www.biologiezentrum.at.

Anders B., Reischmann T., Kostopoulos D. (2007) - Zircon geochronology of basement rocks from the Pelagonian Zone, Greece: Constraints on the pre-Alpine evolution of the westernmost Internal Hellenides. Int. J. Earth Sci., 96(4), 639-661, https://doi.org10.1007/s00531-006-0121-7.

Andersen T.B. (1998) - Extensional tectonics in the Caledonides of southern Norway, an overview. Tectonophysics, 285(3-4), 333-351, https://doi.org/10.1016/S0040-1951(97)00277-1.

Anonymous (1972) - Penrose field conference on ophiolites. Penrose Field Conference on Ophiolites, 17, 24-25.

Argand E. (1911) - Les nappes de recouvrement des Alpes pennines et leurs prolongements structuraux. In Matière carte géologique de Suisse, 31, 1-26). Francke.

Argand E. (1916) - Sur l'arc des Alpes occidentales. Eclogae Geol. Helv., 14, 145-191.

Argand E. (1924a) - Les Alpes et l'Afrique. Bulletin Société Vaudoise Des Sciences Naturelles, 55, 233-236.

Argand E. (1924b) - La tectonique de l'Asie. 13th International Geological Congress, 171-72.

Bailey T.R., Rosenthal Y., McArthur J.M., van de Schootbrugge B., Thirlwall M.F. (2003) - Paleoceanographic changes of the late Pliensbachian-early Toarcian interval: A possible link to the genesis of an Oceanic Anoxic Event. Earth Planet. Sc. Lett., 212(3-4), 307-320, https://doi.org10.1016/S0012-821X(03)00278-4.

Ball P., Eagles G., Ebinger C., McClay K., Totterdell J. (2013) - The spatial and temporal evolution of strain during the separation of Australia and Antarctica. Geochem. Geophy. Geosy., 14(8), 2771-2799, https://doi.org10.1002/ggge.20160.

Barboza S.A., Bergantz G.W., Brown M. (1999) - Regional granulite facies metamorphism in the Ivrea zone: Is the Mafic Complex the smoking gun or a red herring? Geology, 27(5), 447-450, https://doi.org10.1130/0091-7613(1999)027<0447:rgfmit>2.3.co;2.

Bartolini A., Baumgartner P.O., Hunziker J.C. (1996) - Middle and Late Jurassic carbon stable-isotope stratigraphy and radiolarite sedimentation of the Umbria-Marche Basin (Central Italy). Eclogae Geol. Helv., 89, 811-844.

Baumgartner P.O. (2013) - Mesozoic radiolarites accumulation as a function of sea surface fertility on Tethyan margins and in ocean basins. Sedimentology, 60(1), 292-318, https://doi.org10.1111/sed.12022.

Beltrando M., Manatschal G., Mohn G., Dal Piaz G.V., Vitale Brovarone A., Masini E. (2014) - Recognizing remnants of magma-poor rifted margins in high-pressure orogenic belts: The Alpine case study. Earth-Sci. Rev., 131, 88-115. https://doi.org10.1016/j.earscirev.2014.01.001.

Beltrando M., Stockli D.F., Decarlis A., Manatschal G. (2015) - A crustal-scale view at rift localization along the fossil Adriatic margin of the Alpine Tethys preserved in NW Italy. Tectonics, 34(9), 1927-1951, https://doi.org10.1002/2015TC003973.

Bergh S.G., Eig K., Kløvja O.S., Henningsen T., Olesen O., Hansen J.A. (2007) - The Lofoten-Vesterålen continental margin: A multiphase Mesozoic-Palaeogene rifted shelf as shown by offshore-onshore brittle fault-fracture analysis. Norw. J. Geol., 87, 29-58. Retrieved from https://www.researchgate.net/publication/279887584.

Bernoulli D. (1964) - Zur Geologie des Monte Generoso (Lombardische Alpen): ein Beitrag zur Kenntnis der südalpinen Sedimente. In Beitr. Geol. Karte Schweiz (Vol. 118)

https://doi.org/10.3301/GFT.2023.02

Bernoulli D. and Weissert H. (2021) - Oxygen isotopes in ophicalcites: an ever-lasting controversy? Int. J. Earth Sci., 110(1), 1-8, https://doi.org10.1007/S00531-020-01934-5/FIGURES/5.

Bertotti G. (1991) - Early Mesozoic extension and Alpine shortening in the western Southern Alps: The geology of the area between Lugano and Menaggio (Lombardy, Northern Italy) - Mem. Soc. Geol. Padova, 43, 17-123.

Bertrand M. (1884) - Rapports de structure des Alpes de Glaris et du bassin houiller du Nord. Bulletin de La Société Géologique de France, 3(XII), 318-330.

Betlem P., Mohn G., Tugend J., Manatschal G. (2023) - High-resolution digital outcrop models of fossil rifted margins: 3D imaging of extensional detachment systems. First Break 41, 1–10.

Bill M., O'Dogherty L., Guex J., Baumgartner P.O., Masson H. (2001) - Radiolarite ages in Alpine-Mediterranean ophiolites: Constraints on the oceanic spreading and the Tethys-Atlantic connection. Geol. Soc. Am. Bull., 113(1), 129-143, https://doi.org10.1130/0016-7606(2001)113<0129:raiamo>2.0.co;2.

Boillot G., Grimaud S., Mauffret A., Mougenot D., Kornprobst J., Mergoil-Daniel J., Torrent G. (1980) - Ocean-continent boundary off the Iberian margin: A serpentinite diapir west of the Galicia Bank. Earth Planet. Sci. Lett., 48(1), 23-34, https://doi.org10.1016/0012-821X(80)90166-1.

Boillot G., Recq M., Winterer E.L., Meyer A.W., Applegate J., Baltuck M., Bergen J.A., Comas M.C., Davies T.A., Dunham K., Evans C.A., Girardeau J., Goldberg G., Haggerty, J. Jansa L.F., Johnson J.A., Kasahara J., Loreau J.P., Luna-Sierra E., Moullade M., Ogg J., Sarti M., Thurow J., Williamson M. (1987) - Tectonic denudation of the upper mantle along passive margins: a model based on drilling results (ODP leg 103, western Galicia margin, Spain). Tectonophysics, 132(4), 335-342, https://doi.org10.1016/0040-1951(87)90352-0.

Bois C., Pinet B., Roure F. (1989) - Dating lower crustal features in France and adjacent areas from deep seismic profiles. In Mereu R.F., Mueller S., Fountain D.M. (Eds.), Properties and processes of earth's lower crust. American Geophysical Union, Geophysical Monograph Series, 51, 17-31. https://doi.orgdoi:10.1029/GM051p0017.

Bornemann A., Aschwer U., Mutterlose J. (2003) - The impact of calcareous nannofossils on the pelagic carbonate accumulation across the Jurassic-Cretaceous boundary. Palaeogeogr. Palaeocl., 199(3-4), 187-228, https://doi.org10.1016/S0031-0182(03)00507-8.

Bosellini A. (1973) - Modello geodinamico e paleotettonico delle Alpi Meridionali durante il Giurassico-Cretacico. Sue possibili applicazioni agli Appennini. In Moderne Vedute sulla Geologia dell'Appennino, Accademia nazionale dei Lincei, 163-213.

Bousquet R., Oberhänsli R., Goffe B., Jolivet L., Vidal O. (1998) - High-pressure-low-temperature metamorphism and deformation in the Bündnerschiefer of the Engadine window: implications for the regional evolution of the eastern Central Alps. J. Metamorph. Geol., 16(5), 657-674, https://doi.org10.1111/J.1525-1314.1998.00161.X.

Bracciali L., Pandolfi L., Rocchi S. (2014) - A snapshot of the Late Jurassic Western Tethys seafloor composition and morphology provided by the geochemistry of pelitic sediments (Corsica, Central Alps and Northern Apennines). Basin Res., 26(3), 461-485, https://doi.org10.1111/BRE.12036/CITE/REFWORKS.

Braga R., Giacomini F., Messiga B., Tribuzio R. (2001) - The Sondalo gabbroic complex (Central Alps, Northern Italy): Evidence for emplacement of mantle-derived melts into amphibolite-facies metapelites. Phys. Chem. Earth Pt. A, 26(4-5), 333-342, https://doi.org10.1016/S1464-1895(01)00063-1.

Braga R., Callegari A., Messiga B., Ottolini L., Renna M.R., Tribuzio R. (2003) - Origin of prismatine from the Sondalo granulites (Central Alps, northern Italy). Eur. J. Mineral., 15(2), 393-400, https://doi.org10.1127/0935-1221/2003/0015-0393.

Braun J. and Beaumont C. (1989) - A physical explanation of the relation between flank uplifts and the breakup unconformity at rifted continental margins. Geology, 17(8), 760-764. https://doi.org10.1130/0091-7613(1989)017<0760:APEOTR>2.3.CO.

Braun J., Chéry J., Poliakov A., Mainprice D., Vauchez A., Tomassi A., Daignières M. (1999) - A simple parameterization of strain localization in the ductile regime due to grain size reduction: A case study for olivine. J. Geophys. Res., 104(B11), 25,167-25,181, https://doi.org/10.1029/1999JB900214.

Brown M. (2009) - Metamorphic patterns in orogenic systems and the geological record. Geol. Soc., Spec. Publ., 318(1), 37-74, https://doi.org10.1144/SP318.2.

Brune S., Williams S.E., Butterworth N.P., Müller R.D. (2016) - Abrupt plate accelerations shape rifted continental margins. Nature, 536(7615), 201-204. https://doi.org10.1038/nature18319.

Buck W.R. and Poliakov A. (1998) - Abyssal hills formed by stretching of oceanic lithosphere. Nature, 392, 272-275, https://doi.org/10.1038/32636.

https://doi.org/10.3301/GFT.2023.02

Buck W.R., Lavier L.L., Poliakov A.N.B. (1999) - How to make a rift wide. Philos. T. Roy. Soc. A, 357(1753), 671-693, https://doi.org10.1098/rsta.1999.0348.

Butler R.W.H.H. (2013) - Area balancing as a test of models for the deep structure of mountain belts, with specific reference to the Alps. J. Struct. Geol., 52(1), 2-16, https://doi.org10.1016/j.jsg.2013.03.009.

Cadenas P., Manatschal G., Fernández-Viejo G. (2020) - Unravelling the architecture and evolution of the inverted multi-stage North Iberian-Bay of Biscay rift. Gondwana Res., 88, 67-87, https://doi.org10.1016/j.gr.2020.06.026.

Cadisch J. (1932) - Die Schichtreihe von Ardez (Steinsberg) im Unterengadiner Fenster. Eclogae Geol. Helv., 25(1), 17-22.

Cadisch J., Eugster H., Wenk E., Torricelli G., Burkard G. (1968) - Geologischer Atlas der Schweiz, 1: 25.000. In Erläuterungen zu Blatt Scuol-Schuls-Tarasp, 1-68.

Campbell I.H. (2005) - Large igneous provinces and the mantle plume hypothesis. Elements, 1(5), 265-269, https://doi.org10.2113/gselements.1.5.265.

Cecca F., Martin Garin B., Marchand D., Lathuiliere B., Bartolini A. (2005) - Paleoclimatic control of biogeographic and sedimentary events in Tethyan and peri-Tethyan areas during the Oxfordian (Late Jurassic). Palaeogeogr. Palaeocl., 222(1-2), 10-32, https://doi.org10.1016/j.palaeo.2005.03.009.

Channell J.E.T. and Kozur H.W. (1997) - How many oceans? Meliata, Vardar and Pindos oceans in Mesozoic Alpine paleogeography. Geology, 25(2), 183-186, https://doi.org/10.1130/0091-7613(1997)025<0183:HMOMVA>2.3.CO;2.

Chao P., Manatschal G., Chenin P., Ren J., Zhang C., Pang X., Zheng J., Yang L., Kusznir N.J. (2021) - The tectono-stratigraphic and magmatic evolution of conjugate rifted margins: insights from the NW South China Sea. J. Geodyn., 148, 101877, https://doi.org10.1016/j.jog.2021.101877.

Chenin, P. (2016) - Unravelling the impact of inheritance on the Wilson Cycle: A combined mapping and numerical modelling approach applied to the North Atlantic rift system. Université de Strasbourg.

Chenin P., Manatschal G., Lavier L.L., Erratt D. (2015) - Assessing the impact of orogenic inheritance on the architecture, timing and magmatic budget of the North Atlantic rift system: a mapping approach. J. Geol. Soc. London, 172(6), 711-720, https://doi.org10.1144/jgs2014-139.

Chenin P., Manatschal G., Picazo S., Müntener O., Karner G.D., Johnson C., Ulrich M. (2017) - Influence of the architecture of magma-poor hyperextended rifted margins on orogens produced by the closure of narrow versus wide oceans. Geosphere, 13(2), 559-576, https://doi.org10.1130/GES01363.1.

Chenin P., Schmalholz S.M., Manatschal G., Karner G.D. (2018a) - Necking of the lithosphere: A reappraisal of basic concepts with thermo-mechanical numerical modeling. J. Geophys. Res., 123(6), 5279-5299, https://doi.org10.1029/2017JB014155.

Chenin P., Picazo S., Jammes S., Manatschal G., Müntener O., Karner G. (2018b) - Potential role of lithospheric mantle composition in the Wilson cycle: a North Atlantic perspective. Geol. Soc. Spec. Publ., 470(1), 157-172, https://doi.org10.1144/SP470.10.

Chenin P., Jammes S., Lavier L.L., Manatschal G., Picazo S., Müntener O., Karner G.D., Figueredo P.H., Johnson C. (2019a) - Impact of mafic underplating and mantle depletion on subsequent rifting: a numerical modeling study. Tectonics, 38(7), 2185-2207, https://doi.org10.1029/2018TC005318.

Chenin P., Manatschal G., Decarlis A., Schmalholz S.M., Duretz T., Beltrando M. (2019b) - Emersion of distal domains in advanced stages of continental rifting explained by asynchronous crust and mantle necking. Geochem. Geophy. Geosy., 20(8), 3821-3840, https://doi.org10.1029/2019GC008357.

Chenin P., Schmalholz S.M., Manatschal G., Duretz T. (2020a) - Impact of crust-mantle mechanical coupling on the topographic and thermal evolutions during the necking phase of 'magma-poor' and 'sediment-starved' rift systems: A numerical modeling study. Tectonophysics, 786, 228472, https://doi.org10.1016/j.tecto.2020.228472.

Chenin, P., Boesch, Q., Manatschal, G., Tomasi, S. (2020b) - Enseigner les marges passives : un aperçu des innovations scientifiques des deux dernières décennies. Géochronique hors-série 1, 6–22.

Chenin P., Manatschal G., Ghienne J.-F., Chao P. (2022) - The syn-rift tectono-stratigraphic record of rifted margins (Part II): breaking through the proximal/distal interpretation frontier. Basin Res., 34(2), 489-532, https://doi.org10.1111/bre.12628.

Chessex R. (1958) - La géologie de la haute vallée d'Abondance, Haute-Savoie (France). Unpublished Ph.d. thesis, Université de Lausanne.

Chester F.M. and Logan J.M. (1986) - Implications for mechanical properties of brittle faults from observations of the Punchbowl fault zone, California. Pure Appl. Geophysics, 124(1-2), 79-106, https://doi.org10.1007/BF00875720.

https://doi.org/10.3301/GFT.2023.02

Chevalier F., Guiraud M., Garcia J.-P., Dommergues J.-L., Quesne D., Allemand P., Dumont T. (2003) - Calculating the long-term displacement rates of a normal fault from the high-resolution stratigraphic record (early Tethyan rifting, French Alps). Terra Nova, 15(6), 410-416, https://doi.org10.1046/J.1365-3121.2003.00508.X.

Chiari M., Stefano P., Parisi G. (2008) - New stratigraphical data on the Middle-Late Jurassic biosiliceous sediments from the Sicanian basin, Western Sicily (Italy). Swiss J. Geosci., 101(2), 415-429, https://doi.org10.1007/s00015-008-1276-y.

Claudel M.E. and Dumont T. (1999) - A record of multistage continental break-up on the Briançonnais marginal plateau (Western Alps): Early and Middle-Late Jurassic rifting. Eclogae Geol. Helv., 92(1), 45-61.

Clift P. and Vannucchi P. (2004) - Controls on tectonic accretion versus erosion in subduction zones: Implications for the origin and recycling of the continental crust. Rev. Geophys., 42(2), RG2001, https://doi.org10.1029/2003RG000127.

Cobbold P.R. and Quinquis H. (1980) - Development of sheath folds in shear regimes. J. Struct. Geol., 2(1-2), 119-126, https://doi.org10.1016/0191-8141(80)90041-3.

Cohen K.M., Finney S.C., Gibbard P.L., Fan J.-X. (2013) - The ICS International Chronostratigraphic Chart. Episodes, 36(3), 199-204, https://doi.org/10.18814/epiiugs/2013/v36i3/002.

Coleman R.G. (1977) - Ophiolites. Springer-Verlag Berlin, Heidelberg, New York, Heidelberg.

Collettini C. (2011) - The mechanical paradox of low-angle normal faults: Current understanding and open questions. Tectonophysics, 510(3-4), 253-268, https://doi.org10.1016/j.tecto.2011.07.015.

Coltat R. (2020) - Interactions fluides-roches-déformation durant l'exhumation mantellique dans les marges hyper-étendues, la nappe de Platta, Alpes suisses. Unpublished Ph.d. Thesis, Université Rennes.

Coltat R., Boulvais P., Branquet Y., Collot J., Epin M.E., Manatschal G. (2019a) - Syntectonic carbonation during synmagmatic mantle exhumation at an ocean-continent transition. Geology, 47(2), 183-186, https://doi.org10.1130/G45530.1.

Coltat R., Branquet Y., Gautier P., Campos Rodriguez H., Poujol M., Pelleter E., McClenaghan S., Manatschal G., Boulvais P. (2019b) - Unravelling the root zone of ultramafic-hosted black smokers-like hydrothermalism from an Alpine analog. Terra Nova, 31(6), 549-561, https://doi.org10.1111/ter.12427.

Coltat R., Branquet Y., Gautier P., Boulvais P., Manatschal G. (2020) - The nature of the interface between basalts and serpentinized mantle in oceanic domains: Insights from a geological section in the Alps. Tectonophysics, 797, 228646, https://doi.org10.1016/J.TECTO.2020.228646.

Coltat R., Boulvais P., Branquet Y., Poujol M., Gautier P., Manatschal G. (2021) - Discussion to "Oxygen isotope in ophicalcites: an ever-lasting controversy?" Int. J. Earth Sci., 110(3), 1117-1121, https://doi.org10.1007/s00531-021-01983-4.

Condie, K.C. (1993) - Chemical composition and evolution of the upper continental crust: Contrasting results from surface samples and shales. Chem. Geol. 104, 1–37. https://doi.org/10.1016/0009-2541(93)90140-E

Conti P. (1997) - The austroalpine Ortler nappe and the tectonic evolution of the Engadine Dolomites (Switzerland-Italy), Memorie Descrittive della Carta Geologica d'Italia, 53, 102 pp.

Conti P., Manatschal G., Pfister M. (1994) - Synrift sedimentation, Jurassic and Alpine tectonics in the central Ortler nappe (Eastern Alps, Italy). Eclogae Geol. Helv., 87(1), 63-90.

Costa S. and Rey P. (1995) - Lower crustal rejuvenation and growth during post-thickening collapse: Insights from a crustal cross section through a Variscan metamorphic core complex. Geology, 23 (10), 905–908, https://doi.org/10.1130/0091-7613(1995)023<0905:LCRAGD>2.3.CO;2.

Crosby W.O. and Crosby I.B. (1925) - Keystone faults. Bull. Geol. Soc. Am., 36, 623-640, https://doi.org10.1130/GSAB-36-623.

De Graciansky P.C., Roberts D.G., Tricart P. (2011) - The Western Alps, from rift to passive margin to orogenic belt: an integrated geoscience overview. Developments in Earth Surface Processes, Elsevier, 391pp. Retrieved from https://books.google.com/books?hl=fr&lr=&id=_unD4aRUfl4C&pgis=1.

de Saussure H.B. (1779) - Voyages dans les Alpes, précédés d'un essai sur l'histoire naturelle des environs de Genève. Fauche C.S. (Ed.), Neuchâtel, Vol.1, 540 pp.

Decandia F.A. and Elter P. (1969) - Riflessioni sul problema delle ofioliti nell'Appennino settentrionale (nota preliminare). Atti della Società Toscana di Scienze Naturali, Memorie, Serie A, 76, 1-9.

https://doi.org/10.3301/GFT.2023.02

Decandia F.A. and Elter P. (1972) - La "zona" ofiolitifera del Bracco nel settore compreso fra Levento e la Val Graveglia (Appenino ligure). Memorie della Società Geologica Italiana, 11, 503-530.

Decarlis A., Manatschal G., Haupert I., Masini E. (2015) - The tectono-stratigraphic evolution of distal, hyper-extended magma-poor conjugate rifted margins: Examples from the Alpine Tethys and Newfoundland-Iberia. Mar. Petrol. Geol., 68, 54-72, https://doi.org10.1016/j.marpetgeo.2015.08.005.

Decarlis A., Fellin M.G., Maino M., Ferrando S., Manatschal G., Gaggero L., Seno S., Stuart F.M., Beltrando M. (2017a) - Tectono-thermal evolution of a distal rifted margin: constraints from the Calizzano Massif (Prepiedmont-Briançonnais Domain, Ligurian Alps). Tectonics, 36(12), 3209-3228, https://doi.org10.1002/2017TC004634.

Decarlis A., Beltrando M., Manatschal G., Ferrando S., Carosi R. (2017b) - Architecture of the distal Piedmont-Ligurian rifted margin in NW Italy: Hints for a flip of the rift system polarity. Tectonics, 36(11), 2388-2406, https://doi.org10.1002/2017TC004561.

Dercourt J. and Vrielynck B. (1993) - Atlas Tethys paleoenvironmental maps. Gauthier-Villars.

Dercourt J., Zonenshain L.P., Ricou L.E., Kazmin V.G., Le Pichon X., Knipper A.L., Grandjacquet C., Sbortshikov I.M., Geyssant J., Lepvrier C., Pechersky D.H., Boulin J. Sibuet J.C., Savostin L.A., Sorokhtin O., Westphal M., Bazhenov M.L., Lauer J.P., Biju-Duval B. (1986) - Geological evolution of the tethys belt from the Atlantic to the Pamirs since the Lias. Tectonophysics, 123(1-4), 241-315, https://doi.org10.1016/0040-1951(86)90199-X.

Desmurs L. (2001) - Mantle evolution and magmatism in an evolving ocean-continent transition: The Platta nappe, eastern Switzerland. Unpublished Ph.d. Thesis, ETH Zürich.

Desmurs L., Manatschal G., Bernoulli D. (2001) - The Steinmann Trinity revisited: Mantle exhumation and magmatism along an ocean-continent transition: The Platta Nappe, Eastern Switzerland. Geol. Soc. Spec. Publ., 187(1), 235-266, https://doi.org10.1144/GSL.SP.2001.187.01.12.

Desmurs L., Müntener O., Manatschal G. (2002) - Onset of magmatic accretion within a magma-poor rifted margin: a case study from the Platta ocean-continent transition, eastern Switzerland. Contrib. Mineral. Petr., 144(3), 365-382, https://doi.org10.1007/s00410-002-0403-4.

Dewey J.F. and Horsfield B. (1970) - Plate tectonics, orogeny and continental growth. Nature, 225, 521-525, https://doi.org10.1038/227680a0.

Doglioni C. and Bosellini A. (1987) - Eoalpine and mesoalpine tectonics in the Southern Alps. Geol. Rundsch., 76(3), 735-754, https://doi.org10.1007/BF01821061/METRICS.

Dommergues J.L. and Meister C. (1991) - Area of mixed marine faunas between two major paleogeographical realms, exemplified by the Early Jurassic (Late Sinemurian and Pliensbachian) ammonites in the Alps. Palaeogeogr. Palaeocl., 86(3-4), 265-282, https://doi.org10.1016/0031-0182(91)90085-6.

Dommergues, J.L., Meister, C., Manatschal, G. (2012) - Early Jurassic ammonites from Bivio (Lower Austroalpine unit) and Ardez (Middle Penninic unit) areas: A biostratigraphic tool to date the rifting in the Eastern Swiss Alps. Rev. Paléobiologie 31, 43–52.

Dürr S.B., Ring U., Frisch W. (1993) - Geochemistry and geodynamic significance of North Penninic ophiolites from the Central Alps. Schweiz. Miner. Petrog., 73(3), 407-419.

Eberli G.P. (1985) - Die jurassischen Sedimente in den ostalpinen Decken Graubündens: Relikte eines passiven Kontinentalrandes. Unpublished Ph.d. Thesis, ETH Zürich.

Eberli G.P. (1987) - Carbonate turbidite sequences deposited in rift-basins of the Jurassic Tethys Ocean (eastern Alps, Switzerland). Sedimentology, 34(3), 363-388, https://doi.org10.1111/j.1365-3091.1987.tb00576.x.

Eberli G.P. (1988) - The evolution of the southern continental margin of the Jurassic Tethys Ocean as recorded in the Allgäu Formation of the Austroalpine Nappes of Graubünden (Switzerland). Eclogae Geol. Helv., 81(1), 175-214.

Eggenberger U. (1990) - Petrographische und geochemische Untersuchungen im Gebiet zwischen St Moritz und dem Val Bever (Unterostalpin/Err Decke); Geochemischer Vergleich mit anderen Varizischen Intrusiva (Aar/Baveno/ Böttstein/ Bernina/Err/Julier). Univ. Bern.

Engström A. (2006) - Deformation and fluid-flow in magma-poor margins: A study of the Tasna Ocean-Continent transition, SE Switzerland. Unpublished Ph.d. Thesis, Stockholm University.

https://doi.org/10.3301/GFT.2023.02

Epin M.-E (2017) - Morpho-tectono-magmatic evolution and reactivation of ultra-distal magma-poor rifted margins: the fossil Err-Platta Ocean-Continent-Transition (SE Switzerland) and comparison to present-day analogues. Unpublished Ph.d. Thesis, Université de Strasbourg.

Epin M.-E. and Manatschal G. (2018) - Three-dimensional architecture, structural evolution, and role of inheritance controlling detachment faulting at a hyperextended distal margin: the example of the Err detachment system (SE Switzerland). Tectonics, 37(12), 4494-4514, https://doi.org10.1029/2018TC005125.

Epin M.-E., Manatschal G., Amann M. (2017) - Defining diagnostic criteria to describe the role of rift inheritance in collisional orogens: the case of the Err-Platta nappes (Switzerland). Swiss J. Geosci., 110(2), 419-438, https://doi.org10.1007/s00015-017-0271-6.

Epin M.-E., Manatschal G., Amann M., Ribes C., Clausse A., Guffon T., Lescanne M. (2019) - Polyphase tectono-magmatic evolution during mantle exhumation in an ultra-distal, magma-poor rift domain: example of the fossil Platta ophiolite, SE Switzerland. Int. J. Earth Sci., 108, 2443-2467, https://doi.org10.1007/s00531-019-01772-0.

Ernst W.G. (2005) - Alpine and Pacific styles of Phanerozoic mountain building: subduction-zone petrogenesis of continental crust. Terra Nova, 17, 165-188. https://doi.org10.1111/j.1365-3121.2005.00604.x.

Escher A. and Watterson J. (1974) - Stretching fabrics, folds and crustal shortening. Tectonophysics, 22(3-4), 223-231, https://doi.org10.1016/0040-1951(74)90083-3.

Esedo R., van Wijk J., Coblentz D., Meyer R. (2012) - Uplift prior to continental breakup: Indication for removal of mantle lithosphere? Geosphere, 8(5), 1078-1085, https://doi.org10.1130/GES00748.1.

Finger W (1978) Die zone von Samaden (unterostalpine Decken, Graubünden) und ihre jurassischen Brekzien. University Zurich, Zurich

Fletcher R.C. and Hallet B. (1983) - Unstable extension of the lithosphere: A mechanical model for Basin-and-Range structure. J. Geophys. Res., 88(B9), 7457-7466, https://doi.org10.1029/JB088iB09p07457.

Florineth D. and Froitzheim N. (1994) - Transition from continental to oceanic basement in the Tasna Nappe: evidence for Early Cretaceous opening of the Valais Ocean. Schweiz. Miner. Petrog., 74, 437-448.

Fossen H., Gabrielsen R.H., Faleide J.I., Hurich C.A. (2014) - Crustal stretching in the Scandinavian Caledonides as revealed by deep seismic data. Geology, 42(9), 791-794, https://doi.org10.1130/G35842.1.

Franke W. (2006) - The Variscan orogen in Central Europe: construction and collapse. Geological Society, London, Memoirs, 32(1), 333-343, https://doi.org/10.1144/GSL.MEM.2006.032.01.20.

Frasca G., Manatschal G., Cadenas P., Miró J., Lescoutre R. (2021) - A kinematic reconstruction of Iberia using intracontinental strike-slip corridors. Terra Nova, 33, 573-581, https://doi.org/10.1111/ter.12549.

Frisch W. (1979) - Tectonic progradation and plate tectonic evolution of the Alps. Tectonophysics, 60(3-4), 121-139, https://doi.org10.1016/0040-1951(79)90155-0.

Frizon de Lamotte, D., Fourdan, B., Leleu, S., Leparmentier, F., Clarens, P. (2015) - Style of rifting and the stages of Pangea breakup. Tectonics 34, 1009–1029. https://doi.org/10.1002/2014TC003760

Froitzheim N. (1988) - Synsedimentary and synorogenic normal faults within a thrust sheet of the Eastern Alps (Ortler zone, Graubünden, Switzerland). Eclogae Geol. Helv., 81(3), 593-610.

Froitzheim N. and Eberli G.P. (1990) - Extensional detachment faulting in the evolution of a Tethys passive continental margin, Eastern Alps, Switzerland. Geol. Soc. Am. Bull., 102(9), 1297-1308, https://doi.org10.1130/0016-7606(1990)102.

Froitzheim N. and Manatschal G. (1996) - Kinematics of Jurassic rifting, mantle exhumation, and passive-margin formation in the Austroalpine and Penninic nappes (eastern Switzerland). Geol. Soc. Am. Bull., 108(9), 1120-1133, https://doi.org10.1130/0016-7606(1996)108<1120:KOJRME>2.3.CO;2.

Froitzheim N. and Rubatto D. (1998) - Continental breakup by detachment faulting: field evidence and geochronological constraints (Tasna nappe, Switzerland). Terra Nova, 10(4), 171-176, https://doi.org10.1046/J.1365-3121.1998.00187.X.

Froitzheim N., Schmid S.M., Conti P. (1994) - Repeated change from crustal shortening to orogen-parallel extension in the Austroalpine units of Graubunden. Eclogae Geol. Helv., 87(2), 559-612.

https://doi.org/10.3301/GFT.2023.02

Froitzheim N., Schmid S.M., Frey M. (1996) - Mesozoic paleogeography and the timing of eclogite-facies metamorphism in the Alps: A working hypothesis. Eclogae Geol. Helv., 98(1), 81-110.

Froitzheim N., Plašienka D., Schuster R. (2008) - Alpine tectonics of the Alps and Western Carpathians. In: McCann T. (Ed.), The geology of Central Europe, Volume 2: Mesozoic and Cenozoic. Geological Society, London, 1141-1232, https://doi.org/10.1144/CEV2P.6.

Früh-Green G.L., Weissert H., Bernoulli D. (1990) - A multiple fluid history recorded in Alpine ophiolites. J. Geol. Soc. London, 147(6), 959-970, https://doi.org10.1144/gsjgs.147.6.0959.

Furrer H. (1985) - Field Workshop on Triassic and Jurassic sediments in the Eastern Alps of Switzerland: 25th-29th August 1985: Guide Book.

Furrer, H. (1995) - The Prosanto Formation, a marine Middle Triassic Fossil-Lagerstatte near Davos (Canton Graubunden, Eastern Swiss Alps). Eclogae Geol. Helv. 88, 681–684.

Galster F., Cavargna-Sani M., Epard J.L., Masson H. (2012) - New stratigraphic data from the Lower Penninic between the Adula nappe and the Gotthard massif and consequences for the tectonics and the paleogeography of the Central Alps. Tectonophysics, 579, 37-55, https://doi.org10.1016/j.tecto.2012.05.029.

Gawlick H.-J. and Missoni S. (2015) - Middle Triassic radiolarite pebbles in the Middle Jurassic Hallstatt Mélange of the Eastern Alps: implications for Triassic-Jurassic geodynamic and paleogeographic reconstructions of the western Tethyan realm. Facies, 61(13), 1-19, https://doi.org10.1007/s10347-015-0439-3.

Gillard M., Manatschal G., Autin J. (2016a) - How can asymmetric detachment faults generate symmetric Ocean Continent Transitions? Terra Nova, 28(1), 27-34, https://doi.org10.1111/ter.12183.

Gillard M., Autin J., Manatschal G. (2016b) - Fault systems at hyper-extended rifted margins and embryonic oceanic crust: Structural style, evolution and relation to magma. Mar. Petrol. Geol., 76, 51-67, https://doi.org10.1016/j.marpetgeo.2016.05.013.

Gillard M., Tugend J., Müntener O., Manatschal G., Karner G.D., Autin J., Sauter D., Figueredo P.H., Ulrich M. (2019) - The role of serpentinization and magmatism in the formation of decoupling interfaces at magma-poor rifted margins. Earth-Sci. Rev., 196, 102882, https://doi.org10.1016/j.earscirev.2019.102882.

Green R. (1974) - The seismic refraction method—a review. Geoexploration, 12(4), 259-284, https://doi.org10.1016/0016-7142(74)90015-5.

Grove T.L., Chatterjee N., Parman S.W., Médard E. (2006) - The influence of H2O on mantle wedge melting. Earth Planet. Sci. Lett., 249(1-2), 74-89, https://doi.org10.1016/j.epsl.2006.06.043.

Grüler B. (1995) - Geologische Untersuchungen im SW-Teil des Unterengadiner Fensters, Teil I, Geologie der Val Tasna und Umgebung. Beiträge Zur Geologischen Karte Der Schweiz, 166, 2-72.

Gruner U. (1981) - Die jurassischen Breccien der Falknis-Decke und altersäquivalente Einheiten in Graubünden. Beiträge zur Geol. Karte der Schweiz Neue Folge 154, 136.

Handy M.R. (1989) - Deformation regimes and the rheological evolution of fault zones in the lithosphere: the effects of pressure, temperature, grainsize and time. Tectonophysics, 163(1-2), 119-152, https://doi.org10.1016/0040-1951(89)90122-4.

Handy MR. and Zingg A. (1991) - The tectonic and rheological evolution of an attenuatted cross section of the continental crust: Ivrea crustal section, southern Alps, northwestern Italy and southern Switzerland. Geol. Soc. Am. Bull., 103(2), 236-253, https://doi.org10.1130/0016-7606(1991)103<0236:TTAREO>2.3.CO;2.

Handy, M.R., Herwegh, M., Kamber, B.S., Tietz, R., Villa, I.M. (1996) - Geochronologic, petrologic and kinematic constraints on the evolution of the Err-Platta boundary, part of a fossil continent-ocean suture in the Alps (eastern Switzerland). Schweizerische Mineral. und Petrogr. Mitteilungen 76, 453–474.

Handy M.R., Franz L., Heller F., Janott B., Zurbriggen R. (1999) - Multistage accretion and exhumation of the continental crust (Ivrea crustal section, Italy and Switzerland). Tectonics, 18(6), 1154-1177, https://doi.org10.1029/1999TC900034.

Handy M.R., Schmid S., Bousquet R., Kissling E., Bernoulli D. (2010) - Reconciling plate-tectonic reconstructions of Alpine Tethys with the geological-geophysical record of spreading and subduction in the Alps. Earth-Sci. Rev., 102(3-4), 121-158, https://doi.org10.1016/j.earscirev.2010.06.002.

Hanžl P., Verner K., Buriánek D., Šíma J., Janderkova J., Paleček M., Hroch T., Martínek K., Megerssa L., Hrdličková K., Metelka V. (2018) - Basic principles of geological and thematic mapping. Czech Geological Survey, https://doi.org10.13140/RG.2.2.12898.99523.

https://doi.org/10.3301/GFT.2023.02

Hardy S. (1993) - Numerical modelling of the response to variable stretching rate of a domino fault block system. Mar. Petrol. Geol., 10(2), 145-152, https://doi.org10.1016/0264-8172(93)90019-O.

Hart N.R., Stockli D.F., Lavier L.L., Hayman N.W. (2017) - Thermal evolution of a hyperextended rift basin, Mauléon Basin, western Pyrenees. Tectonics, 36(6), 1103-1128, https://doi.org10.1002/2016TC004365.

Haug E. (1909) - Les géosynclinaux de la chaîne des Alpes pendant les temps secondaires. Comptes Rendus de l'Academie des Sciences de Paris, 148, 1637.

Haupert I. (2015) - Etude des hauts et bas topographiques dans les marges profondes de type "upper plate" : Exemple des unités du Briançonnais et du Prépiémontais dans les Alpes et comparaison avec des analogues modernes. Unpublished Ph.d. Thesis, Université de Strasbourg.

Haupert I., Manatschal G., Decarlis A., Unternehr P. (2016) - Upper-plate magma-poor rifted margins: stratigraphic architecture and structural evolution. Mar. Petrol. Geol., 69, 241-261, https://doi.org10.1016/j.marpetgeo.2015.10.020.

Hauser A. (2011) - The ocean-continent-transition in the Lower Engadine: Petrologic, geochemical and geochronological insights constraining paleogeographic geometry and evolution (Tasna-Nauders Area, CH-A). Unpublished master's Thesis, University of Lausanne.

Hendrie D.B., Kusznir N.J., Hunter R.H. (1993) - Jurassic extension estimates for the North Sea 'triple junction' from flexural backstripping: implications for decompression melting models. Earth Planet. Sci. Lett., 116(1-4), 113-127, https://doi.org10.1016/0012-821X(93)90048-E.

Hermann J., Müntener O. (1992) - Strukturelle Entwicklung im Grenzbereich zwischen dem penninischen Malenco-Ultramafitit und dem Unterostalpin (Margna-und Sella-Decke). Schweizerische Mineral. und Petrogr. Mitteilungen 72, 225–240.

Hermann J. and Müntener O. (1996) - Extension-related structures in the Malenco-Margna-system: Implications for paleogeography and consequences for rifting and Alpine tectonics. Schweiz. Miner. Petrog., 76(3), 501-520.

Hermann J., Müntener O., Trommsdorff V., Hansmann W., Piccardo G.B. (1997) - Fossil crust-to-mantle transition, Val Malenco (Italian Alps). J. Geophys. Res., 102(B9), 20123-20132, https://doi.org10.1029/97JB01510.

Hess H.H. (1962) - History of ocean basins. In: Engel A.E.J., James H.L., Lonard B.F. (Eds.), Petrologic Studies: A Volume to Honor Buddington A.F., Geological Society of America, 599-620.

Hesse R. (1974) - Long-distance continuity of turbidites: Possible evidence for an Early Cretaceous trench abyssal plain in the east Alps. Geol. Soc. Am. Bull. 85, 859-870.

Hitz L. (1996) - The deep structure of the Engadine Window: Evidence from deep seismic data. Eclogae Geol. Helv., 89(2), 657-675.

Hölker A. (2001) - Seismic structure and response of ocean-continent transition zones in magma-poor rifted continental margins. Unpublished Ph.d. Thesis, ETH Zürich.

Hölker A.B., Manatschal G., Holliger K., Bernoulli D. (2002) - Seismic structure and response of ocean-continent transition zones - A comparison of an ancient Tethyan and a present-day Iberian site. Mar. Geophys. Res., 23(4), 319-334, https://doi.org10.1023/A:1025706125747.

Holmes A. (1931) - Radioactivity and Earth Movements. Transactions of the Geological Society of Glasgow, 18(3), 559-606, https://doi.org10.1144/transglas.18.3.559.

Hosseinpour M., Williams S., Seton M., Barnett-Moore N., Müller R.D. (2016). Tectonic evolution of Western Tethys from Jurassic to present day: coupling geological and geophysical data with seismic tomography models. Int. Geol. Rev., 58(13), 1616-1645, https://doi.org10.1080/00206814.2016.1183146.

Huang C. and Hesselbo S.P. (2014) - Pacing of the Toarcian Oceanic Anoxic Event (Early Jurassic) from astronomical correlation of marine sections. Gondwana Res., 25(4), 1348-1356, https://doi.org10.1016/j.gr.2013.06.023.

Hubbard R.J. (1988) - Age and significance of sequence boundaries on Jurassic and Early Cretaceous rifted continental margins. Am. Assoc. Petr. Geol. B., 72(1), 49-72, https://doi.org10.1306/703c81c8-1707-11d7-8645000102c1865d.

Huismans R.S. and Beaumont C. (2008) - Complex rifted continental margins explained by dynamical models of depth-dependent lithospheric extension. Geology, 36(2), 163-166, https://doi.org10.1130/G24231A.1.

Huismans R. and Beaumont C. (2011) - Depth-dependent extension, two-stage breakup and cratonic underplating at rifted margins. Nature, 473(7345), 74-78, https://doi.org10.1038/nature09988.

https://doi.org/10.3301/GFT.2023.02

Huismans R.S., Podladchikov Y.Y., Cloetingh S.A.P.L. (2001) - Transition from passive to active rifting: Relative importance of asthenospheric doming and passive extension of the lithosphere. J. Geophys. Res., 106(B6), 11,271-11,291.

Hunziker J.C., Desmons J., Hurford A.J. (1992) - Thirty-two years of geochronological work in the Central and Western Alps: a review on seven maps. Cueno (Italy): Mémoires de Géologie (Lausanne) n°13.

Incerpi N. (2017) - Hydrothermal systems in distal rifted margins and their role in the thermal evolution of sedimentary successions: study of two fossil analogues in the Swiss Alps and Pyrenees. Unpublished Ph.d. Thesis, Université de Strasbourg, Università degli studi di Torino.

Incerpi N., Martire L., Manatschal G., Bernasconi S.M. (2017) - Evidence of hydrothermal fluid flow in a hyperextended rifted margin: the case study of the Err nappe (SE Switzerland) - Swiss J. Geosci., 110(2), 439-456, https://doi.org10.1007/s00015-016-0235-2.

Incerpi N., Martire L., Bernasconi S.M., Manatschal G., Gerdes A. (2018) - Silica-rich septarian concretions in biogenic silica-poor sediments: A marker of hydrothermal activity at fossil hyper-extended rifted margins (Err nappe, Switzerland). Sediment. Geol., 378, 19-33, https://doi.org10.1016/j.sedgeo.2018.10.005.

Incerpi N., Martire L., Manatschal G., Bernasconi S.M., Gerdes A., Czuppon G., Palcsu L., Karner G.D., Johnson C.A., Figueredo P.H. (2020a) - Hydrothermal fluid flow associated to the extensional evolution of the Adriatic rifted margin: Insights from the pre- to post-rift sedimentary sequence (SE Switzerland, N Italy). Basin Res., 32(1), 91-115, https://doi.org10.1111/bre.12370.

Incerpi N., Manatschal G., Martire L., Bernasconi S.M., Gerdes A., Bertok C. (2020b) - Characteristics and timing of hydrothermal fluid circulation in the fossil Pyrenean hyperextended rift system: new constraints from the Chaînons Béarnais (W Pyrenees). Int. J. Earth Sci., 109, 1071-1093, https://doi.org/10.1007/s00531-020-01852-6.

Jaupart C. and Mareschal J.C. (2007) - Heat flow and thermal structure of the lithosphere. In: Watts A.B., Schubert G. (Eds.), Treatise on Geophysics, Volume 6, Crust and lithosphere dynamics, Elsevier, 217-251.

Jenkyns H.C. (1988) - The early Toarcian (Jurassic) anoxic event: stratigraphic, sedimentary, and geochemical evidence. Am. J. Sci., 288(2), 101-151, https://doi.org10.2475/ajs.288.2.101.

Jenkyns H.C. (2010) - Geochemistry of oceanic anoxic events. Geochem. Geophy. Geosy., 11(3), Q03004, https://doi.org10.1029/2009GC002788.

Ji W.Q., Malusà M. G., Tiepolo M., Langone A., Zhao L., Wu F.Y. (2019) - Synchronous Periadriatic magmatism in the Western and Central Alps in the absence of slab breakoff. Terra Nova, 31(2), 120-128, https://doi.org10.1111/TER.12377.

Jolivet L., Gorini C., Smit J., Leroy S. (2015) - Continental breakup and the dynamics of rifting in back-arc basins: The Gulf of Lion margin. Tectonics, 34(4), 662-679, https://doi.org10.1002/2014TC003570.

Kaus B.J., Connolly J.A., Podladchikov Y.Y., Schmalholz S.M. (2005) - Effect of mineral phase transitions on sedimentary basin subsidence and uplift. Earth Planet. Sci. Lett., 233(1-2), 213-228, https://doi.org10.1016/j.epsl.2005.01.032.

Kley J. and Voigt T. (2008) - Late Cretaceous intraplate thrusting in Central Europe: Effect of Africa-Iberia-Europe convergence, not Alpine collision. Geology, 36(11), 839-842, https://doi.org10.1130/G24930A.1.

Kooi H. Cloetingh S., Burrus J. (1992) - Lithospheric necking and regional isostasy at extensional basins 1. Subsidence and gravity modeling with an application to the Gulf of Lions Margin (SE France). J. Geophys. Res., 97(B12), 17553-17571, https://doi.org10.1029/92JB01377.

Kröner U. and Romer R.L. (2013) - Two plates - Many subduction zones: The Variscan orogeny reconsidered. Gondwana Res., 24(1), 298-329, https://doi.org10.1016/j.gr.2013.03.001.

Kusznir N.J. and Ziegler P.A. (1992) - The mechanics of continental extension and sedimentary basin formation: A simple-shear/pure-shear flexural cantilever model. Tectonophysics, 215(1-2), 117-131, https://doi.org10.1016/0040-1951(92)90077-J.

Kusznir N.J., Marsden G., Egan S.S. (1991) - A flexural-cantilever simple-shear/pure-shear model of continental lithosphere extension: applications to the Jeanne d'Arc Basin, Grand Banks and Viking Graben, North Sea. Geol. Soc. Spec. Publ., 56(1), 41-60, https://doi.org10.1144/GSL.SP.1991.056.01.04.

Laubscher H. and Bernoulli D. (1977) - Mediterranean and Tethys. In: Nairn A.E.M., Kanes W.H., Stehli F.G. (Eds.), The Ocean Basins and Margins, 4A, The Eastern Mediterranean Plenum. Springer Boston, US, New York, 1-28. https://doi.org/10.1007/978-1-4684-3036-3.

https://doi.org/10.3301/GFT.2023.02

Lavier L.L. and Manatschal G. (2006) - A mechanism to thin the continental lithosphere at magma-poor margins. Nature, 440(7082), 324-328, https://doi.org10.1038/nature04608.

Le Breton E., Handy M.R., Molli G., Ustaszewski K. (2017) - Post-20 Ma motion of the Adriatic Plate: New constraints from surrounding orogens and Implications for Crust-Mantle decoupling. Tectonics, 36(12), 3135-3154, https://doi.org10.1002/2016TC004443.

Leeder M.R. and Gawthorpe R. L. (1987) - Sedimentary models for extensional tilt-block/half-graben basins. In: Coward M.P., Dewey J.F., Hancock P.L (Eds.), Continental extensional tectonics, Geol. Soc. Spec. Publ., 28, 139-152, https://doi.org10.1144/gsl.sp.1987.028.01.11.

Lemoine M. (1961) - La marge externe de la fosse piémontaise dans les Alpes occidentales. Rev. Géogr. Phys. Géol. Dyn, 2, 163-180.

Lemoine M. (1967) - Brèches sédimentaires marines à la frontière entre les domaines briançonnais et piémontais dans les Alpes occidentales. Geol. Rundschau, 56(1), 320-335, https://doi.org10.1007/BF01848723.

Lemoine M., Bas T., Arnaud-Vanneau A., Arnaud H., Dumont T., Gidon M., Bourbon M., de Graciansky P.C., Rudkiewicz J.L., Megard-Galli J., Tricart P. (1986) - The continental margin of the Mesozoic Tethys in the Western Alps. Mar. Petrol. Geol., 3(3), 179-199, https://doi.org10.1016/0264-8172(86)90044-9.

Lemoine M., Tricart P., Boillot G. (1987) - Ultramafic and gabbroic ocean floor of the Ligurian Tethys (Alps, Corsica, Apennines): In search of a genetic model. Geology, 15(7), 622-625, https://doi.org10.1130/0091-7613(1987)15.

Lescoutre R. and Manatschal G. (2020) - Role of rift-inheritance and segmentation for orogenic evolution: example from the Pyrenean-Cantabrian system. B. Soc. Geol. Fr., 191(1), 1-18, https://doi.org10.1051/bsgf/2020021.

Lewis D.S., Ross E., Leander M. (2014) - New insights into late synrift subsidence from detailed well ties and seismic mapping, Campos Basin, Brazil. In: Pindell J., Horn B., Rosen N., Weimer P., Dinkleman M., Lowrie A., Fillon R., Granath J., Kennan L. (Eds.), Sedimentary basins: origin, depositional histories and petroleum systems, SEPM - Society for Sedimentary Geology, 98-115, https://doi.org/10.5724/gcs.14.33.

Lin A.T., Watts A.B., Hesselbo S. P. (2003) - Cenozoic stratigraphy and subsidence history of the South China Sea margin in the Taiwan region. Basin Res., 15(4), 453-478, https://doi.org10.1046/j.1365-2117.2003.00215.x.

Liniger M.H. (1992) - Der ostalpin-penninische Grenzbereich im Gebiet der nördlichen Margna-Decke (Graubünden, Schweiz). Unpublished Ph.D. Thesis, ETH Zurich.

Lister G.S., Etheridge M.A., Symonds P.A. (1986) - Detachment faulting and the evolution of passive continental margins. Geology, 14(3), 246-250, https://doi.org/10.1130/0091-7613(1986)14<246:DFATEO>2.0.CO;2.

Lory C. (1860) - Description géologique du Dauphiné pour servir d'explication à la carte géologique de cette province (F. Savy (ed.)). Grenoble: Librairie de la Société Géologique de France.

Lovecchio J.P., Rohais S., Joseph P., Bolatti N.D., Kress P.R., Gerster R., Ramos V.A. (2018) - Multistage rifting evolution of the Colorado basin (offshore Argentina): Evidence for extensional settings prior to the South Atlantic opening. Terra Nova, 30(5), 359-368, https://doi.org10.1111/ter.12351ï.

Lugeon M. (1902) - Les grandes nappes de recouvrement des Alpes du Chablais et de la Suisse. B. Soc. Géol. Fr., 4(1), 723-825.

Luo P., Manatschal G., Ren J., Zhao Z., Wang H., Tong D. (2021) - Tectono-magmatic and stratigraphic evolution of final rifting and breakup: evidence from the tip of the southwestern propagator in the South China Sea. Mar. Petrol. Geol., 129, 105079, https://doi.org10.1016/J.MARPETGEO.2021.105079.

Mac Niocaill C., Van der Pluijm B.A., Van der Voo R. (1997) - Ordovician paleogeography and the evolution of the Iapetus Ocean. Geology, 25(2), 159-162, https://doi.org/10.1130/0091-7613(1997)025<0159:OPATEO>2.3.CO;2.

Mählmann R.F. (1996) - The pattern of diagenesis and metamorphism by vitrinite reflectance and illitecrystallinityin Mittelbunden and in the Oberhalbstein. 2. Correlation of coal petrographical and mineralogical parameters. Schweiz. Miner. Petrogr., 76, 23–46.

Manatschal G. (1999) - Fluid- and reaction-assisted low-angle normal faulting: evidence from rift-related brittle fault rocks in the Alps (Err Nappe, eastern Switzerland). J. Struct. Geol., 21(7), 777-793, https://doi.org10.1016/S0191-8141(99)00069-3.

Manatschal G. (2004) - New models for evolution of magma-poor rifted margins based on a review of data and concepts from West Iberia and the Alps. Int. J. Earth Sci., 93(3), 432-466, https://doi.org10.1007/s00531-004-0394-7.

https://doi.org/10.3301/GFT.2023.02

Manatschal, G., Müntener, O. (2009) - A type sequence across an ancient magma-poor ocean--continent transition: the example of the western Alpine Tethys ophiolites. Tectonophysics 473, 4–19. https://doi.org/10.1016/j.tecto.2008.07.021

Manatschal G. and Nievergelt P. (1997) - A continent-ocean transition recorded in the Err and Platta nappes (Eastern Switzerland). Eclogae Geol. Helv., 90, 3-27.

Manatschal G. and Bernoulli D. (1999) - Architecture and tectonic evolution of nonvolcanic margins: Present-day Galicia and ancient Adria. Tectonics, 18(6), 1099-1119, https://doi.org10.1029/1999TC900041.

Manatschal G., Marquer D., Früh-Green G.L. (2000) - Channelized fluid flow and mass transfer along a rift-related detachment fault (Eastern Alps, Southeast Switzerland). Bull. Geol. Soc. Am., 112(1), 21-33, https://doi.org10.1130/0016-7606(2000)112<21:CFFAMT>2.0.CO;2.

Manatschal G., Froitzheim N., Rubenach M., Turrin B.D. (2001) - The role of detachment faulting in the formation of an ocean-continent transition: Insights from the Iberia Abyssal Plain. Geol. Soc. Spec. Publ., 187(1), 405-428, https://doi.org10.1144/GSL.SP.2001.187.01.20.

Manatschal G., Engström A., Desmurs L., Schaltegger U., Cosca M., Müntener O., Bernoulli D. (2006) - What is the tectono-metamorphic evolution of continental break-up: The example of the Tasna Ocean-Continent Transition. J. Struct. Geol., 28(10), 1849-1869, https://doi.org10.1016/j.jsg.2006.07.014.

Manatschal G., Sauter D., Karpoff A.M., Masini E., Mohn G., Lagabrielle Y. (2011) - The Chenaillet Ophiolite in the French/Italian Alps: An ancient analogue for an Oceanic Core Complex? Lithos, 124(3-4), 169-184, https://doi.org10.1016/j.lithos.2010.10.017.

Manatschal G., Lavier L.L., Chenin P. (2015) - The role of inheritance in structuring hyperextended rift systems: Some considerations based on observations and numerical modeling. Gondwana Res., 27(1), 140-164, https://doi.org10.1016/j.gr.2014.08.006.

Manatschal G., Chenin P., Lescoutre R., Miró J., Cadenas P., Saspiturry N., Masini E., Chevrot S., Ford M., Jolivet L., Mouthereau F., Thinon I., Issautier B., Calassou S. (2021) - The role of inheritance in forming rifts and rifted margins and building collisional orogens: a Biscay-Pyrenean perspective. B. Soc. Geol. Fr., 192(1), 55, https://doi.org/10.1051/bsgf/2021042.

Manatschal G., Chenin P., Ghienne J.-F., Ribes C., Masini E. (2022) - The syn-rift tectono-stratigraphic record of rifted margins (Part I): insights from the Alpine Tethys. Basin Res., 34(1), 457-488, https://doi.org10.1111/bre.12627.

Masini E. (2011) - L'évolution tectono-sédimentaire syn-rift des bassins de marge passive profonde: exemples du bassin de Samedan (Alpes centrales, Suisse) et du bassin de Mauléon (Pyrénées basques françaises). Unpublished Ph.D. Thesis, Université de Strasbourg.

Masini E., Manatschal G., Mohn G., Ghienne J.F., Lafont F. (2011) - The tectono-sedimentary evolution of a supra-detachment rift basin at a deep-water magma-poor rifted margin: The example of the Samedan Basin preserved in the Err nappe in SE Switzerland. Basin Res., 23(6), 652-677, https://doi.org10.1111/j.1365-2117.2011.00509.x.

Masini E., Manatschal G., Mohn G., Unternehr P. (2012) - Anatomy and tectono-sedimentary evolution of a rift-related detachment system: The example of the Err detachment (central Alps, SE Switzerland). Geol. Soc. Am. Bull., 124(9-10), 1535-1551, https://doi.org10.1130/B30557.1.

Masini E., Manatschal G., Mohn G. (2013) - The Alpine Tethys rifted margins: Reconciling old and new ideas to understand the stratigraphic architecture of magma-poor rifted margins. Sedimentology, 60, 174-196, https://doi.org10.1111/sed.12017.

Masson H., Bussy F., Eichenberger M., Giroudd N., Meilhac C., Presniakov S. (2008) - Early Carboniferous age of the Versoyen ophiolites and consequences: Non-existence of a "Valais ocean" (Lower Penninic, western Alps). Bull. Soc. Geol. Fr., 179(4), 337-355, https://doi.org10.2113/gssgfbull.179.4.337.

McArthur J.M., Cohen A.S., Coe A.L., Kemp D.B., Bailey R.J., Smith D.G. (2008) - Discussion on the Late Palaeocene-Early Eocene and Toarcian (Early Jurassic) carbon isotope excursions: A comparison of their time scales, associated environmental change, causes and consequences. J. Geol. Soc. London, 165(4), 875-880, https://doi.org10.1144/0016-76492007-157.

McCarthy A., Tugend J., Mohn G., Candioti L., Chelle-Michou C., Arculus R., Schmalholz S. M., Müntener O. (2020) - A case of Ampferer-type subduction and consequences for the Alps and the Pyrenees. Am. J. Sci., 320(4), 313-372, https://doi.org10.2475/04.2020.01.

McClay K.R., Norton M.G., Coney P., Davis G.H. (1986) - Collapse of the Caledonian orogen and the Old Red Sandstone. Nature, 323, 147-149, https://doi.org/10.1038/323147a0.

https://doi.org/10.3301/GFT.2023.02

McKenzie D. (1978) - Some remarks on the development of sedimentary basins. Earth Planet. Sci. Lett., 40(1), 25-32, https://doi.org10.1016/0012-821X(78)90071-7.
McKerrow W.S., Mac Niocaill C., Ahlberg P.E., Clayton G., Cleal C.J., Eagar R.M.C. (2000a) - The Late Palaeozoic relations between Gondwana and Laurussia. Geol. Soc. Spec. Publ., 179(1), 9-20, https://doi.org10.1144/GSL.SP.2000.179.01.03.
McKerrow W.S., Mac Niocaill C., Dewey J.F. (2000b) - The Caledonian Orogeny redefined. J. Geol. Soc. London, 157(6), 1149-1154, https://doi.org10.1144/jgs.157.6.1149.
Meier A. (2003) - The Periadriatic fault system in Valtellina (N-Italy) and the evolution of the southwestern segment of the Eastern Alps. Unpublished Ph.D. Thesis, ETH Zurich.
Meissner R. (1999) - Terrane accumulation and collapse in central Europe: seismic and rheological constraints. Tectonophysics, 305(1-3), 93-107, https://doi.org10.1016/S0040-1951(99)00016-5.
Miller D.J. and Christensen N.I. (1997) - Seismic velocities of lower crustal and upper mantle rocks from the slow-spreading Mid-Atlantic Ridge, south of the Kane Transform Zone (MARK). Proceedings of the Ocean Drilling Program, Scientific Results, 153, 437-454. Retrieved from http://cat.inist.fr/?aModele=afficheN&cpsidt=2817434.
Miró J., Cadenas P., Manatschal G., Munoz J.A. (2021) - Reactivation of a hyperextended rift system: the Basque-Cantabrian Pyrenees case. Basin Res. 33, 3077–3101. https://doi.org/10.1111/bre.12595
Miyashiro A. (1961) - Evolution of metamorphic belts. J. Petrol., 2(3), 277-311, https://doi.org10.1093/petrology/2.3.277.
Mohn G. (2010) - L'évolution tectono-sédimentaire des marges de la Téthys Alpine au cours de l'amincissement lithosphérique. Unpublished Ph.D. Thesis, Université de Strasbourg.
Mohn G., Manatschal G., Müntener O., Beltrando M., Masini E. (2010) - Unravelling the interaction between tectonic and sedimentary processes during lithospheric thinning in the Alpine Tethys margins. Int. J. Earth Sci., 99, 75-101, https://doi.org10.1007/s00531-010-0566-6.
Mohn G., Manatschal G., Masini E., Müntener O. (2011) - Rift-related inheritance in orogens: a case study from the Austroalpine nappes in Central Alps (SE-Switzerland and N-Italy). Int. J. Earth Sci., 100(5), 937-961, https://doi.org10.1007/s00531-010-0630-2.
Mohn G., Manatschal G., Beltrando M., Masini E., Kusznir N. (2012) - Necking of continental crust in magma-poor rifted margins: Evidence from the fossil Alpine Tethys margins. Tectonics, 31(1), TC1012, https://doi.org10.1029/2011TC002961.
Mohn G., Manatschal G., Beltrando M., Haupert I. (2014) - The role of rift-inherited hyper-extension in Alpine-type orogens. Terra Nova, 26(5), 347-353, https://doi.org10.1111/ter.12104.
Mohn G., Karner G.D., Manatschal G., Johnson C.A. (2015) - Structural and stratigraphic evolution of the Iberia-Newfoundland hyper-extended rifted margin: a quantitative modelling approach. Geol. Soc. Spec. Publ., 413(1), 53-89, https://doi.org10.1144/SP413.9.
Montadert L., de Charpal O., Roberts D., Guennoc P., Sibuet J.-C. (1979) - Northeast Atlantic passive continental margins: Rifting and subsidence processes. In Talwani M., Hay W., Ryan W.B.F. (Eds.), Deep drilling results in the Atlantic Ocean: Continental margins and paleoenvironment, Volume 3. American Geophysical Union (AGU), 154-186, https://doi.org10.1029/me003p0154.
Müller R.D., Seton M., Zahirovic S., Williams S.E., Matthews K.J., Wright N.M., Shephard G.E., Maloney K.T., Barnett-Moore N., Hosseinpour M., Bower D.J., Cannon J. (2016) - Ocean basin evolution and global-scale plate reorganization events since Pangea breakup. Ann. Rev. Earth Pl. Sci., 44(1), 107-138, https://doi.org10.1146/annurev-earth-060115-012211.
Müntener O., Hermann R.G., Trommsdorff V. (2000) - Cooling history and exhumation of lower-crustal granulite and upper Mantle (Malenco, Eastern Central Alps). J. Petrol., 41(2), 175-200.
Müntener O., Pettke T., Desmurs L., Meier M., Schaltegger U. (2004) - Refertilization of mantle peridotite in embryonic ocean basins: trace element and Nd isotopic evidence and implications for crust-mantle relationships. Earth Planet. Sci. Lett., 221, 293-308, https://doi.org10.1016/S0012-821X(04)00073-1.
Müntener O., Manatschal G., Desmurs L., Pettke T. (2010) - Plagioclase peridotites in ocean-continent transitions: Refertilized mantle domains generated by melt stagnation in the shallow mantle lithosphere. J. Petrol., 51(1-2), 255-294, https://doi.org10.1093/petrology/egp087.

https://doi.org/10.3301/GFT.2023.02

Murillas J., Mougenot D., Boulot G., Comas M.C., Banda E., Mauffret A. (1990) - Structure and evolution of the Galicia Interior Basin (Atlantic western Iberian continental margin). Tectonophysics, 184(3-4), 297-319, https://doi.org10.1016/0040-1951(90)90445-E.

Nance R.D. and Linnemann U. (2008) - The Rheic Ocean: Origin, evolution, and significance. GSA Today, 18(12), 4-12, https://doi.org10.1130/GSATG24A.1.

Nance R.D., Gutiérrez-Alonso G., Keppie J.D., Linnemann U., Murphy J.B., Quesada C., Strachan R.A., Woodcock N.H. (2010) - Evolution of the Rheic Ocean. Gondwana Res. 17, 194–222. https://doi.org/10.1016/j.gr.2009.08.001.

Nievergelt P., Liniger M., Froitzheim N., Mählmann R.F. (1996) - Early to mid-Tertiary crustal extension in the Central Alps: The Turba Mylonite Zone (Eastern Switzerland). Tectonics, 15(2), 329-340, https://doi.org10.1029/93TC02312.

Nirrengarten M., Manatschal G., Yan X., Kusznir N., Millot B. (2016) - Application of the critical Coulomb wedge theory to hyper-extended, magma-poor rifted margins. Earth Planet. Sci. Lett., 442, 121-132, https://doi.org/10.1016/j.epsl.2016.03.004.

Nirrengarten M., Manatschal G., Tugend J., Kusznir N., Sauter D. (2018) - Kinematic evolution of the Southern North Atlantic: Implications for the formation of hyperextended rift systems. Tectonics, 37(1), 89-118, https://doi.org10.1002/2017TC004495.

Officer C.B. and Ewing M. (1954) - Geophysical investigations in the emerged and submerged Atlantic coastal plain: Part VII. Continental shelf, continental slope, and continental rise south of Nova Scotia. Geol. Soc. Am. Bull., 65(7), 653-670, https://doi.org/10.1130/0016-7606(1954)65[653:GIITEA]2.0.CO;2.

Ogg, J.G., Ogg, G., Gradstein, F.M. (2016) - A concise geologic time scale. Elsevier, Amsterdam.

Osmundsen P.T. and Péron-Pinvidic G. (2018) - Crustal-scale fault interaction at rifted margins and the formation of domain-bounding breakaway complexes: Insights from offshore Norway. Tectonics, 37, 935-964, https://doi.org/10.1002/2017TC004792.

Peacock S.M., Rushmer T., Thompson A.B. (1994) - Partial melting of subducting oceanic crust. Earth Planet. Sci. Lett., 121(1-2), 227-244, https://doi.org10.1016/0012-821X(94)90042-6.

Pérez-Gussinyé M., Ranero C.R., Reston T.J. (2003) - Mechanisms of extension at nonvolcanic margins: Evidence from the Galicia Interior Basin, west of Iberia. J. Geophys. Res., 108(B5), 2245, https://doi.org10.1029/2001JB000901.

Pérez-Gussinyé M., Andrés-Martínez M., Araújo M., Xin Y., Armitage J., Morgan J.P. (2020) - Lithospheric strength and rift migration controls on synrift stratigraphy and breakup unconformities at rifted margins: Examples from numerical models, the Atlantic and South China Sea margins. Tectonics, 39(12), e2020TC006255, https://doi.org10.1029/2020TC006255.

Péron-Pinvidic, G., Manatschal, G. (2009) The final rifting evolution at deep magma-poor passive margins from Iberia-Newfoundland: A new point of view. Int. J. Earth Sci. 98, 1581–1597. https://doi.org/10.1007/s00531-008-0337-9

Péron-Pinvidic G., Shillington D.J., Tucholke B.E. (2010) - Characterization of sills associated with the U reflection on the Newfoundland margin: evidence for widespread early post-rift magmatism on a magma-poor rifted margin. Geophys. J. Int., 182, 113-136, https://doi.org10.1111/j.1365-246X.2010.04635.x.

Peters T. (2005) - Blatt Nr. 1257 St.Moritz. - Geol. Atlas der Schweiz 1:25'000, Karte 118, mit Erläuterungen. Bundesamt für Wasser und Geologie. Bern.

Peters T. (2007) - Blatt Nr. 1256 Bivio. - Geol. Atlas der Schweiz 1:25'000, Karte 124, mit Erläuterungen. Bundesamt für Wasser und Geologie. Bern.

Petri, B. (2014) - Formation et exhumation des granulites permiennes. Université de Strasbourg.

Petri B., Mohn G., Štípská P., Schulmann K., Manatschal G. (2016) - The Sondalo gabbro contact aureole (Campo unit, Eastern Alps): implications for mid-crustal mafic magma emplacement. Contrib. Mineral. Petr., 171(5), 52, https://doi.org10.1007/s00410-016-1263-7.

Petri B, Skrzypek E., Mohn G., Mateeva T., Galster F., Manatschal G. (2017) - U-Pb geochronology of the Sondalo gabbroic complex (Central Alps) and its position within the Permian post-Variscan extension. Int. J. Earth Sci., 106, 2873-2893, https://doi.org10.1007/s00531-017-1465-x.

Petri B., Duretz T., Mohn G., Schmalholz S.M., Karner G.D., Müntener O. (2019) - Thinning mechanisms of heterogeneous continental lithosphere. Earth Planet. Sci. Lett., 512, 147-162, https://doi.org10.1016/J.EPSL.2019.02.007.

Pfiffner O.A., Lehner P., Heitzmann P., Mueller S., Steck A. (1997) - Deep structure of the Swiss Alps: results of NRP 20. Birkhäuser.

https://doi.org/10.3301/GFT.2023.02

Pfiffner O.A., Schlunegger F., Buiter S.J.H. (2002) - The Swiss Alps and their peripheral foreland basin: Stratigraphic response to deep crustal processes. Tectonics, 21(2), 1-16, https://doi.org10.1029/2000tc900039.

Picazo S., Manatschal G., Cannat M., Andréani M. (2013) - Deformation associated to exhumation of serpentinized mantle rocks in a fossil Ocean Continent Transition: The Totalp unit in SE Switzerland. Lithos, 175, 255-271, https://doi.org10.1016/j.lithos.2013.05.010.

Picazo S., Müntener O., Manatschal G., Bauville A., Karner G.D., Johnson C. (2016) - Mapping the nature of mantle domains in Western and Central Europe based on clinopyroxene and spinel chemistry: evidence for mantle modification during an extensional cycle. Lithos, 266-267, 233-263, https://doi.org10.1016/j.lithos.2016.08.02.

Pinto V.H. (2014) - Linking tectonic evolution with fluid history in hyperextended rifted margins: Examples from the fossil Alpine and Pyrenean rift systems and the present-day Iberia rifted margin. Unpublished Ph.D. Thesis, Université de Strasbourg.

Pinto V.H.G., Manatschal G., Karpoff A.-M., Viana A. (2015) - Tracing mantle-reacted fluids in magma-poor rifted margins: The example of Alpine Tethyan rifted margins. Geochem. Geophy. Geosy., 16(9), 3271-3308, https://doi.org10.1002/2015GC005830.

Pinto V.H.G., Manatschal G., Karpoff A.M., Ulrich M., Viana A.R. (2017) - Seawater storage and element transfer associated with mantle serpentinization in magma-poor rifted margins: A quantitative approach. Earth Planet. Sci. Lett., 459, 227-237, https://doi.org10.1016/j.epsl.2016.11.023.

Quick J.E., Sinigoi S., Negrini L., Demarchi G., Mayer A. (1992) - Synmagmatic deformation in the underplated igneous complex of the Ivrea-Verbano zone. Geology, 20(7), 613-616, https://doi.org10.1130/0091-7613(1992)020<0613:sditui>2.3.co;2.

Ranero C.R. and Pérez-Gussinyé M. (2010) - Sequential faulting explains the asymmetry and extension discrepancy of conjugate margins. Nature, 468(7321), 294-299, https://doi.org10.1038/nature09520.

Reston T.J. and McDermott K.G. (2011) - Successive detachment faults and mantle unroofing at magma-poor rifted margins. Geology, 39(11), 1071-1074, https://doi.org10.1130/G32428.1.

Reston T.J., Krawczyk C.M., Hoffmann H.J. (1995) - Detachment tectonics during Atlantic rifting: Analysis and interpretation of the S reflection, the west Galicia margin. Geol. Soc. Spec. Publ., 90(1), 93-109, https://doi.org10.1144/GSL.SP.1995.090.01.05.

Rey P. (1993) - Seismic and tectono-metamorphic characters of the lower continental crust in Phanerozoic areas: a consequence of post-thickening extension. Tectonics, 12(2), 580-590, https://doi.org10.1029/92TC01568.

Ribes C., Manatschal G., Ghienne J.-F., Karner G.D., Johnson C.A., Figueredo P.H., Incerpi N.N., Epin M. (2019a) - The syn-rift stratigraphic record across a fossil hyper-extended rifted margin: the example of the northwestern Adriatic margin exposed in the Central Alps. Int. J. Earth Sci., 108(6), 2071-2095, https://doi.orgHTTPS://DOI.ORG10.1007/s00531-019-01750-6.

Ribes C., Ghienne J.-F., Manatschal G., Decarlis A., Karner G.D., Figueredo P.H., Johnson C.A. (2019b) - Long-lived mega fault-scarps and related breccias at distal rifted margins: insights from present-day and fossil analogues. J. Geol. Soc. London, 176(5), 801-816, https://doi.org10.1144/jgs2018-181.

Ribes C., Petri B., Ghienne J., Manatschal G., Galster F., Karner G.D., Figueredo P.H., Johnson C.A. & Karpoff A. (2019c) - Tectono-sedimentary evolution of a fossil ocean-continent transition: Tasna nappe, central Alps (SE Switzerland). Geol. Soc. Am. Bull., 132(7-8), 1427-1446, https://doi.org10.1130/B35310.1/4863878/b35310.pdf.

Ribes C., Ghienne J.F., Manatschal G., Dall'Asta N., Stockli D.F., Galster F., Gillard M., Karner G.D. (2020) - The Grès Singuliers of the Mont Blanc region (France and Switzerland): stratigraphic response to rifting and crustal necking in the Alpine Tethys. Int. J. Earth Sci., 109(7), 2325-2352, https://doi.org10.1007/s00531-020-01902-z.

Ring U. (1994) - The influence of preexisting structure on the evolution of the Cenozoic Malawi rift (East African rift system). Tectonics, 13(2), 313-326, https://doi.org10.1029/93TC03188.

Ring U., Ratschbacher L., Frisch W., Dürr S., Borchert S. (1990) - The internal structure of the Arosa Zone (Swiss-Austrian Alps). Geol. Rundsch., 79(3), 725-739, https://doi.org10.1007/BF01879211.

https://doi.org/10.3301/GFT.2023.02

Roberts D. (2003) - The Scandinavian Caledonides: event chronology, palaeogeographic settings and likely modern analogues. Tectonophysics 365, 283–299. https://doi.org/10.1016/S0040-1951(03)00026-X.

Robertson A. (2004) - Development of concepts concerning the genesis and emplacement of Tethyan ophiolites in the Eastern Mediterranean and Oman regions. Earth-Sci. Rev., 66(3-4), 331-387, https://doi.org10.1016/j.earscirev.2004.01.005.

Rosenbaum G. and Lister G.S. (2005) - The Western Alps from the Jurassic to Oligocene: Spatio-temporal constraints and evolutionary reconstructions. Earth-Sci. Rev., 69(3-4), 281-306, https://doi.org10.1016/j.earscirev.2004.10.001.

Rosenbaum G., Lister G.S., Duboz C. (2002) - Relative motions of Africa, Iberia and Europe during Alpine orogeny. Tectonophysics, 359(1-2), 117-129, https://doi.org10.1016/S0040-1951(02)00442-0.

Rüpke L.H., Morgan J.P., Hort M., Connolly J.A.D. (2004) - Serpentine and the subduction zone water cycle. Earth Planet. Sci. Lett., 223(1-2), 17-34, https://doi.org10.1016/j.epsl.2004.04.018.

Sang Chan L., Shen W., Pubellier M. (2010) - Polyphase rifting of greater Pearl River Delta region (South China): Evidence for possible rapid changes in regional stress configuration. J. Struct. Geol., 32, 746-754, https://doi.org10.1016/j.jsg.2010.04.015.

Sauter D., Cannat M., Rouméjon S., Andreani M., Birot D., Bronner A., Brunelli D., Carlut J., Delacour A., Guyader V., MacLeod C.J., Manatschal G., Mendel V., Ménez B., Pasini V., Ruellan E., Searle R. (2013) - Continuous exhumation of mantle-derived rocks at the Southwest Indian Ridge for 11 million years. Nat. Geosci., 6, 314-320, https://doi.org10.1038/ngeo1771.

Schaltegger U. (1997) - Magma pulses in the Central Variscan Belt: episodic melt generation and emplacement during lithospheric thinning. Terra Nova, 9(5/6), 242-245, https://doi.org10.1046/j.1365-3121.1997.d01-43.x.

Schaltegger U., Desmurs L., Manatschal G., Muntener O., Meier M., Frank M., Bernoulli D. (2002) - The transition from rifting to sea-floor spreading within a magma-poor rifted margin: field and isotopic constraints. Terra Nova, 14(3), 156-162, https://doi.org10.1046/j.1365-3121.2002.00406.x.

Schardt H. (1898) - Les régions exotiques du versant N des Alpes suisses. Bulletin de La Société Vaudoise de Sciences Naturelles, 34, 114-219.

Schmid S.M. and Froitzheim N. (1993) - Oblique slip and block rotation along the Engadine line. Eclogae Geol. Helv., 86(2), 569-593.

Schmid S.M., Zingg A., Handy M. (1987) - The kinematics of movements along the Insubric Line and the emplacement of the Ivrea Zone. Tectonophysics, 135(1-3), 47-66, https://doi.org10.1016/0040-1951(87)90151-X.

Schmid S.M., Pfiffner O.A., Froitzheim N., Schönborn G., Kissling E. (1996) - Geophysical-geological transect and tectonic evolution of the Swiss-Italian Alps. Tectonics, 15(5), 1036-1064, https://doi.org10.1029/96TC00433.

Schmid S.M., Fgenschuh B., Kissling E., Schuster R., Fügenschuh B. (2004) - Tectonic map and overall architecture of the Alpine orogen. Eclogae Geol. Helv., 97, 93-117, https://doi.org10.1007/s00015-004-1113-x.

Schmid S.M., Kissling E., Diehl T., van Hinsbergen D.J.J., Molli G. (2017) - Ivrea mantle wedge, arc of the Western Alps, and kinematic evolution of the Alps-Apennines orogenic system. Swiss J. Geosci., 110(2), 581-612, https://doi.org10.1007/S00015-016-0237-0.

Schmid S.M., Fügenschuh B., Kounov A., Maţenco L., Nievergelt P., Oberhänsli R., Pleuger J., Schefer S., Schuster R., Tomljenović B., Ustaszewski K., van Hinsbergen D.J.J. (2020) - Tectonic units of the Alpine collision zone between Eastern Alps and western Turkey. Gondwana Res., 78, 308-374, https://doi.org10.1016/J.GR.2019.07.005.

Schumacher M.E., Schönborn G., Bernoulli D., Laubscher H.P. (1997) - Rifting and collision in the Southern Alps. Deep Structure of the Swiss Alps: Results of the National Research Program, 20, 186-204.

Schüpbach M.A. (1974) - Comparison of slope and basinal sediments of a marginal cratonic basin (Pedregosa Basin, New Mexico) and a marginal geosynclinal basin (southern border of Piemontais Geosyncline, Bernina Nappe, Switzerland) - Rice University.

Schwizer B. (1983) - Die Tristel-Formation: Vergleichende Untersuchung in Graubünden, Liechtenstein, Vorarlberg und Bayern. Unpublished Ph.D. Thesis, University of Bern.

https://doi.org/10.3301/GFT.2023.02

Şengör A.M.C. (1990) - Plate-tectonics and orogenic research after 25 years - a Tethyan perspective. Earth-Sci. Rev., 27(1-2), 1-201, https://doi.org/10.1016/0012-8252(90)90002-D.

Senkans A., Leroy S., d'Acremont E., Castilla R., Despinois F. (2019) - Polyphase rifting and break-up of the central Mozambique margin. Mar. Petrol. Geol., 100, 412-433, https://doi.org10.1016/j.marpetgeo.2018.10.035.

Seymour N.M., Stockli D.F., Beltrando M., Smye A.J. (2016) - Tracing the thermal evolution of the Corsican lower crust during Tethyan rifting. Tectonics, 35, 2439-2466, https://doi.org10.1002/2016TC004178.

Sibuet J.C. and Tucholke B.E. (2013) - The geodynamic province of transitional lithosphere adjacent to magma-poor continental margins. Geol. Soc. Spec. Publ., 369(1), 429-452, https://doi.org10.1144/SP369.15.

Simon N.S.C. and Podladchikov Y.Y. (2008) - The effect of mantle composition on density in the extending lithosphere. Earth Planet. Sci. Lett., 272(2), 148-157, https://doi.org10.1016/j.epsl.2008.04.027.

Smye A.J. and Stockli D.F. (2014) - Rutile U-Pb age depth profiling: A continuous record of lithospheric thermal evolution. Earth Planet. Sci. Lett., 408, 171-182, https://doi.org10.1016/j.epsl.2014.10.013.

Spillmann P. (1993) - Die Geologie des penninisch-ostalpinen Grenzbereichs im südlichen Berninagebirge. Unpublished Ph.D. Thesis, ETH Zurich.

Spillmann P. and Büchi H.J. (1993) - The Pre-Alpine Basement of the Lower Austro-Alpine Nappes in the Bernina Massif (Grisons, Switzerland; Valtellina, Italy). In: von Raumer J.F., Neubauer F. (Eds), Pre-Mesozoic geology in the Alps, Springer, Berlin, Heidelberg, 457-467, https://doi.org10.1007/978-3-642-84640-3_27.

Springhorn R. (2007) - Geology of the Engadine Window, especially the upper Val Fenga (east Switzerland). Z. Dtsch. Ges. Geowiss., 158(1), 67-87, https://doi.org10.1127/1860-1804/2007/0158-0067.

Stampfli G.M. (1993) - Le Briançonnais, terrain exotique dans les Alpes? Eclogae Geol. Helv., 86(1), 1-45.

Staub R. and Cadisch J. (1921) - Zur Tektonik des Unterengadiner Fensters. Eclogae Geol. Helv., 16, 223-285.

Steffen D., Jaques C., Nydegger T.H., Petroons D., Wildi W. (1993) - La Brèche du Chablais à son extrémité occidentale (Hte Savoie, France): Sédimentologie, éléments stratigraphiques et interprétation paléogéographique. Eclogae Geol. Helv., 86(2), 543-568.

Steinmann G. (1905) - Geologische Beobachtungen in den Alpen. Wagners Universitäts-Buchdruckerei.

Stern C.R. (2011) - Subduction erosion: Rates, mechanisms, and its role in arc magmatism and the evolution of the continental crust and mantle. Gondwana Res., 20, 284-308, https://doi.org10.1016/j.gr.2011.03.006.

Stern R.J. (2004) - Subduction initiation: spontaneous and induced. Earth Planet. Sci. Lett., 226, 275-292, https://doi.org10.1016/j.epsl.2004.08.007.

Streckeisen A. (1976) - To each plutonic rock its proper name. Earth-Sci. Rev., 12(1), 1-33, https://doi.org10.1016/0012-8252(76)90052-0.

Suess E. (1875) - Die Entstehung der Alpen. Braumüller W. (Ed.), Wien.

Sutra E. and Manatschal G. (2012) - How does the continental crust thin in a hyperextended rifted margin? Insights from the Iberia margin. Geology, 40(2), 139-142, https://doi.org10.1130/G32786.1.

Sutra E., Manatschal G., Mohn G., Unternehr P. (2013) - Quantification and restoration of extensional deformation along the Western Iberia and Newfoundland rifted margins. Geochem. Geophy. Geosy., 14(8), 2575-2597, https://doi.org10.1002/ggge.20135.

Svartman Dias A.E., Lavier L.L., Hayman N.W. (2015) - Conjugate rifted margins width and asymmety: The interplay between lithospheric strength and thermomechanical processes. J. Geophys, Res.-Solid Ea., 120, 8672-8700, https://doi.org10.1002/2015JB012074.

Switzerland Generaldirektion der Post-, Telegraphen- und Telephonverwaltung (1955) -

Termier P. (1904) - Les nappes des Alpes orientales et la synthèse des Alpes. B. Soc. Geol. Fr., 4(3), 843-928.

Thinon I., Matias L., Réhault J.P., Hirn A., Fidalgo-González L., Avedik F. (2003) - Deep structure of the Armorican Basin (Bay of Biscay): a review of Norgasis seismic reflection and refraction data. J. Geol. Soc. London, 160, 99-116, https://doi.org/10.1144/0016-764901-103.

https://doi.org/10.3301/GFT.2023.02

Thöni M. (1981) - Degree and evolution of the Alpine metamorphism in the Austroalpine unit W of the Hohe Tauern in the light of K/Ar and Rb/Sr age determinations on micas. Jahrb. der Geol. Bundesanstalt 124, 111–174.

Torsvik T.H. (1998) - Palaeozoic palaeogeography: A North Atlantic viewpoint. GFF, 120, 109-118.

Torsvik T.H., Van der Voo R., Preeden U., Mac Niocaill C., Steinberger B., Doubrovine P.V., van Hinsbergen D.J.J., Domeier M., Gaina C., Tohver E., Meert J.G., McCausland P.J.A., Cocks L.R.M. (2012) - Phanerozoic polar wander, palaeogeography and dynamics. Earth-Sci. Rev. 114, 325–368. https://doi.org/10.1016/j.earscirev.2012.06.007.

Tribuzio R., Thirlwall M.F., Messiga B. (1999) - Petrology, mineral and isotope geochemistry of the Sondalo gabbroic complex (Central Alps, Northern Italy): implications for the origin of post-Variscan magmatism. Contrib. Mineral. Petr., 136(1-2), 48-62, https://doi.org10.1007/s004100050523.

Trommsdorff V. (1983) - Metamorphose magnesiumreicher Gesteine: Kritischer Vergleich von Natur, Experiment und thermodynamischer Datenbasis. Fortschr. Mineral., 61, 283-308.

Trommsdorff V., Piccardo G.B., Montrasio A. (1993) - From magmatism through metamorphism to sea floor emplacement of subcontinental Adria lithosphere during pre-Alpine rifting (Malenco, Italy). Schweiz. Miner. Petrog., 73(2), 191-203.

Trümpy R. (1972) - Zur Geologie des Unterengadins. Ergebnisse Der Wissenschaftlichen Uneterunchugen Im Schweizerschen Nationalpark, 12, 71-87.

Trümpy R. (1980) - Geology of Switzerland: A Guide-Book. Basel: Wepf & Co. Schweizerische Geologische Kommission.

Trümpy R., Schmid S.M., Conti P., Froitzheim N. (1997) - Erläuterungen zur Geologischen Karte 1:50000 des Schweizerischen Nationalparks (Geologische Spezialkate Nr. 122) (Issue 87). Zernez: Landeshydrologie und geologie (Buwal), Bern.

Tucholke B.E., Sawyer D.S., Sibuet J. (2007) - Breakup of the Newfoundland--Iberia rift. In: Karner G.D., Manatschal G., Pinheiro L.M. (Eds.), Imaging, mapping and modelling continental lithosphere extension and breakup, Geol. Soc. Spec. Publ., 282(3), 9-46, https://doi.org10.1144/SP282.2.

Tugend J., Manatschal G., Kusznir N.J., Masini E. (2014) - Characterizing and identifying structural domains at rifted continental margins: application to the Bay of Biscay margins and its Western Pyrenean fossil remnants. Geol. Soc. Spec. Publ., 413, 171-203, https://doi.org10.1002/2014TC003529.

Tugend J., Manatschal G., Kusznir N. (2015) - Spatial and temporal evolution of hyperextended rift systems: implication for the nature, kinematics and timing of the Iberian-European plate boundary. Geology, 43(1), 15-18, https://doi.org/10.1130/G36072.1.

Ullmann C.V., Thibault N., Ruhl M., Hesselbo S.P., Korte C. (2014) - Effect of a Jurassic oceanic anoxic event on belemnite ecology and evolution. P. Natl. Acad. Sci. USA, 111(28), 10073-10076, https://doi.org10.1073/pnas.1320156111.

Uyeda S. (1981) - Subduction zones and back arc basins - A review. Geol. Rundsch., 70(2), 552-569, https://doi.org10.1007/BF01822135.

Van Staal C.R., Barr S.M. (2012) - Lithospheric architecture and tectonic evolution of the canadian appalachians and associated atlantic margin. In: Percival J.A., Cook F.A., Clowed R.M. (Eds.), Tectonic styles in Canada: The LITHOPROBE perspective, Geological Association of Canada, Special Paper, 49, 41-95.

Villa I.M., Hermann J., Müntener O., Trommsdorff V. (2000) - ^{39}Ar-^{40}Ar dating of multiply zoned amphibole generations (Malenco, Italian Alps). Contrib. Mineral. Petrol. 140, 363-381, https://doi.org/10.1007/s004100000197.

Vine F.J. and Matthews D.H. (1963) - Magnetic anomalies over oceanic ridges. Nature, 199(4897), 947-949, https://doi.org10.1038/199947a0.

von Blanckenburg F. and Davies J.H. (1995) - Slab breakoff: A model for syncollisional magmatism and tectonics in the Alps. Tectonics, 14(1), 120-131, https://doi.org10.1029/94TC02051.

Von Quadt A., Grunenfelder M., Buchi H. (1994) - U-Pb zircon ages from igneous rocks of the Bernina nappe system (Grisons, Switzerland). Schweiz. Miner. Petrog., 74(3), 373-382.

Waibel A.F. and Frisch W. (1989) - The Lower Engadine Window: sediment deposition and accretion in relation to the plate-tectonic evolution of the Eastern Alps. Tectonophysics, 162(3-4), 229-241, https://doi.org10.1016/0040-1951(89)90246-1.

Wegener A. (1915) - Die Entstehung der Kontinente und Ozeane. Braunschweig, Friedrich Vieweg und Sohn.

https://doi.org/10.3301/GFT.2023.02

Weissel J.K. and Karner G.D. (1989) - Flexural uplift of rift flanks due to mechanical unloading of the lithosphere during extension. J. Geophys. Res.-S. Ea., 94(B10), 13919-13950, https://doi.org10.1029/JB094iB10p13919.

Weissert H.J. and Bernoulli D. (1985) - A transform margin in the Mesozoic Tethys: evidence from the Swiss Alps. Geol. Rundsch., 74(3), 665-679, https://doi.org10.1007/BF01821220.

Wernicke B. (1985) - Uniform-sense normal simple shear of the continental lithosphere. Can. J. Earth Sci., 22(1), 108-125, https://doi.org10.1139/e85-009.

Wernicke B. and Axen G.J. (1988) - On the role of isostasy in the evolution of normal fault systems. Geology, 16(9), 848-851, https://doi.org/10.1130/0091-7613(1988)016<0848:OTROII>2.3.CO;2.

White R. and McKenzie D. (1989) - Magmatism at rift zones: The generation of volcanic continental margins and flood basalts. J. Geophys. Res., 94(B6), 7685-7729, https://doi.org10.1029/JB094iB06p07685.

Whitmarsh R.B., Manatschal G., Minshull T.A. (2001) - Evolution of magma-poor continental margins from rifting to seafloor spreading. Nature, 413(6852), 150-154, https://doi.org10.1038/35093085.

Willett S., Beaumont C., Fullsack P. (1993) - Mechanical model for the tectonics of doubly vergent compressional orogens. Geology, 21(4), 371-374, https://doi.org10.1130/0091-7613(1993)021<0371:MMFTTO>2.3.CO.

Wilson R.C.L., Manatschal G., Wise S. (2001) - Rifting along non-volcanic passive margins: Stratigraphic and seismic evidence from the Mesozoic successions of the Alps and Western Iberia. Geol. Soc. Spec. Publ., 187(1), 429-452, https://doi.org10.1144/gsl.sp.2001.187.01.21.

Withjack M.O., Schilsche, R.W., Olsen P.E. (2012) - Development of the passive margin of eastern North America: Mesozoic rifting, igneous activity, and breakup. In: Roberts D.G., Bally. A.W. (Eds.), Regional geology and tectonics: Phanerozoic rift systems and sedimentary basins, Elsevier, 301-335, https://doi.org10.1016/B978.

Woodhead J., Eggins S., Gamble J. (1993) - High field strength and transition element systematics in island arc and back-arc basin basalts: Evidence for multi-phase melt extraction and a depleted mantle wedge. Earth Planet. Sci. Lett., 114(4), 491-504, https://doi.org10.1016/0012-821X(93)90078-N.

Xie X.N., Müller R.D., Li S., Gong Z., Steinberger B. (2006) - Origin of anomalous subsidence along the Northern South China Sea margin and its relationship to dynamic topography. Mar. Petrol. Geol., 23(7), 745-765, https://doi.org10.1016/j.marpetgeo.2006.03.004.

Yamasaki T., O'Reilly B., Readman P. (2006) - A rheological weak zone intensified by post-rift thermal relaxation as a possible origin of simple shear deformation associated with reactivation of rifting. Earth Planet. Sci. Lett., 248(1-2), 119-131, https://doi.org10.1016/j.epsl.2006.05.019.

Yielding G. (1990) - Footwall uplift associated with Late Jurassic normal faulting in the northern North Sea. J. Geol. Soc. London, 147(2), 219-222, https://doi.org10.1144/gsjgs.147.2.0219.

Zanchetta S., Malusà M.G., Zanchi A. (2015) - Precollisional development and Cenozoic evolution of the Southalpine retrobelt (European Alps). Lithosphere, 7(6), 662-681, https://doi.org10.1130/L466.1.

Ziegler P.A. (1988) - Evolution of the Arctic-North Atlantic and the Western Tethys. Am. Assoc. Petr. Geol., Memoir, 43, 164-196.

Zwaan F., Chenin P., Erratt D., Manatschal G., Schreurs G. (2021) - Complex rift patterns, a result of interacting crustal and mantle weaknesses, or multiphase rifting? Insights from analogue models. Solid Earth, 12(7), 1473-1495, https://doi.org10.5194/SE-12-1473-2021.

Manuscript received 04 November 2022; accepted 28 February 2023; published online 30 May 2023;
editorial responsibility and handling by S. Tavani.

https://doi.org/10.3301/GFT.2023.02